

NKS-439
ISBN 978-87-7893-531-1

Thermal Hydraulic Phenomena of the Suppression Pool

Pavel Kudinov¹
Xicheng Wang¹
Dmitry Grishchenko¹
Markku Puustinen²
Antti Räsänen²
Eetu Kotro²
Kimmo Tielinen²
Timo Pättikangas³
Ari Silde³

¹Division of Nuclear Engineering, Kungliga Tekniska Högskolan (KTH)
Sweden

²Lappeenranta-Lahti University of Technology (LUT)
Finland

³VTT Technical Research Centre of Finland Ltd

June 2020

Abstract

KTH reports further development and validation of the Effective Momentum Source and the Effective Heat Source (EMS/EHS) models for spargers using source terms and boundary conditions approaches. Fluent and GOTHIC codes have been applied in the analysis to design sparger (H2P3) and integral (H2P4) test series in PANDA facility. Results of the analysis suggest that proposed design allows to achieve test objectives and obtain PIV data needed for model development and validation from H2P3, and to reach prototypic levels of pressurization within a reasonable time in H2P4. The progress on development of the image analysis for post processing the data from the SEF-POOL tests is presented.

Nine steam injection tests in SEF-POOL facility at LUT University. Analysis of the tests helps to understand the key effects and factors that can be neglected in model development. Main findings are: both the Jacob and Mach number have a significant effect; at large Ja effective momentum is significantly reduced; effective momentum has a maximum at $Ja \sim 0.02-0.04$; injection hole diameter and chamfer have no significant influence on the effective momentum except for the maximum value of C, which is reached at larger values of Ja number for smaller holes.

Result of VTT work suggest that the EHS/EMS models could be implemented in the Apros 6-equation model. The EHS/EMS models can increase capability of Apros for computationally efficient simulation of pool stratification/mixing phenomena in plant geometry. Simulation on thermal stratification has been done with Fluent for an experiment performed in the PPOOLEX test facility with steam injection through a vertical sparger. The effect of steam injection was modelled by using the EMS/EHS. Qualitatively correct behavior of the thermal stratification was obtained, however, pool temperature was lower than in the experiment due to the heat loss on the pool surface. Further analysis is ongoing in order to improve the results.

Key words

Steam Condensation, Pool Stratification, Mixing, Pressure Suppression Pool, Thermal Hydraulic, BWR, Containment, CFD, GOTHIC

NKS-439
ISBN 978-87-7893-531-1
Electronic report, June 2020
NKS Secretariat
P.O. Box 49
DK - 4000 Roskilde, Denmark
Phone +45 4677 4041
www.nks.org
e-mail nks@nks.org

Thermal Hydraulic Phenomena of the Suppression Pool

Final Report from the NKS-THEOS

(Contract: NKS_R_2019_130)

Pavel Kudinov¹, Xicheng Wang¹, Dmitry Grishchenko¹
Markku Puustinen², Antti Räsänen², Eetu Kotro², Kimmo Tielinen²
Timo Pättikangas³, Ari Silde³

¹Division of Nuclear Engineering, Kungliga Tekniska Högskolan (KTH),

²Lappeenranta-Lahti University of Technology (LUT),

³VTT Technical Research Centre of Finland Ltd

Table of contents

1.	Introduction	3
1.1.	BACKGROUND	3
1.2.	MOTIVATION AND GOALS FOR THE THEOS PROJECT	4
2.	Description of activities in 2019	5
2.1.	SUMMARY OF ACTIVITIES AT KTH	5
2.2.	SUMMARY OF ACTIVITIES AT LUT	6
2.3.	SUMMARY OF ACTIVITIES AT VTT	8
3.	References	10

Appendix A:

Development of the EHS/EMS models and analytical support to PANDA and SEF-POOL experiments

Appendix B:

SEF-POOL tests on small-scale phenomena of steam discharge into subcooled water

Appendix C:

Assessment of implementation of the effective heat and momentum source models in Apros

Appendix D:

CFD analysis of pressure suppression pool by using effective heat and momentum source models

1. Introduction

1.1. Background

Containment is the last physical barrier that prevents radioactive fission products release into the environment. Boiling Water Reactors (BWR) employ a large water pool (Pressure Suppression Pool (PSP)) to condense steam released from the primary coolant system [1]. The PSP is used both in accidents and in normal operation to control reactor vessel pressure. It also serves as a water source for the Emergency Core Cooling System (ECCS), containment spray, and as a scrubber in case of a core damage accident with release of radioactive aerosols.

A thermally stratified pool has higher temperature at the surface compared to a completely mixed pool with the same averaged temperature. The pool surface temperature determines the steam partial pressure in the containment gas space, while bottom layer of the pool might remain cold. Higher pool temperature results in higher partial pressure of steam in the containment atmosphere and respectively higher total containment pressure. If water temperature at the steam injection point is close to saturation, condensation can be very violent leading to large dynamic loads. If saturation conditions are reached in the vicinity of the steam injection, steam can bypass the pool without condensation. Thus, thermal stratification reduces pressure suppression capacity of the pool. For instance, containment pressure in Fukushima Daiichi Unit 3 accident was increasing much faster than prediction done with the assumption of completely mixed PSP [7, 8].

There are several scenarios of where PSP operation can be affected by interactions between (i) stratification and mixing phenomena, (ii) operation of emergency core cooling systems (ECCS), spray, residual heat removal system (RHR), (iii) water balance in the containment compartments, and (iv) pool behavior diagnostics and emergency operation procedures. Those scenarios include (i) different LOCAs scenarios e.g. with steam line break inside the radiation shield, broken blowdown pipes, and leaking safety relief valves (SRV); (ii) station blackout; (iii) severe accidents.

In a BWR, steam can be injected into the pool through blowdown pipes (in case of LOCA) and spargers [2]. The blowdown pipes connect the drywell to the wetwell and play important role in LOCA accidents. Spargers connect the primary coolant system to the wetwell pool, inject steam through multiple small holes, and are used to control the pressure in the vessel. Direct Contact Condensation (DCC) of steam injected into a water pool is as a source of heat and momentum. A competition between these sources determines whether the PSP will be thermally stratified or mixed [3, 4]. Momentum depends on the steam condensation regime e.g. chugging, oscillatory bubbles, and stable jets. If steam injection results in a low momentum source incapable to overcome buoyancy forces, the heat can be deposited in the layer above the injection point, while water below remains cold [5, 6]. If steam injection results in a higher momentum source, it can lead to the development of a large scale circulation in the pool which can erode or even break the stratification [5, 6].

Validated codes are needed for the simulation of realistic accident scenarios that can adequately resolve the interplay between phenomena, safety systems and operational procedures. However, the prediction of thermal stratification and mixing in a PSP remains a

challenging task, due to the lack of models for direct contact condensation phenomena [9, 10, 11] that could be effectively used to simulate large-scale pools with numerous steam injection devices operated during long-term transients.

Effective Heat Source (EHS) and Effective Momentum Source (EMS) models [3, 4, 12] have been proposed at KTH to enable the prediction of thermal stratification and mixing phenomena in a BWR containment and pressure suppression pool. The EHS/EMS models have been under development for steam injection through the blowdown pipes [3, 4, 12, 13, 14, 16, 17, 18, 19, 20, 21, 22, 23, 24, 25, 26] and the spargers [27, 28, 29, 30, 31, 32, 33, 34]. The models provide a computationally affordable approach by exploiting the gap between the spatial and temporal scales of the large pool and direct contact condensation phenomena. The models postulate that the effects of steam injection on the development of thermal stratification and mixing in a large pool can be predicted using only “effective”, i.e. time and space averaged, sources of heat and momentum created by steam injection without explicit resolution of the steam/water interfaces. The development of the EHS/EMS models was greatly supported by cooperation with the experimental teams first at Lappeenranta University of Technology (LUT) in the framework of NKS and NORTHNET RM3 projects and then with the Paul Scherrer Institute (PSI) in the framework of OECD/NEA HYMERES and HYMERES-2 projects.

1.2. Motivation and goals for the THEOS project

Validation of the EHS/EMS models was done by KTH using experimental data from the PPOOLEX and SEF-POOL facilities at LUT, Finland, and the PANDA facility at PSI, Switzerland. The validated models have been applied to analysis of steam injection through spargers in a full-scale Nordic BWR Pressure Suppression Pool (PSP). The results show that strong thermal stratification of potential safety importance can develop in the pool during prototypic steam injection conditions. The analysis results suggest that further development of the EHS/EMS correlations and computational models are necessary in order to enable modeling of regimes and conditions, which have not yet been studied in experiments, but are critically important and can completely change the PSP stratification and mixing behavior. More specifically, non-condensable gases in case of steam injection through blowdown pipes can affect chugging phenomena and thus pool mixing. Steam injection regimes through spargers, azimuthal velocity distribution and turbulence generated at sparger head and the effect of the load reduction rings are also very influential factors according to the analysis. The effects of other safety systems such as sprays and strainers have also not been addressed in experiments. In this project, KTH will provide analytical support for the new tests in the SEF-POOL and PPOOLEX facilities at LUT and in the PANDA facility at PSI (in the framework of the OECD/HYMERES-2 project). Obtained experimental data will be used by KTH for the development and validation of the models in order to address the remaining important sources of uncertainty for prediction of the pool behavior.

A set of experiments with spargers were performed in the PPOOLEX facility at LUT. The experiments were mainly focused on the oscillatory bubble regime, and exploratory tests were done in chugging and stable jet regimes. The experimental data were used by KTH to address important phenomena governing the pool behavior and to validate the computational models. A small-scale Separate Effect Facility (SEF-POOL) was built to measure directly the effective momentum induced by steam injection through a sparger. The tests provided a possibility to quantify the effective momentum correlations that are used in the simulations

performed at KTH and a validation effort of CFD models at VTT. Important variables affecting the effective momentum magnitude in full-scale plant need to be further analyzed in order to provide closures for the EMS model development for spargers by KTH. Furthermore, data on direct contact condensation gathered with the help of sophisticated instrumentation is needed for the improvement of calculation models of CFD codes at VTT. For this purpose, further development of the experimental facilities for obtaining systematic data relevant to PSP phenomena and conditions will be carried out in this project. Particularly, design for new experiments that can address possible effect of initial steam enthalpy to clarify most adequate definition of Jacob number for steam injection conditions, the effect of hole size on the value of Jacob number at which effective momentum reaches its maximum, the entrainment rate for the jet created by steam injection and respective effect of momentum distribution in azimuthal direction, turbulence generated by steam condensation and chugging regimes in spargers will be developed. Feasibility of a new experimental campaign in the PPOOLEX facility will be evaluated, considering remaining uncertainties in the phenomena such as the effect of spray activation in the drywell and/or wetwell on a thermally stratified pool, the combined effect of sparger head and load reduction rings, etc.

Computational Fluid Dynamics (CFD) simulations will be performed by VTT for the direct-contact condensation and thermal stratification experiments of LUT. The simulations will be done by using the commercial ANSYS Fluent code. The EHS/EMS models developed at KTH will be implemented in the Fluent code by using user-defined functions. In the model, the sparger of the vent pipe in the pressure suppression pool will be described with mass, heat and momentum sources. Simulations of stratification and mixing experiments performed with the PPOOLEX facility will be performed with the Fluent code. The results will be compared to the experiments of LUT and to the results calculated by KTH. In addition, possibilities to implement an approach based on the EHS/EMS model in the Apros system code will be studied. CFD calculations will be performed to validate the implemented EHS/EMS model for stratification and mixing. In addition, the implementation of the approaches based on the EHS/EMS model in the Apros system code will be tested.

2. Description of activities in 2019

2.1. Summary of activities at KTH

Detailed description of the project activities at KTH is provided in Appendix A. KTH is providing analytical support to SEF-POOL and PANDA tests in order to select the most important parameters for model development and validation conditions and to provide necessary measurement systems. Further development and validation of the EHS/EMS models for spargers is ongoing in order to: (i) include the effect of Jacob and Mach numbers on the effective momentum rate in subsonic and sonic injection regimes (ii) include jet entrainment rate in the definition of the momentum profile around the sparger head, (iii) to implement revised EMS model for the load reduction rings and (iv) to further develop the Richardson correlation for predicting the erosion velocity of the cold stratified layer.

In this report we describe the progress achieved in addressing main technical tasks, i.e.: (i) development validation of the EHS/EMS models for spargers using OECD/HYMERES-1 PANDA HP5 test series; (ii) pre-test analysis in support of the experimental for SEF-POOL facility at LUT and PANDA facility at PSI; (iii) post-test analysis using the new test data.

In Section 3 of Appendix A we provide an overview of previous works on direct contact condensation and pool phenomena and modeling approaches. The need and the progress in further development of the EHS/EMS models for spargers is described in Sections 4 of Appendix A. Two approaches to EMS model implementation are discussed (i) based on the source terms in the momentum equation and (ii) using boundary conditions for liquid velocity. Advantages and disadvantages of both approaches are discussed in detail. Results of the model calibration and validation against the data available from the PANDA HP5 tests are presented.

In Section 5 of Appendix A application of the developed EHS/EMS models to pre-test analysis in support of the PANDA H2P3 tests with sparger injection are presented. Scoping calculations were carried out to specify geometrical setup (pool depth, elevation of the sparger and number of open LRR holes), initial pool temperature, injection procedures, arrangement of thermocouples, PIV setup, for sparger tests (H2P3-1,2,3) and LRR tests (H2P3-4,5,6).

In Section 6 of Appendix A we present results of the pre-test analysis for the integral H2P4 test series in PANDA facility. The aim of the tests is to study the effect of pool stratification and mixing phenomena on containment pressurization. Results of the analysis are used for selection of the test configuration, i.e. the vessels to be used and connections between them, water pool level, duration and mass flow rates for different injection phases. Results of the analysis suggest that it is feasible to achieve prototypic levels of pressurization during a reasonable time for the tests.

In Section 7 of Appendix A the progress in development of the image analysis for post-processing of the data from the SEF-POOL tests are presented. Gas bubbles are used in the tests in order to visualize water velocity in the vicinity of the jet induced by steam injection. The first data from the analysis of the bubbles rise in a stagnant pool was obtained and results are being analyzed. The current work is focused on the further analysis of bubbles flow during steam injection and the data from SEF S-29 test has been processed. Further work will aim to optimize (i) experimental setup to resolve several issues related to bubble formation and size, and (ii) image analysis and develop reliable approach to the estimation of flow velocity and entrainment rate.

2.2. Summary of activities at LUT

Detailed description of the project activities at LUT University is provided in Appendix B. Prediction of the effective momentum induced by the oscillatory bubble and oscillatory cone jet regimes is necessary for the modelling of the pool behavior. This is especially relevant for BWRs, where the development of thermal stratification or mixing during a steam injection through spargers can affect the performance of the suppression pool. In order to directly measure the effective momentum, the SEF-POOL facility was built at LUT University and an extensive test series is being carried out. The reference system for the SEF-POOL facility is an SRV sparger pipe of a BWR plant. Hence, the facility is designed in such a way that discharge of steam through the injection holes at the sparger lower end into the sub-cooled pool water can be simulated representatively.

Analysis of the previous tests by KTH has shown that oscillatory bubble motions are a very efficient mechanism of transferring the force from the steam to the mean flow liquid. The main goal of the SEF-POOL tests in 2019 was to provide data of the characteristics of the small-scale phenomena, which affect the effective momentum sources in case of steam injection through a sparger into a sub-cooled pool of water. This information will then be used in the validation of the simplified EHS/EMS models for spargers by KTH. Furthermore, the SEF-POOL tests support the validation effort of the DCC and interfacial area models of CFD codes for steam injection through spargers at VTT and LUT.

Nine steam injection tests were performed in the SEF-POOL facility in 2019. The following issues were addressed:

- i) Effect of high Jacob number on the effective momentum, i.e. steam injection into initially highly subcooled pool in sonic and sub-sonic regimes.
- ii) Effective momentum in the transition regime, i.e. effect of transition from subsonic to sonic flow conditions.
- iii) Effective momentum at mass fluxes higher than 300 kg/m²s.
- iv) Effect of nozzle chamfer.

Preliminary analysis of the tests by LUT and KTH reveal that the results fit well with the previous data and are very helpful for the understanding of the key effects and factors that can be neglected when the EMS/EHS models are developed further. Based on the results, the following new findings from the SEF-POOL tests in 2019 can be summarized.

- 1) Both the Jacob and Mach number have a significant effect on the effective momentum coefficient C (i.e. the ratio of the liquid momentum rate to the theoretical value of the momentum rate of steam). New data provides a possibility to quantify the effect of the Mach number, which was only qualitatively noticeable in the previous data set.
- 2) In choked flow conditions, except for the cases with a very large Jacob number, the steam mass flow rate (or theoretical Mach number) has no effect on the effective momentum coefficient, which is close to ~ 0.8 in this regime.
- 3) The Jacob number has a minor and nearly linear effect on the effective momentum coefficient, which is increasing as the Jacob number is decreasing.
- 4) At very large Jacob numbers ($\sim 0.16-0.2$), the condensation rate is very large, which leads to rapid reduction of the effective momentum coefficient. This effect can be observed even at choked flow conditions (as mentioned above) when the theoretical Mach number for steam was relatively small, $\sim 1-1.3$.
- 5) As the Jacob number approaches to zero, the effective (time-averaged) momentum coefficient behaves non-monotonically, i.e. it reaches a maximum value at $Ja \sim 0.02-0.04$ and then decreases.
- 6) There is no apparent dependency of the effective momentum coefficient on chamfer in the injection holes.
- 7) Comparison with the previous data suggests that the hole diameter also doesn't have an effect on the effective momentum coefficient, except with the value of the Ja number at which C reaches its maximum value.
- 8) Comparison of the earlier test results (the S3 and S17 tests with the $\varnothing 8$ mm orifice) indicate that the maximum value of C can be reached with larger values of Jacob number when the hole size is smaller. This can be an indication that the Weber and/or Reynolds number might play a role in the transition.

Bubble parameters, which have been estimated through the image processing of the highspeed videos of the SEF-POOL tests by KTH, include the collapse and bubble life frequencies, maximum bubble radius, bubble velocities, pressure gradient, and heat transfer coefficients. A

good agreement is observed in the data and proposed correlations. Regarding the heat transfer coefficient, further tests are required to reduce the uncertainties associated with its strong time-dependency and the steam flow entering the bubble.

2.3. Summary of activities at VTT

Detailed description of the project activities at VTT on model development and validation is provided in Appendix C and D for Apros and CFD respectively.

VTT aims to assess the implementation of the EHS/EMS models in Apros, i.e., whether the implementation is possible and how it should be done. Both the lumped parameter containment model and six-equation thermal hydraulic model of Apros are considered. The EHS/EMS models are adapted in the CFD or system codes using a single-phase liquid solver. Due to totally different approach used in the Apros lumped parameter (LP) code, the EHS/EMS models cannot be directly used for LP simulation. However, the work revealed some other interesting approaches, which might be exploited in the Apros LP modelling for pool stratification/mixing. The EHS/EMS models could be implemented in the Apros 6-equation model using the suitable correlations for the effective steam momentum calculated by Apros.

The recommendations for future work are that the EHS/EMS models associated with steam injection through spargers will first be implemented in the Apros 6-equation model. Possibility to use 2D nodalisation in the pool to allow circulation flows should be studied. Selected POOLEX experiments could be simulated to verify/validate the new modelling approach. The suitable PPOOLEX experiments are e.g. SPA-T2 and SPA-T3. The tests should be selected for simulations in leverage on the respective development at VTT with the Fluent CFD code. This work shows that adoption of the EHS/EMS model for Apros can be worthwhile. Pool thermal stratification, as seen e.g. in the Fukushima accident, is typically a long-term phenomenon, and an accurate modelling of stratification phenomena and associated steam condensation regimes is challenging and time-consuming when using the current code models. The EHS/EMS models increase capability of Apros for computationally efficient simulation of pool stratification/mixing phenomena in real plant geometry.

VTT is also developing implementation of EHS/EMS modeling approaches in Fluent. Test simulation on thermal stratification of pressure suppression pool has been done for an experiment performed with the PPOOLEX test facility. In the experiment, steam was injected into water through a vertical sparger pipe submerged into the pressure suppression pool. The condensation of steam was not calculated directly but it was modelled by using the Effective Momentum Source and the Effective Heat Source (EMS/EHS) models developed by [18]. The calculation was performed with the commercial ANSYS Fluent code, where the EMS/EHS model was implemented with user-defined functions. In the EMS/EHS model, the momentum and enthalpy resulting from the steam condensation are added as source terms directly into liquid water phase. The CFD simulation resulted in qualitatively correct behavior of the thermal stratification. The calculated pool temperatures were, however, clearly lower than in the experiment. The reason for this was the heat loss on the pool surface. The beginning of the mixing part of the stratified layer was also calculated and the initial phase of the mixing was observed. The present approach must be modified and a new simulation with modified boundary conditions is in progress. It seems, however, that in future some major changes in the simulations method should be made in order get improved results. During the present

experiment, the amount of injected steam is so large that the surface level in the pool changed significantly. In order to take this properly into account, Volume Of Fluid Method or moving mesh approach should be used were the evolution of the surface level can be calculated. This method would also properly treat the problematic heat losses on the pool surface.

Acknowledgements

NKS conveys its gratitude to all organizations and persons who by means of financial support or contributions in kind have made the work presented in this report possible. The support from the Finnish nuclear safety program, the SAFIR2022-program, the Swedish Radiation Safety Authority for the work is gratefully acknowledged.

Disclaimer

The views expressed in this document remain the responsibility of the author(s) and do not necessarily reflect those of NKS. In particular, neither NKS nor any other organization or body supporting NKS activities can be held responsible for the material presented in this report.

3. References

1. Pershagen, B., 1994. Light Water Reactor Safety. Pergamon Press.
2. Lahey, R.T., Moody, F.J., 1993. The Thermal Hydraulics of a Boiling Water Nuclear Reactor, 2nd edition, American Nuclear Society, La Grange Park, Ill, USA.
3. Li, H., Kudinov, P., 2010. Effective Approaches to Simulation of Thermal Stratification and Mixing in a Pressure Suppression Pool. OECD/NEA & IAEA Workshop CFD4NRS-3, Bethesda, MD, USA, September 14-16, 2010.
4. Li, H., Villanueva, W., Kudinov, P., 2014. Approach and Development of Effective Models for Simulation of Thermal Stratification and Mixing Induced by Steam Injection into a Large Pool of Water. Science and Technology of Nuclear Installations, 2014, Article ID 108782, 11 pages.
5. Laine, J., Puustinen, M., Räsänen, A., 2013. PPOOLEX experiments on the dynamics of free water surface in the blowdown pipe. Nordic Nuclear Safety Research, NKS-281.
6. J. Laine, M. Puustinen, A. Räsänen, PPOOLEX Experiments with a Sparger, Nordic Nuclear Safety Research, 2015, NKS-334.
7. Mizokami, S., Yamada, D., Honda, T., Yamauchi, D., Yamanaka, Y., 2016. Unsolved issues related to thermal-hydraulics in the suppression chamber during Fukushima Daiichi accident progressions. Journal of Nuclear Science and Technology, 53, 630-638.
8. Mizokami, S., Yamanaka, Y., Watanabe, M., Honda, T., Fuji, T., Kojima, Y., PAIK, C.Y., Rahn, F., 2013. State of the art MAAP analysis and future improvements on TEPCO Fukushima-Daiichi NPP accident. NURETH-15: The 15th International Topical Meeting on Nuclear Reactor Thermal Hydraulics, Pisa, Italy, May 12-17, paper number 536.
9. Tanskanen, V., Jordan, A., Puustinen, M., Kyrki-Rajamäki, R., 2014. CFD simulation and pattern recognition analysis of the chugging condensation regime. Annals of Nuclear Energy, 66, 133-143.
10. Patel, G., Tanskanen, V., Hujala, E., Hyvärinen, J., 2017. Direct contact condensation modeling in pressure suppression pool system. Nuclear Engineering and Design, 321, 328-342.
11. Pellegrini, M., Naitoh, M., 2016. Application of two-phase flow DFC to the phenomena expected in Fukushima Daiichi S/C. OECD/NEA & IAEA Workshop CFD4NRS-6.
12. Li, H., Villanueva, W., Puustinen, M., Laine, J., Kudinov, P., 2014. Validation of Effective Models for Simulation of Thermal Stratification and Mixing Induced by Steam Injection into a Large Pool of Water. Science and Technology of Nuclear Installations, 2014, Article ID 752597, 18 pages.
13. Li, H., Villanueva, W., Puustinen, M., Laine, J., Kudinov, P., 2017. Thermal stratification and mixing in a suppression pool induced by direct steam injection. Annals of Nuclear Energy, 111, 487-498.
14. Villanueva, W., Li, H., Puustinen, M., Kudinov, P., 2015. Generalization of experimental data on amplitude and frequency of oscillations induced by steam injection into a subcooled pool. Nuclear Engineering and Design, 295, 155-161.
15. Li, H. and Kudinov, P., 2009. An Approach to Simulation of Mixing in a Stratified Pool with the GOTHIC code. ANS Transactions, paper 210976.
16. Li, H., Villanueva, W., Kudinov, P., 2011. Development and implementation of effective models in GOTHIC for the prediction of mixing and thermal stratification in a

- BWR pressure suppression pool. Proceedings of ICAPP 2011, Nice, France, May 2-5, 2011, Paper 11256.
17. Li, H. and Kudinov, P., 2008. An approach toward simulation and analysis of thermal stratification and mixing in a pressure suppression pool. NUTHOS-7, Seoul, Korea, October 5-9, Paper 243.
 18. Gallego-Marcos, I., Villanueva, W., Kudinov, P., 2018. Modelling of Pool Stratification and Mixing Induced by Steam Injection through Blowdown Pipes. *Annals of Nuclear Energy*, 112, 624-639.
 19. Li, H. and Kudinov, P., 2009. Condensation, Stratification and Mixing in a Boiling Water Reactor Suppression Pool. NORTHNET Roadmap 3 Report, Division of Nuclear Power Safety, Royal Institute of Technology (KTH), Stockholm, Sweden, 70p.
 20. Li, H., Villanueva, W., Kudinov, P., 2010. Investigation of containment behavior with activation of rupture disks in system 361/362 with GOTHIC simulation. Swedish Radiation Safety Authority (SSM) Project Report, Royal Institute of Technology (KTH), Stockholm, Sweden, 25p.
 21. Li, H., Kudinov, P., Villanueva, W., 2010. Modeling of Condensation, Stratification and Mixing Phenomena in a Pool of Water. NKS Report, NKS-225, Division of Nuclear Power Safety, KTH, Stockholm, Sweden, 91p.
 22. Li, H., Kudinov, P., Villanueva, W., 2010. Condensation, Stratification and Mixing in a Boiling Water Reactor Suppression Pool. NORTHNET Roadmap 3 Report, Division of Nuclear Power Safety, Royal Institute of Technology (KTH), Stockholm, Sweden, 88p.
 23. Li, H., Villanueva, W., Kudinov, P., 2012. Development, Implementation and Validation of EHS/EMS Models for Spargers. Westinghouse project report. Division of Nuclear Power Safety, Royal Institute of Technology (KTH), Stockholm, Sweden, 98p.
 24. Li, H., Villanueva, W., Kudinov, P., 2012. Effective Momentum and Heat Flux Models for Simulation of Stratification and Mixing in a Large Pool of Water. NKS-ENPOOL Research report, NKS-266, 58p.
 25. Li, H., Villanueva, W., Kudinov, P., 2012. Effective Models for Prediction of Stratification and Mixing Phenomena in a BWR Suppression Pool. NORTHNET Roadmap 3 Report, Division of Nuclear Power Safety, Royal Institute of Technology (KTH), Stockholm, Sweden, 87p.
 26. Li, H., Villanueva, W., Kudinov, P., 2014. Effective Models for Simulation of Thermal Stratification and Mixing Induced by Steam Injection into a Large Pool of Water. Nordic Nuclear Safety Research, NKS-316.
 27. Gallego-Marcos, I., Villanueva, W., Kapulla, R., Paranjape, S., Paladino, D., Kudinov, K., 2016. Modeling of thermal stratification and mixing induced by steam injection through spargers into a large water pool. OECD/NEA & IAEA Workshop CFD4NRS-6, Cambridge, MA, USA, September 13-15.
 28. Gallego-Marcos, I., Villanueva, W., Kapulla, R., Paranjape, S., Paladino, D., Kudinov, K., 2016. Scaling and CFD Modelling of the Pool Experiments with Spargers Performed in the PANDA Facility. NUTHOS-11: The 11th International Topical Meeting on Nuclear Reactor Thermal Hydraulics, Operation and Safety Gyeongju, Korea, October 9-13, N11P0670.
 29. Gallego-Marcos, I., Villanueva, W., Kudinov, P., 2016. Scaling of the Erosion of a Thermally Stratified Layer in a Large Water Pool during a Steam Injection Through Spargers. NUTHOS-11: The 11th International Topical Meeting on Nuclear Reactor Thermal Hydraulics, Operation and Safety, Gyeongju, Korea, October 9-13, N11P0525.
 30. Gallego-Marcos, I., Villanueva, W., Kudinov, P., 2016. Modeling of Thermal Stratification and Mixing in a Pressure Suppression Pool Using GOTHIC. NUTHOS-

- 11: The 11th International Topical Meeting on Nuclear Reactor Thermal Hydraulics, Operation and Safety, Gyeongju, Korea, October 9-13, N11P0524.
31. Gallego-Marcos, I., Villanueva, W., Kudinov, P., et al., 2019. Pool Stratification and Mixing Induced by Steam Injection through Spargers: CFD modeling of the PPOOLEX and PANDA experiments. *Nuclear Engineering and Design*, 347, 67-85.
 32. Gallego-Marcos, I., Filich, L., Villanueva, W., Kudinov, P., 2015. Modelling of the Effects of Steam Injection through Spargers on Pool Thermal Stratification and Mixing. NKS Report 347.
 33. Gallego-Marcos, I. Villanueva, W., Kudinov, P., 2016. Thermal Stratification and Mixing in a Large Pool Induced by Operation of Spargers, Nozzles, and Blowdown Pipes". NKS Report 369.
 34. Gallego-Marcos, I., Villanueva, W., Kudinov, P., 2017. Modelling of a Large Water Pool during Operation of Blowdown Pipes, Spargers, and Nozzles. NKS-393.

Appendix A

Development of the EHS/EMS models and analytical support to PANDA and SEF-POOL experiments



**Development of the EHS/EMS models and analytical
support to PANDA and SEF-POOL experiments**

**Project: Thermal Hydraulics of the Suppression Pool
NKS-THEOS
(Contract: NKS_R_2019_130)**

Xicheng Wang, Dmitry Grishchenko, Pavel Kudinov

Royal Institute of Technology (KTH),
Division of Nuclear Engineering
Roslagstullsbacken 21, 106 91 Stockholm, Sweden

June 2020
Stockholm

Table of contents

1.	INTRODUCTION	5
2.	GOALS AND TASKS.....	11
3.	STATE OF THE ART REVIEW	12
3.1.	<i>Experiments on direct contact condensation</i>	12
3.2.	<i>Experiments on pool behavior</i>	13
3.3.	<i>Modelling approaches</i>	13
3.4.	<i>EHS/EMS models</i>	14
4.	DEVELOPMENT OF EHS/EMS MODELS FOR SPARGER.....	16
4.1.	<i>Introduction of PANDA HP5 tests</i>	16
4.2.	<i>Calibration of the EHS/EMS models implemented using source terms</i>	17
4.2.1.	EHS/EMS models for spargers by source terms	17
4.2.2.	Calibration of the EHS/EMS models	22
4.3.	<i>Development of EHS/EMS models using SCR approach</i>	24
4.3.1.	Single-phase turbulent jets	25
4.3.2.	SCR model for a single jet induced by steam injection	26
4.3.3.	Comparison of analytical and CFD results for single jet flow.....	27
4.3.4.	SCR model for multiple condensed jets.....	30
4.4.	<i>Implementation of SCR for spargers in Fluent</i>	31
4.4.1.	Computational domain	31
4.4.2.	Lumped velocity profile.....	32
4.4.3.	Boundary conditions	34
4.4.4.	Turbulence model	35
4.5.	<i>Validation against HP5 tests</i>	35
4.6.	<i>Summary of EHS/EMS model development for sparger</i>	39
5.	PRE-TEST SIMULATIONS FOR PANDA H2P3 TESTS	40
5.1.	<i>Pre-test simulations for H2P3 spargers tests</i>	40
5.1.1.	Pool configuration.....	40
5.1.2.	Steam injection procedure.....	43
5.1.3.	3D PIV setup.....	44
5.1.4.	CFD analysis of velocity field around sparger	47
5.1.5.	Optimization of the PIV window orientation.....	51
5.2.	<i>Pre-test simulations for H2P3 LRR tests</i>	54
5.3.	<i>Summary of pre-test analysis for H2P3 test series in PANDA facility</i>	57
6.	PRE-TEST SIMULATIONS FOR PANDA H2P4 TESTS	58
6.1.	<i>Motivation and background</i>	58
6.2.	<i>Initial test configuration for the H2P4 series</i>	58
6.3.	<i>Model setup for H2P4 scoping analysis</i>	59
6.4.	<i>Model validation</i>	61
6.5.	<i>Results of the scoping analysis</i>	63
6.5.1.	Two-vessel configuration with open IPs.....	63
6.5.2.	Two-vessel configuration with closed bottom IP	66

6.5.2.1.	Effect of the water pool depth	67
6.5.2.2.	Effect of initial water pool temperature.....	69
6.5.2.3.	Effect of the hot layer thickness	70
6.5.2.4.	Effect of steam injection rate.....	72
6.5.2.5.	Effect of nozzle spray location	72
6.5.3.	Pool preconditioning	75
6.6.	<i>Summary of H2P4 scoping analysis.....</i>	76
7.	ANALYSIS OF SEF-POOL TESTS.....	78
7.1.	<i>Motivation and background.....</i>	78
7.2.	<i>Experimental setup.....</i>	78
7.3.	<i>Entrainment rate analysis</i>	82
7.3.1.	Image calibration and error analysis	82
7.3.2.	SEF stagnant pool	84
7.3.3.	Discussion of the results	87
7.4.	<i>Summary of development of image analysis for SEF-POOL experiment.....</i>	87
8.	SUMMARY.....	88
	ACKNOWLEDGEMENTS.....	90
	DISCLAIMER	91
	REFERENCES.....	92

1. INTRODUCTION

Containment is an essential part of the reactor safety design and is the last physical barrier that prevents the release of radioactive fission products into the environment. Boiling Water Reactors (BWR) do not need to accommodate the steam generators used in Pressurized Water Reactors (PWR) and thus can be built with a smaller containment. In Loss-Of-Coolant Accident (LOCA) scenarios large amount of steam is released into the containment from reactor vessel. The smaller volume of the containment can lead to a rapid pressurization. Therefore BWRs utilize a large water pool (Pressure Suppression Pool (PSP)) where steam is condensed [1]. The PSP can be used in normal operation to reduce reactor vessel pressure and can be employed as a passive safety system for storing large amounts of decay heat in long-term transients such as Station Black Outs (SBO). It also serves as a water source for the Emergency Core Cooling System (ECCS), spray, and as a scrubber in case of a core damage accident with release of radioactive aerosols. Advanced PWRs (e.g. AP1000, APR1400, EPR, etc.) have In-containment Refuelling Water Storage Tank (IRWST) that carries out similar functions as the PSP in the BWRs [73].

The PSP and overall containment performance can be affected by physical phenomena such as mixing and stratification. A stratified pool will have higher temperature at the surface compared to completely mixed pool with the same averaged temperature. The pool surface temperature determines the steam partial pressure in the containment gas space. Higher pool temperature results in higher partial pressure of steam in the containment atmosphere and respectively higher total containment pressure, while bottom layer of the pool remains cold. If the water temperature at the steam injection point is close to saturation, condensation can be very violent leading to large dynamic loads. If saturation conditions are reached in the vicinity of the steam injection, steam can bypass the pool without condensation. Thus thermal stratification reduces pressure suppression capacity of the pool.

For instance, containment pressure in Fukushima Daiichi Unit 3 accident was rapidly increasing during the first 12 hours of the operation of the Reactor Core Isolation Cooling (RCIC) system [7, 8]. The system was driven by a steam turbine which exhaust is connected to the pressure suppression pool. The automated protection system shut down the RCIC when the pressure reached 400 kPa. The lumped parameter codes under-estimated the rate of pressure increase and resulting maximum pressure by about 160 kPa using a mixed pool assumption [7]. The underprediction was attributed to the development of thermal stratification in the suppression pool.

There are several scenarios of where PSP operation can be affected by interactions between (i) stratification and mixing phenomena, (ii) operation of emergency core cooling systems (ECCS), spray, residual heat removal system (RHR), (iii) water balance in the containment compartments, and (iv) pool behaviour diagnostics and emergency operation procedures. Those scenarios include (i) different LOCAs scenarios e.g. with steam line break inside the radiation shield, broken blowdown pipes, and leaking safety relief valves (SRV); (ii) station blackout; (iii) severe accidents.

In order to prevent build-up of thermal stratification, some designs (e.g. Nordic BWRs) employ nozzles that inject water into the pool at high momentum. However, as an active system, such nozzles will not be available in case of an SBO scenario and the state of the pool will be determined solely by steam injection phenomena.

In a BWR, steam can be injected into the pool through blowdown pipes (in case of LOCA) and spargers [2]. The large size blowdown pipes connect the drywell to the wetwell, inject steam vertically downwards, and play important role in LOCA accidents. Spargers connect the primary coolant system to the wetwell pool, inject steam through multiple small holes, and are used to control the pressure in the vessel. Direct Contact Condensation (DCC) of steam injected into a water pool is as a source of heat and momentum. A competition between these sources determines whether the PSP will be thermally stratified or mixed [3, 4]. Momentum depends on the steam condensation regime e.g. chugging, oscillatory bubbles, and stable jets. If steam injection results in a low momentum source incapable to overcome buoyancy forces, the heat can be deposited in the layer above the injection point, while water below remains cold [5, 6]. If steam injection results in a higher momentum source, leading to the development of a large scale circulation in the pool which can erode or even break the stratification [5, 6].

Validated codes are needed for simulation of realistic accident scenarios that can adequately resolve the interplay between phenomena, safety systems and operational procedures. However, the prediction of thermal stratification and mixing in a PSP remains a challenging task, due to the lack of models for direct contact condensation phenomena [9, 10, 11] that could be effectively used to simulate large-scale pools with numerous steam injection devices operated during long-term transients.

Effective Heat Source (EHS) and Effective Momentum Source (EMS) models [3, 4, 12] have been proposed to enable the prediction of thermal stratification and mixing phenomena in a BWR containment and pressure suppression pool. The models EHS/EMS models have under development for steam injection through the blowdown pipes [3, 4, 12, 13, 14, 16, 17, 18, 19, 20, 21, 22, 23, 24, 25, 26] and the spargers [27, 28, 29, 30, 31, 32, 33, 34]. The models provide a computationally affordable approach by exploiting the gap between the spatial and temporal scales of the large pool and direct contact condensation phenomena. The models postulate that the effects of steam injection on the development of thermal stratification and mixing in a large pool can be predicted using only “effective”, i.e. time and space averaged, sources of heat and momentum created by steam injection without explicit resolution of the steam/water interfaces.

The development of this models greatly benefited from the cooperation with the experimental teams first at Lappeenranta University of Technology (LUT) in the framework of NKS and NORTHNET RM3 projects and then with the Paul Scherrer Institute (PSI) in the framework of OECD/NEA HYMERES project.

After the Fukushima Daiichi BWRs research community was startled with the realization that some of the containment phenomena that have a significant impact on the accident progression could not be reliably predicted by contemporary safety analysis tools. This realization reignited the international research community with an interest in containment and pool behavior. OECD/NEA HYMERES-1 project (2014-2017) was the first internationally supported effort that addressed pressure suppression pool phenomena in a dedicated HP5 series of experiments in PANDA facility which is a unique, large-scale, multi-purpose facility well instrumented for performing thermal-hydraulics experiments on containment phenomena.

In the HP5 series of the HYMERES-1 project, tests were performed to study “thermal stratification build-up” in a first test phase and “homogenization” in a second test phase in a water pool at different initial temperatures, under the effect of steam venting through a vertical sparger or water injection through a horizontal nozzle. These two phenomena were obtained by varying the steam flow rate. For the lower steam flow rates prevailed thermal stratification

build-up and for the higher flow rate prevailed thermal homogenization of the water pool. In one test a mixture of helium/steam was vented in phase 2 and the homogenization time was drastically reduced. Also for the tests in which water was injected through a horizontal nozzle in phase 2, the water temperature was varied in different tests to enhance either buoyancy or inertia of the water jet.

KTH has started post-test validation of the Effective Heat and Momentum Source (EHS/EMS) models implemented in GOTHIC and CFD code Fluent [27, 28, 29, 30, 31, 32, 33, 34, 36]. The EHS/EMS models were extended to the condensation regimes appearing in spargers. However, more detailed post-test validation revealed potential deficiencies in current modeling approaches. Preliminary results suggest that modeling of the slow erosion of the stratified layer, observed in the PANDA experiments with spargers, requires adequate selection of numerical approaches and modifications in the turbulence modeling with respect to the buoyancy effects. Also, further development, calibration and validation of the EHS/EMS models, especially for steam injection through spargers, would require an extended experimental database. Specifically, more data would be needed in order to clarify:

- The effect of buoyancy forces across the interface of the stratified layer on turbulence;
- Stability of large scale flow structures in the pool.
- Effective momentum induced by steam injection through spargers;
- The effect of non-condensable gases on the pool mixing.

Following the success of the first phase of the OECD/NEA HYMERES-1 project, the second phase (HYMERES-2) project has been initiated (starting from October 2017) and supported by the project partners, including some new members, such as US-NRC. One of the topics of the HYMERES-2 is to address the remaining issues on pressure suppression pool and BWR systems. Specifically, it is proposed

- *“... to extend the database on the pool related phenomena. The test conditions for the new series will be selected based on scoping calculations. The effect of the following parameters will be considered: Height of the pool and depth of the sparger; sparger design including blowdown pipe; BWR containment system tests, which involve the interplay of e.g. Drywell, Wetwell, Reactor Pressure Vessel and components e.g. venting pipes, vacuum breaker, spray, etc. These tests would allow a progressive validation of computational tools dedicated to pool phenomena.”*

With respect to the HP5 series in HYMERES-1, the following parameters could be varied in HYMERES-2:

- Height of the pool and depth of the sparger.
- Sparger design including blowdown pipe.
- BWR containment system tests, which involve the inter-playing of e.g. Drywell, Wetwell, sparger, blowdown pipe, spray, vacuum breakers, etc.

A schematic for the PANDA test configuration addressing the suppression pool is shown in Figure 1. The tests involve the interplay of different compartments e.g. Drywell, Wetwell, RPV and components e.g. venting pipes, vacuum breaker, spray, etc. An example of the PANDA configuration for representing a Main Steam Line Break (MSLB) scenario is shown in Figure 2. The tests would include the,

- Cyclic mixture flow venting from the Drywell to the Wetwell
- Cyclic opening of vacuum breaker and mixture flow returning from the Wetwell to the drywell.

Tests addressing specific open issues related to the Fukushima Daiichi containment behavior identified in the last years including those which arose during the activities of the OECD/NEA Benchmark Scenarios at the Fukushima (BSAF) are also planned to be addressed in the HYMERES-2 project.

It is instructive to note that PSI experimentalist have developed advanced techniques for using particle image velocimetry that can be used in application to the two-phase flows in the pool tests.

As in the first phase of the HYMERES project, the relevance and usefulness of the experimental data for understanding of the Nordic BWR containment phenomena, for model development and validation, will be dependent on the analytical support. KTH has developed a unique team that is leading research in the area of the pressure suppression pool modeling and has experience in guiding experimental research efforts.

The project will contribute to further development and retention of the national expertise in containment thermal hydraulic phenomena and analysis methods. The work will also strengthen SSM and Swedish participation in the international cooperation in the area of containment thermal-hydraulics.

The ultimate aim of the tests and analysis is to make a significant step towards plan applications. In the preliminary discussion with the PANDA operators following topics have been identified as of high potential interest for SSM that can be addressed in the experimental and analytical work in the framework of the HYMERES-2 project.

Two groups of tests are foreseen:

- Integral effect tests (IET)
- Separate effect tests (SET).

The aims of the IETs are:

- Observation of the interaction between different
 - phenomena and
 - equipmentin complex scenarios relevant to different accident progression sequences.
- Development and validation of adequate modeling approaches applicable for plant conditions that combine:
 - Reduced numerical resolution.
 - To address the complete containment system behavior.
 - Reliable modeling of the key physical phenomena and equipment

In total ~2 integral tests (plus shake-down and repeatability) are expected to be carried out. Scenarios of interest for each test are determined by relevancy to:

- LOCA scenarios
- SBO scenarios
 - With possibility of late power recovery.

Issues to be addressed in the tests are relevant to potential effects of

- Vacuum breakers.
- Spray.
- Break location.

- Location of the venting system inlet in the containment.
- Gas phase stratification.
 - Provides a link to the other test series in the projects concerned with gas phase mixing stratification and spray/cooler activation.

on performance of:

- ECCS and spray
- Pressure suppression function.
- Containment venting.
 - Potential for air ingress in the containment
 - activation of non-filtered containment venting
 - at the time when large fraction of non-condensable gases is present in the drywell.
 - Potential effect on aerosols distribution between the drywell and wetwell.
 - Non-condensable gases distribution between drywell and wetwell.

Extensive pre-test analysis with a plant model and a full model of the PANDA facility will be necessary in order to identify potentially important feedbacks and suggest how to address those in the tests.

The integral effect tests are expected to be of direct interest for SSM in interpretation and potential identification of safety issues.

The aim of the separate effect tests (SETs) is

- To provide necessary data for development and validation of the separate effect models.

In total about 5-6 SETs on development of stratification and mixing can be carried out using:

- High priority:
 - Sparger.
 - Blowdown pipe.
- Medium priority:
 - Spray – can be included in IET.
- Lower priority:
 - Nozzles.
 - Strainers.

The test conditions will be defined to provide necessary complementary knowledge to existing databases recently produced in the framework of the NKS projects in LUT and in HYMERES-1 project.

This report formulates goals and tasks in Section 2. An overview of previous works on direct contact condensation and pool phenomena and modeling approaches are provided in Section 3. The progress in development of the EHS/EMS models for spargers is described in Sections 4. Application of the developed EHS/EMS models in pre-test analysis for support of PANDA H2P3 tests are presented in Section 5. Pre-test analysis for the integral H2P4 test series in PANDA facility are presented in Section 6. Development of image analysis approach for post-processing the data from the SEF-POOL tests are provided in Section 7.

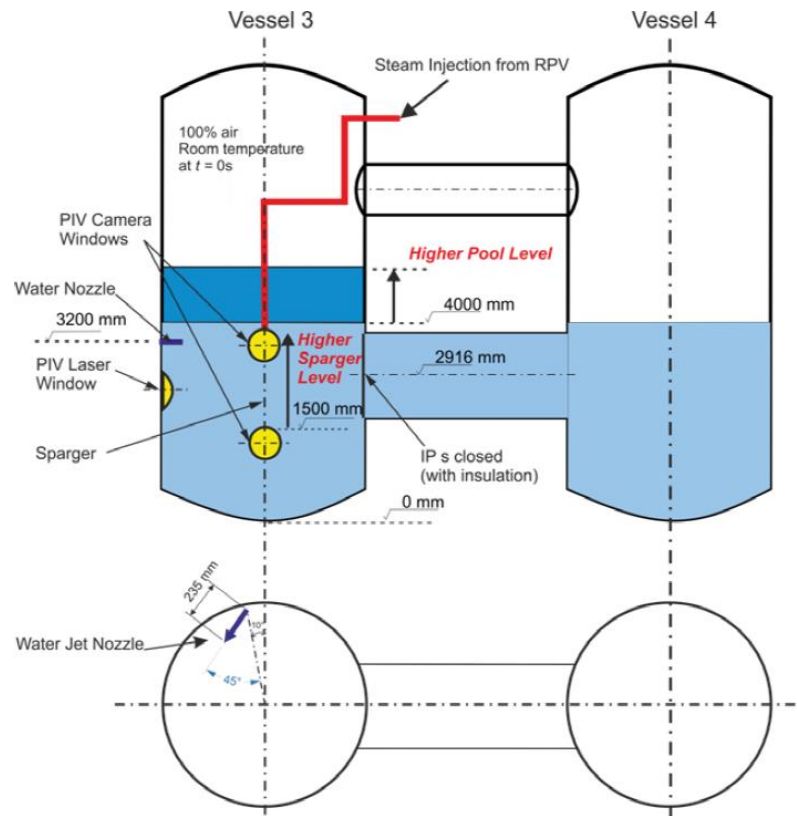


Figure 1: Example for the PANDA test configuration addressing suppression pool.

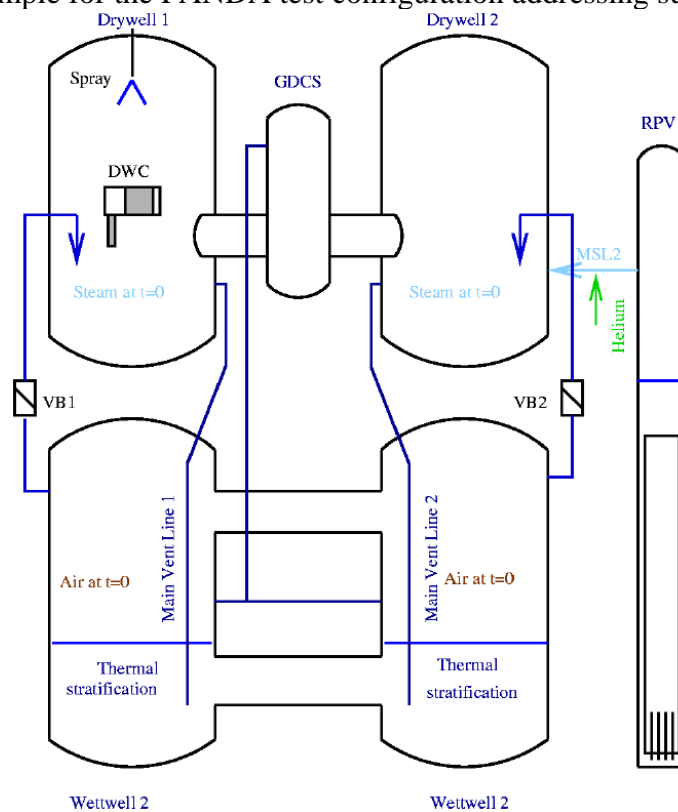


Figure 2: Example for the PANDA test configuration addressing suppression pool.

2. GOALS AND TASKS

The goal of the project is to provide pre- and post-test analytical support to the HYMERES-2 and NKS-THEOS experimental activities in order to ensure the success of the tests and maximize the value of the tests for model development and validation.

The following main tasks to be addressed in order to achieve the goal of the project:

- Task-1: To develop EHS/EMS models for spargers and validate them against OECD/HYMERES-1 PANDA HP5 test series.
- Task-2: To provide pre-test analysis in order to support the design and selection of the test conditions for the pressure suppression pool test series in SEF-POOL facility at LUT and PANDA facility at PSI.
- Task-3: To provide post-test analysis for the tests, aiming to develop and further validate predictive capabilities for the pressure suppression pool phenomena.

3. STATE OF THE ART REVIEW

The behavior of the pressure suppression pool is affected by a large number of phenomena. This section provides an overview of relevant experimental data and analytical approaches.

3.1. Experiments on direct contact condensation

Sonic and sub-sonic are the two main regimes of steam condensation in a pool. Sonic regimes occur when the injection pressure is about 0.53 times higher than the ambient. The high steam velocity creates large shear between liquid and vapor, which creates highly diffused interfaces before gradually turning into a single-phase jet flow. Sonic regimes are usually referred as “stable regimes” because macroscopic jet parameters such as penetration length, expansion ratio, heat transfer coefficient, etc., remain relatively constant in time. Experiments in [37] that the aforementioned parameters are mainly determined by the steam mass flux, pool subcooling, and diameter of the injection hole [37, 38, 39]. Wu et al. shown that high pressures after a shockwave cause an expansion of the jet. Steam condensation is negligible during the expansion. The jet is confined to a divergent section [40]. The expanded jet can accelerate the flow to super-sonic conditions, leading to another shockwave. Successive contraction-expansion waves can occur depending on the pressure inside the sparger and in the pool.

In the sub-sonic regime, heat transfer is smaller compared to sonic conditions [42]. Therefore a jet can expand, produce bubbles, which detach collapse and condense [43, 44], in so called oscillatory bubble regime. The frequency of the bubble growth-detach-collapse for single and multi-hole injections was observed to vary from 50 to 600 Hz [45, 46, 47], and is a function of the hole diameter and pool subcooling. Tang et al. [48] studied the mechanism of the detached bubble collapse and proposed a regime map. At low steam flux the map includes chugging regime, where the collapse of bubbles causes volumetric condensation, sudden pressure drop and rapid suction of liquid from the pool into the injection pipe [49]. The transition from the oscillatory bubble to chugging regimes is characterized by a monotonic decrease of the bubble detachment frequency which occurs in the range of steam mass flux of 20-60 kg/(m²s) [50]. Aust & Seeliger [51] showed that chugging can be suppressed in a blowdown pipe with outlet cut at 45° which prevented large bubbles from forming for steam mass fluxes up to 100 kg/(m²s). At very low steam mass fluxes all steam is condensed inside the blowdown pipe.

The condensation regime maps as functions of mass flux and pool subcooling for sub-sonic flows have been proposed in [43, 53, 54, 54]. Petrovic de With et al. [55] included the injection hole diameter as a third parameter. Gregu et al. [56] investigated different chugging regime modes. Wu et al. [57] proposed regime maps for multi-hole injection with transition from sonic to sub-sonic flow occurring at approximately 330 kg/(m²s).

In a BWR, the area of the blowdown pipes is much larger than a possible area of a break in the primary system. Therefore, steam mass fluxes are too low for transition to sonic flow. The large pressure difference between the primary coolant system and the wetwell is more likely to result in sonic flows through spargers, especially at the initial stages of the Automatic Depressurization System (ADS) activation, or during the intermittent operation of the Safety Relief Valves (SRVs). For LOCA, long-term ADS operations, or exhaust of safety systems such as the RCIC, sub-sonic regimes are expected to dominate during the transient.

Single-phase jets induced by the steam condensation were investigated by Choo et al. [58] using Particle Image Velocimetry (PIV). A self-similar feature of the liquid jet was observed after a certain distance from the orifice. Correlations were proposed to model the turbulent profile as a function of the injection conditions. Van Wissen et al. [59] measured the turbulent intensities of the liquid, which maximum values can be about 30%.

3.2. Experiments on pool behavior

Experiments are usually performed in reduced scale facilities. In this case, adequate scaling becomes an essential ingredient for the design of the tests and interpretation of the results [58]. The full-scale Marviken-FCSB tests [61] showed that chugging can occur during prototypic LOCA transients in a BWR Mark II containment. Thermal stratification was observed when chugging was suppressed at reduced steam mass flux. Extensive experimental campaigns were carried out by General Electric in a 1:130 reduced scale facility to for the pool swelling, pressure increase, pool temperature, etc. during a LOCA in a BWR Mark I [62], Mark II [63, 64], and Mark III [65, 66, 67]. LOCA type experiments were also performed in Japan by JAERI [62, 69] in a full size 1/18 sector of a BWR. Chugging was observed in most of the JAERI tests, but duration of the test (few hundred seconds) was too short for development of thermal stratification.

To study the development of thermal stratification and mixing at the late stages of a LOCA in ESBWR the LINX facility [70] at PSI was developed with steam injection through a single-hole 40 mm vertical sparger. Injection of pure steam lead to development of stratification with temperature differences up to 30°C [71], while adding air in concentrations above 5% in mass caused complete pool mixing. In experiments with prototypic multi-hole spargers of an APR1400 in the sonic regimes performed by Moon et al. [72] no stratified layer was observed. Zhang et al. [73] using the scaled models of the AP1000 quencher and IRWST showed that considerable thermal stratification can develop in prototypic steam injection conditions, especially for the quenchers with a low submergence.

Extensive experimental campaigns were carried out in the POOLEX/PPOOLEX facility in Lappeenranta University of Technology (LUT), Finland, and in the PANDA facility in PSI, Switzerland, using blowdown pipes [74, 75, 76, 77, 78, 79] and spargers [6, 33, 36]. Separate effect experiments were conducted in these schemes to investigate the effect of parameters such as the diameter of the pipe, volume of the drywell, steam injection conditions, etc.

Solom et al. [81] studied thermal stratification that can develop during prototypic steam injections of the RCIC system. Song et al. [83] showed that the Richardson number can be used to predict transition between thermal stratification and mixing. Fernando et al. [82, 84, 86] showed that the Richardson number defines regimes of interactions between the stratified layer and turbulent eddies and that the erosion velocity of a stratified layer is a function of the Richardson number.

3.3. Modelling approaches

Analytical models for bubble diameter and detachment frequency in the oscillatory bubble regime were developed in [87, 88] using the Rayleigh-Plesset equation and momentum balances across the bubble. Chugging models were also developed by Aya & Nariai [49] and Pitts [89] using the conservation equations and extended to include the non-condensable gases

in [90]. Comparison to experimental data showed a good prediction of the frequency and amplitude of the oscillations. Stability analysis performed by Brennen [91] showed that chugging is usually sustained in the natural, manometer type, oscillation of the system.

Pattikangas et al. [87] used ANSYS Fluent to simulate the chugging regime in the PPOOLEX experiments. An improved prediction of the heat transfer was obtained in the work done by Tanskanen et al. [9] and Patel [10]. Pellegrini et al. [11] used a Rayleigh-Taylor instability model to simulate the direct contact condensation heat transfer during chugging.

Based on the work done by Gamble et al. [93], KAERI proposed a modelling approach called Steam Condensation Region Model (SCRM) [28, 72, 94, 95, 96]. The SCRM is based on equations of mass, momentum, and energy in a control volume inside which steam condensation is assumed to be complete. This allows to introduce single-phase flow analysis and boundary conditions for the liquid velocity. The SCRM approach implemented in Star CCM+ and ANSYS Fluent showed good agreement with the results of the where complete mixing was observed. However, no thermal stratification and mixing transients were addressed with the model.

To enable prediction of the PSP performance in long-term thermal stratification and mixing transients EHS/EMS models have been proposed by Li & Kudinov [3, 4]. Similar to SCRM, EHS/EMS model aims to resolve only the effect of the direct contact condensation on the large pool. It is achieved by introducing effective sources of heat and momentum while details of the microscale phenomena at the steam/water interface are not resolved. The implementation of these models in GOTHIC [18, 34] showed good agreement with the PPOOLEX STB and MIX experiments [75, 78, 79], which were performed at different injection conditions and pool geometry, etc. The EHS/EMS models were further developed and applied to steam injection through multi-hole spargers by Gallego-Marcos et al. [31, 34, 97].

The EHS/EMS models can be implemented in a CFD code by (i) introducing volumetric momentum and heat source terms in transport equations [31], or (ii) by imposing boundary conditions on an interface (similar to the Steam Condensation Region (SCR) [72, 94, 95, 96]) that yield the same effective sources of heat and momentum. The method that uses the source terms has been validated against PPOOLEX [6] and PANDA tests [36], showing a good agreement with experimental data on temperature distributions in the pool, if the value of the effective momentum is properly calibrated. However, later experiments that measured the magnitude of momentum produced by steam condensation in a Separate Effect Facility (SEF) [98] suggested that the values of the effective momentum that gave good results were significantly under-estimated. Thus the need for further development of the predictive capabilities of the EHS/EMS model was identified.

3.4. EHS/EMS models

Explicit modeling of direct contact condensation (DCC) of steam is a challenge for contemporary codes. The small time and length scale of steam condensation behavior requires very small mesh size and time step when using CFD type analysis [9, 10, 11]. Lumped and 1D codes are inadequate for prediction of 3D, transient mixing phenomena. Thermal-hydraulic codes such as GOTHIC [99], and RELAP5 [100], do not provide a model for prediction of the effect of steam injection through blowdown pipes or spargers. Available condensation models are mostly designed for pipe flow regimes such as bubbly, churn, film, etc.

Therefore, the concept of Effective Heat Source (EHS) and Effective Momentum Source (EMS) models have been proposed to enable the prediction of the pool behavior induced by the steam condensation. The main idea of the effective models is that large scale pool behavior is not affected by the details of the DCC phenomena occurring at the small temporal and spatial scales. Therefore, only the time-averaged “effective” heat and momentum sources induced by steam in a large pool need to be modelled. The effective heat Q_{eff} and momentum M_{eff} sources can be presented as [4]

$$Q_{eff}(t) = \frac{1}{\Delta t} \int_{t-\Delta t}^t Q(\tau) d\tau \quad (1)$$

$$M_{eff}(t) = \frac{1}{\Delta t} \int_{t-\Delta t}^t M(\tau) d\tau \quad (2)$$

where the integrals represent the time-average of the instantaneous variations of the sources over a period Δt of time. These variations are due to the oscillatory nature of direct contact condensation. For example, the large scale motions of the liquid inside the pipe during the chugging regime, the small scale oscillatory bubble behavior, etc.

The chart for estimation of the effective heat and momentum sources in the EHS/EMS models is shown in Figure 3. First condensation regime is estimated for the given steam injection and pool conditions, then respective heat and momentum sources are calculated.

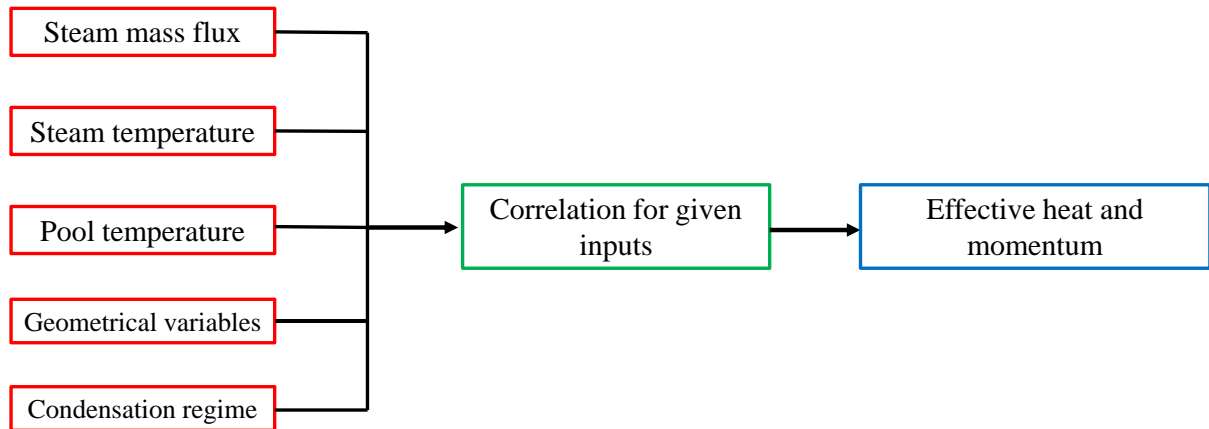


Figure 3. Chart of the EHS/EMS models.

4. DEVELOPMENT OF EHS/EMS MODELS FOR SPARGER

The multi-hole spargers are used to discharge steam from the primary circuit into the PSP. They can be used in the exhaust of safety systems such as the RCIC [8] as well. The horizontal injection through multi-hole leads to different regimes compared to the blowdown pipes, and therefore, requires further development of the EHS/EMS models [34].

In this section we introduce PANDA HP5 tests and the results of calibration of EHS/EMS models implemented using source effective source terms. Then, the development of EHS/EMS models using SCR approach is discussed in Section 4.3. Finally, the implementation in Fluent together with the validation against HP5 tests are given given in Section 4.4 and Section 4.5.

4.1. Introduction of PANDA HP5 tests

PANDA [108] is a multipurpose test facility designed to address containment thermal hydraulics phenomena and safety issues in LWRs. The facility consist of 2 wet well vessels and 2 dry well vessels and has a 1.5 MW steam generator. The experiments for steam injection through multi-hole spargers were done in one of the drywell as shown in Figure 4. The vessel was filled with water up to 4 m at room temperature 25°C. The interconnecting pipe (IP) was blocked by a thermally insulated lid to reduce the heat transfer between the vessels. The sparger was placed along the central axis of the pool at 1511 mm elevation above the bottom of the vessel.

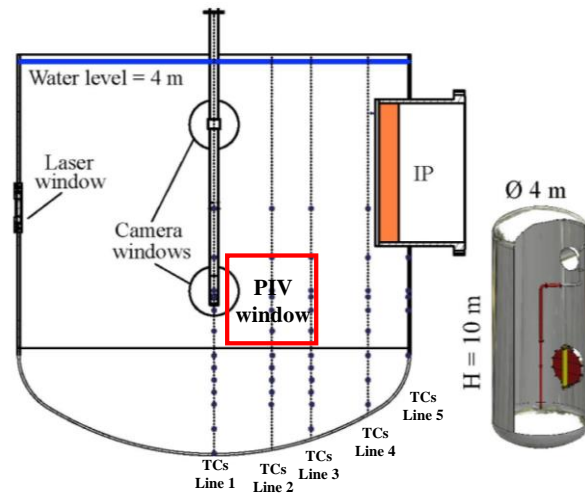


Figure 4. PANDA facility in the HP5 tests with sparger.

Five vertical trains of thermocouples (TCs) were mounted in a TC plane at different distance from the sparger (See TC points in Figure 4). The TC plane was positioned 250 mm away from the central plane. The vessel has three windows installed to enable 2D PIV measurements of the fluid velocity. One window was used to pass the laser sheet into the vessel and the other two windows were used for making video recording of the flow field with the PIV camera [109]. The geometrical characteristics of the multi-hole sparger used in the tests are shown in Figure 5. The sparger head has 32 holes arranged in 4 rings. Each hole has inner diameter of 9.5 mm and a conical chamfer.

Test matrix of selected test from the PANDA HP5 series is presented in Table 1 including steam injection procedures and initial pool temperatures. Each test had two phases for

development of thermal stratification and mixing respectively. Low steam mass flow rate (minimum flow rate avoiding the chugging regime [43, 46]) was used to develop stratification in the pool. After the temperature difference between the top and bottom of the pool reached certain value, the mass flow rate was increased to mix the pool. Further details of the experiments and their analysis can be found in [34, 36].

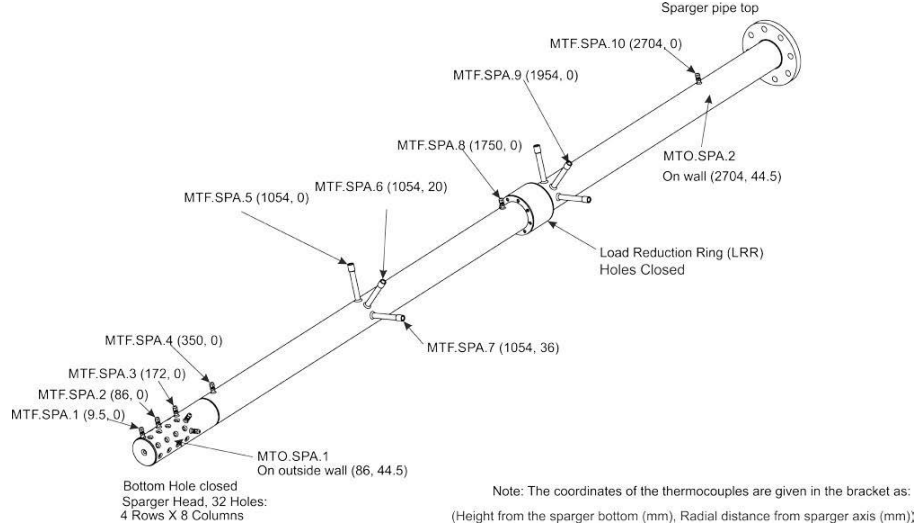


Figure 5. Geometry of sparger pipe [36].

Table 1. HP5 tests matrix

Test	Pool Initial Conditions		Phase 1: Stratification		Phase 2: Mixing	
	Temperature (°C)	Water level (m)	Flow (kg/s)	Duration (s)	Flow (kg/s)	Duration (s)
HP5-1	~25	4	0.16	6000	0.37	2500
HP5-2	~45	4	0.16	6000	0.26	5600
HP5-3	~23	4	0.16	6000	0.26	8100

4.2. Calibration of the EHS/EMS models implemented using source terms

The momentum and heat induced by steam injection into the pool can be modelled in the simulation using source terms in the transport equations or using boundary conditions. A good agreement between the experiments and simulations was achieved when the source term was calibrated based on PANDA data. However, the magnitude of effective momentum source was later found to be under-estimated in the simulations [31, 98] based on the SEF-POOL data. results of EHS/EMS models calibration implemented using source terms are discussed in this section.

4.2.1. EHS/EMS models for spargers by source terms

The EMS model for multi-hole spargers requires models for the (i) magnitude of the momentum, (ii) downward inclination of the momentum, and (iii) profile of velocity (or

momentum distribution) in vertical and azimuthal directions. When steam is injected into a subcooled pool through the multi-hole spargers, the effective heat and momentum induced by the steam condensation can be computed by Eqs. (1) and (2) respectively [4]. With some simplifications [31], the effective momentum source can be written as:

$$\dot{M}_{eff} = C\dot{M}_{th} = C\rho_s A_0 U_s^2 \quad (3)$$

$$C = 4.28\Delta T^{-0.35} \quad (4)$$

where ρ_s and U_s are the density and velocity of steam, A_0 is the injection hole area and ΔT is water subcooling, C is the condensation regime coefficient which is introduced as a ratio of the effective momentum to the momentum of the steam. This coefficient (or the effective momentum induced by multi-hole steam injection) was not measured directly in PPOOLEX and PANDA experiments. CFD simulations [31] were used to calibrate the value of C based on the temperature evolution in the pool (see Figure 6). C was measured later in the Separate Effect Facility (SEF) [98], and approximated by an empirical correlation (4) as a function of the pool subcooling.

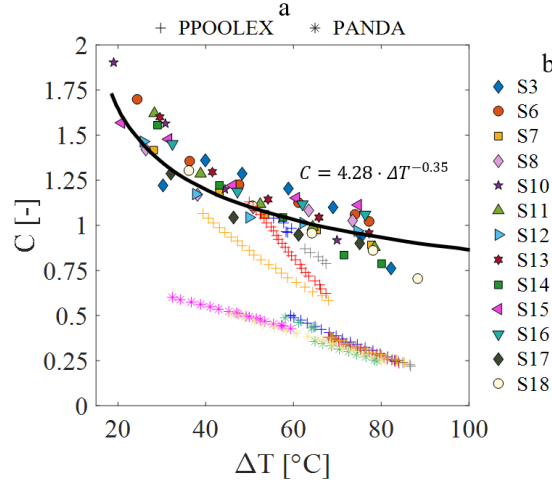


Figure 6. Comparison between C measured in the SEF facility and estimated from CFD simulations of PPOOLEX and PANDA experiments with spargers.

Comparison between the values of C estimated by CFD simulations (+, *) and measured in SEF experiments are summarized in Figure 6. The values of C calibrated from the CFD simulations under-estimate the measurements of C by 20 – 300%. The difference might be explained by the fact that the azimuthal profile of velocity (APV) was not measured in the PANDA and PPOOLEX tests and thus is an uncertain parameter in the model. The goal of this section is to calibrate the EMS model by using the updated correlation for the C coefficient and adjusting the spatial distributions of the momentum. When correlation (4) is applied with the previous modelling setup for the spatial distribution of the momentum, increased value of the momentum is expected to intensify pool mixing.

Sensitivity studies suggest that the downward inclination has a significant effect on the motion of thermocline [31]. The jets induced by steam condensation have a downward inclination according to the TC mesh measurements in the PPOOLEX and PIV images in PANDA tests (Figure 7). The inclination is created by the downward component of the steam at the sparger hole outlet. The ratio between the area of the injection hole to the pipe cross-section area is

around 0.41 and the thickness of the wall is 4 *mm* provides an angle of 15° for both PPOOLEX and PANDA [36]. The angle was estimated to be about 10° in a separate gas-to-gas injection experiment as shown in Figure 7(a). The difference might be attributed to the secondary flows inside the sparger and buoyancy effect of the plume. The angle can be also affected by the injection conditions according to the PIV data in the PANDA tests with flow pattern determined by the competition between the jet buoyancy and inertia.

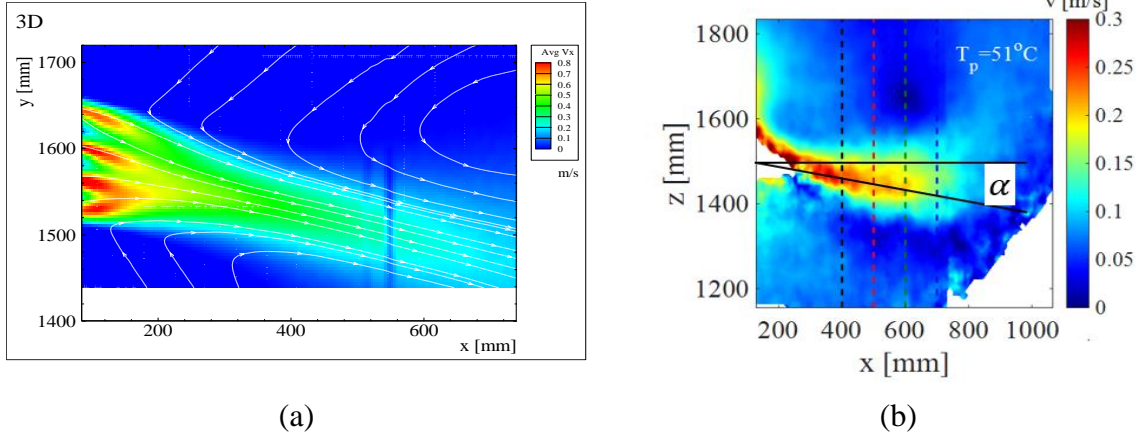


Figure 7. PIV data from (a) PANDA gas-to-gas experiment, (b) low steam injection phase of the PANDA HP5-2 experiment. Velocity data were time-averaged over 200s [36].

A single-phase jet injected into a still water develops a self-similarity velocity profile in non-dimensional coordinates. Jets injected through the adjacent nozzles have a tendency to merge into a single jet at certain distance downstream. The distance can be estimated as 3 times the pitch plus diameter [36] which agrees well with the temperature and velocity measurements in PANDA tests. Figure 7(b) shows a merged jet observed in PANDA HP5-2 test with the steam flux of 71 kg/m^2s . Self-similarity of the velocity profile in the vertical cross section of the jet was also observed.

The model for the Vertical Profile of Velocity (VPV) was developed to describe the velocity profile in the vertical direction. It includes two parameters, the length of the condensation zone where the momentum is applied in the vertical direction and its distribution in this zone. According to the standard round jet equation as Eq. (5), the VPV model can be defined as:

$$U_0(x, r) = U_0(x) \exp\left(-K \frac{r^2}{x^2}\right) \quad (5)$$

The centerline velocity $U_0(x)$ estimated by Figure 7(b), is about $0.1/x$. The jet expansion factors K , for round and plane jets, are 77 and 50 respectively in a single-phase flow [110, 121]. Analysis of the PIV data from PANDA experiments suggests that the K is about 40 or less (see Figure 8). The difference could be due to the effect of multi-hole sparger injection, condensation regime and turbulence. Note that all PANDA tests were performed with steam mass fluxes below 170 kg/m^2s . In this work, the VPV model is kept the same as in the previous work [31]. The length of the condensation zone in vertical is assumed 50 *mm* and it starts at the height of 1560 *mm*. Since the momentum sources are distributed in a radial range of 40 – 150 *mm*, the distribution profile in the vertical can be simplified as a top-hat profile where the velocity magnitude is independent of the elevation.

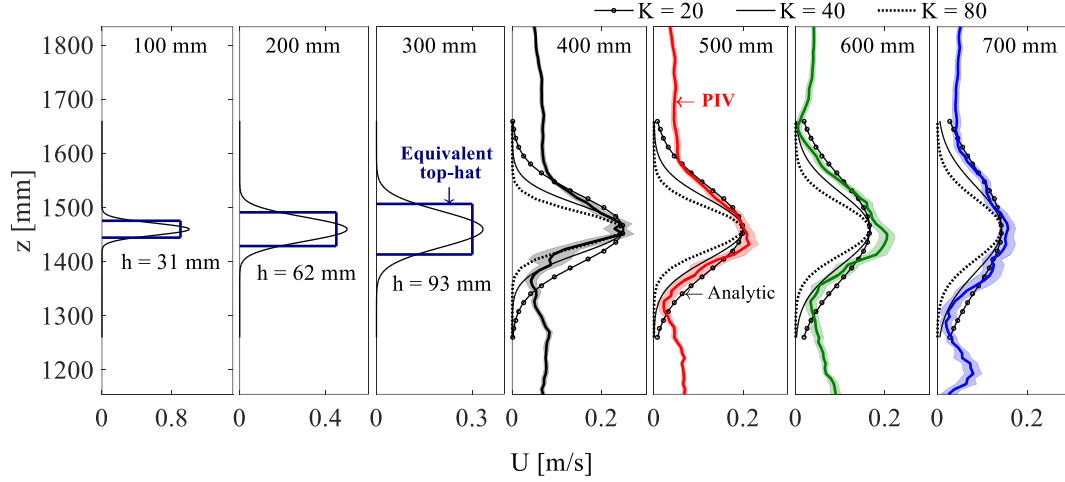


Figure 8. Comparison between the PIV data from Figure 7(b) and the analytical velocity profile described by Eq. (5) using different K [36].

Non-uniformities of the azimuthal velocity were observed in the work done by Song, et al [96]. The jet resembles a rectangular one which expands mostly in the horizontal direction. In this work, the momentum distribution in the azimuthal direction is described by the Azimuthal Profile of Velocity (APV) model. The model involves two variables, namely the length of the condensation zone in the radial direction and its distribution profile in this region.

In previous work [31], the length of the condensation zone in the radial direction was assumed as 50 mm starting at the $r = 90$ mm as shown in Figure 9(a) and the distribution profile was estimated by (5) using $K = 40$. With such setup, the effective momentum coefficient C was under-estimated. In this work, the calibration of the EHS/EMS model is carried out by adjusting the distribution of the source terms in vertical and azimuthal directions using the condensation regime coefficient C defined by (4).

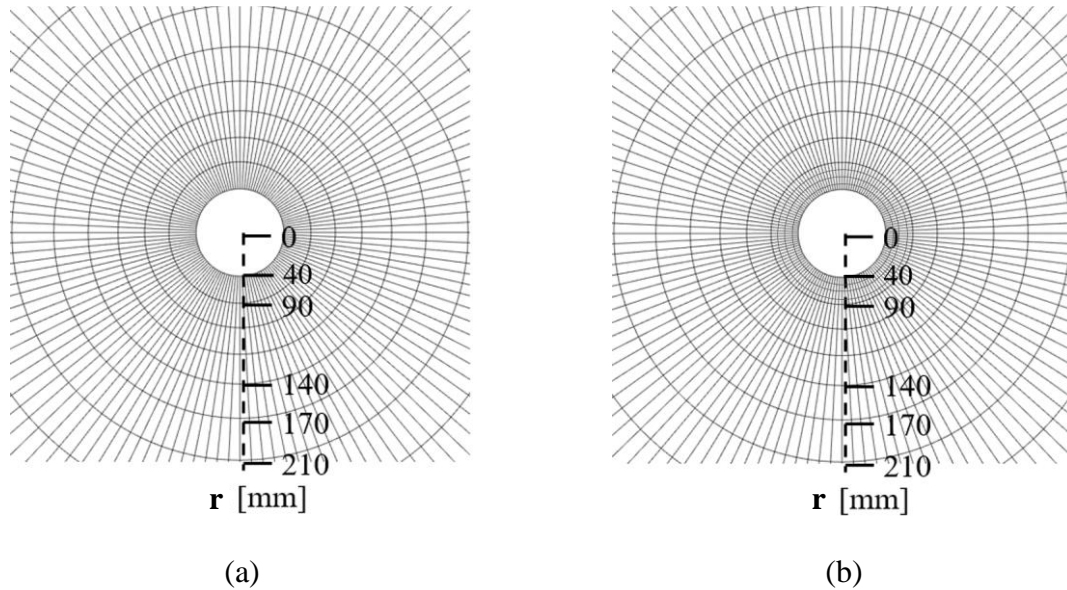


Figure 9. Top view of the azimuthal condensation zone. (a) Mesh in Fluent and (b) refined mesh within 40 – 90 mm.

Expansion factor K controls the shape of the azimuthal velocity profile. Comparison of azimuthal velocity profiles obtained using different values of K is presented in Figure 10. Note that the stepwise shape of the profiles is selected for convenient interpolation in the ANSYS Fluent. The integral of these profiles should be equal to 2π to keep the same overall momentum for different expansion factors K . The profile becomes more homogenous as K is decreased. When K is below 5, the jets merge. The erosion velocity of the thermocline is determined by the effective momentum. Sensitivity studies using $K = 40, 20$ and 10 suggest that the erosion velocity of the thermocline was slower for smaller K (Figure 11). Note that the total effective momentum was the same in all simulations, only the azimuthal velocity distribution was different.

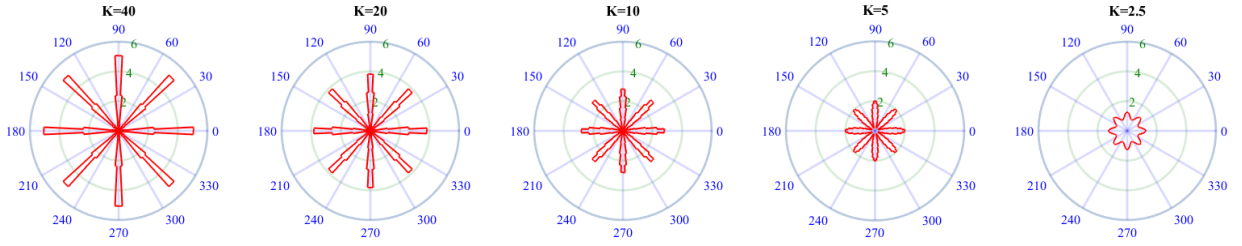


Figure 10. Comparison between the azimuthal velocity distribution profiles with different expansion factor K .

A combination of the effective momentum coefficient C , expansion coefficient K , azimuthal condensation zone length and location define intensity of the effective momentum and its impact on the erosion rate.

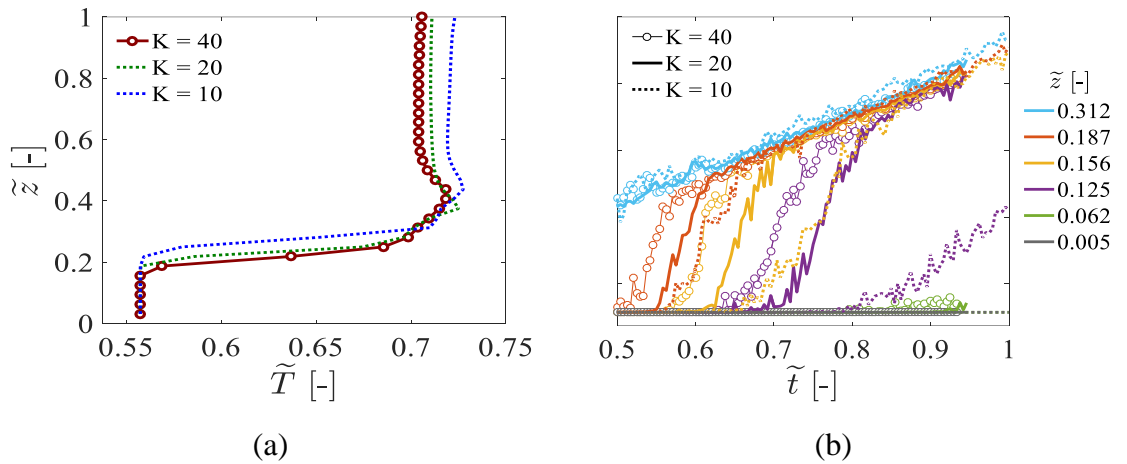


Figure 11. Effect of the expansion K on the temperature and the erosion of the pool obtained in the simulation of PANDA HP5-3. (a) Temperature profile during the low steam injection phase, $\tilde{t} = 0.42$ and (b) temperature evolution during the high steam injection phase [31].

The Effective Heat Source (EHS) is uniformly distributed in the same region as the effective momentum. The value of the EHS is calculated by

$$\dot{q}_s = \dot{m}_s h_s \quad (6)$$

where \dot{m}_s and h_s are the mass flow rate and enthalpy of the steam.

4.2.2. Calibration of the EHS/EMS models

PANDA HP5-3 experiment data was used to calibrate the model. The temperature evolution of HP5-3 and results of CFD modeling using old EHS/EMS models are presented in Figure 12. In the new implementation of the EMS model following parameters can be adjusted (i) the C coefficient defined by (4), (ii) the condensation zone size and position, and (iii) the expansion factor K for the azimuthal profile. The downward inclination and the VPV model are kept the same as in the old implementation model. The cases for the old model and new models are summarized in Table 2. The mesh for case 4 (C4) is refined in the region $40 - 90 \text{ mm}$ as shown in Figure 9(b) to enable the changes in the condensation region size and position.

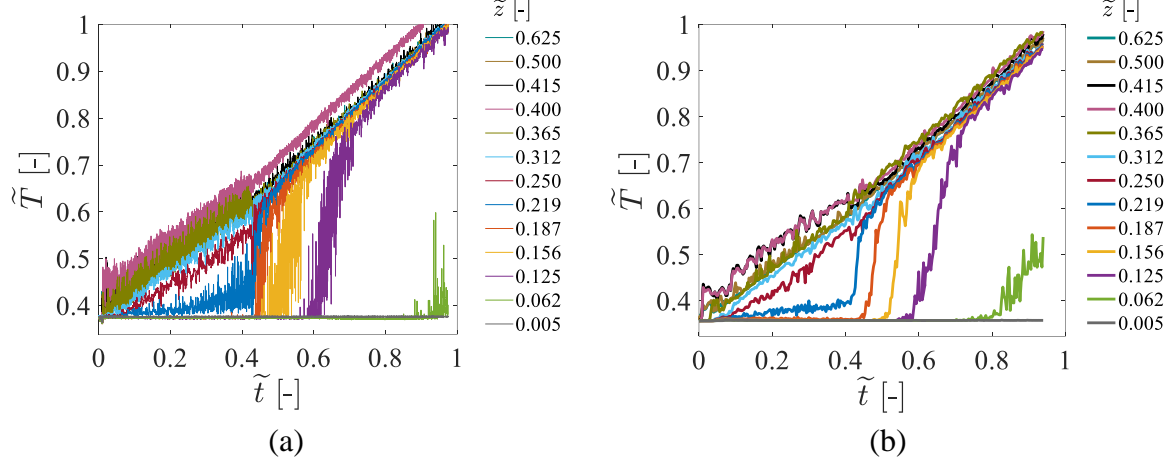


Figure 12. PANDA HP5-3 (a) experiment and (b) Fluent simulation using old EHS/EMS model with the C coefficient about $0.24 - 0.53$ (Figure 6). Temperature evolution along a vertical line of thermocouples (TCs line 1) in the pool [31].

Implementation of the EHS/EMS models in ANSYS Fluent was introduced by Gallego-Marcos et al. [31]. Calibration of the EHS/EMS models against PANDA HP5-3 test is presented in the following part. The normalized temperature evolutions along the vertical TCs line 1 for these four cases are shown in Figure 13 and Figure 14.

Table 2. Comparison between the old and calibrated EHS/EMS models

Case name	Condensation regime coefficient C [-]	APV model		VPV model	
		Condensation zone in radial [mm]	Distributed profile K [-]	Condensation zone in vertical [mm]	Distributed profile [-]
Old model	0.24-0.53	90-140	40		
C1	$C = 4.28\Delta T^{-0.35}$	90-140	20	1560-1610	Top hat
C2		90-140	3.5		
C3		40-140	3.5		
C4		40-80	40		

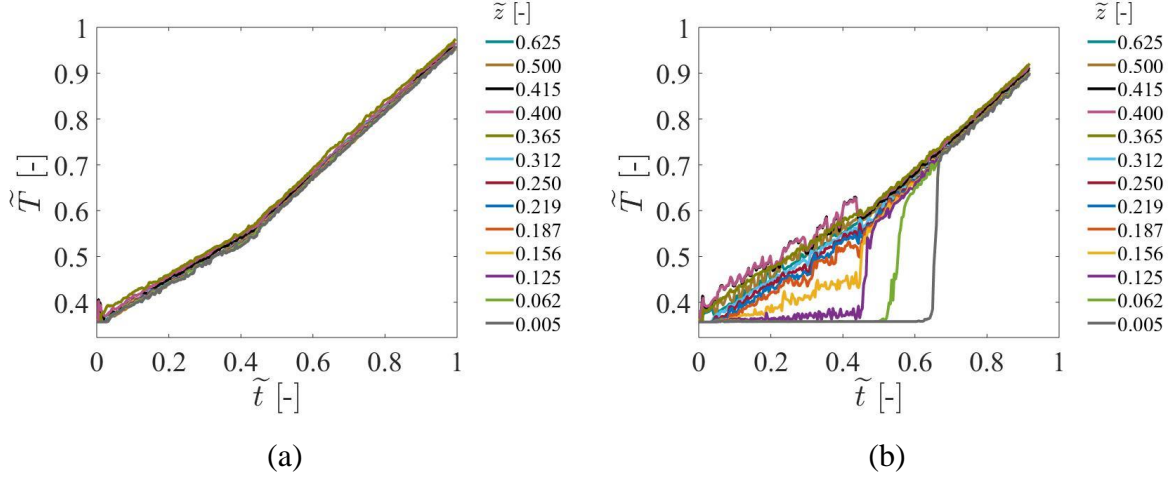


Figure 13. Pool temperature evolution (TC train 1). Fluent results of (a) C1 and (b) C2.

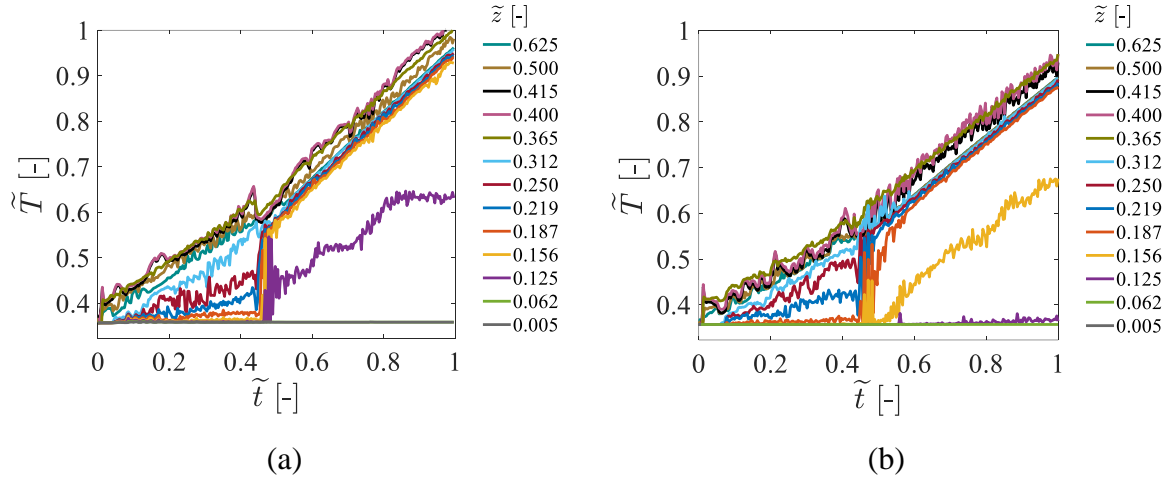


Figure 14. Pool temperature evolution (TC train 1). Fluent results for (a) C3 and (b) C4.

In C1 completely mixed pool was predicted in the simulations. This suggests that the decrease of K from 40 to 20 is not sufficient to compensate for the large increase in the magnitude of the momentum source (i.e. C coefficient). Further decrease of K from 20 to 3.5 (C2) provides a better agreement with the experimental data. However, erosion of thermocline in simulations is still faster compared to the measurements (Figure 12a). Temperature measured at the height of $\tilde{z} = 0.219$ is increased during the first injection phase faster than in the old model in Figure 12(b). The erosion velocity of the thermocline becomes even larger in the second injection phase. The extension of the condensation zone from 90 – 140 mm to 40 – 140 mm (C3) provides a better agreement with the experiment. However, the erosion velocity of the thermocline during the high steam injection phase is slower than in the experiment. The rate of temperature increase in the locations $\tilde{z} = 0.250$ and $\tilde{z} = 0.125$ are small compared to the experiment.

In C4, the azimuthal condensation zone starts at the sparger wall at $r = 40$ mm and the expansion factor K is 40. If condensation zone starts at the sparger wall, fluid can enter the condensation region only from top and bottom, resulting in an increased hydrodynamic resistance to acceleration of fluid in the condensation region. A good agreement is achieved between experimental data and simulations in C4 case for temperature evolution in the first injection phase was achieved. In addition, positioning of the condensation zone starting from

the sparger wall can help to reproduce the local circulation pattern which was observed in HP53 PIV measurements (Figure 15) but is not observed in the cases where condensation zone starts at $r = 90 \text{ mm}$ (Figure 16). However, the discrepancy between experiment and simulation data for the temperature evolutions in the high steam injection phase suggest that further calibration of the EHS/EMS models with respect to the APV model, namely dependency of the azimuthal profile on the steam injection conditions such as flow rate and water subcooling is needed.

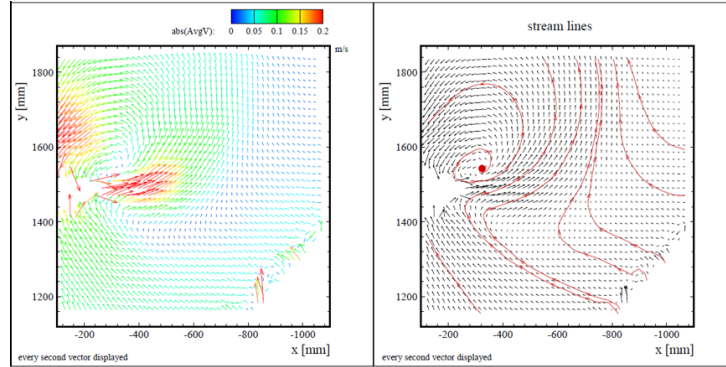


Figure 15. 2D PIV measurement of velocity at $t = 2900\text{s}$ [132]. The blank area at the sparger exit is due to the presence of the bubbles. The data is time-averaged over 200s.

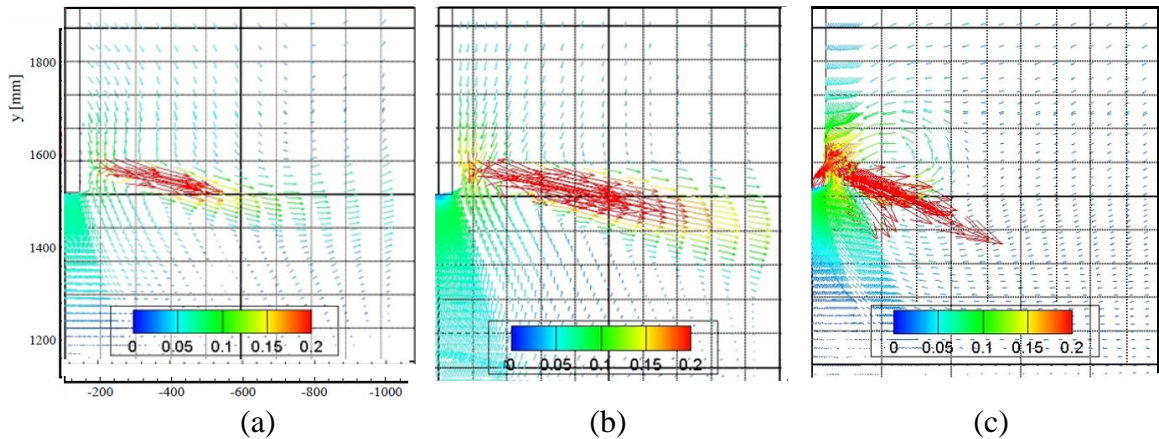


Figure 16. Velocity vectors obtained from CFD simulations of (a) old EHS/EMS models, (b) case 1, and (c) case 4 at $T = 2900\text{s}$.

In summary, after the uncertainty in C coefficient is reduced according to the SEF-POOL data (4), further calibration of the EHS/EMS model is needed in order to reproduce the pool behavior observed in the test. Results of calibrations show that the decreasing of expansion factor K and moving the location of the condensation region closer to the axis can help to reproduce a stratified layer at the low steam injection phase. The significant difference between experiment and simulation at high flow rate conditions suggest that the remaining calibratable parameters of the model are dependent on the steam injection regime.

4.3. Development of EHS/EMS models using SCR approach

Although a good agreement between experiment and simulations can be achieved using the source terms approach to implementation of the EHS/EMS, currently available test data is insufficient for a reliable calibration of the model parameters. Specifically, characteristics of spatial distribution of the momentum source. There are two approaches to solving this problem.

One approach is to measure the azimuthal velocity profiles in the future pool tests in different steam injection regimes, as discussed in section 5.1. Another approach is to resolve in the model interactions between the jets produced by individual steam injection holes. In this case the EHS/EMS model can be implemented using boundary conditions at the surface of the sparger, or at the interface of the Steam Condensation Region (SCR).

In this section we develop implementation of the EHS/EMS models using SCR approach. In this method, a velocity profile is imposed on the interface where jets from different injection holes are fully merged. The details of steam condensation inside the condensation region are neglected. The velocity can be derived based on a “Unit Cell” model where a group of individual jets is directly modelled.

4.3.1. Single-phase turbulent jets

Thermal stratification and mixing in a large pool are determined by a competition between buoyancy and momentum induced by the steam injection. The momentum created by injection through a multi-hole sparger [133] is introduced in a form of jets created by condensing steam. Characteristics of the velocity in the far-field (after condensation is finished) for such jets are similar to the single-phase turbulent jets [28, 72, 95, 133].

We consider a water jet injected through a nozzle into a large tank with stagnant water (Figure 17). The domain that contains the turbulent jet has a conical shape. Regardless of the type of fluid (water or air) and other conditions (such as nozzle diameter and discharge speed), the expansion angle is a constant [134] of 11.8° .

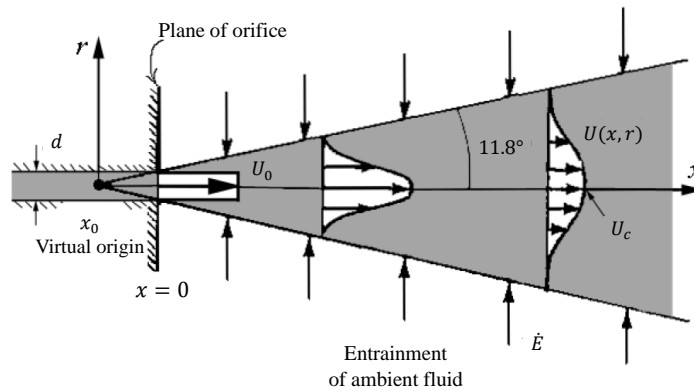


Figure 17. Schematic of a jet penetrating in a still fluid.

The mean centerline velocity $U_c(x)$ can be expressed by Eq. (7) [121]

$$\frac{U_c(x)}{U_0} = \frac{Bd}{(x - x_0)} \quad (7)$$

where U_0 is the mean exit velocity, B the decay rate, d the nozzle diameter and x_0 the so called virtual origin of the jet.

The fully developed axisymmetric velocity profile obeys a law of self-similarity as given by Eq. (5). By considering the effect of virtual origin, this profile can be presented as:

$$U(x, r) = U_c(x) e^{\left(-K \frac{r^2}{(x-x_0)^2}\right)} \quad (8)$$

To integrate the square of velocity over the cross-section of the jet with the fluid density, the momentum rate of the jet is:

$$\dot{M} = \int_0^\infty \rho U(x, r)^2 2\pi r dr = \frac{1}{4} \pi d^2 \rho U_0^2 \cdot \frac{2B^2}{K} \quad (9)$$

Since the decay rate and expansion ratio are constant for a given jet, the jet momentum is conserved at any downstream cross section of the jet and equal to its initial momentum $\pi d^2 \rho U_0^2 / 4$. Hence, we can deduce a rough relation between B and K given by Eq. (10), which shows that a jet with faster decay of the centerline velocity should also expand faster.

$$2B^2 \sim K \quad (10)$$

Investigation of velocity characteristics induced by air, water, and steam jets shows for the fully developed jets $2B^2/K = 0.88 \sim 1.05$ [133]. The mass flow rate \dot{Q} is not conserved because of the entrainment of ambient fluid. The jet mass flow rate can be calculated by integration (11).

$$\dot{Q} = \int_0^\infty 2\pi r \rho U(x, r) dr = \pi d \rho U_0 \frac{B}{K} \cdot (x - x_0) \quad (11)$$

The entrainment rate \dot{E} is defined as the rate at which the jet mass flow rate grows along the jet axis.

$$\dot{E} = \frac{d\dot{Q}}{dx} = \pi d \rho U_0 \frac{B}{K} \quad (12)$$

4.3.2. SCR model for a single jet induced by steam injection

Before studying a group of jets and their effect on the pool behavior, it is important to understand the behavior of a single jet induced by steam injection. As shown in Figure 18, SCR model for a single jet can be characterized by two regions: the Steam Condensation Region (SCR) and the Condensed Jet Region (CJR). SCR is a control volume in which the injection steam is expected to condense completely over a short distance. The DCC phenomena in this region are not resolved, only their effects on the mean flow are taken into account by solving simplified conservation equations of mass, momentum, and energy. Downstream of SCR, the condensed jet region is a domain where single-phase turbulent jet develops. In SCR, the conservation of mass is described by:

$$\dot{m}_c = \dot{m}_s + \dot{m}_e \quad (13)$$

where \dot{m}_c is the mass flow rate of condensing jet, \dot{m}_s and \dot{m}_e are the mass flow rate of injected steam and entrained water, respectively.

The conservation of energy and momentum is achieved by the EHS/EMS models which provide the time-averaged momentum and heat transferred from the injection steam to the pool water. The equations can be found in Eqs. (3), (4) and (6). Since the velocity characteristics of the condensed jet are similar to the single-phase turbulent jet [96]. It is reasonable to describe the condensed jet velocity profile using equations (7) and (12).

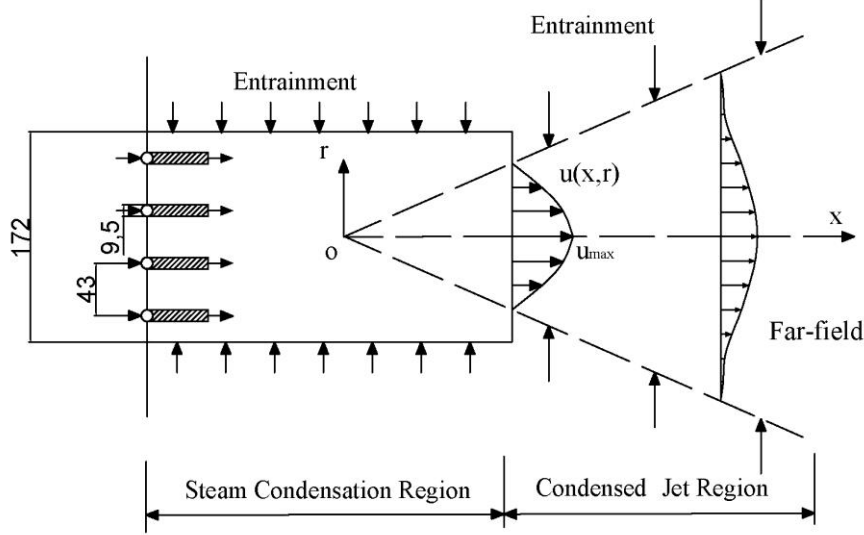


Figure 18. Schematic of SCR model for single condensing jet.

The dimensions of SCR are determined by two parameters, namely the steam penetration length L and expansion width δ . The penetration length is a function of the steam flux, pool subcooling, and sparger geometry. Experimental works [96] showed that for Mach number $Ma > 1$ a stable sonic jets condenses within 2 to 11 sparger hole diameters. Since the PPOOLEX and PANDA pool tests are focused on the unstable bubble regime where $Ma < 0.8$, its penetration length would be smaller than in the case of a sonic jet. We can define the radius δ which contains 98% of the jet momentum in a given cross section

$$\begin{aligned} \dot{M} &= \int_0^\delta \rho U(x,r)^2 2\pi r dr = \int_0^\delta \rho U_c(x) e^{\left(-K \frac{r^2}{(x-x_0)^2}\right)^2} 2\pi r dr = 98\% M_{initial} \\ &= 0.98 \cdot \frac{1}{4} \pi d^2 \rho U_0^2 \cdot \frac{2B^2}{K} \end{aligned} \quad (14)$$

$$\delta = 2(x - x_0)/B \quad (15)$$

The radius δ can be used to set boundary conditions for the velocity at the SCR exit surface.

4.3.3. Comparison of analytical and CFD results for single jet flow

In this section we discuss comparison of predictions for a single jet by the analytical model and CFD code Fluent. In the SEF tests [98] only the effective momentum induced by steam injection was measured. Other experimental data [58, 72, 95, 96] for condensed steam jets are available in sonic and super-sonic injection regimes. The velocity profile data for a single jet induced by steam condensation in the oscillatory bubble regime is not available. Therefore, a

typical single-phase turbulent round jet [134] is used in this validation. Its main parameters are summarized in Table 3.

Table 3. Parameters of a typical turbulent round jet

	Re	B	K	x_0	d	U_0
	[-]	[-]	[-]	[mm]	[mm]	[m/s]
Theory	95500	5	40	-25	10	9.6

The dimensions of SCR and the velocity profile at the SCR exit surface are important parameters for prediction of the pool behavior. An approach to estimation of the entrainment rate in the SEF tests is under development now and will enable estimation of the decay rate B and expansion factor K as described in (12).

In this simulations the jet is injected with a uniform velocity of $U_0 = 9.6 \text{ m/s}$ within a circular region with diameter $d = 10 \text{ mm}$. The $k - \omega$ BSL model is used to resolve the turbulence characteristics. More details of the turbulence model can be found in section 4.4.4. Only the boundary conditions for the turbulence characteristics, namely, turbulent intensity and turbulent viscosity ratio, are the uncertain parameters. These two parameters are adjusted in order to fit the far-field velocity profiles according to (7) and (8). As a result the turbulence intensity of 50% and the turbulent viscosity ratio of 3000 were selected in the analysis.

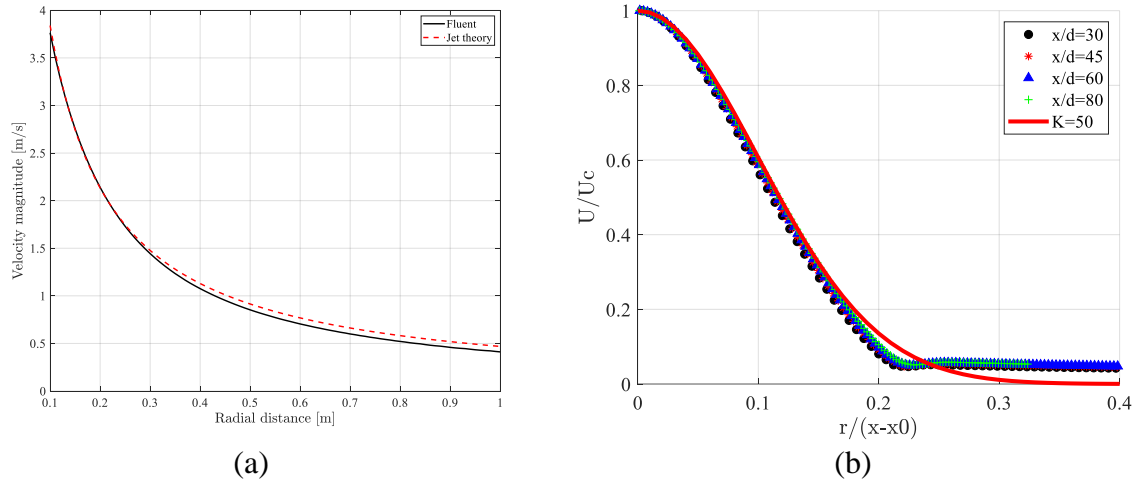


Figure 19. Comparison between Fluent and jet theory of (a) centerline velocity versus distance along the radial direction and (b) mean axial velocity versus radial distance at different slices.

A comparison of the centerline velocity profile between the Fluent and the analytical model is presented in Figure 19(a). Self-similarity of the axial velocity profile is clearly seen in different sections of the jet showing a nearly Gaussian shape (Figure 19b). The velocity is scaled by the cross-section centerline velocity and the axial distance by the distance between the jet virtual origin and the coordinate of the cross section $x - x_0$. Theoretical profile by Eq. (8) with $K=50$ is plotted for comparison. Good agreement between analytical and CFD predictions for the velocity profile suggests that a single condensed jet model can be implemented in Fluent and can reproduce a round jet by appropriate selection of the turbulent characteristics, namely, the turbulence intensity and turbulent viscosity ratio. Although the simulation was carried out for

a single-phase liquid jet, the SCR approach should be applicable to simulating a jet induced by condensed steam due to the similarity of the jet characteristics in the far-field.

The momentum and entrainment integrated over different cross sections of the jet are presented in Table 4. Theoretical values are calculated by (9), (11), and (12). The momentum and entrainment rates are slowly decreasing along the jet axis, probably due to the energy dissipation or the effect of the walls in the finite computational domain. In general, we can conclude that described SCR model can be used for a single condensed jet.

Table 4. Momentum and entrainment at different slices

Distance [m]	Theory	Inlet	0.05	0.3	0.45	0.6	0.8
Momentum rate [N]	7.22	7.20	7.34	6.76	6.60	6.40	6.38
Entrainment rate [kg/ms]	30.07	29.30	30.01	25.38	24.83	24.27	24.10

4.3.4. SCR model for multiple condensed jets

Compared to single hole steam injection, a multi-hole sparger introduces phenomena of interactions between the jet. The interactions can be directly modelled, e.g. using SCR approach for each jet created by condensed steam from each sparger hole [135]. However resolving flow for each individual jet would require significant computational resources even for PANDA test as there are 32 holes in the PANDA sparger (Figure 20). In plant applications, the number of spargers and holes in each sparger pipe are too large making such analysis practically unfeasible. Instead we develop a model that can be used to simulate a group of condensed steam jets using approaches similar to the SCR model for a single jet.

As shown in Figure 21 two regions are introduced: the steam condensation region which includes a group of jets, and the condensed jet region. Jets injected from adjacent nozzles into undisturbed surroundings tend to merge into a single jet at a certain downstream distance. The length of SCR is no longer the steam penetration length but the downstream distance where the parallel jets are fully merged. The distance can be estimated as 3 times the pitch plus diameter [36] which agrees well with the temperature and velocity measurements in PANDA tests. For instance, Figure 7(b) shows completely merged jets in PANDA HP5-2 test with the steam flux of $71 \text{ kg/m}^2\text{s}$ and pool subcooling of 55°C . The blank area around the sparger is caused by unreliable PIV data in the region with high concentration of small gas bubbles produced in the steam condensation region. This effect was especially severe at high steam flux conditions.

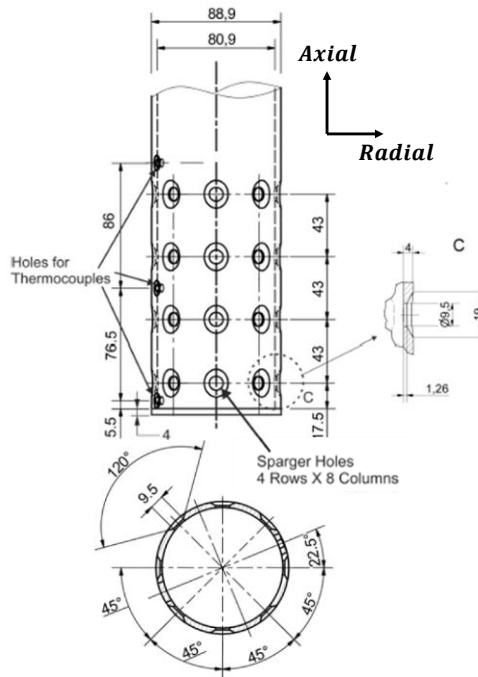


Figure 20. Geometry of multi-hole sparger head in PANDA HP5 tests [36] with a pitch to hole diameter ratio of $p/d = 4.53$.

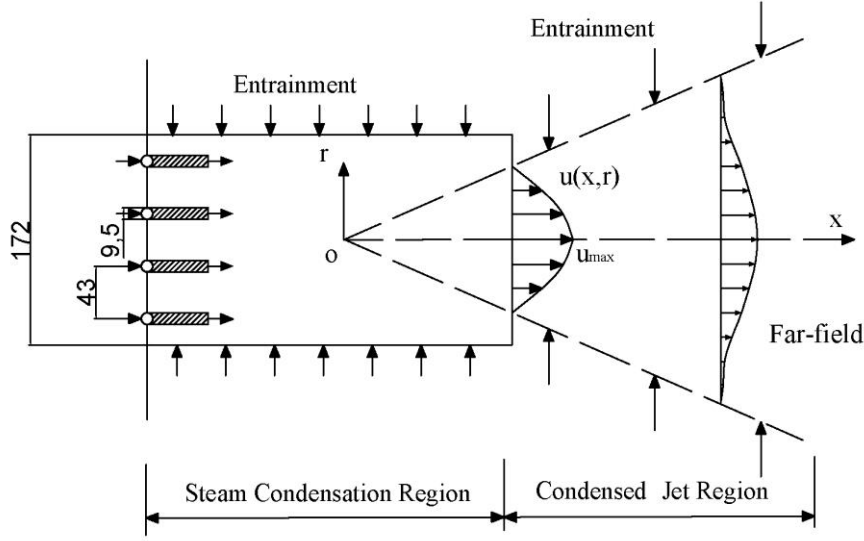


Figure 21. Schematic of SCR model for multiple jets induced by injection of condensing steam.

Self-similar behavior of the far-field velocity profile in vertical cross section was also observed for the merged jets induced by steam injection through several neighboring holes in PANDA tests. However, azimuthal profile of velocity was not measured by PIV and is expected to be non-uniform according to the results of EHS/EMS models calibration in section 4.2. The merged jet resembles a rectangular jet with little widening of the jet in the vertical direction and more intensive expansion in the horizontal (azimuthal) direction. The velocity profile for the merged condensed jet can be described by (16) in analogy with the profile of the single turbulent jet given by Eq. (8).

$$U(x, y, z) = U_c(x) \cdot e^{-\frac{K_A y^2 + K_V z^2}{(x-x_0)^2}} \quad (16)$$

where the asymmetry of velocity profile is described by the expansion ratio of K_A and K_V in azimuthal (or horizontal) and vertical directions respectively.

4.4. Implementation of SCR for spargers in Fluent

SCR approach for multi-hole spargers (multiple jets) can be implemented in any CFD code. ANSYS Fluent 19.3 is used as an example in this work. In this section we describe numerical approaches to prediction of the pool behavior in PANDA HP5 test series.

4.4.1. Computational domain

The computational domain for simulation of the jet induced by steam injection through a multi-hole sparger is presented in Figure 22. Several sectors (22.5° , 180° and 360°) were used in the simulation. Data from HP51 was used to validate the models. The height of the water level and sparger head are 4 m and 1.51 m above the bottom of the pool. The effect of grid refinement on the solution was carried out in order to reduce sensitivity of the results to grid resolution [31]. For a full domain (360°) 128 cells in the azimuthal direction were used and the size of cells in the vertical direction above/below sparger are about $50/25\text{ mm}$ respectively.

Steam condensation region has three boundaries, namely entrainment top, entrainment bottom, and inlet. SCR length $L = 0.2 \text{ m}$ was selected to make sure that it is longer than the distance where jets can completely merge, which is equal to $3 \times (43 + 9.5) = 157.5 \text{ mm}$. According to the velocity profile at the distance L (Figure 23b), the height of 0.08 m for the condensation zone was selected. According to PIV measurements [135] the elevation of the central horizontal plane of the SCR is $H \approx 1.475 \text{ m}$, which is a bit lower than the geometric location of the central plane according to the simulations ($H \approx 1.55 \text{ m}$, Figure 23a). The discrepancy might be attributed to the single-phase modeling approach in the unit model simulations where the DCC phenomena within the condensation core region are not resolved. An increase of the injection inclination angle produced a little effect. To be consistent with the sparger geometry, $H \approx 1.55 \text{ m}$ was used in the analysis.

Energy equation and dynamic mesh with laying method are turned on. PISO algorithm and Quick spatial discretization scheme in momentum, turbulent kinetic energy (k), specific dissipation rate (ω), and energy were used. The simulation is considered fully converged when the residual was below $1e - 6$ for energy and $1e - 3$ for other variables.

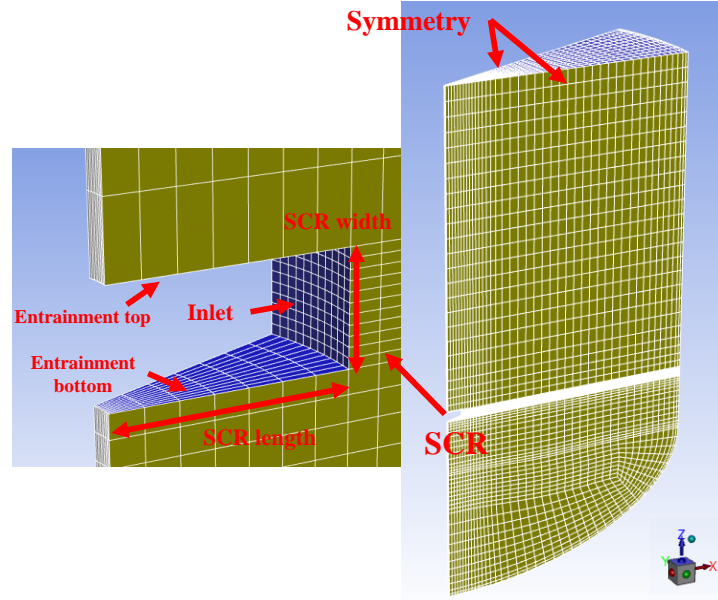


Figure 22. Hexagonal meshing grid of SCR model for multiple condensing jets.

4.4.2. Lumped velocity profile

One of the most important steps in the SCR model for multiple condensed jets is to reproduce the lumped velocity profile (shown in Eq. (16)) by fitting the results from the Unit model. The Unit model [135] has a 22.5° sector domain with 4 injection holes (Figure 20, Figure 21). In each hole, a uniform effective velocity profile was imposed according to the EMS model and equations (3), (4), (17), and (18).

$$\dot{M}_{eff} = C\dot{M}_{th} = C\rho_s A_0 U_s^2 = \rho_l A_{eff} U_{eff}^2 \quad (17)$$

where ρ_l is the density of the liquid, A_{eff} is the effective area equal to the area of the injection hole, thus:

$$U_{eff} = \sqrt{\frac{C\rho_s}{\rho_l}} U_s \quad (18)$$

Validation of the model against PANDA HP53 test with respect to the pool temperature evolution suggests that this Unit model can provide a good prediction in the low steam flux phase. However, a faster mixing was observed in the high flux phase [135]. In order to address this issue, an adjustment of the initial turbulent characteristics was done to make the jet more diffused. However, this approach resulted in numerical oscillation of the solution. The oscillations might be caused by the enforced symmetry boundary of the 22.5° domain. Therefore larger domains ($1/2$ and a full size) were considered. The SCR model for the merged jets was used for larger size of the domain.

The velocity profile predicted by the Unit model in a vertical cross section are shown in Figure 23. The cross section is located at $x = 0.2 \text{ m}$ from the sparger axis (Figure 23a). Apparently the jets have merge completely prior to the selected cross section. Predicted 15° downward inclination angle for the merged jet agrees well with the PIV measurement shown in Figure 7(b) and the gas-to-gas injection case in [36].

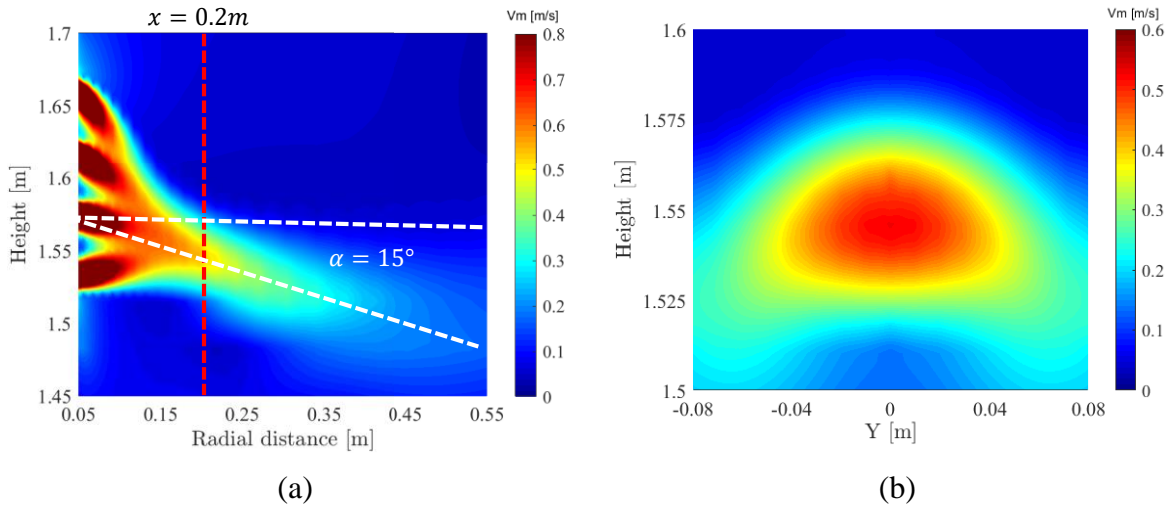


Figure 23. Velocity contours obtained in HP53 simulations by Unit model at $\tilde{t} = 0.13$ in (a) vertical direction and (b) azimuthal direction.

The inclination of the jet is taken into account in the fitting process for calibration of the parameters in (16). A transformation from the Cartesian coordinate systems where x axis is parallel to the jet is applied (Figure 24(a)) by rotating around y axis counterclockwise by α degree. The relationships between these two systems is given by (19). By substituting (19) into (16), we can obtain the jet velocity profile in the $x'y'z'$ system (20).

$$\begin{aligned} x &= x' \cos \alpha - z' \sin \alpha \\ y &= y' \\ z &= z' \cos \alpha + x' \sin \alpha \end{aligned} \quad (19)$$

$$U(x', y', z') = U_c(x') \cdot e^{-\frac{K_A y'^2 + K_V (z' \cos \alpha + x' \sin \alpha)^2}{(x' \cos \alpha - z' \sin \alpha - x_0')^2}} \quad (20)$$

The maximum velocity $U_c(0.2)$ over the slice at $x = 0.2m$ served as centerline velocity is equal to $0.53 m/s$ at $\tilde{t} = 0.13$ and the rotation degree is about $\alpha = 15^\circ$. The rest of the parameters are fitted through Matlab cftool, giving $K_A = 9.3$, $K_V = 50.5$ and $x'_0 = -0.043 m$. A similar value for the vertical jet expansion coefficient $K_V = 40$ was obtained in previous work [36] using fitting to PIV measurement. The velocity contours provided by the fitting equation is presented in Figure 24.

To apply this velocity profile in a transient simulation, the decay ratio D defined by the centerline velocity over the effective velocity of a single condensing jet (U_{eff} , see Eq. (18)) is used to provide the estimation of the centerline velocity $U_c(x, t)$ at a specific distance from the sparger axis. This ratio is obtained by extracting both velocities from the Unit model results at $\tilde{t} = 0.13$, $\tilde{t} = 0.20$, $\tilde{t} = 0.29$ and $\tilde{t} = 0.46$, resulting in a range of $0.172 \sim 0.188$. The averaged value $D = 0.18$ is selected in the following simulations. The merged jet velocity profile can be described as:

$$U(x, y, z) = 0.18 \cdot U_{eff} \cdot e^{-\frac{9.3 \cdot y^2 + 50.5 \cdot z^2}{(0.2 + 0.043)^2}} \quad (21)$$

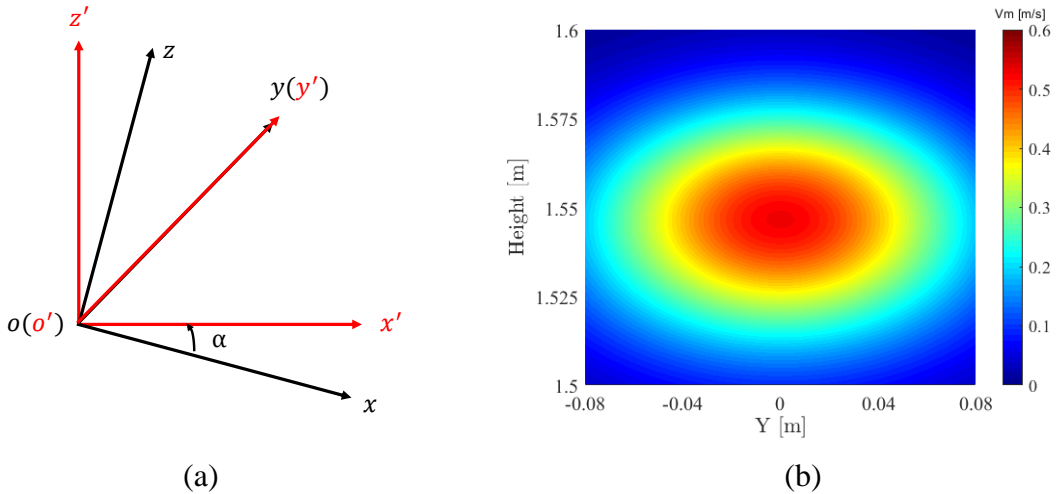


Figure 24. (a) A transformation of then Cartesian coordinate system by rotation around y by angle α to an $x'y'z'$ system, and (b) velocity contours obtained by fitting obtained profiles at $\tilde{t} = 0.13$ with $\alpha = 15^\circ$.

4.4.3. Boundary conditions

In the SCR approach the momentum induced by steam injection is modelled by water injection. Resulting mass flow rate of water can be many times larger than the steam flow rate. In order to preserve the mass balance, some part of the injected water should be taken out of the computational domain. We can remove the water through the surfaces named “entrainment top & bottom” (see Figure 22) with a total mass flow rate given by Eq. (22). In order to respect the heat balance, the EHS model was used with the time-averaged heat source estimated by Eq. (6). In the simulation, when mass is taken out from the entrainment surface, the energy will be removed as well. To compensate the loss of removed heat, the enthalpy of the injection water h_l^{in} should be defined by Eqs. (23), (24). The h_l^{in} is implemented by setting the inlet boundary conditions for the temperature according to Eq. (25).

$$\dot{m}_{out} = 0.5 \cdot (\dot{m}_{in} - \dot{m}_s) \quad (22)$$

$$\dot{q}_{in} = \dot{q}_s + \dot{q}_{out} \quad (23)$$

$$h_l^{in} \cdot \dot{m}_{in} = h_s \cdot \dot{m}_s + h_l^{out} \cdot \dot{m}_{out} \quad (24)$$

$$T^{in} = \frac{h_s \cdot \dot{m}_s + C_p(T^{out} - 273.15) \cdot (\dot{m}_{in} - \dot{m}_s)}{C_p \dot{m}_{in}} + 273.15 \quad (25)$$

where \dot{m}_{in} is the mass flow rate of inlet liquid, calculated by the user defined function (UDF), sub-indexes l and s are indicating liquid and steam respectively, in and out are indicating the input and output, C_p and T are the specific heat capacity and water temperature, respectively.

4.4.4. Turbulence model

Stable stratification with significant temperature difference between the cold and hot layer was observed in all PPOOLEX and PANDA experiments. The development of the stratified layer is governed by the buoyancy, which is modelled by the temperature-dependent water density. In order to model the effect of buoyancy on turbulence source terms for turbulent kinetic energy k and specific dissipation rate ω are modified respectively. Details of the turbulence model implementation can be found in [31].

The turbulence model is $k - \omega$ BSL model with low-Re corrections which provided the best agreement between prediction and experimental temperature evolution in PANDA & PPOOLEX pool tests [31, 135]. Kato-Launder production term and production limiter are turned on to limit the build-up of k in the stagnation regions (i.e. the cold layer below the thermocline).

The flow pattern in the pool is sensitive to the boundary conditions for characteristics of turbulence [135]. Turbulence intensity and turbulent viscosity ratio are used to estimate calculate the boundary conditions for the turbulent kinetic energy and dissipation rate. Turbulence intensity in a water jet induced by steam condensation was estimated in [59] to be around 25 – 35% at 0.25 m downstream from the injection orifice. These values have been further confirmed in [95, 96]. With $I = 30\%$, the turbulent viscosity ratio can be estimated as $\mu_t/\mu_l = 1000$ [27]. These two values should be considered as a rough estimate. Significantly larger values were obtained in PIV data from previous PANDA tests. Further investigations of the new PIV data in the PANDA tests should be carried out to clarify.

4.5. Validation against HP5 tests

Validation of the model described in the previous sections is carried out against PANDA HP51 test data on temperature evolutions and PIV measurements. The HP5 tests were done at atmospheric conditions in PANDA facility and discussed in more detail in section 4.1. The temperature evolutions obtained in HP51 TCs and Fluent simulations of 360°, 180°, and 22.5° domains are shown in Figure 25 and Figure 26. The measurements at TCs line 1 are chosen for comparison. Note that these measurements are representative for the whole pool temperature due to the uniformity of the temperature profile in the horizontal (radial) direction in the pool [36], (Figure 4).

There are noticeable differences between the three simulation cases with respect to the temperature evolution. Location of the thermocline during the first injection phase is predicted at the height between $\tilde{z} = 0.250$ and $\tilde{z} = 0.219$ for the 22.5° domain and between $\tilde{z} = 0.219$ and $\tilde{z} = 0.187$ for the 180° and 360° domains, which agrees well with the TCs measurements of HP51 test. Pool temperature oscillation were observed in all PANDA experiments and are also visible in the simulations with 180° and 360° domains. A similar behavior was reported by Gallego-Marcos et al. [31] where such instabilities were reproduced in a full 3D domain and not in a 45° sector. A faster erosion of thermocline and flow instability during the transient from low to high steam injection phases were observed in the simulations with the slice domains of 22.5° [135] and 45° [31], respectively.

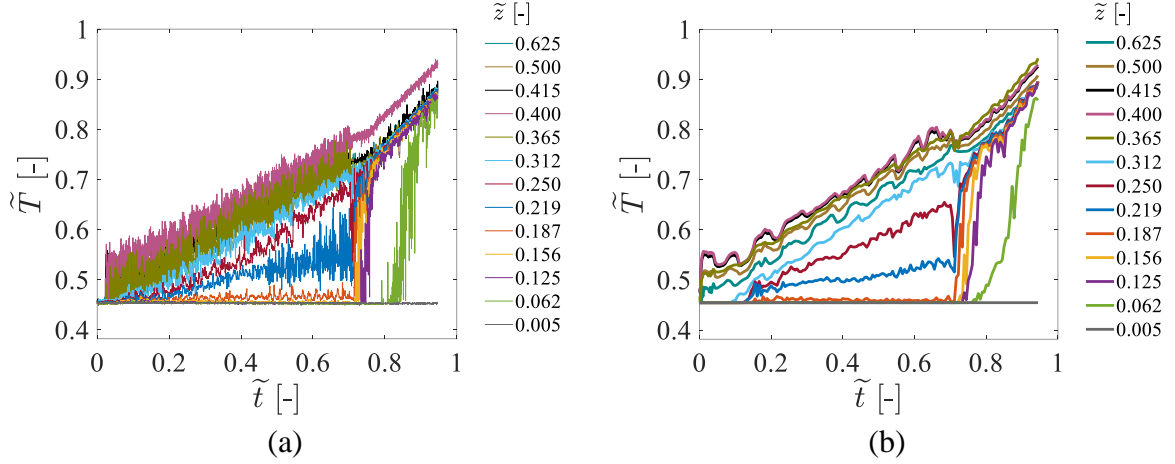


Figure 25. PANDA HP51 (a) experiment and (b) Fluent simulation using SCR approach in a 360° domain.

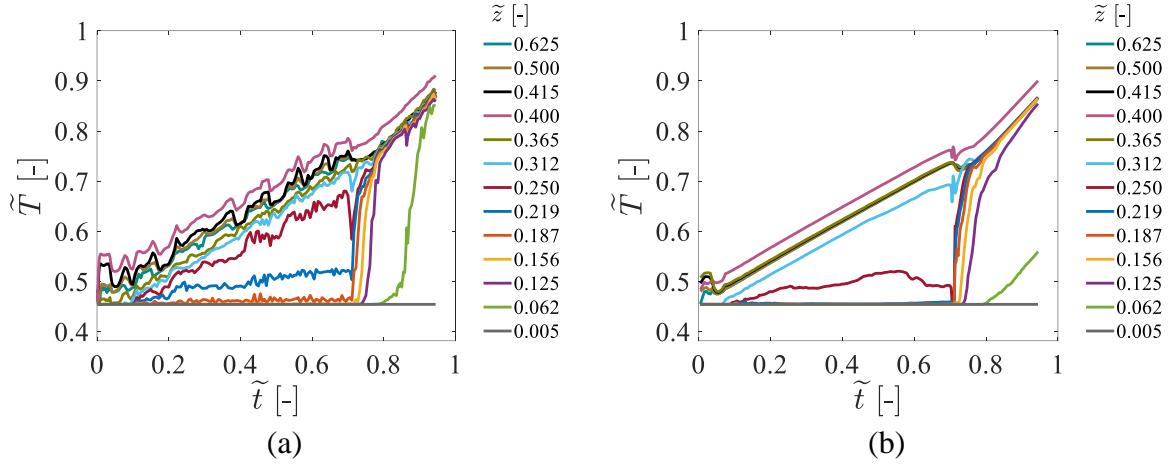


Figure 26. PANDA HP51. Fluent simulation using SCR approach in an (a) 180° domain and (b) 22.5° domain. Data are normalized with $T = 55^\circ\text{C}$, $t = 9200\text{ s}$, $z = 4\text{ m}$.

These observations indicate that modelling of stratification and mixing induced by steam injection through spargers in the PANDA pool requires sufficiently large 3D domain (at least 180°). The artificial instabilities can be attributed to the lower degrees of freedom of reduced size 3D and 2D simulation, which prevents large scale vortices from accommodation of changes in the flow pattern. Another advantage of using the 3D model is that the effect of Interconnecting Pipe (IP) can be resolved directly. This component slightly intrudes inside the cylindrical shape of the vessel, which can serve as factor for symmetry-breaking and increased unsteadiness of the flow [31]. Therefore, a 3D domain with at least 180° was used in the following simulations.

HP52 and HP53 tests (Table 1) were analyzed with the same numerical setup used for simulation of HP51. Comparison of the temperature evolutions obtained in the simulations and experiments are presented in Figure 27 and Figure 28. Proposed modelling approach provides an adequate prediction of the pool behavior in different steam injection conditions. The motion of thermocline is well captured at low steam injection conditions. The large temperature gradient across the thermocline is also resolved in the high injection phase.

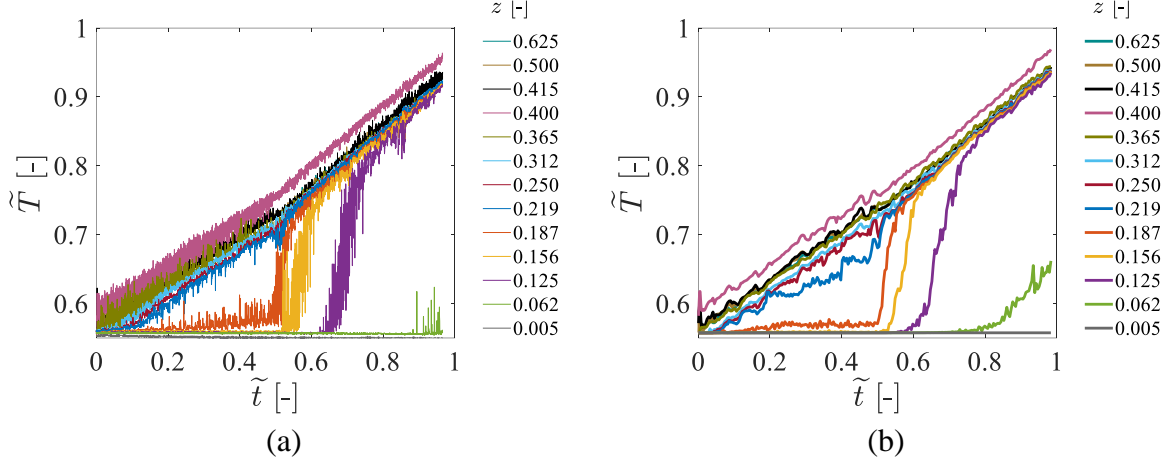


Figure 27. PANDA HP52 (a) experiment and (b) Fluent simulation using SCR approach in a 180° domain.

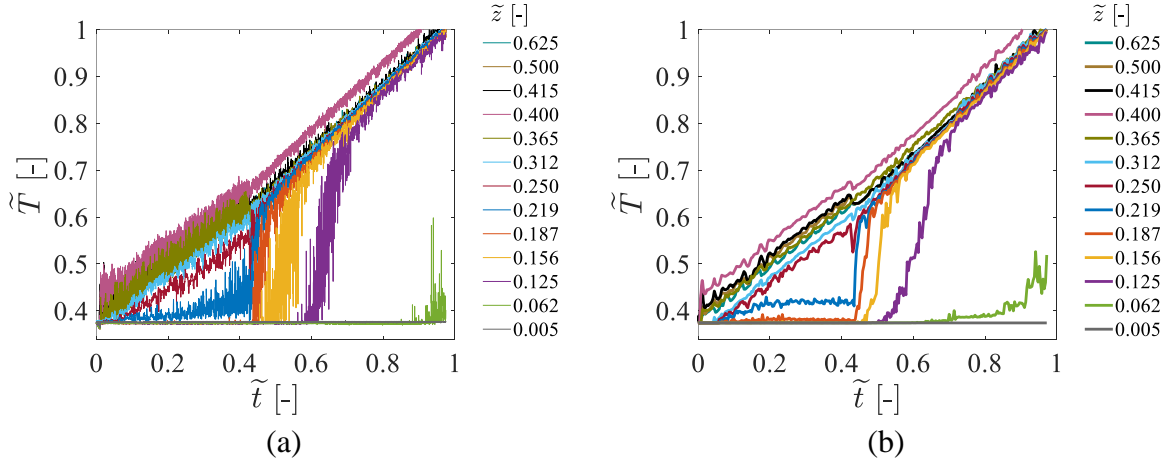


Figure 28. PANDA HP53 (a) experiment and (b) Fluent simulation using SCR approach in a 180° domain.

Figure 29 and Figure 30 provide a comparison of experimental (PIV) and simulation data for the velocity fields in vertical cross sections. PIV measurements were unreliable in some parts of the domain (dark blue areas) due to presence of a large number of gas bubbles. Despite the incompleteness of the PIV field of view, a reasonable agreement of simulation with the experiment on the buoyancy/inertia-driven jets in all phases of steam injection can be observed. Merging of the jets at radial distance of ~ 0.2 m was observed in PIV. This confirms that selected length of SCR is reasonable. The velocity magnitude agrees well with the experiment, indicating that the merged jet velocity profile and selected boundary conditions for turbulence characteristics provide an adequate estimation. Further improvement of the simulations can be achieved by calibration of the boundary conditions for turbulence characteristics, which has considerable effect on the flow patterns (Figure 46).

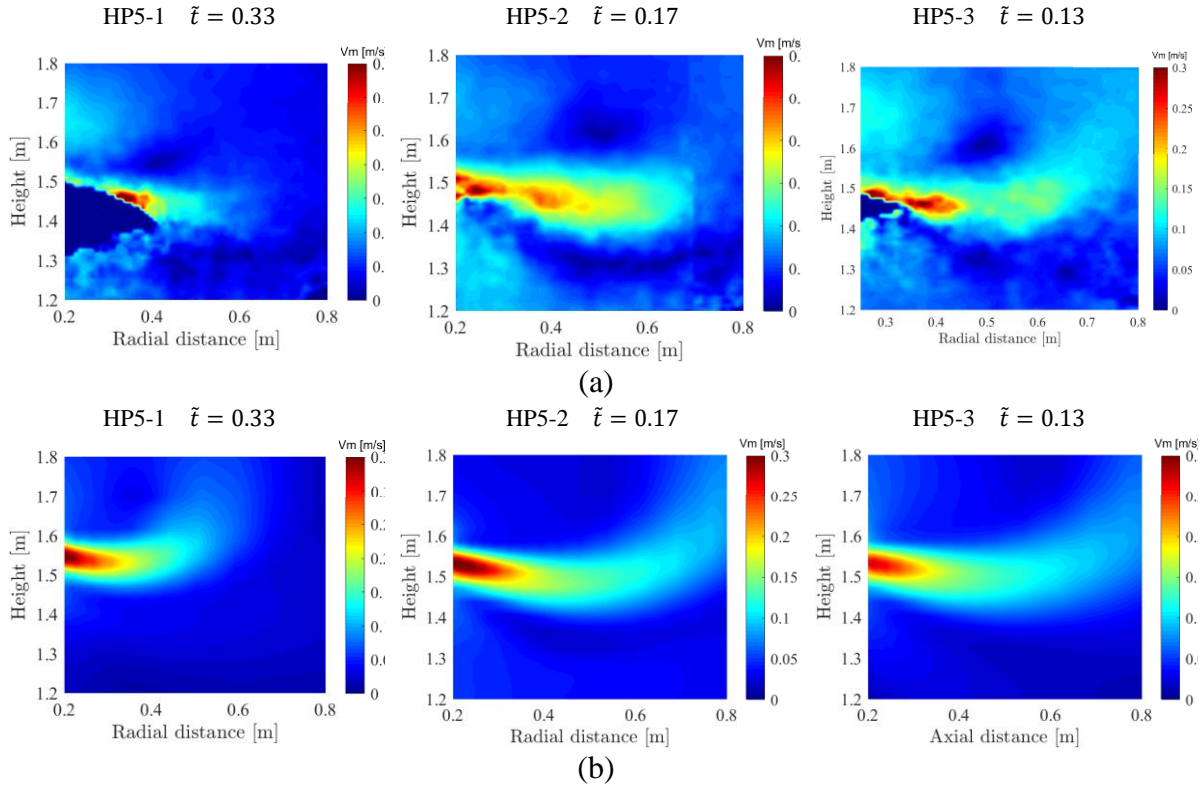


Figure 29. Velocity contours during the low steam injection phases obtained in (a) PIV data from PANDA HP5 tests and (b) Fluent simulations. Data have been time-averaged over 200s.

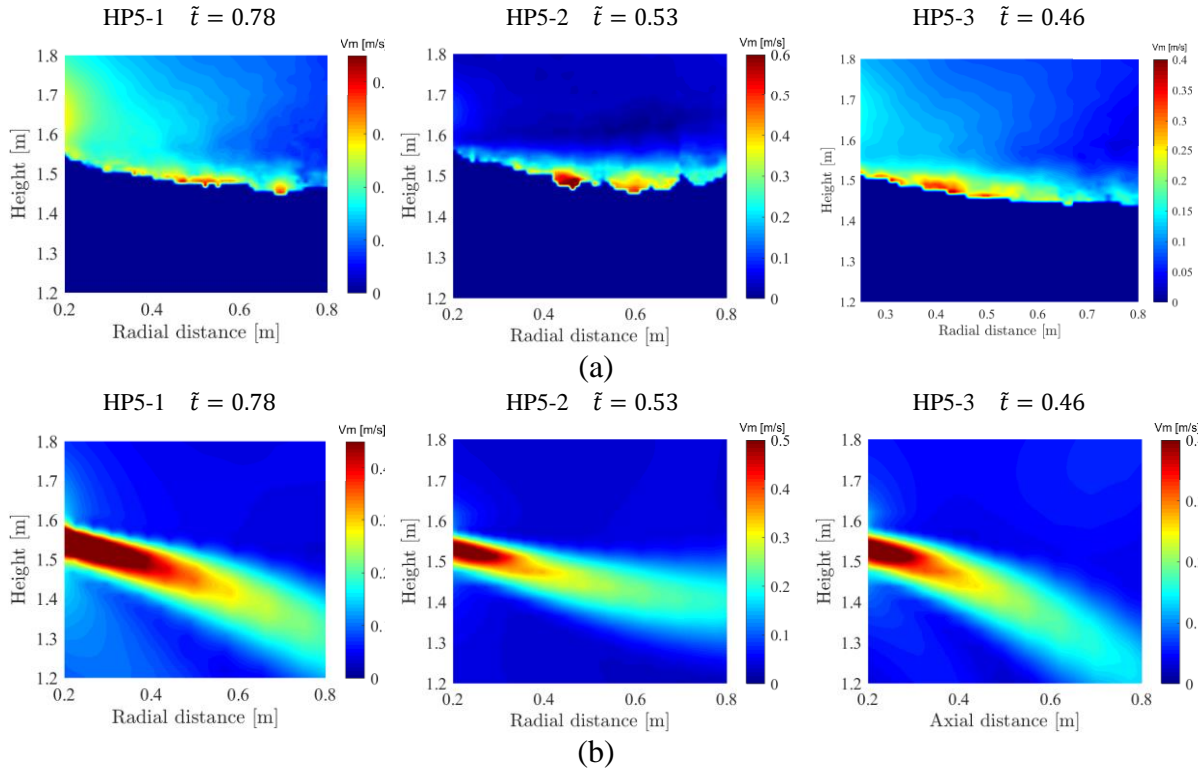


Figure 30. Velocity contours during the high steam injection phases obtained in (a) PIV data from PANDA HP5 tests and (b) Fluent simulations. Data have been time-averaged over 200s.

4.6. Summary of EHS/EMS model development for sparger

In this section we present results of EHS/EMS models development for prediction of the pool behavior induced by the steam injection through a multihole sparger.

First, we discuss calibration of the EHS/EMS models implemented using a source term approach. The results suggest that the temperature evolutions are sensitive to the geometrical characteristics of the domains where EHS/EMS source terms are introduced. Although a good agreement can be achieved between simulations and experiments, a robust calibration process of the model is needed.

Second, we discuss implementation of the EHS/EMS models using steam condensation region (SCR) approach. Main findings and features of the modelling approach are listed below:

- Prototypic pool behavior has large spatial and temporal scales. Single-phase solver is used in order to achieve necessity computational efficiency in resolving the effects of steam condensation in a CFD code.
- Effective momentum is introduced by through boundary conditions and injection of liquid. The temperature of the injected liquid is defined in order to conserve the energy. In order to conserve mass excessive amount of liquid is removed from the domain through the top and bottom surfaces of the SCR.
- A 3D calculation domain with at least 180° is required to obtain a reasonable agreement between simulations and experiment on the temperature evolution and to avoid a large scale flow instability during transition from small to large steam flow rate.
- The velocity profile for the merged jets induced by steam condensation is derived by analytical fitting of the results obtained from the “Unit cell” model. In this model, all individual jets and interactions between the jets are explicitly modelled.

Validation against PANDA HP5 test series suggest that this model can provide a reasonably accurate prediction of the pool behaviour. Compared to the previous modeling approach where the EHS/EMS models were implemented using source terms, SCR approach avoids uncertainty in the distribution of the momentum source, which can significantly affect temperature evolution in the pool.

5. PRE-TEST SIMULATIONS FOR PANDA H2P3 TESTS

The OECD/NEA HYMERES-2 project aims to carry out 24 tests in PANDA facility. The tests are grouped in 6 series each addressing a set of safety-relevant containment phenomena. PANDA H2P3 pool test series is intended to study phenomena of thermal stratification development and mixing in a large water pool induced by steam injection through multi-hole spargers and Load Reduction Ring (LRR).

In order to maximize the usefulness of the experimental data for the development and validation of the containment thermal hydraulics codes and EHS/EMS models, we provide pre-test simulations and analytical support for the test design, initial and boundary conditions for the H2P3 tests. Here we present results of the pre-test analysis for H2P3 sparger tests (H2P3-1,2,3) where the steam is injected into the pool only through sparger and for H2P3 LRR tests (H2P3-4,5,6) where only LRR holes are opened for steam injection.

5.1. Pre-test simulations for H2P3 spargers tests

The H2P3 tests will be carried out using the same vessel and sparger as in the HP5 series (see section 4.1). The aim of the tests with steam injection through sparger head is to address (i) the effect of the distance between sparger head and thermocline on the rate of thermocline erosion; (ii) the azimuthal velocity profile and its dependence on the steam injection conditions. The pre-test simulations were carried out to support the selection of: (i) the sparger elevation above the bottom of the pool, pool depth and arrangement of TCs; (ii) the test procedure for steam injection and (iii) PIV setup for velocity measurements.

Implementation of EHS/EMS models using the source terms approach (Figure 12) was used for the analysis of the effect of the distance between sparger head and thermocline. “Unit cell” model was used to study the velocity profile of the multiple interacting condensed steam jets [135] to support the selection of PIV setup.

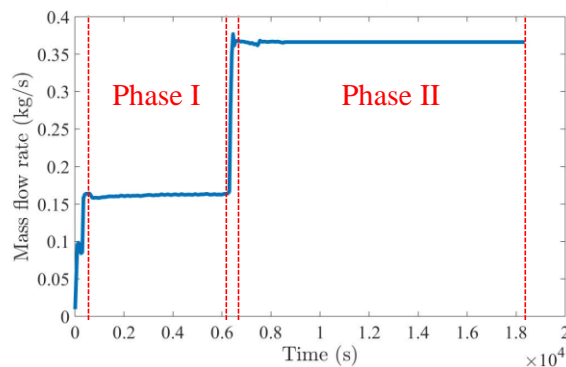


Figure 31. Steam mass flow rate in the simulations of H2P3-2.5 and H2P3-3.3.

5.1.1. Pool configuration

The elevation of the sparger head should be sufficient to study the effect of the distance between the thermocline and sparger head on the erosion velocity of the stratified layer. Two options were considered with sparger elevation of 2.5 m (H2P3-2.5) and 3.3m (H2P3-3.3). The same numerical setup was used in both cases. The steam injection conditions are the same as in HP51 (Table 1) with extended duration of the second phase (Figure 31). The detailed setup including

the mesh sensitivity, turbulence model, boundary condition, numerical solver and source terms approach are described in [31].

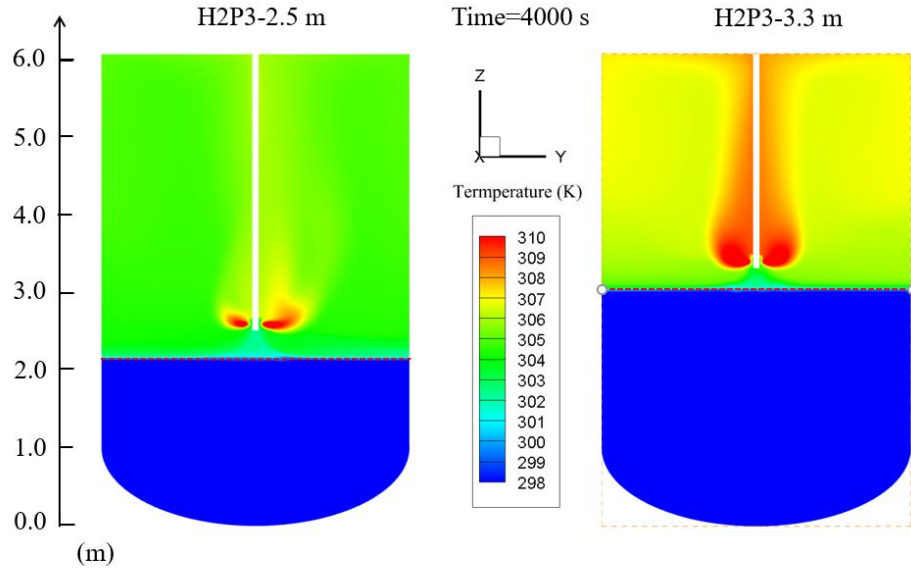


Figure 32. Comparison of temperature contours of H2P3-2.5 and H2P3-3.3 at $T = 4000s$.

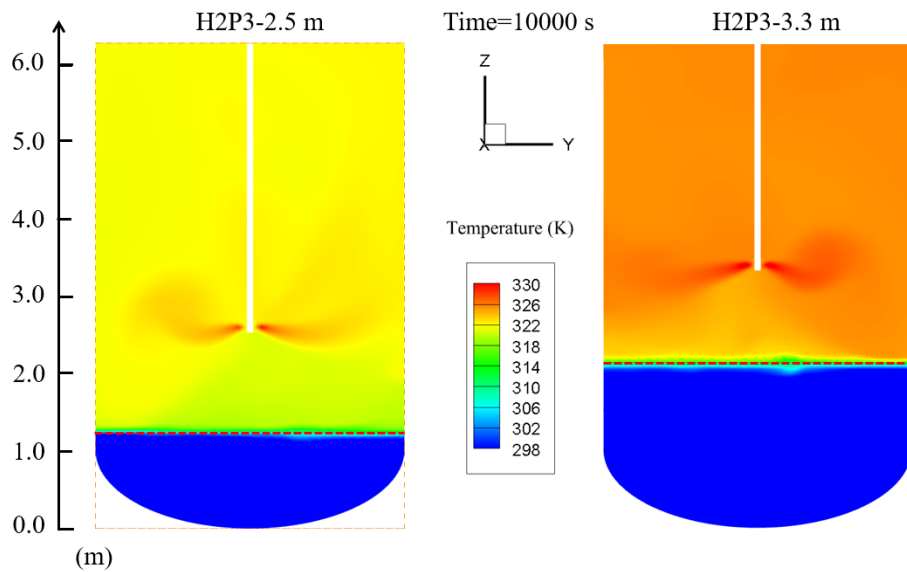


Figure 33. Comparison of temperature contours of H2P3-2.5 and H2P3-3.3 at $T = 10000s$.

Comparisons of the temperature fields for both cases at $t = 4000s$ and $t = 10000s$ (phase I and phase II respectively) are presented in Figure 32 and Figure 33. Locations of the thermocline, where the largest temperature gradient is observed, are highlighted with a red dashed line for both cases. The evolution of the thermocline elevation and velocity are shown in Figure 34. In both cases, the elevation of the thermocline decreases rapidly at the beginning of a steam injection phase, then reaches a stable position with near zero erosion velocity. Note that decreasing water subcooling slowly increases effective momentum (see (3) and (4)), which helps to maintain a certain rate of erosion of the cold layer.

The temperature evolution and motion of thermoclines in both considered cases have very similar trends (see Figure 35). The distance between the sparger head and the thermocline is

slightly smaller in case with sparger elevation of 3.3 m. This is because hot layer in this case is thinner and has higher temperature and respectively larger density difference with the cold layer at the same time moment compared to the case with 2.5 m sparger head elevation. Both options enable capturing the effect of the distance from the sparger head on the erosion rate including the regime of practical stagnation of the thermocline. Configuration with 2.5 m sparger head elevation was eventually selected for the H2P3-1,2,3 tests, considering that it was more suitable for implementing 3D PIV setup than configuration with elevation of 3.3 m.

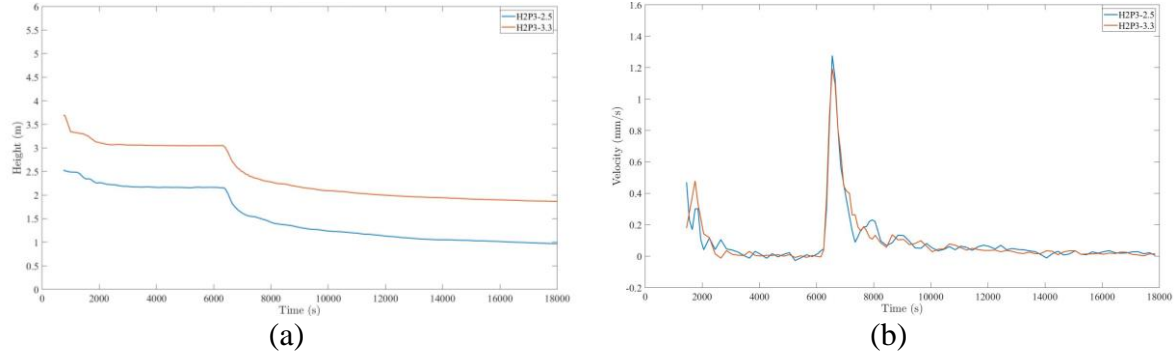


Figure 34. Comparison between H2P3-2.5 and H2P3-3.3 of (a) evolutions of thermocline and (b) erosion velocity of the stratified layer.

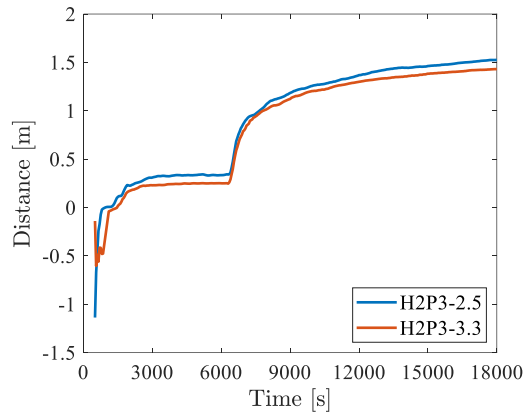


Figure 35. Comparison between H2P3-2.5 and H2P3-3.3 of the distance from the sparger head to the thermocline.

Based on the analysis results following recommendations were provided for optimization of the thermocouples (TCs) positioning. It is important to provide at least one vertical train of TCs with refined resolution (25 mm step between the TCs) below the sparger head at a distance of 250 mm away from the vertical axis of the pool (TC line 1 in Figure 4). The other two trains can be used with larger (about 100-150 mm) steps between TCs in vertical direction and be placed at a distance of 500 and 1000 mm away from the sparger. No additional TCs in the pool would be necessary due to the uniformity of the temperature profile in the radial direction [36].

5.1.2. Steam injection procedure

One of the goals of H2P3 was to study the effect of the distance from the sparger to thermocline and to achieve a few configurations with nearly stagnant position of the thermocline. Respectively, three cases were proposed for H2P3 (Table 5 and Figure 36). All of them involve four injection phases with different mass flow rates and durations. All tests start with injection at 0.16 kg/s which is minimum flow rate to avoid chugging [6] (Figure 36) and end with the maximum flow rate that was possible to achieve in the test. For comparison with the HP5 tests, some flow rates in H2P3 were kept similar to those in HP5 test matrix. In all cases the same boundary conditions and water pool depth of a 6 m were used. The difference was in the duration of the steam injection phases and steam mass flow rates.

Table 5. Steam injection procedures of H2P3-1,2,3.

Test	Initial conditions	Phase 1		Phase 2		Phase 3		Phase 4	
	Temperature (°C)	Flow (kg/s)	Time (s)	Flow (kg/s)	Time (s)	Flow (kg/s)	Time (s)	Flow (kg/s)	Time (s)
H2P3-1	20	0.16	4000	0.27	4000	0.37	4000	0.45	4000
H2P3-2	20	0.16	4000	0.27	4000	0.37	8000	0.45	5000
H2P3-3	45	0.16	4000	0.27	4000	0.37	4000	0.45	4000

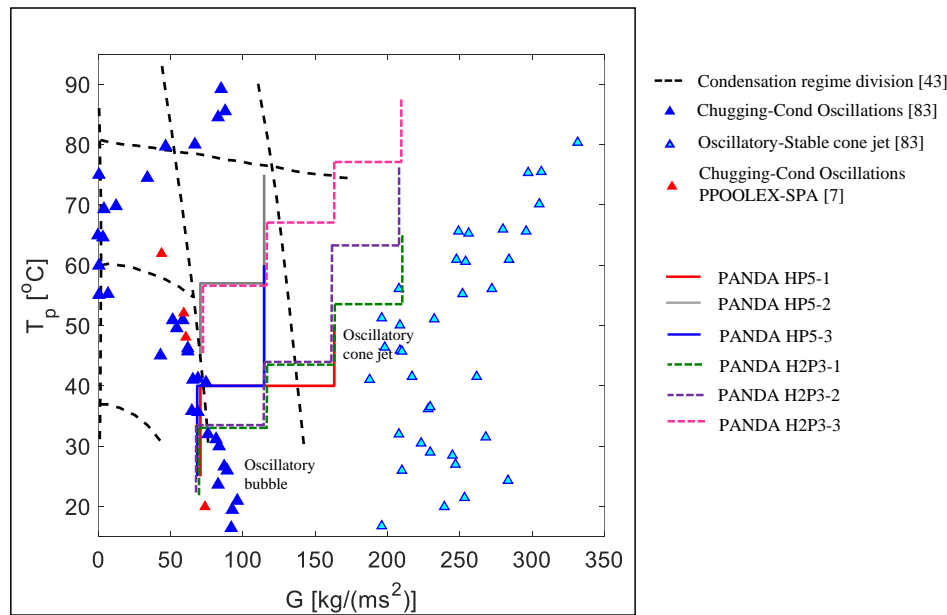


Figure 36. Condensation regime map of PANDA HP5, H2P3 tests [6, 43, 96]. G is the steam mass flux through the injection holes and T_p is the pool bulk temperature.

Results of simulations presented in Figure 34 show that the stratified layer nearly stagnates at $\sim 4000\text{s}$ after the transition. Therefore 4000s is selected as a typical duration for each steam injection phase. Pre-test simulations of the H2P3-1, show that the stagnation of the thermocline in phases 3 and 4 is not observed (Figure 37). Analysis of H2P3-2 show no significant qualitative effect from extending duration of the last two injection phases. However, the extended duration of the injection phases provides a possibility to compare data from H2P3-1

and H2P3-2 at different pool configurations. Therefore, it was suggested to keep 4000s duration for each phase in H2P3-1 and perform H2P3-2 with extended injection time. In H2P3-3 a higher initial pool temperature was selected to investigate the effects of subcooling on the motion of thermocline.

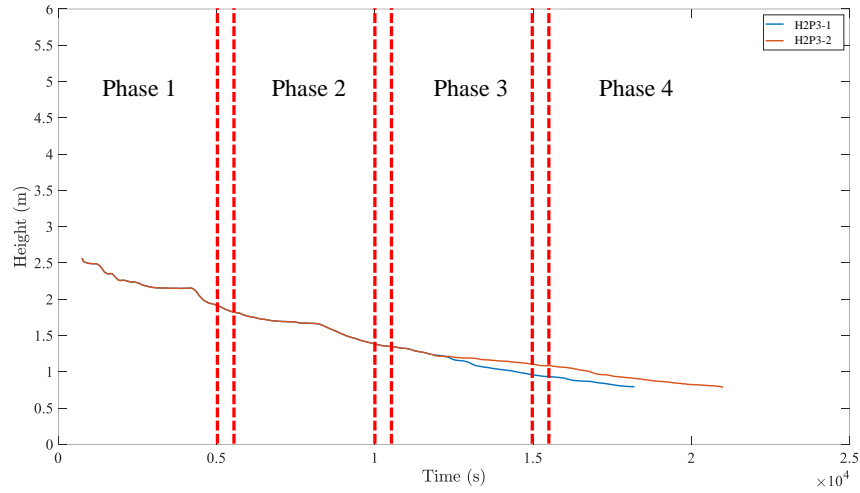


Figure 37. Evolution of thermocline elevation obtained in pre-test simulations of H2P3-1 and H2P3-2.

5.1.3. 3D PIV setup

Particle Image Velocimetry (PIV) was used in previous PANDA tests for measurements of the velocity profile in vertical cross section near the sparger [36]. One of the main tasks for H2P3 tests is to provide measurements that can be used to calibrate modeling approaches for the azimuthal distribution of the fluid velocity in the vicinity of the sparger. A new 3D PIV window $\sim 1 \times 1 \text{ m}$ was prepared for this purpose. Pre-test analysis was carried out in order to optimize position of the PIV window for measurement of the merged jets velocity profiles in the azimuthal direction.

The first pre-test analysis was performed using MATLAB and equation (5) to describe the jet velocity field. The effects of the expansion factor K on the velocity profile is illustrated in Figure 38. As discussed in section 4.2.1, the azimuthal profile of velocity is smoother at smaller values of K . In Figure 39 velocity profiles are shown in different horizontal cross-sections with different distances between the PIV plane and sparger head. A horizontal PIV plane was studied as an option that provides more detailed information about dependency of the velocity on the distance from the sparger. However, small gas bubbles, usually produced in the steam condensation region, can create difficulties for measurements of the velocity near the sparger. Also there are technical difficulties with implementing a horizontal PIV plane in PANDA, therefore the option with horizontal PIV window was eventually discarded.

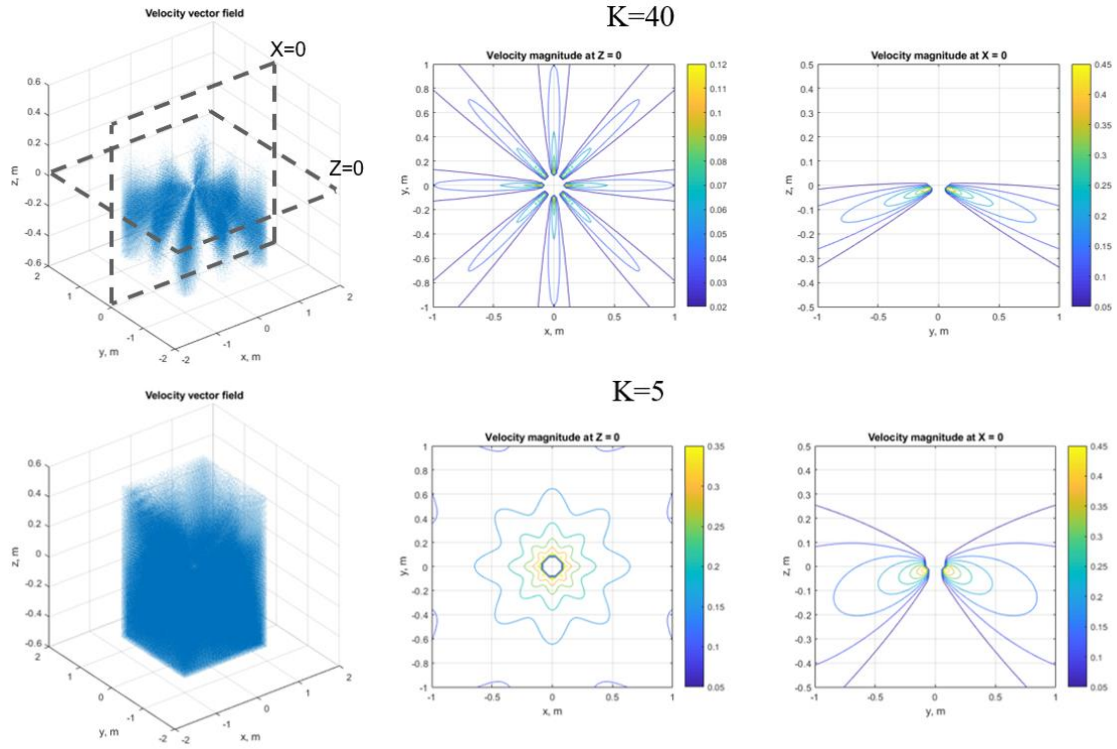


Figure 38. Characteristic map of velocity filed around a sparger with different K .

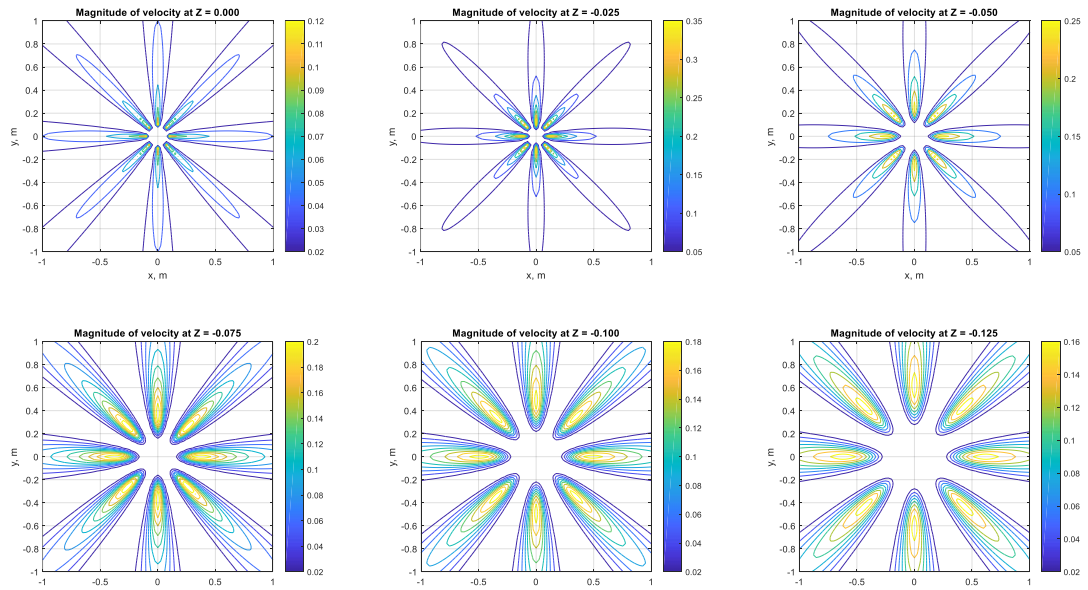


Figure 39. Horizontal cross-sections of velocity profile at the different heights using $K = 40$.

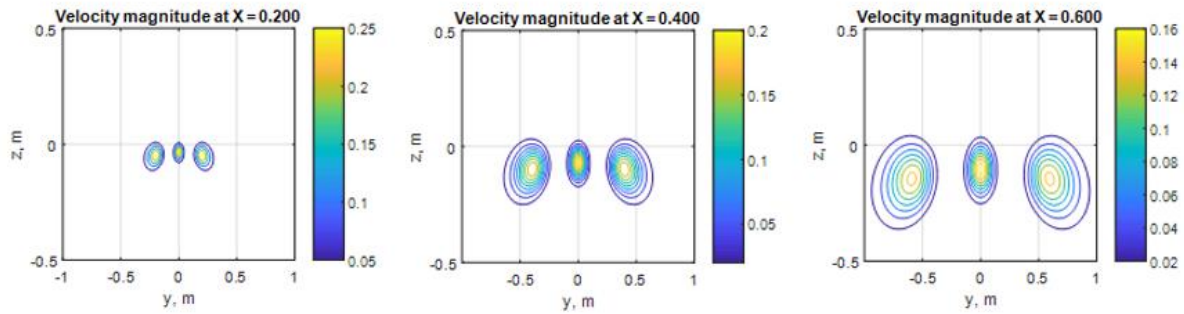


Figure 40. Vertical cross-sections of the velocity field at different distances from the sparger axis with $K = 40$.

Velocity profiles in vertical cross-sections with different distances from the sparger axis are shown in Figure 40. Vertical PIV plane can provide a reasonable coverage for the jet velocity field. However, given the limitation on the size of the PIV window, the coverage is significantly reduced at larger distances (e.g. larger than ~ 0.6 m). An optimization of the PIV window positioning with respect to sparger is needed to maximize the value of the obtained data. The PIV plane is located in the middle section of the pool at the level of the sparger head (Figure 41). The sparger is mounted on two parallel rails and can be moved to control the distance to the PIV plane. However, the sparger can't be moved during the test.

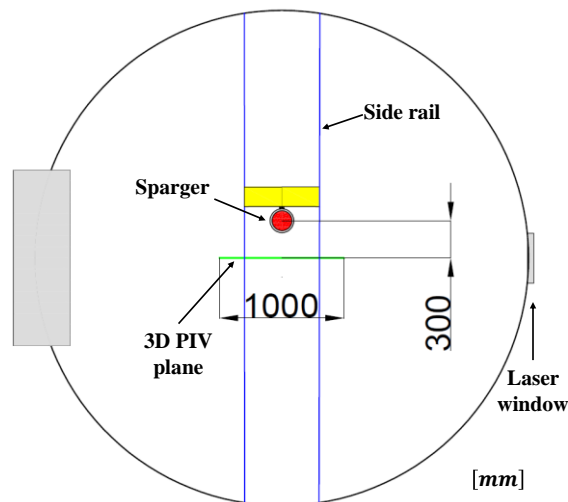


Figure 41. PIV configuration for H2P3 tests for the measurements of azimuthal velocity profiles of the jet.

5.1.4. CFD analysis of velocity field around sparger

To maximize the value of obtained measurements, pre-test simulations were performed to study details of the velocity field around the sparger using CFD. In this section, the “Unit cell” model [135] with a 22.5° sector domain is used. Validation of the approach against PIV data from the HP53 test [132] showed a reasonable qualitative agreement with the experimental data. Comparison of the centerline velocity predicted by Fluent and obtained from PIV is shown in Figure 42.

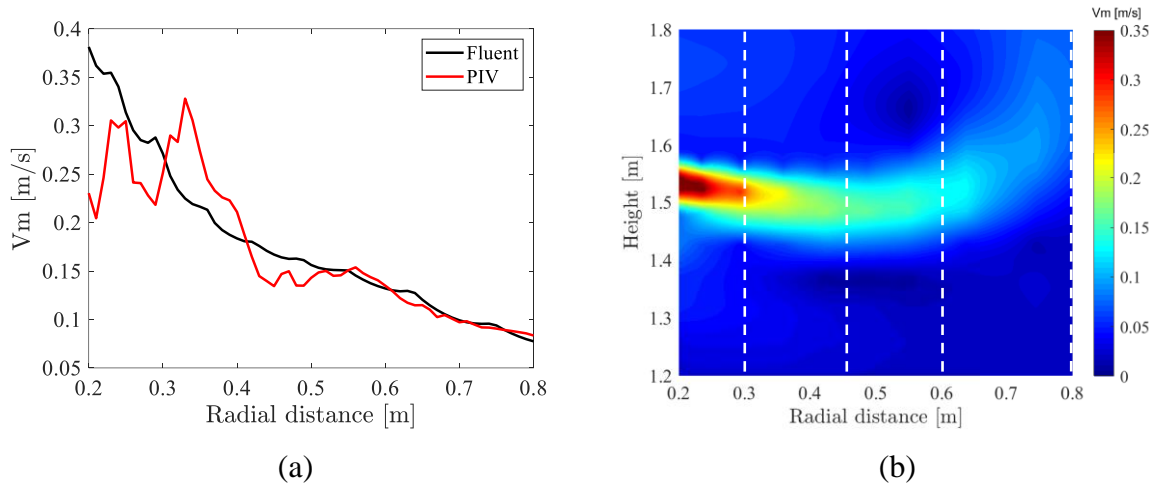


Figure 42. Velocity characteristics at $t = 1800s$: (a) comparison of Fluent predictions and PIV data for centerline velocity, and (b) velocity field predicted by Fluent. The data from PIV was time-averaged over 200s.

There is a noticeable deviation between experiment and simulation in the region before $x = 0.4 m$. In Figure 29(a) the dark blue area around the sparger where no data was recorded is shown. The centerline velocity in the PIV data was defined as the maximum velocity in a cross section. Given that only part of the region is resolved, the value of the maximum velocity can be under-estimated. Further discussion regarding the measurement uncertainty can be found in [109, 132]. A good agreement in the far-field ($x > 0.5m$) suggests that the “Unit cell” model can quantitatively be used to predict the far-field velocity profile induced by steam injection.

Comparison of the radial velocity profiles in different cross sections (see dashed lines in Figure 42b) is given in Figure 43. Individual jets can be seen at $x = 0.05 m$. In reality, however, the steam jets might not be condensed yet at this point. The radial velocity profile in both PIV and simulations can be described as a single jet at the radial distances of $x = 0.3, 0.45, 0.6 m$. A reasonable agreement between prediction and experiment is obtained with boundary conditions for turbulence intensity $I = 50\%$ and viscosity ratio $\nu_T/\nu_L = 3000$ (section 4.3.3). A buoyant jet is predicted by Fluent at the far-field (Figure 42(b)) agrees reasonably well with the PIV measurements (HP53 in Figure 29). These observations suggest that the “Unit cell” model can provide an adequate prediction of the velocity field.

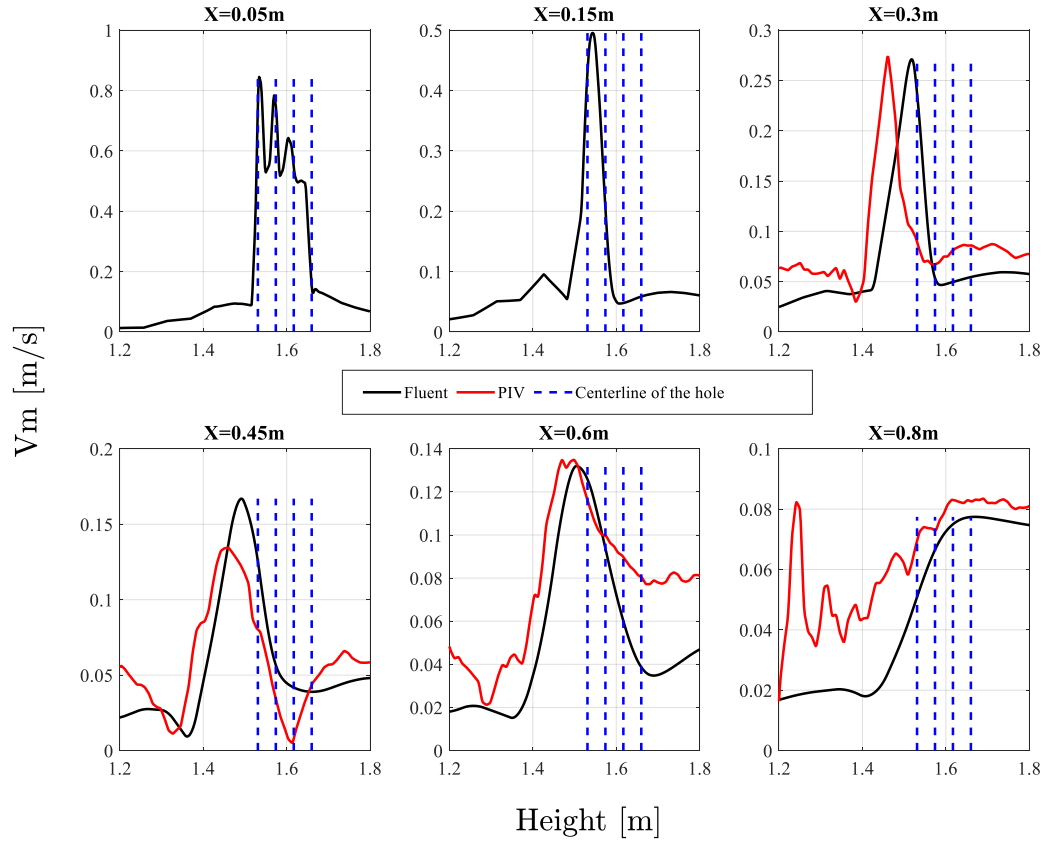


Figure 43. Comparison of radial velocity profiles between Fluent and test results over the PIV plane. The centerline of the hole drawn by blue dashed lines is used to verify the downward inclination of the jets.

The “Unit cell” model was used in pre-test simulations to support the optimization of the PIV setup. Note that the velocity field can be affected by the pool temperature due to (i) dependency of the condensation regime coefficient C on pool subcooling, (ii) buoyancy effects on the mean flow and turbulence. According to (3) and (4) pool temperature variation in the tests will cause relatively small change of the condensation regime coefficient. Buoyancy driven jet was observed by PIV data in PANDA HP5 tests only in the low steam injection phase $\dot{m}_s = 0.16 \text{ kg/s}$ [31, 36]. When the steam flow rate was increased to 0.27 kg/s and 0.37 kg/s , buoyancy was no longer a dominant factor. Pool temperature had little effect on the jet flow pattern. It can be expected that the differences between water temperature in H2P3 tests would not change the velocity field dramatically. Therefore, the pre-test simulations are performed using initial conditions and injection procedures of H2P3-1 (Table 5).

The velocity contours in the vertical direction obtained from the simulation are presented in Figure 44. The velocity field in H2P3-1 first phase is expected to be similar to HP53 (Figure 42(b)) that was carried out at the same conditions. A buoyancy driven jet is observed in the first injection phase where $\dot{m}_s = 0.16 \text{ kg/s}$, similar to the data from PIV.

After the steam flow rate was increased to 0.27 kg/s , inertia becomes the dominant factor. Simulation results at $t = 8000 \text{ s}$ are also in a good agreement with the experimental observations (Figure 30a). Although half of the domain is invisible, one can see that jet penetration is more pronounced compared to the low steam flow rate conditions.

The main differences between the last three injection phases are the magnitude of the velocity and the inclination of the jet. The velocity is increased due to the increase of the steam flow rate and the decrease of the subcooling. The jet with higher effective momentum is less diffused and changes jet inclination angle. This is probably due to the fact that the turbulent viscosity ratio in the boundary conditions is set to 3000 during the whole transient.

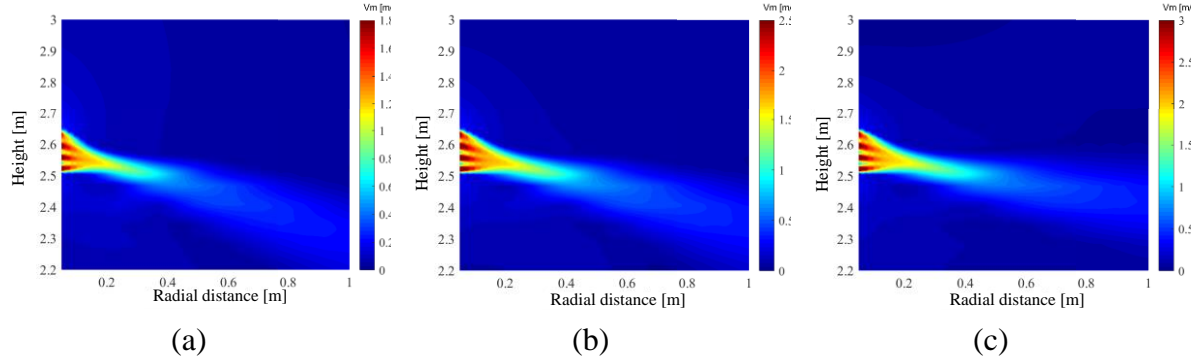


Figure 44. Velocity contours obtained in Fluent at (a) $\dot{m}_s = 0.27 \text{ kg/s}$, $t = 8000 \text{ s}$ (b) $\dot{m}_s = 0.37 \text{ kg/s}$, $t = 12000 \text{ s}$ (c) $\dot{m}_s = 0.45 \text{ kg/s}$, $t = 16000 \text{ s}$.

The velocity fields obtained in Fluent at different cross sections are presented in Figure 45. The figure shows velocity fields at the end of each injection phase. The four condensing jets almost merge together at a distance of 150mm away from the sparger head (Figure 44, Figure 45). According to the empirical formula [36], the distance where jets merge can be estimated as three times the pitch plus hole diameter, which corresponds to 157.5 mm for PANDA sparger. Similar observation was done based on the analysis of temperature and PIV data from PANDA tests [36].

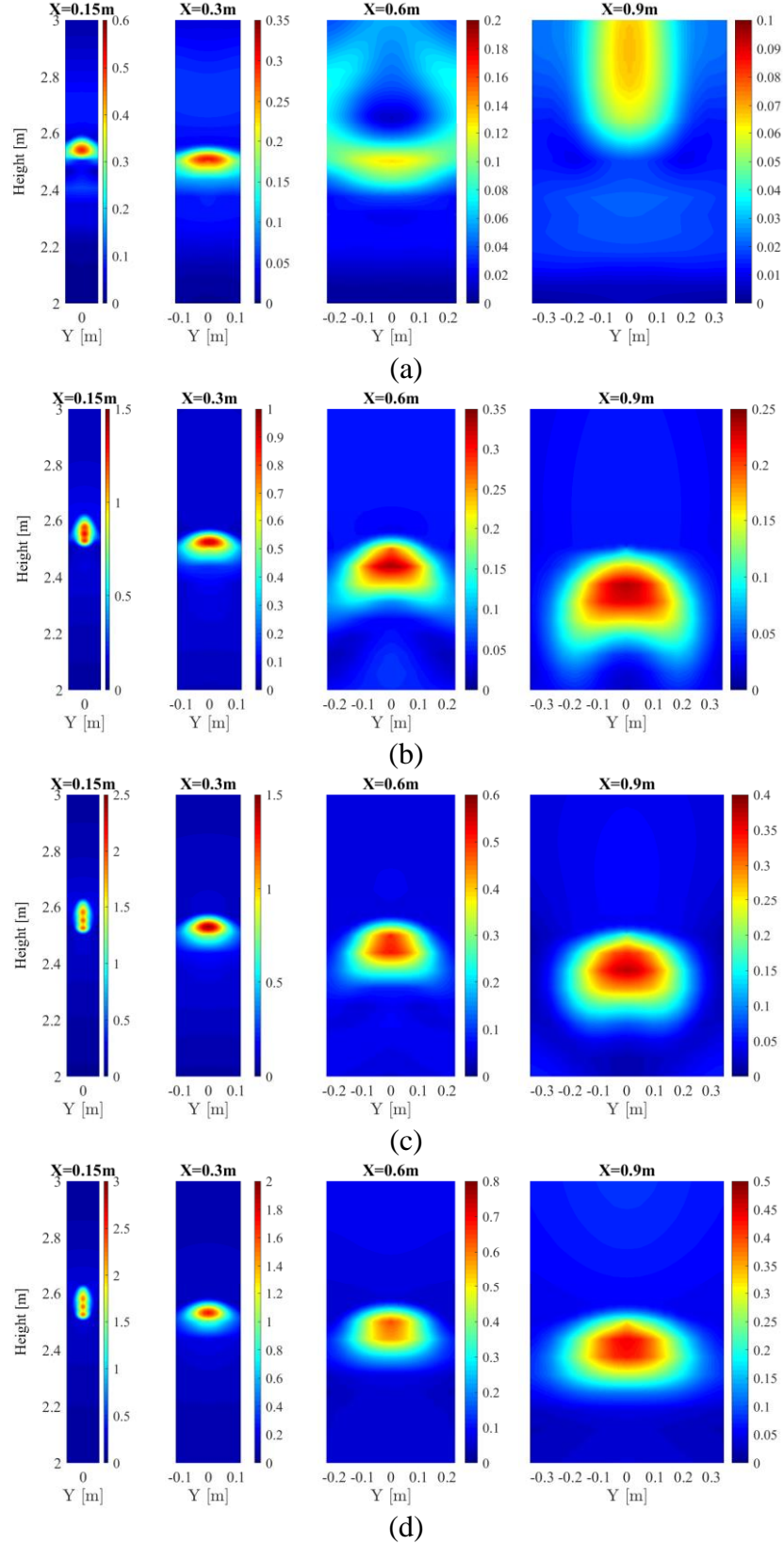


Figure 45. Velocity contours at different slices obtained in Fluent. (a) $\dot{m}_s = 0.16 \text{ kg/s}$, $t = 4000\text{s}$ (b) $\dot{m}_s = 0.27 \text{ kg/s}$, $t = 8000\text{s}$ (c) $\dot{m}_s = 0.37 \text{ kg/s}$, $t = 12000\text{s}$ (d) $\dot{m}_s = 0.45 \text{ kg/s}$, $t = 16000\text{s}$.

Non axisymmetric velocity field is observed in Fluent simulation (Figure 45) in all injection phases. It is a typical behavior for the multiple jets. Observed profiles can be described using equation (16). As the distance from orifice increases, the jet expands in the azimuthal direction,

resulting in a change from near-planar to elliptical jet. The jet velocity profile evolution is seen in Figure 46, where the buoyancy effect and downward inclination are not modelled.

The jet at the end of the first injection phase is driven upward by the buoyancy (see sections at $X = 0.6\text{ m}$ and $X = 0.9\text{ m}$). For these conditions the PIV window should be placed closer ($X = \sim 0.3\text{ m}$). Inertia dominates jet behavior at higher flow rates, and no qualitative differences in the velocity profile can be seen. Turbulent diffusion effect can explain the differences between velocity profiles in the far-field obtained at different injection conditions. Higher momentum jets can penetrate farther with less diffusion.

Sensitivity of the velocity profile in azimuthal direction to the turbulent viscosity ratio was carried out (Figure 46). The jet with higher viscosity ratio result in more elliptical shape of the jet. This means that boundary conditions for turbulence characteristics have significant influence on the jet velocity field. In order to reproduce specific profile in Fluent the proper boundary conditions for turbulence are needed.

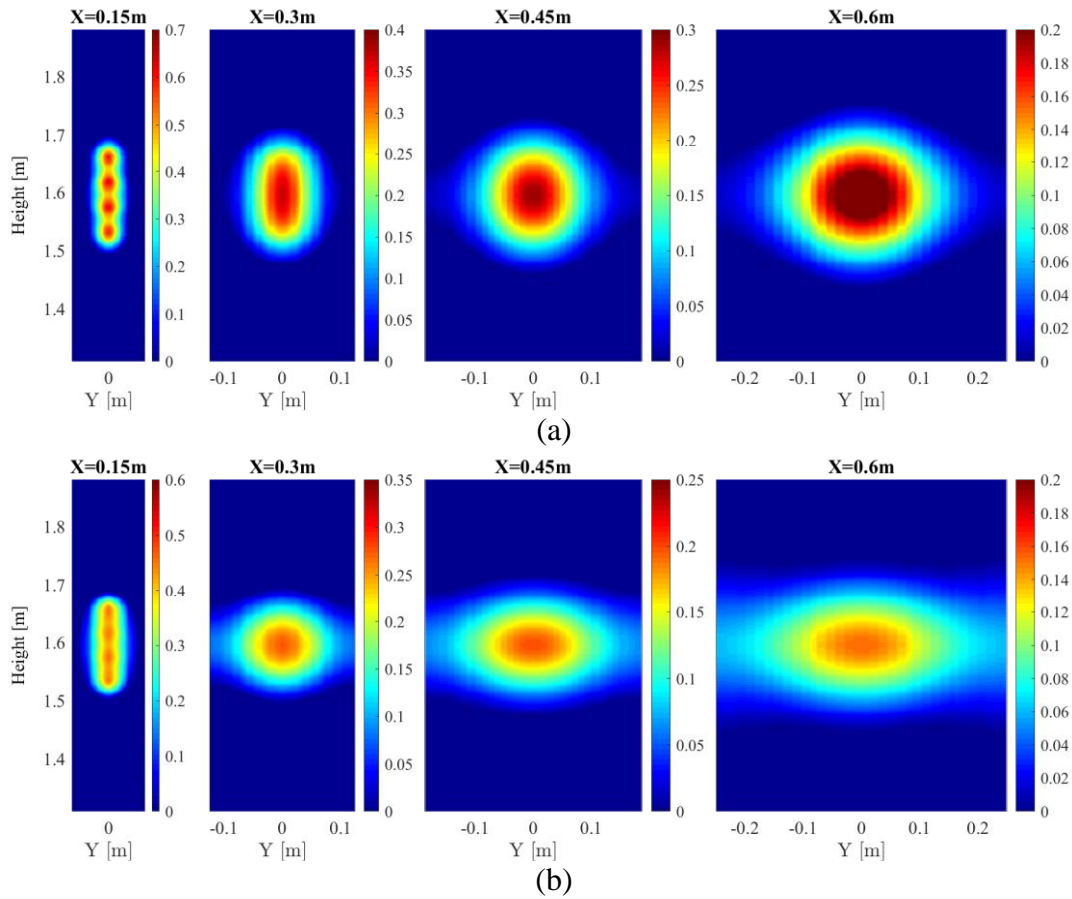


Figure 46. Velocity contours at different slices in the first injection phase, iso-thermal, and no downward inclinations. (a) $I = 50\%$, $\nu_T/\nu_L = 1000$ and (b) $I = 50\%$, $\nu_T/\nu_L = 3000$.

5.1.5. Optimization of the PIV window orientation

The sparger head position with respect to the PIV window can be optimized to maximize the value of the PIV data by measuring jet velocity with a single PIV plane in as many jet cross sections as possible. Since the centerline velocity is one of the important parameters of

calibration of the azimuthal profile model, the measurement should also capture as many centerline points of the jets as possible. The PIV setup is optimized by selecting (i) the distance d between sparger head and PIV plane, and (ii) angle α of the sparger head rotation along the vertical axis. The PIV might be unreliable at close distances to the sparger. In the high steam injection phase of HP53 almost half of the PIV window becomes unusable (Figure 30(a)). In this region dense bubbles affect the passage of light from the illumination plane to the camera. Therefore a minimum distance of 300 mm between the PIV plane and the sparger is selected for the low steam injection conditions.

In order to make a quantitative optimization of PIV plane orientation we introduce an effective length. The length is defined as a sum of projections of the PIV cross sections of different jets on the centerline axes of the respective jets (Figure 47). If different jets are crossed in the same place, effective length is counted only for one of the cross sections.

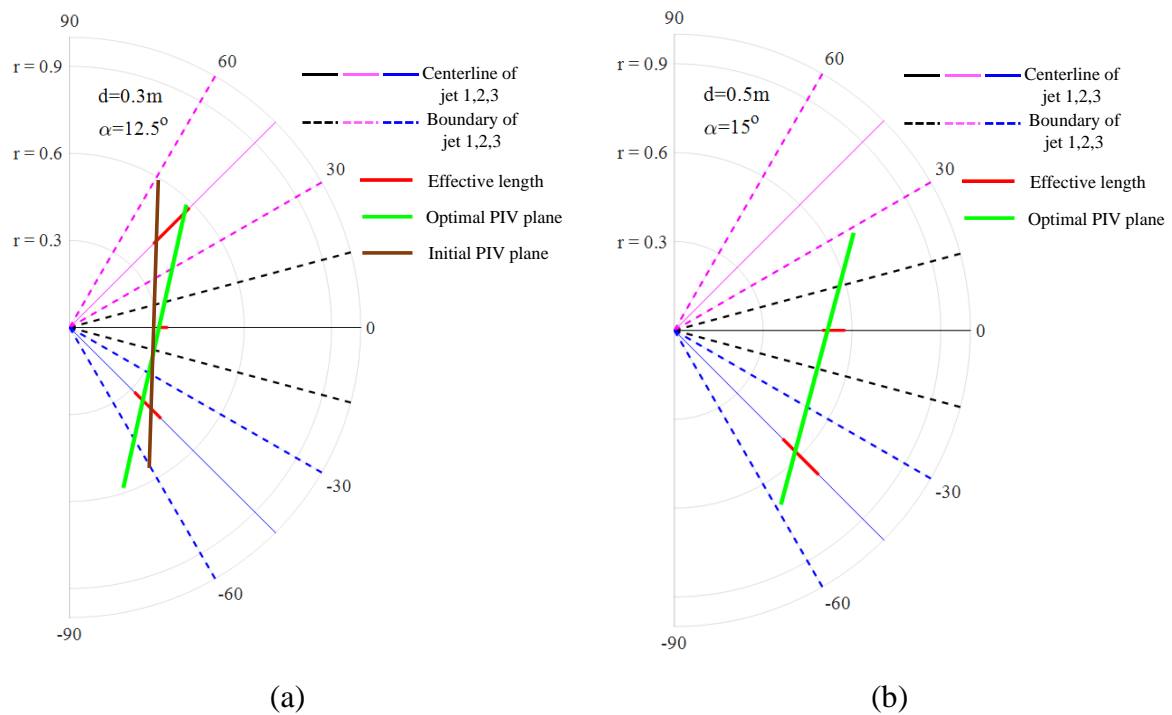


Figure 47. Optimal PIV configuration of a range of (a) 300 – 500 mm and (b) 500 – 800 mm in a view along the sparger axis. r is radial distance and the sparger at $r = 0$.

In the analysis we consider three turbulent jets with expansion angle 30° and symmetric with respect to the centerline. The PIV plane was aligned with the centerline of jet 1 $\alpha = 90^\circ$ and $d = 0$ m (Figure 47) in the previous tests [36] to measure the velocity profile in a vertical cross section. For H2P3 measurements of the velocity distribution in azimuthal direction, the optimization is started with $\alpha = 0^\circ$ (plane shown as brown line in Figure 47). Optimal angle of rotation depends on the distance from the sparger. Centerline velocities for three jets can be measured if the distance from the PIV plane to the sparger is in a range between 300 – 500 mm. In this case the optimization gives $\alpha = 12.5^\circ$ and $d = 300$ m (Figure 47(a)). The PIV plane intersection with the jet 1 centerline is 5 cm away from the edge of the PIV plane. For the range of the distances 500 – 800 mm, it is possible to measure only two centerline velocities with a 1 m wide PIV window. The optimization results in $\alpha = 15^\circ$ and $d = 500$ m (Figure 47(b)). At the distances larger than 900 mm only one centerline velocity can be measured.

Given the distance of the PIV window will be fixed during each test, the distribution of the above introduced three regions should be discussed. For the strongest jet (e.g. H2P3-3 last injection phase) the PIV window should be located at a distance of 900 *mm*. Sparger rotation can be set between 0° or ~43°. For the conditions of H2P3-2 second, third and fourth injection phases the PIV window can be located at the distance of 500 *mm* with rotation angle of 15°. For H2P3-1 first injection phase the PIV plane can be located at the distance of 300 *mm* with rotation angle 12.5°.

5.2. Pre-test simulations for H2P3 LRR tests

Three tests of H2P3-4,5,6 are planned to be carried out with LRR holes open and with the sparger head holes closed. The LRR, is located at 1800 mm from the bottom of the sparger (Figure 5 and Figure 48) and has 8 holes with 9.5 mm inner diameter, distributed in 1 ring. In this section we provide pre-test analysis to select the test conditions. The aim of the test is to maintain stratification in the pool during the whole transient and study gradual erosion of the cold layer as the steam flow rate is changed. We study the effect of (i) the elevation of LRR holes above the pool bottom, (ii) the number of open LRR holes, and (iii) the flow rate and duration in each steam injection phase.

The pre-test simulations are carried out using the EHS/EMS models implemented by SCR approach for a single jet (section 4.3.2). Results of the model validation (section 4.3.3) demonstrated that jet induced by condensing steam can be simulated by injecting liquid with a uniform velocity profile that provides the same effective momentum. Flow symmetry was assumed and a 22.5° sector was used as a computational domain with a half of the injection hole.

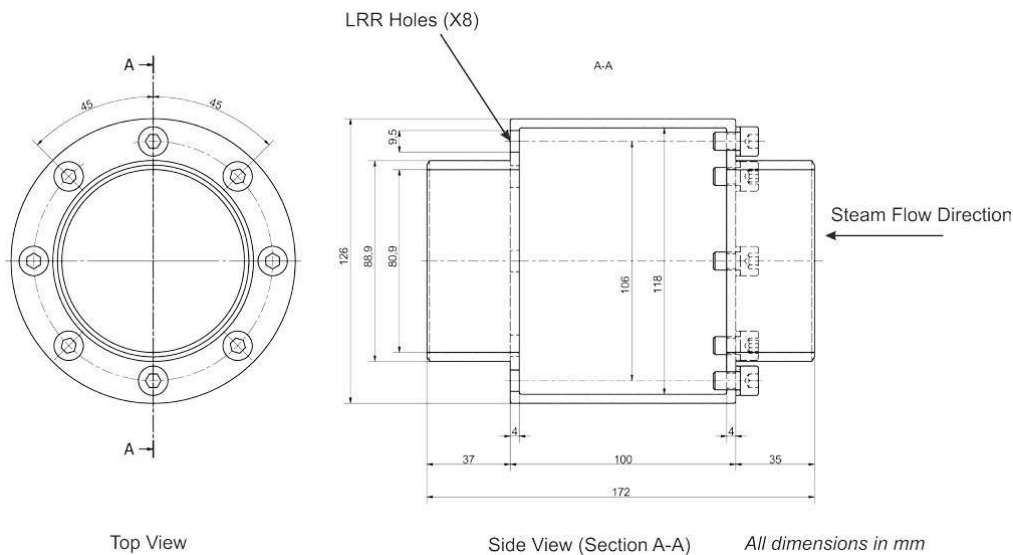


Figure 48. Details of the Load Reduction Ring (LRR).

The water pool level is 6 m . The pre-test analysis with LRR holes positioned at 3300 mm ($1500 + 1800$) above the pool bottom and steam injection procedure similar to H2P3 was carried out first. Results of the analysis showed that vertical jets from LRR holes can penetrate into the cold layer by about $2000 - 2500\text{ mm}$ even at relatively small flow rates. To avoid rapid mixing of the pool, the elevation of the sparger head was increased from 1.5 m to 2.5 m with elevation of LRR holes 4300 mm .

Further pre-test simulations with the 2.5 m sparger head elevation were carried out to investigate the effect of steam injection procedures. Initial pool temperature of 15°C was selected to achieve a prototypic subcooling, minimum steam flux $G = 85\text{ kg/m}^2\text{s}$ was chosen to avoid chugging (see regimes map in Figure 36). Temperature fields shown in Figure 49 illustrate the effect of steam mass flux increase from $85\text{ kg/m}^2\text{s}$ to $160\text{ kg/m}^2\text{s}$ at $T = 4000\text{ s}$. A stratified layer can be observed in the first injection phase, but it is eroded rapidly by the increased momentum of the jet.

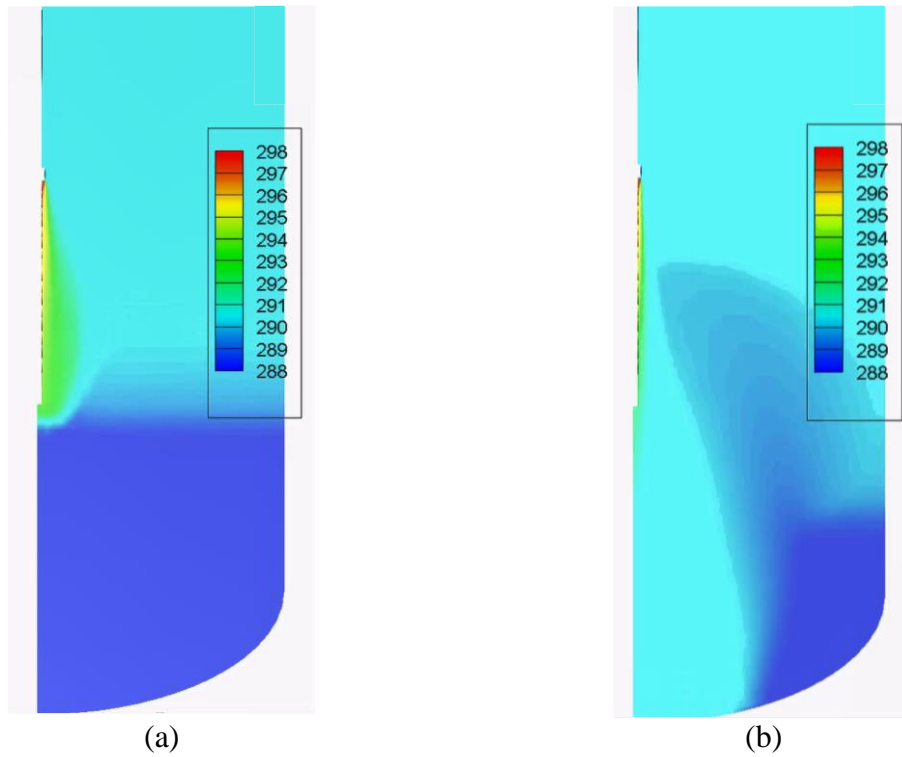


Figure 49. Temperature field predicted for H2P3 LRR tests at (a) $t = 4000$ s with $G = 85$ $\text{kg/m}^2\text{s}$, and (b) at $t = 4300$ s with $G = 160$ $\text{kg/m}^2\text{s}$.

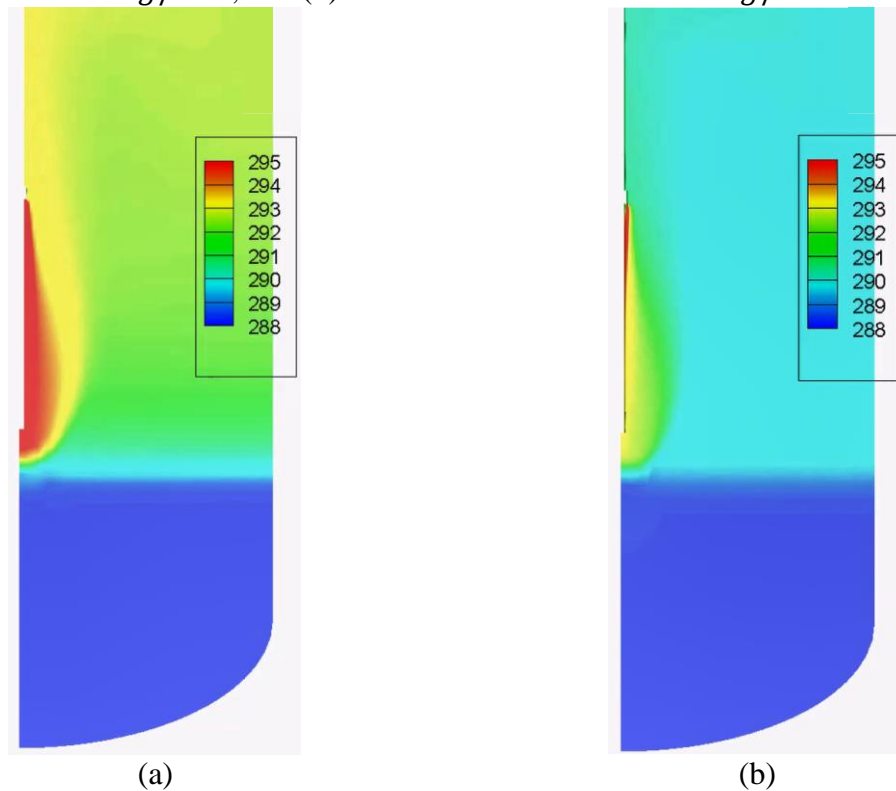


Figure 50. Temperature field predicted for H2P3 LRR tests at $t = 6000$ s, $G = 85$ $\text{kg/m}^2\text{s}$ with (a) 8 holes open, and (b) 4 holes open.

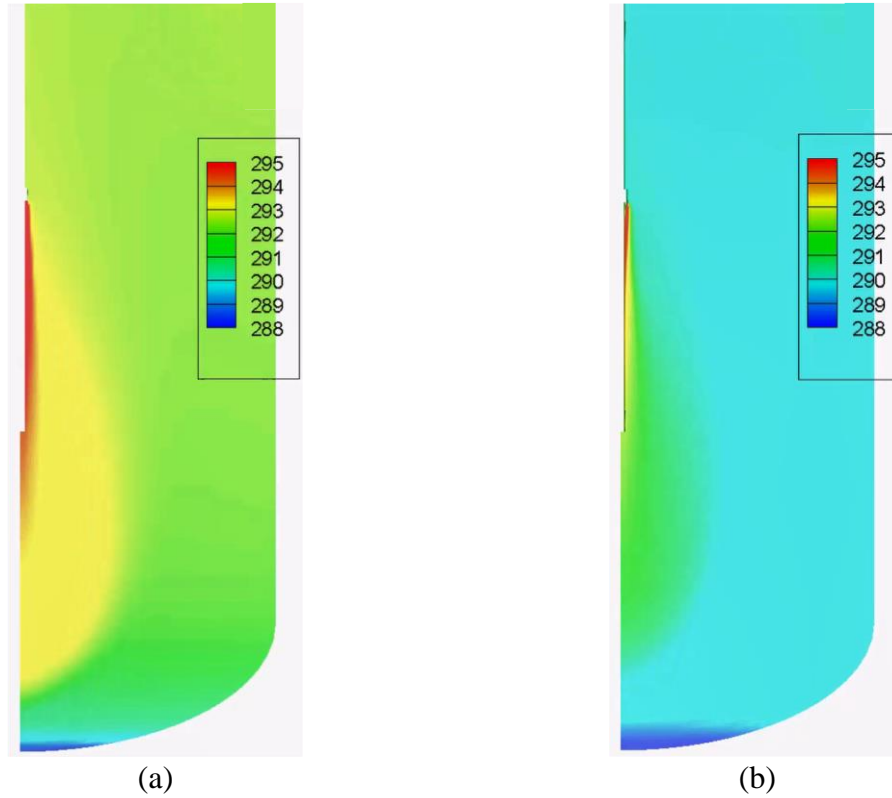


Figure 51. Temperature field predicted for H2P3 LRR tests at $t = 7000$ s, $G = 125$ kg/m²s with (a) 8 holes open, and (b) 4 holes open.

Based on the analysis results, it was suggested to increase the duration of the first phase to 6000 s in order to achieve a larger density (temperature) difference between the cold and the hot layers to increase resistance to the erosion at higher flow rates. In fact, 8000 s would be even better in this respect, however it was considered that the overall duration of the test still should be reasonable. The mass flux in the second phase was decreased to 125 kg/m²s in order to reduce the momentum source. Predicted temperature fields are shown in Figure 50 and Figure 51. Increased duration for the first injection phase indeed created a stronger thermocline with a larger temperature gradient (compared to the case with 4000 s for the first injection phase Figure 49). A thin layer of cold water (Figure 51a) remains at the end of the second phase, which suggests that $G = 125$ kg/m²s can be used in the last phase.

We found that the effect of the number of LRR holes on the jet penetration depth at the same steam flux is minor (Figure 50b and Figure 51b). Smaller number of holes (and respectively reduced flow rate) results in increased time needed to develop a stratified layer. Therefore, it was proposed to keep 8 holes opened. The setup suggested for H2P3 LRR tests has water level 6 m, sparger head elevation 2.5 m and 8 open LRR holes. The injection procedures are summarized in Table 6 and Table 7. In total 4 injection phases are set for H2P3-4,5 and eight phases for H2P3-6. In the first phase of steam injection flux is set to 85 kg/m²s (0.048 kg/s) in order to create a stratified pool. Then steam flow rate is increased in steps. Initial temperature in H2P3-5 is set to 35°C.

Amount of gas bubbles generated at small steam flow rates in the LRR tests is expected to be relatively small. There is a hope that at such conditions PIV can provide valuable data for code validation such as velocity field and turbulence characteristics of the jet. In H2P3-6 the number of the injection phases is increased to 8 and the duration of each phase is decreased to 2500 s

(Table 7). First, the flow rate is increased from 48 g/s to 60 g/s in 4 steps. The pool is expected to be almost completely mixed at that point. Then flow rate is reduced to 40 g/s. Chugging can be avoided at such small flow rates as the pool temperature is sufficiently increased. Then flow rate is increased again in several steps.

Table 6. Steam injection procedures of H2P3-4,5.

Test	Initial conditions	Phase 1		Phase 2		Phase 3		Phase 4	
	Temperature (°C)	Flow (kg/s)	Time (s)	Flow (kg/s)	Time (s)	Flow (kg/s)	Time (s)	Flow (kg/s)	Time (s)
H2P3-4	15	0.048	6000	0.053	4000	0.058	4000	0.07	4000
H2P3-5	35	0.048	6000	0.053	4000	0.058	4000	0.07	4000

Table 7. Steam injection procedures of H2P3-6.

Test	Initial conditions	Phase 1(5)		Phase 2(6)		Phase 3(7)		Phase 4(8)	
	Temperature (°C)	Flow (kg/s)	Time (s)	Flow (kg/s)	Time (s)	Flow (kg/s)	Time (s)	Flow (kg/s)	Time (s)
H2P3-6	15	0.048	2500	0.052	2500	0.056	2500	0.060	2500
		0.040	2500	0.052	2500	0.056	2500	0.060	2500

5.3. Summary of pre-test analysis for H2P3 test series in PANDA facility

Pre-test simulations have been carried out to support definition of the PANDA H2P3 test series. Scoping calculations are carried out to specify geometrical setup (pool depth, elevation of the sparger and number of open LRR holes), initial pool temperature, injection procedures, arrangement of thermocouples, PIV setup, for sparger tests (H2P3-1,2,3) and LRR tests (H2P3-4,5,6).

6. PRE-TEST SIMULATIONS FOR PANDA H2P4 TESTS

6.1. Motivation and background

OECD/HYMERES-2 project test series H2P4 aims to address integral phenomena of a BWR containment behavior with pressurization caused by pool stratification. We consider an SBO scenario with steam injection into wetwell at relatively small rates through a sparger. Conditions similar to those observed in the Fukushima Units 2 and 3 were taken as a reference for defining the H2P4 series of tests. Specifically, containment pressurization to ~4 bar with temperature of water ~140 °C and then activation of spray and slow depressurization of the containment.

The goal of the H2P4 test series is to provide data in relevant for plant conditions regimes for validation of code predictive capabilities for (i) development of thermal stratification in the pool induced by steam injection and condensation; (ii) containment pressurization due to development of the pool stratification with increased temperature of the pool surface and thus higher partial steam pressure in the containment gas space; (iii) the effect of spray activation on the pool stratification and containment pressure.

The primary goal of the pre-test scoping analysis is to provide basis for selection of test design options that would enable achieving within a reasonable test time: (i) pool thermal stratification, (ii) system pressurization ~4 Bar, (iii) pool temperature ~140 °C and (iv) study the effects of spray activation on pool stratification and containment pressure.

The secondary goals for the test design are: (i) to minimize the effects of irrelevant and/or not measured phenomena in the experiments, e.g. gravity driven counter current flows through the interconnecting pipes and (ii) to optimize experimental efforts, e.g. reduce facility modifications compared to H2P3 test configuration.

To achieve the goals of the scoping analysis the following tasks have been addressed: (i) to develop a fast running model, (ii) to calibrate and validate the model and (iii) to carry out scoping parametric analysis for selection of H2P4 test configuration and test matrix.

It should be mentioned that at the time of the writing of this report selection of the H2P4 test conditions has not been completed, and discussions related to the technical implementation of specific design solutions in the PANDA facility were still ongoing.

6.2. Initial test configuration for the H2P4 series

The H2P4 test series will be carried out in the PANDA experimental facility. The PANDA facility [136] consists of four interconnected vessels that are scaled to represent drywell and wetwell of a BWR. The facility was used to study the passive decay heat removal systems and containment response of the Simplified Boiling Water Reactor (SBWR) and the Economic Simplified Boiling Water Reactor (ESBWR) designs from General Electric (GE), as well as of the SWR1000 design from Siemens-KWU (now KERENA design from AREVA) in the case of accident transients. During the H2P4 series the injection of steam into the wetwell pool through a sparger must develop thermal stratification and with time pressurization of the drywell. The drywell vessels were disconnected in order to reduce gas volume and achieve faster pressurization within a realistic time for an experiment.

The preliminary experimental setup for the scoping analysis is comprised of two vessels (see Figure 52). The vessels are connected using two pipes one at the bottom (ID1420) and one at the top (ID928). Both vessels are filled in with water, steam injection into the pool is performed into the left (in the Figure 1) vessel through a sparger. The water pool represents the wetwell and gas gap above it – the drywell. Experimental parameters included in the scoping analysis:

- steam injection rate:
 - affects the rate of system heat-up and pool mixing / stratification.
- sparger submergence,
- water pool depth:
 - affects the volume of gas space for pressurization
- water pool initial temperature:
 - affects time required for system heat up during steam injection
 - can also affects stability of the thermocline due to temperature difference between the hot and cold layers
- configuration of the vessels:
 - single vs two vessel configuration
- spray location (vessel and elevation above water pool surface),

In addition, scoping simulations also included analysis of experimental procedures for possible pool preconditioning.

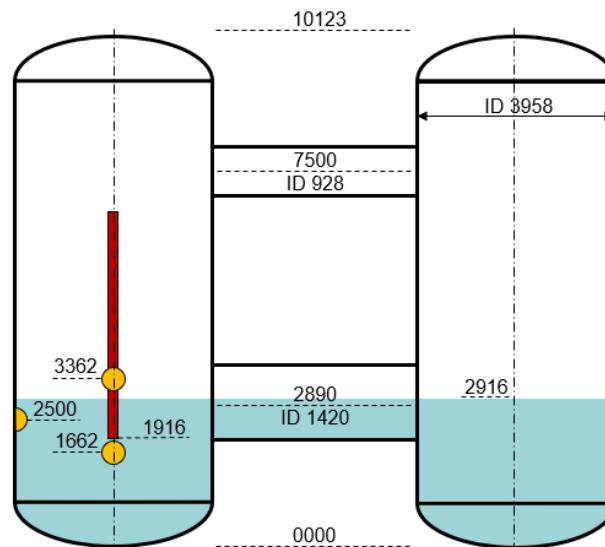


Figure 52. PANDA experimental facility for H2P4 scoping analysis

6.3. Model setup for H2P4 scoping analysis

GOTHIC 8.3 code was selected for the pre-test analysis. GOTHIC is a general-purpose thermal-hydraulic code used for modelling of power plant containments, confinement buildings and system components. It provides 3D capability based on Cartesian mesh and porous body approximation, has a wide validation database and is used for design and licensing applications.

To achieve required computational efficiency several simplifications were made in the model setup:

- To model sparger effect on the pool we introduced
 - Mass source: source of saturated water located in the pool cell with the sparger tip
 - Heat source: volumetric homogeneous heat source distributed vertically along the submerged section of the sparger to account for steam latent heat.
- The thickness of the hot layer (that defines position of the thermocline) was fixed in the model input to avoid the need for detailed 3D modelling of the steam momentum effect on the pool mixing.
 - The thermocline depth was varied as a part of the scoping analysis to account for available knowledge on the erosion of the cold layer by steam injection at different steam flow rates.
- In order to allow for convective energy redistribution within the hot layer a coarse 3x3x4 mesh was used.
- Convection in the gas space above the water pool was modelled using coarse 3x3x4 mesh. In the later stage of calculations nodalization in the gas space was increased to study steam transport behavior in more detail.
- Vessel walls were modelled to account for thermal inertia of the steel. Adiabatic boundary conditions were setup for all simulation cases at the external surface of the vessel covered with thermal insulation.
- The two interconnecting pipes (IPs) between the vessels were modelled using single flow paths with stratified flow option.

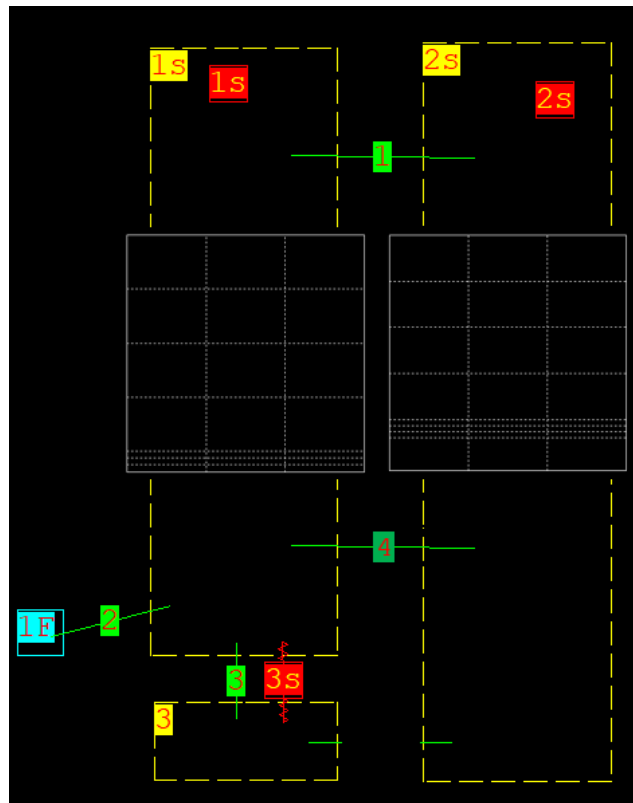


Figure 53. Initial GOTHIC model for H2P4 scoping analysis

Initial model implementation is shown in Figure 53. The two inserts in the figure show the cross-section of the nodalization for the control volumes 1s and 2s. The left vessel is modelled as two control volumes:

- control volume 3 for the cold layer of the pool and
- control volume 1s for the hot layer of the pool and the gas space above it.

Control volumes 1s and 3 are connected using a flow path and a thermal conductor. The thermal conductor is introduced to account for heat transfer between the hot and cold layer through the thermocline. The flow path is included mainly to allow for flow between the bottom of the vessel 3 and vessel 2s. The respective flow path was not used in the initial model and is not shown in the illustration.

The two interconnecting pipes are modelled as flow paths 4 and 1. Stratified flow conditions was activated to model possible counter flow of water and steam.

It should be noted that described here model corresponds to the one of several configurations studied in the scoping analysis.

6.4. Model validation

The ultimate goal of the model was to assess the rate of the pool heat-up and system pressurization given conditions of steam injection and expected thermocline depth (based on previous tests and/or accompanying CFD EMS/EHS simulations).

The model was validated against Phase 1 of HP5_1_2 test [80]. In the test steam was injected into the left vessel through a sparger. The sparger end was positioned 1.5 m below the initial water level. The pressure in the gas space above the water pool was kept constant by opening the vessel to atmosphere. The position of the thermocline was measured in the experiment and provided as an input to the model (refer to Figure 54a and b), specifically:

- Hot layer thickness: 3 m
- Thermocline thickness: 0.25 m
- Cold layer thickness: 0.75 m

Other initial and boundary conditions:

- Water pool initial depth 4 m and temperature 25°C
- Sparger submergence 1.5 m.
- Steam injection (as equivalent mass source of saturated water and volumetric heat):
 - Flow rate: 161.74 g/s
 - Temperature: 110°C

Two relevant System Response Quantities were selected for model validation: (i) water pool heat up rate and (ii) water pool surface temperature. The latter is believed to be one of the dominating factor for vessel pressurization. The results of the model validation are provided in the Figure 55.

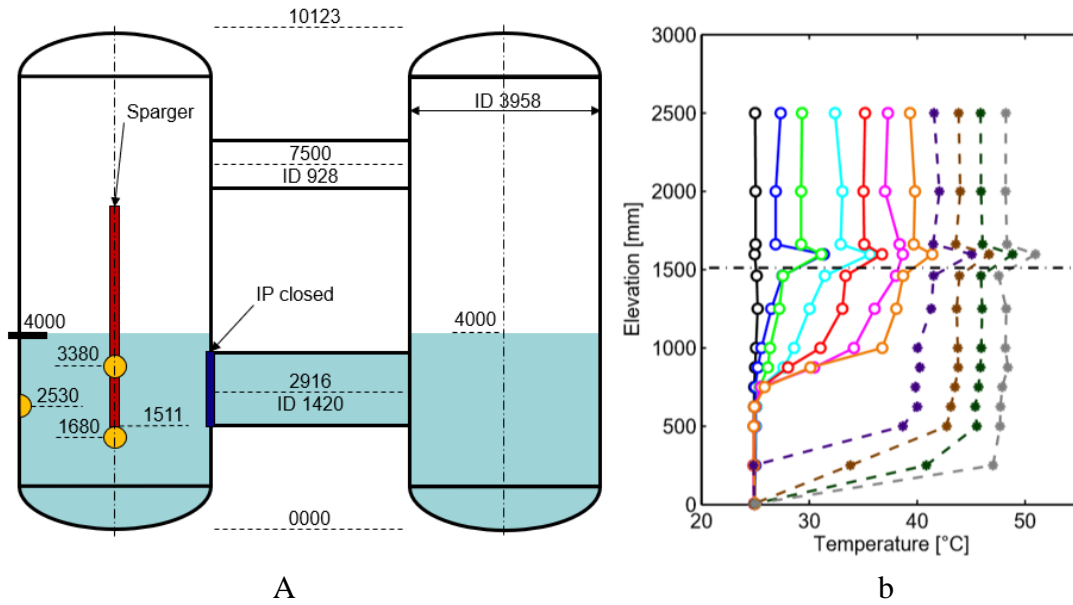


Figure 54. HP5_1_2 test: a – initial setup, b – temperature profile at different times for Phase 1 (solid lines) and Phase 2 (dashed lines) of the test.

The predicted rate of pool heat-up satisfactory agrees with the experimental data: at 6325 s the estimated temperature of the pool surface was 42.3°C - close to the experimental value of about 43°C. The vertical temperature difference in the hot layer was underestimated: about 2.3K in the simulation vs ~4.6K in the experiment. The discrepancy is attributed to the coarse meshing in the pool in the vertical direction (4x0.9m). The discrepancy was considered as acceptable tradeoff for the needed computations efficiency.

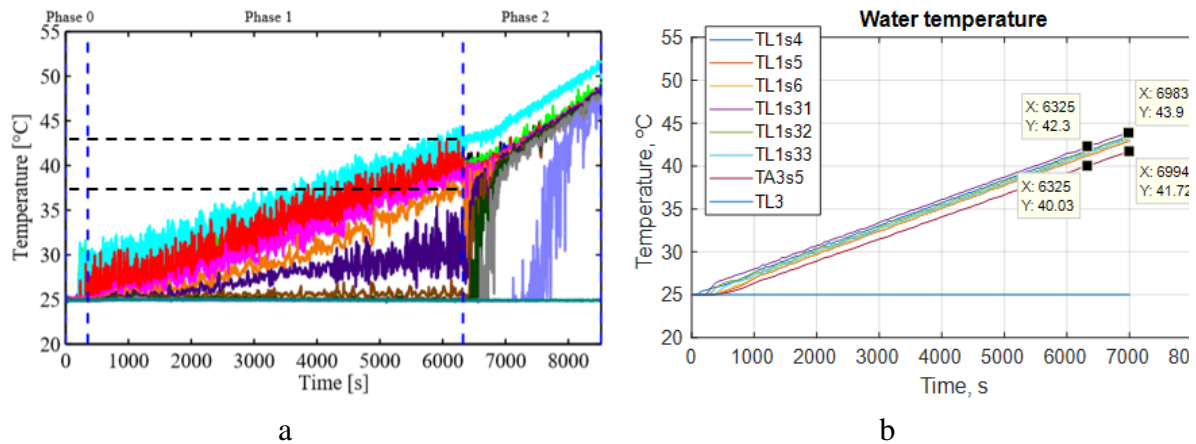


Figure 55. HP5_1_2 test evolution of the pool temperature: a – experiment, b – simulation.

6.5. Results of the scoping analysis

Preliminary heat balance calculations were carried out to estimate the magnitude of the steam injection necessary to heat the pool to 100-140°C assuming zero thermal losses and no evaporation. The results (see Table 8) suggest that scoping calculations should be performed for steam injection of 160 and 260 g/s. Higher rates of steam injection will increase the potential for complete mixing of the pool; while at lower flow rates heating and pressurization will take long time to develop.

Table 8. Heat balance calculation for different steam injection rates

Thermocline depth m	Injection rate kg/s	Time [h] to reach water pool temperature				
		100 °C	110 °C	120 °C	130 °C	140 °C
0.7	0.056	4.72	5.35	5.98	6.60	7.23
1	0.056	6.74	7.64	8.54	9.43	10.33
1.3	0.056	8.76	9.93	11.10	12.26	13.43
1.2	0.161	2.81	3.19	3.56	3.94	4.31
1.5	0.161	3.52	3.98	4.45	4.92	5.39
1.8	0.161	4.22	4.78	5.34	5.91	6.47
1.5	0.262	2.16	2.45	2.74	3.02	3.31
1.9	0.262	2.74	3.10	3.47	3.83	4.20
2.2	0.262	3.17	3.59	4.01	4.44	4.86

6.5.1. Two-vessel configuration with open IPs

The first set of GOTHIC calculations was carried out for the two-vessel configuration (as shown in Figure 56) for conditions listed in Table 9. For Cases 1-3 the depth of the hot layer as function of the steam injection rate was obtained from HP5_3 experiment. For Case 4 hot layer thickness was reduced by reducing water pool depth and raising the sparger elevation.

Table 9. Calculation cases for two-vessel configuration with open top and bottom interconnecting pipes

#	Pool depth m	Sparger position m	Steam injection rate g/s	Hot layer thickness m	Initial water pool temperature °C
1	4	1.5	161	3.0	25
2	4	1.5	262	3.4	25
3	4	1.5	161	3.0	45
4	2.9	1.9	161	1.5	25

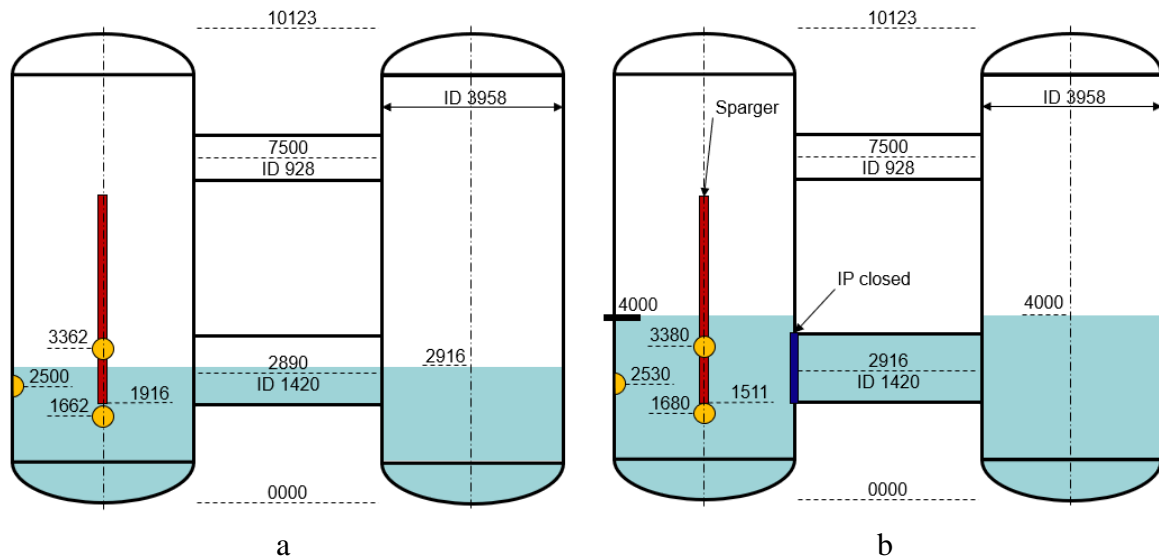


Figure 56. Calculation cases for two-vessel configuration with open IPs
(a – Case 4; b – Case 1-3)

In all cases the results were similar in that after 15000 sec pool temperature was around 60°C, gas temperature was 45-60°C and system pressure 1.2 Bar. Heat transfer from vessel 3 pool to the vessel 4 pool significantly slows down system pressurization. Furthermore, connections between the two vessels introduce counter-current gravity driven flows in a pipe that are not relevant for plant conditions, difficult to measure in the test and not easy to model. For example, when water level is within the elevation of the bottom interconnecting pipe (IP), hot water from the left vessel will flow through the IP in to the right vessel and cold water from the right vessel will flow in opposite direction. The two counter-current flows will (i) be stratified (with hot layer above the cold layer), (ii) have different velocities due to varied cross section of the IP and (iii) partially mix due to the Kelvin-Helmholtz instability. Detailed modelling of flow in the IP will be necessary to capture the dynamics of thermal stratification in both vessels. The experiment is not well instrumented for measuring details of the flow in the interconnecting pipes and modelling of the IPs is not directly relevant from the perspective of a plant accident.

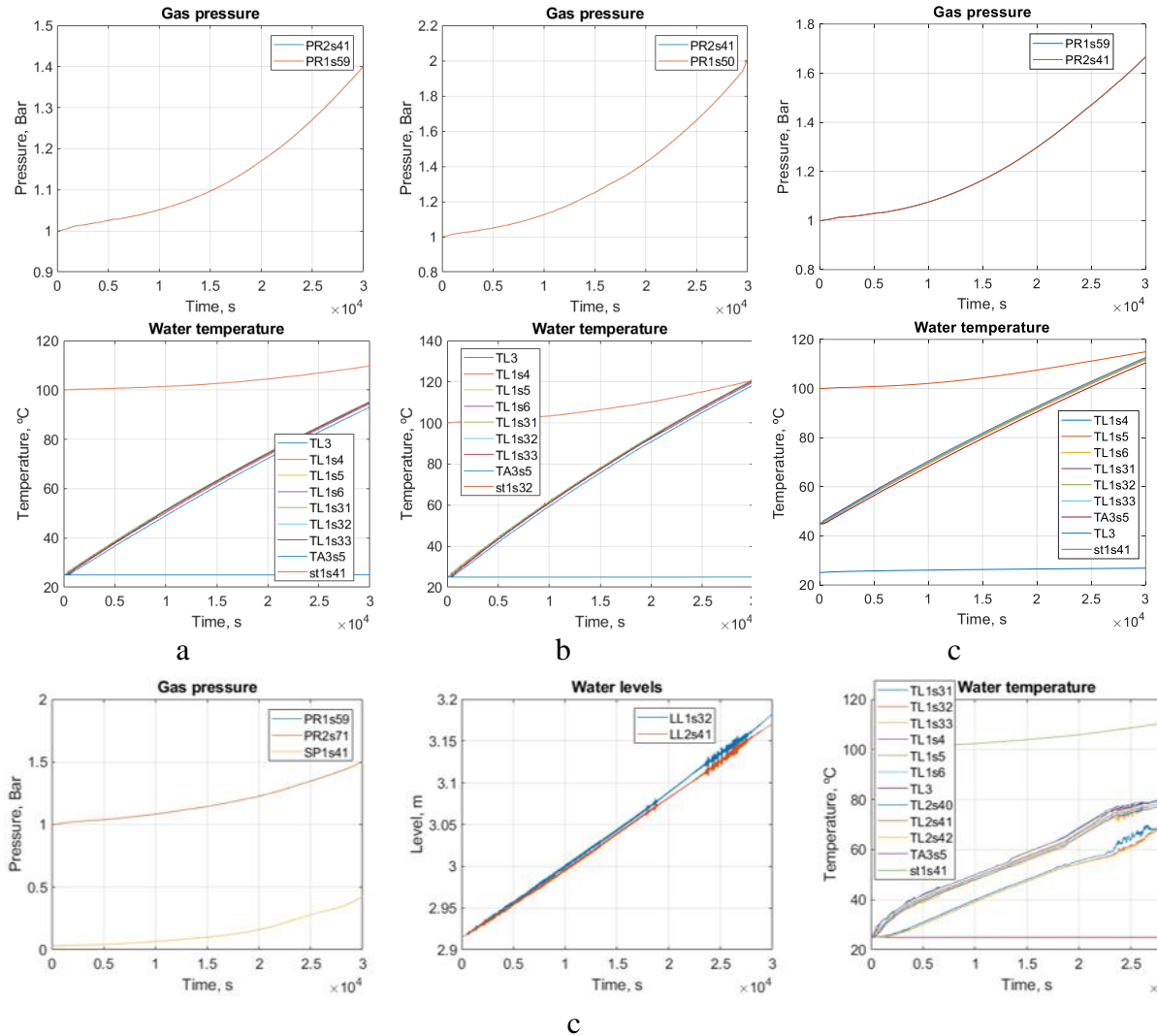


Figure 57. Calculation results for two vessel configuration with open IPs
(a – Case 1; b – Case 2; c - Case 3; d – Case 4)

Legend notation:

PR2, PR1 – gas pressure in the control volumes 2s and 1s

SP1 – saturation pressure in the control volume 1s

TL1, TL3 – water temperature in the control volumes 1s and 3

st1 – saturation temperature in the control volume 1s

LL1, LL2 – water level in the control volumes 1s and 2s

Based on the results of the first series of calculations, it was suggested that both interconnecting pipes should be closed. Instead small diameter lines (interconnecting steam line and interconnecting water line) could be introduced to balance hydrostatic pressure of the two pools and pressure in the gas space in both vessels (see Figure 58).

6.5.2. Two-vessel configuration with closed bottom IP

A second series of calculations has been carried (refer to Table 10 for the list of the most relevant cases), including 4 cases for sparger injection, 2 cases for pool preconditioning and different configurations of interconnecting pipes and interconnecting lines. The results are summarized in the following subsections.

Table 10. List of simulations carried out in the second series of calculations

Case	Steam injection	Depth			Initial water temperature	Top interconnecting pipe	Interconnecting line		Spray	
		Therm ocline	Pool	Sparger			Bot.	Top	kg/s	position
	g/s	m	m	m	°C					
C10.01	161	1	3	2.5	25	open	yes	no	-	-
C10.02	262	1.4	3	2.5	25	open	yes	no	-	-
C10.03	161	1.4	3	2.5	25	open	yes	no	-	-
C10.04	262	1.9	3	2.5	25	open	yes	no	-	-
C10.01b	161	1	3	2.5	25	closed	yes	yes	-	-
C10.02b	262	1.4	3	2.5	25	closed	yes	yes	-	-
C10.03b	161	1.4	3	2.5	25	closed	yes	yes	-	-
C10.04b	262	1.9	3	2.5	25	closed	yes	yes	-	-
C11.01	161	1	6	5.5	25	open	yes	no	-	-
C11.02	262	1.4	6	5.5	25	open	yes	no	-	-
C11.03	161	1.4	6	5.5	25	open	yes	no	-	-
C11.04	262	1.9	6	5.5	25	open	yes	no	-	-
C11.01b	161	1	6	5.5	25	closed	yes	yes	-	-
C11.02b	262	1.4	6	5.5	25	closed	yes	yes	-	-
C11.03b	161	1.4	6	5.5	25	closed	yes	yes	-	-
C11.04b	262	1.9	6	5.5	25	closed	yes	yes	-	-
C08.01	161	3	4	2.5	25	open	no	no	-	-
C08.02	161	3	4	2.5	45	open	no	no	-	-
C10.01c	161	1	3	2.5	15	closed	yes	yes	-	-
C10.02s1	262	1.4	3	2.5	25	closed	yes	yes	5	V3-top
C10.02s2	262	1.4	3	2.5	25	closed	yes	yes	1	V3-top
C10.02s3	262	1.4	3	2.5	25	closed	yes	yes	5	V3-bot
C10.02s4	262	1.4	3	2.5	25	closed	yes	yes	5	V4-top
Preconditioning 1 – hot water injection for 1h at the top of pool										
Preconditioning 2 – hot water injection for 1h at 0.5 depth										

6.5.2.1. Effect of the water pool depth

Water pool depth (assumed initially the same in both vessels) changes the volume of gas that needs to be pressurized during the test. In addition, it brings the surface of the two pools closer to each other (closer to the top interconnecting pipe or line) and consequently can increase the rate of steam transport from the hot pool in Vessel 3 to the cold pool in Vessel 4. Initial conditions for calculations performed to investigate the effect of the water pool depth correspond to the cases C10.01, C10.02, C11.01, C11.02 (refer to Table 10) with C10 referring to shallow and C11 to deep pool cases (refer to Figure 58).

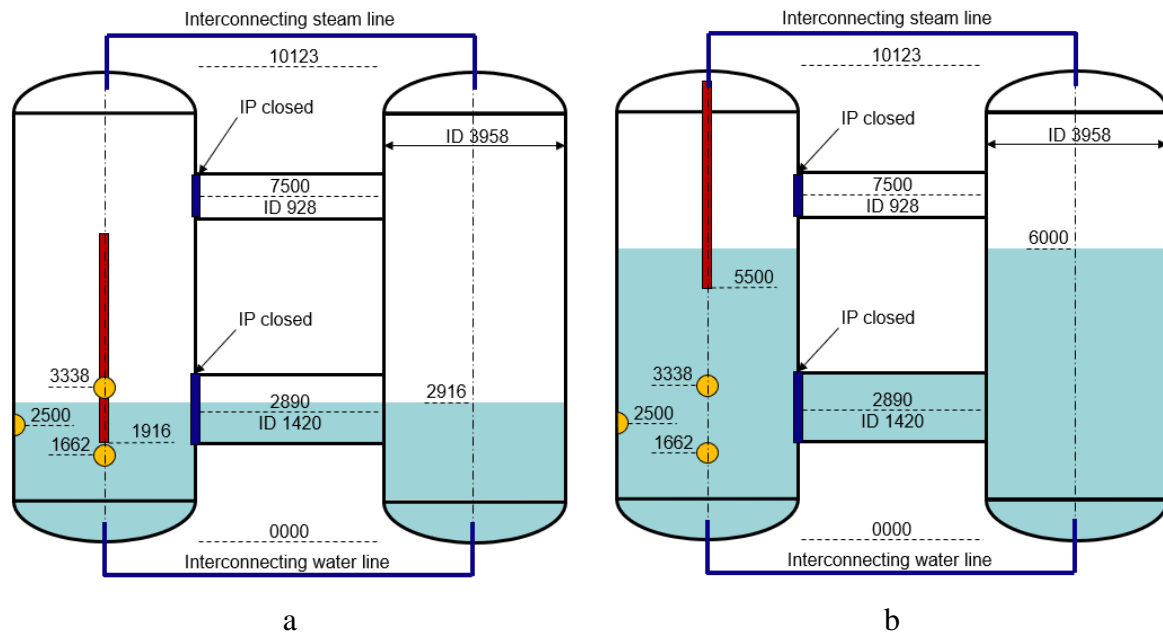


Figure 58. Calculation cases for two vessel configuration with closed IPs

In all cases sufficiently high temperatures have been established in the water pool. The initial pressure rise was found to be faster for deeper water pool cases. However, higher pressures were established in case of a shallow pool (see Figure 59). Follow-up analysis indicated that increased transport of steam in the simulations is established between the two vessels that prevented further pressurization in the case of deep water pool. Since increased transport of steam could be attributed to the used coarse mesh in the gas space a new set of calculations has been performed with refined mesh.

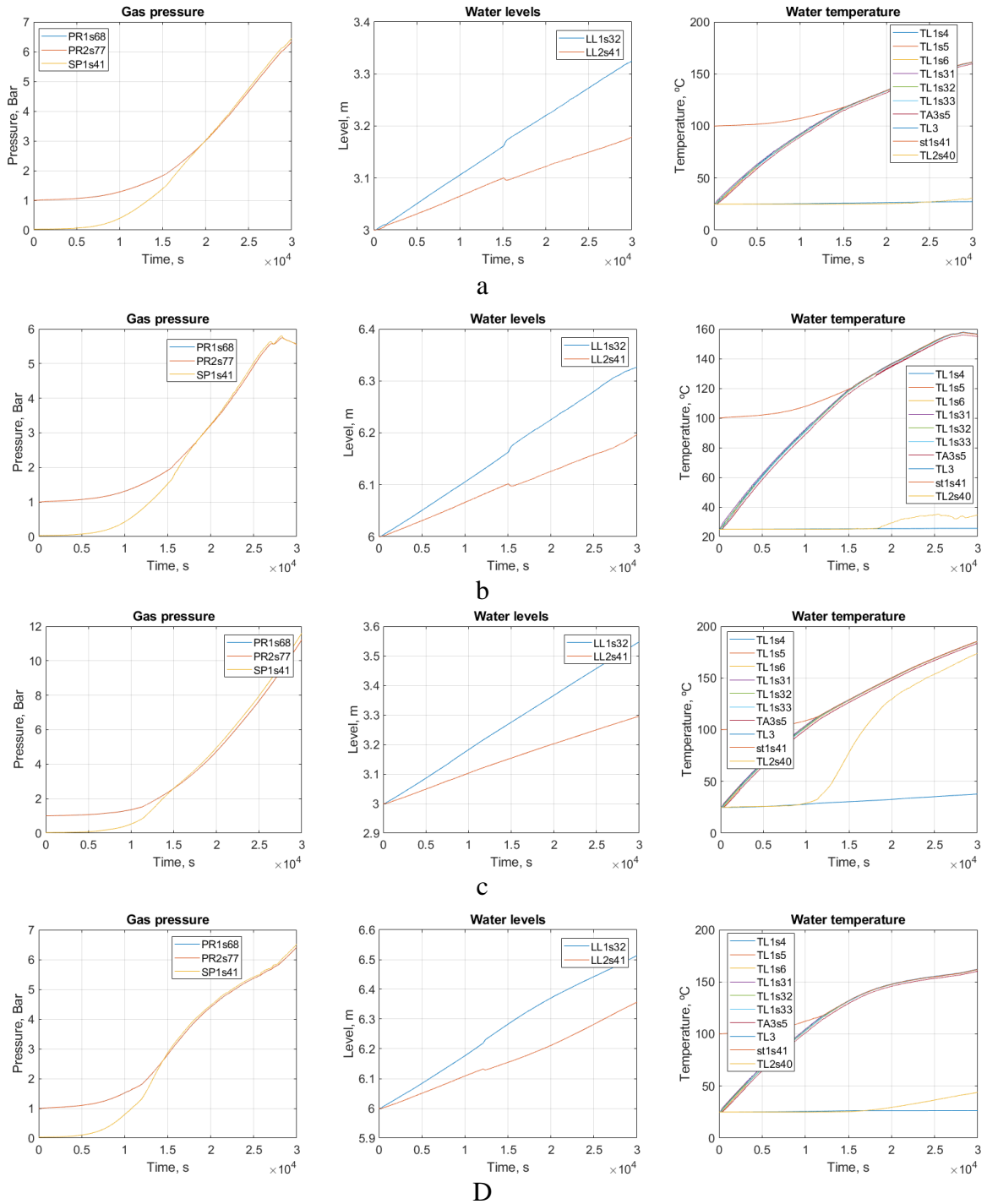


Figure 59. Calculation results for the effect of the water pool depth
(a – C10.01; b – C11.01; c – C10.02; d – C11.02)

Legend notation:

PR2, PR1 – gas pressure in the control volumes 2s and 1s

SP1 – saturation pressure in the control volume 1s

TL1, TL3 – water temperature in the control volumes 1s and 3

st1 – saturation temperature in the control volume 1s

LL1, LL2 – water level in the control volumes 1s and 2s

The results for the cases with shallow pool depth were not affected by the mesh size. However, for the deep pool with finer mesh steam transport was reduced and higher pressure was

predicted in the simulation for deep water pool (see Figure 60 for the mesh effect and compare Figure 60a vs Figure 59c (left plot)).

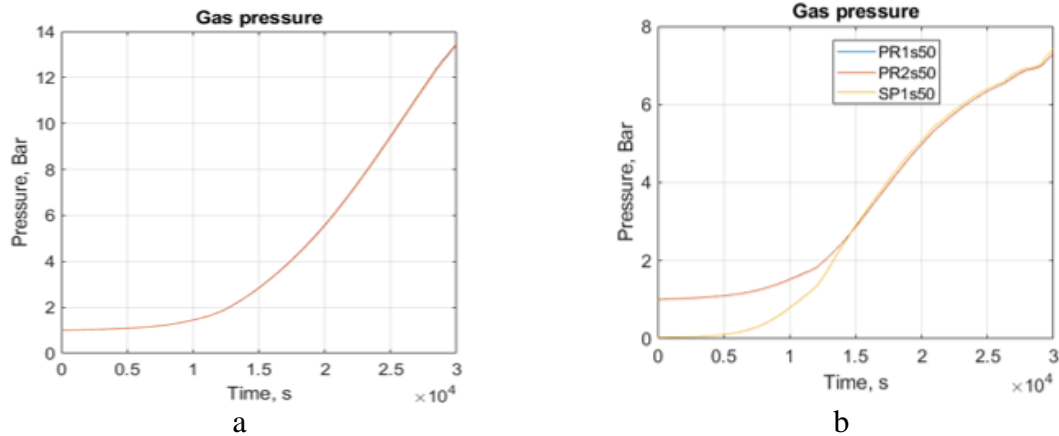


Figure 60. Effect of the mesh size for deep water pool case (a – fine mesh, b – coarse mesh)

Time required to establish 4 Bar pressure was predicted to be between 6.25h and 5.00h depending on the steam flow rate, the effect of the water pool depth was found to be less important with deep pools providing 20-30 min advantage.

6.5.2.2. Effect of initial water pool temperature

Lower initial water temperature can facilitate thermal stratification, i.e. increase the stability of the cold layer to erosion due to larger density difference between the hot and cold layers. Two simulations have been carried out with shallow water to investigate the effect of initial water pool temperature on pressurization. It was found that reduction of initial pool temperature from 25 °C to 15 °C has a penalizing effect on the pressurization. At 20 000 sec pressure in the initially colder pool was 0.5 Bar lower than that in the initially hotter pool. The difference is increased to about 0.7 Bar at 25 000 sec (see Figure 61). The effect of the initial water pool temperature is likely enhanced by the initial temperature of the test section walls (which at the start of the calculation is assumed equal to the initial water pool temperature). The time delay due to reduction of the initial pool temperature from 25°C to 15°C is about 2250 sec.

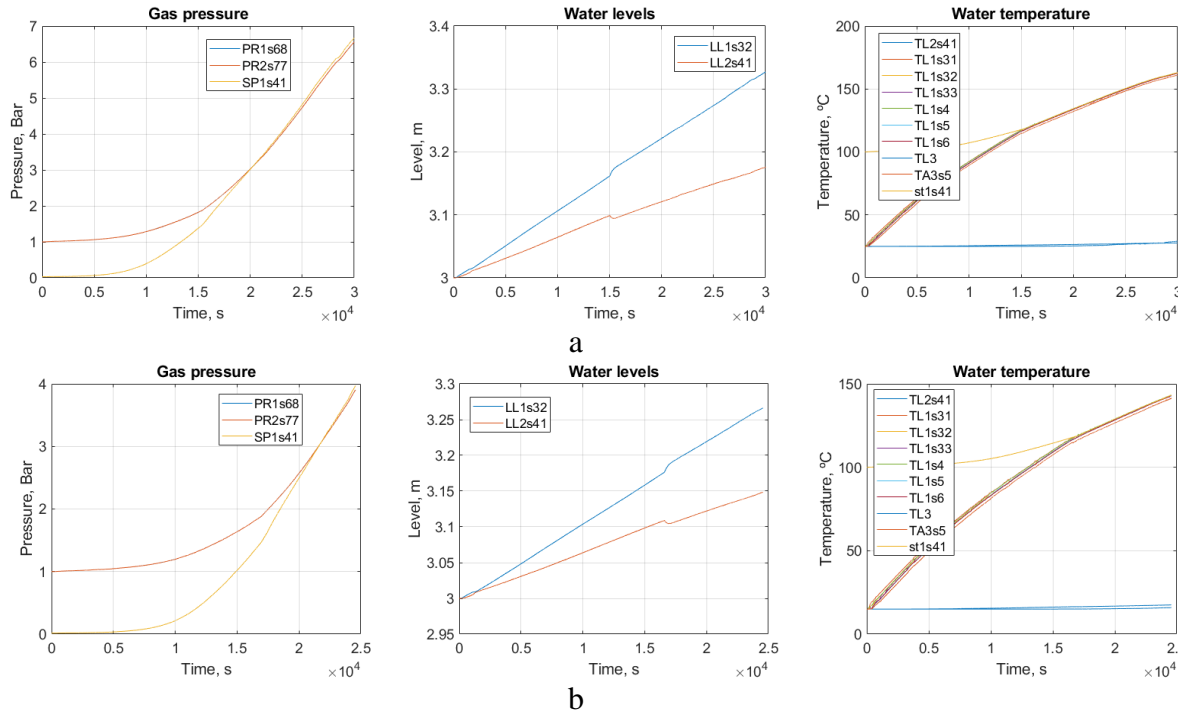


Figure 61. Calculation results for the effect of the initial water pool temperature
(a – Case 10.02b initial temperature 25°C; b – Case 10.01c initial temperature 15°C)

Legend notation:

PR2, PR1 – gas pressure in the control volumes 2s and 1s

SP1 – saturation pressure in the control volume 1s

TL1, TL3 – water temperature in the control volumes 1s and 3

st1 – saturation temperature in the control volume 1s

LL1, LL2 – water level in the control volumes 1s and 2s

6.5.2.3. Effect of the hot layer thickness

The location of the thermocline below the sparger on the distance from the sparger head and is determined by the competition between the density difference between cold and hot water layers and the effective momentum generated by condensing steam, which depends on parameters such as water temperature and steam flow rate.

Implemented in this work model does not directly simulate effective steam momentum, using instead a fixed hot layer depth to represent the effect of partial pool mixing. We used this model to investigate the effect of the hot layer thickness on the pressurization. The effect was studied for both shallow and deep-water pools. The results of the simulations are summarized in Figure 62.

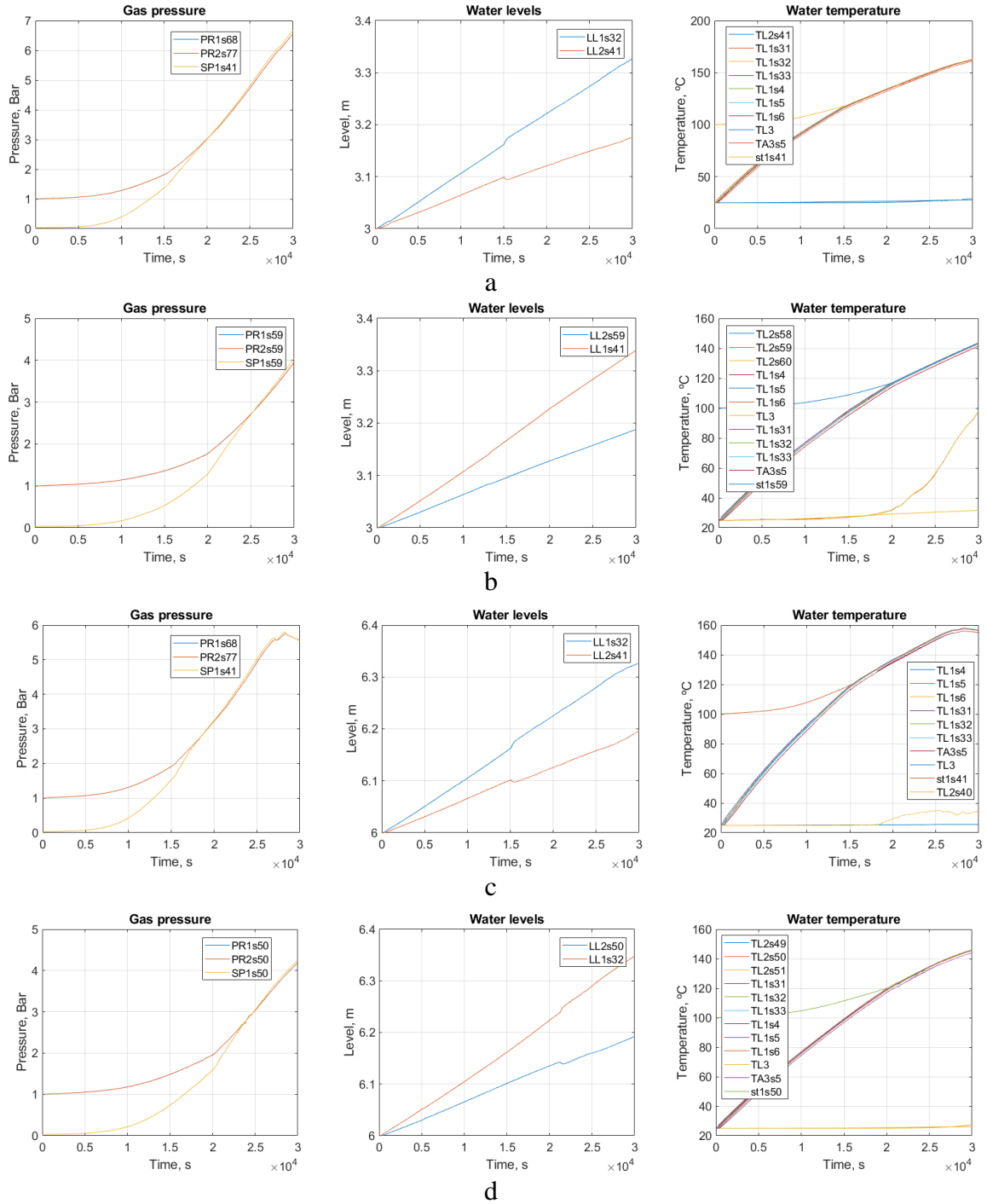


Figure 62. Calculation results for the effect of the water pool depth
(a – C10.01b; b – C10.03b; c – C11.01b; d – C11.03b)

Legend notation:

PR2, PR1 – gas pressure in the control volumes 2s and 1s

SP1 – saturation pressure in the control volume 1s

TL1, TL3 – water temperature in the control volumes 1s and 3

st1 – saturation temperature in the control volume 1s

LL1, LL2 – water level in the control volumes 1s and 2s

It was found that reducing the depth of the hot layer from 1.4 m to 1.0 m almost doubles the rate of pressure rise making this parameter the most influential among all considered in this study. For instance, the time required to reach 4 Bar pressure in case of a shallow water pool

would be reduced from 8.3h to 6.25h if hot layer thickness could be sustained at 1m instead of 1.4.

High sensitivity of the pressure to the thickness of the hot layer suggests that proposed experimental configuration is well suited for validation of the effective momentum source models and the effect of pool stratification/mixing on containment pressurization.

6.5.2.4. Effect of steam injection rate

Experimentally it is not possible to study separately the effect of the steam injection rate from other parameters. Change in the steam injection will change the effective momentum [4, 12, 15] and consequently the erosion rate of the cold layer. Two simulations have been carried out with different injection rates (161 and 262 g/s) and consequently different thermocline positions (1.0 and 1.4 m respectively – values obtained in HP5 series for given steam injection rates). The effect appeared to be comparable to the effect of hot layer thickness. Increase in the steam injection from 161 to 262 g/s almost doubled the rate of pressure rise (clarify Figure 63).

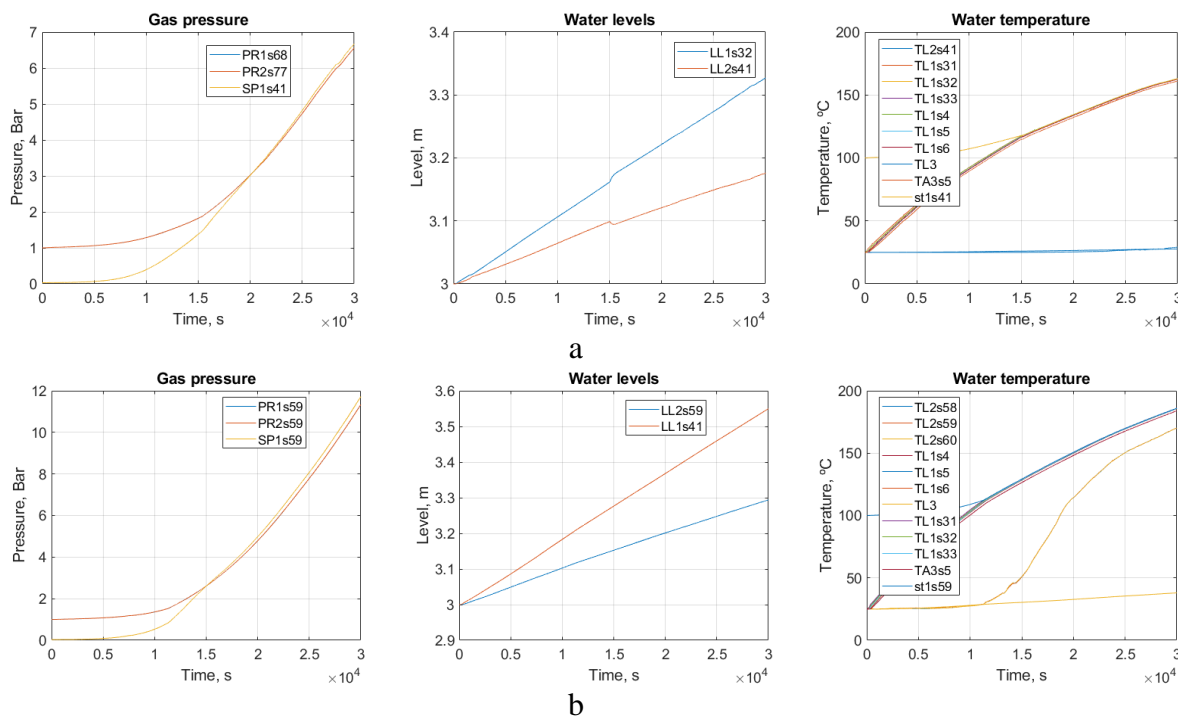


Figure 63. Calculation results for the effect of the initial water pool temperature
(a – Case 10.01b; b – Case 10.02b)

Legend notation:

PR2, PR1 – gas pressure in the control volumes 2s and 1s

SP1 – saturation pressure in the control volume 1s

TL1, TL3 – water temperature in the control volumes 1s and 3

st1 – saturation temperature in the control volume 1s

LL1, LL2 – water level in the control volumes 1s and 2s

6.5.2.5. Effect of nozzle spray location

Investigation of the effect of spray on the depressurization of the vessels is planned in the H2P4 series. In the pre-test analysis we studied effects of (i) water mass flow rate on the rate of depressurization and (ii) spray nozzles location (refer to Figure 64).

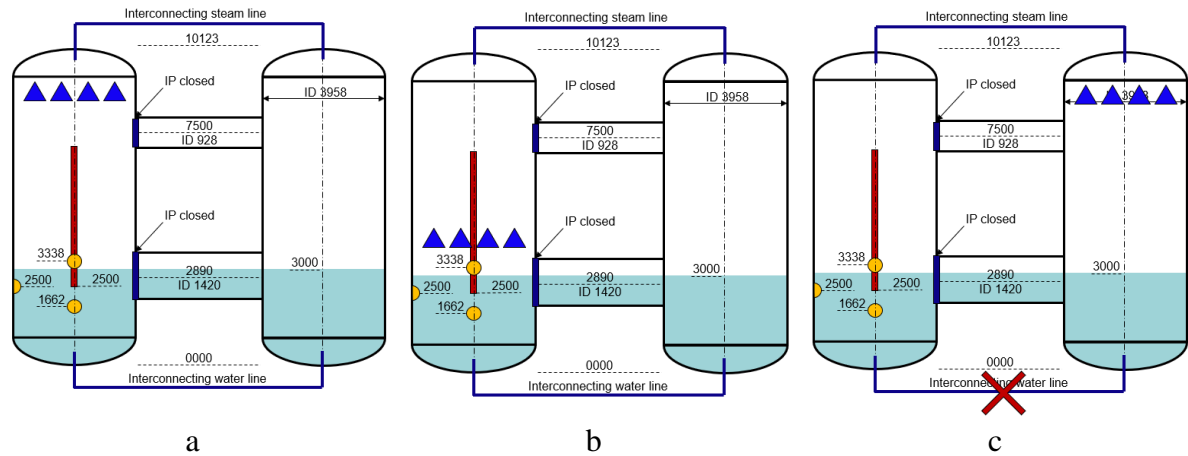


Figure 64. Simulated configurations of spray nozzles in the PANDA facility
(a – spray at the top of vessel 3; b – spray above the water level of vessel 3; c – spray at the top of vessel 4)

It was found that moving spray nozzles down to the water surface had marginal effect on system depressurization (at least at 5 kg/s of water supply to sprays). Depressurization might be dominated by the surface temperature of the water pool (see Figure 65a and b). The data further shows that shortly after spray activation system pressure rises above the saturation pressure causing volumetric condensation of steam and depressurization.

Placing spray into the vessel 4, i.e. above the cold-water pool produced counter intuitive result, i.e. depressurization rate was similar to the case where sprays were located above the hot water pool. However, the mechanisms of depressurization appeared to be different. In case when sprays are in vessel 3 depressurization is driven by cooling of the hot pool, and gas pressure is above saturation pressure. In case when sprays are in the cold vessel the pressure drops due to increased evaporation from the hot pool and gas pressure is below the saturation pressure (compare Figure 65b and c). From experimental point of view, system pressure rapidly falling below saturation point may lead to volumetric boiling of the hot pool potentially endangering instrumentation.

System depressurization appeared to be most sensitive to the water mass flow rate of spray water. At 5 kg/s of coolant flow rate the system pressure reduced by 92% within 1h, at 1kg/s only 16% reduction was established within the same period (compare Figure 65a and d).

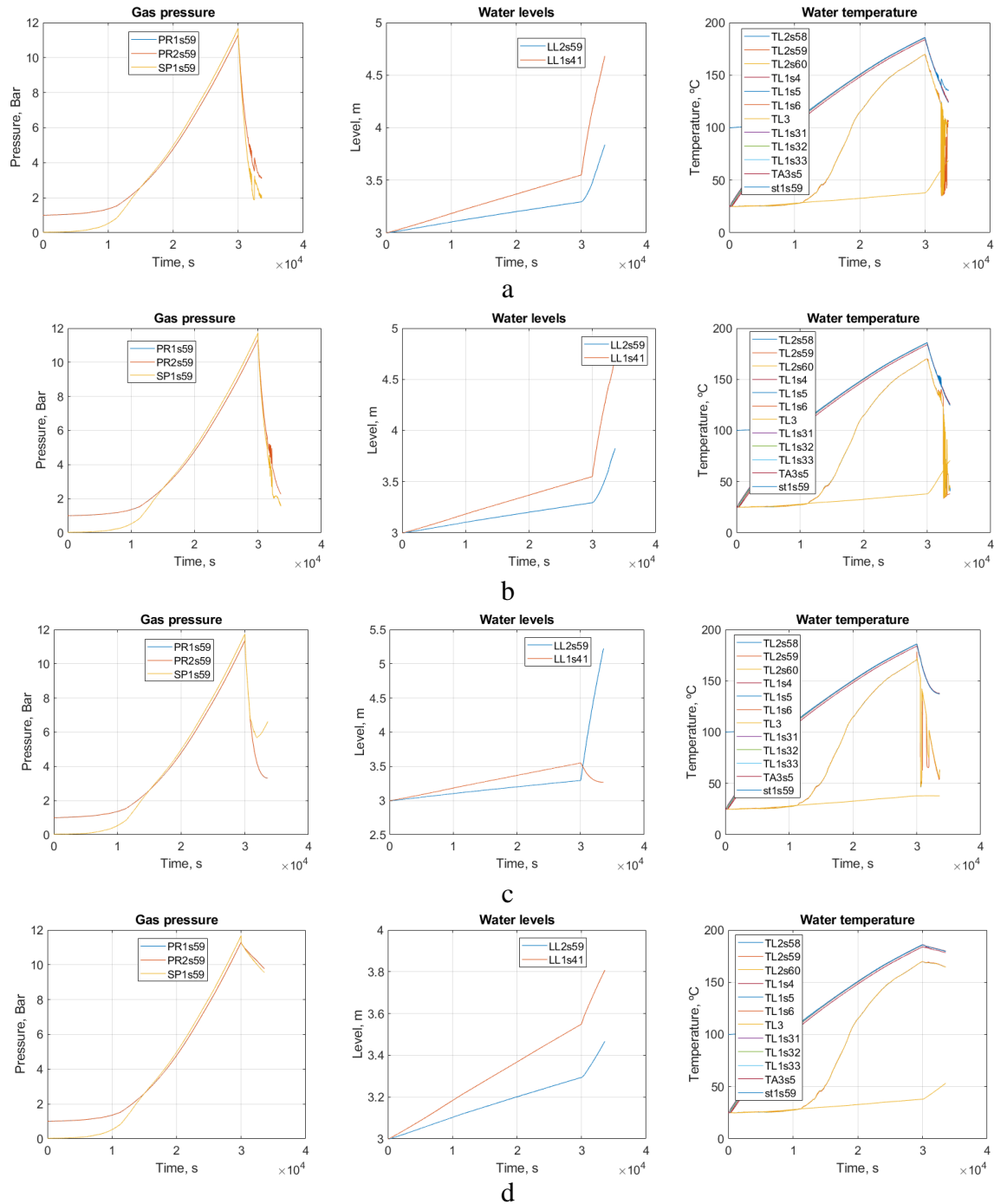


Figure 65. Calculation results for the effect of spray nozzles elevation
(a – Case 10.02s1; b – Case 10.02s3; c – Case 10.02s4; d – Case 10.02s2)

Legend notation:

PR2, PR1 – gas pressure in the control volumes 2s and 1s;

SP1 – saturation pressure in the control volume 1s;

TL1, TL3 – water temperature in the control volumes 1s and 3s;

st1 – saturation temperature in the control volume 1s

LL1, LL2 – water level in the control volumes 1s and 2s

6.5.3. Pool preconditioning

To reduce overall duration of the experiment and thus providing more time for observation and measurement of more important phenomena two pool preconditioning procedures were suggested and simulated. Both procedures aim at artificial development of stratified pool by injection of hot water during filling procedure.

The first option includes the following (Procedure #1):

- connect vessel 3 and vessel 4 using bottom interconnecting line
- establish cold water pool in both vessels with water level according to H2P4 test conditions
- for the period of 3600 s:
 - inject hot water (95°C) just under water surface at a rate of 5 l/s and simultaneously
 - remove cold water from the bottom of the pool at a rate of 5 l/s

This procedure will allow to establish hot water layer at the surface of the cold pool and gradually extend the hot layer downwards. Simulation of this procedure predicted an hour reduction of the experiment duration if the hot water could be prepared in advance. Results of the simulation are shown in Figure 66.

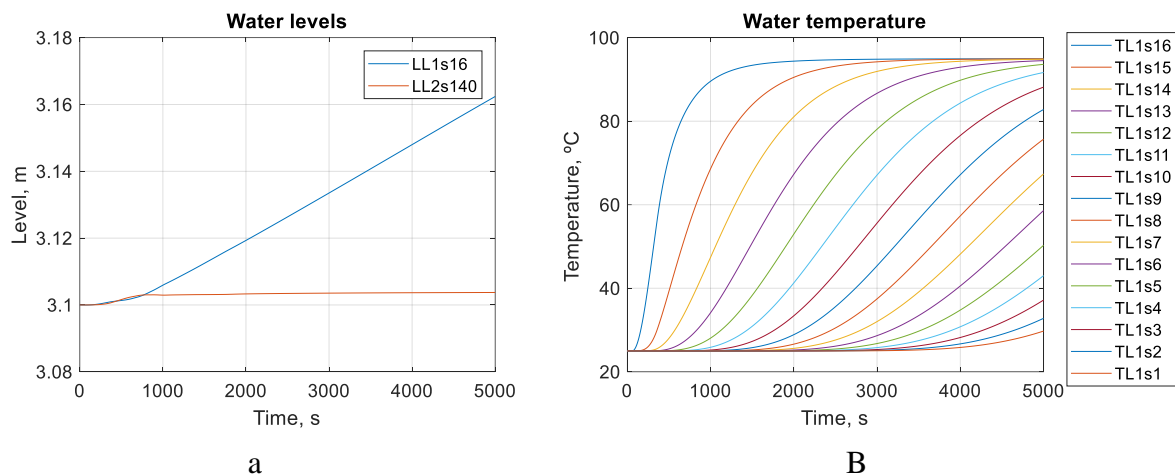


Figure 66. Pool heat up during filling procedure #1 (a – water level, b – temperature evolution)

The second option is based on the following (Procedure #2):

- connect vessel 3 to the vessel 4 at the bottom using interconnecting line
- establish cold water pool in both vessels with water level 0.5 m below H2P4 test conditions
- for the period of ~3600 s:
 - Inject hot water (95°C) at the initial pool level at a rate of 5 l/s
 - Stop injection when water level reaches H2P4 predefined level
 - water level can be adjusted by supplying or removing cold water into / from vessel 4

Since hot water injection will create momentum, some mixing with cold layer may occur. Also injection into a pool while level gradually increases will create a temperature gradient resulting in the pool temperature profiles shown in Figure 67.

While both procedures will reduce experiment time, their implementation might meet difficulties from practical perspective. It should be noted that Procedure #2 requires much less control over the supply of hot and cold water and therefore can be easier to implement.

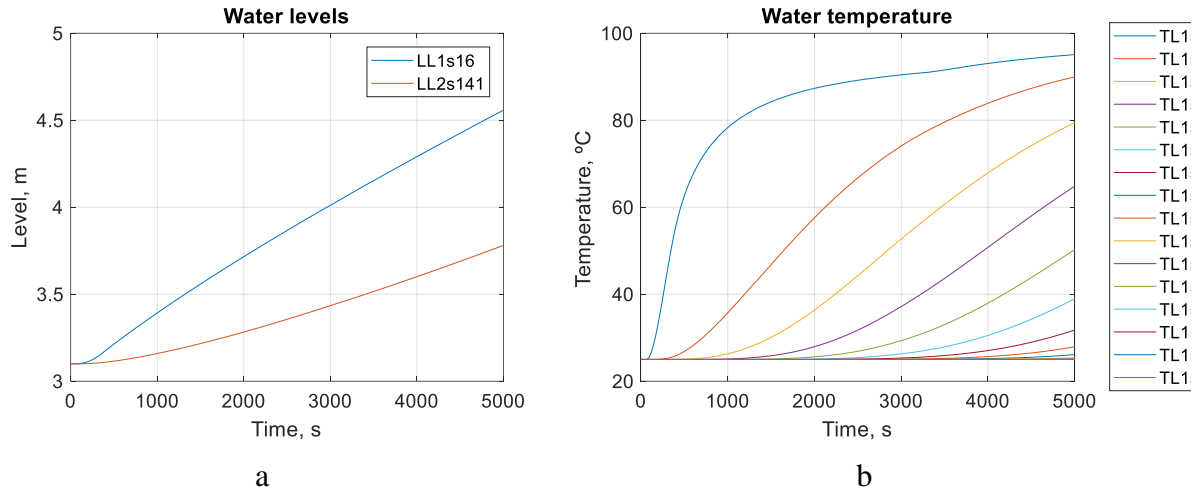


Figure 67. Pool heat up during filling procedure #1 (a – water level, b – temperature evolution)

6.6. Summary of H2P4 scoping analysis

In shallow water pool configuration, opened bottom interconnecting pipe, can significantly increase time for pressurization caused by additional amount water that will be heated up in the second vessel. Two most influential model input parameters are steam injection rate, hot layer thickness and spray water injection rate. Experimentally, only steam and water injection rates can be controlled, actual hot layer thickness is not known for high-pressure high-temperature conditions.

The characteristics times to reach 4 Bar pressure are in the range between 23000-30000 sec for 161 g/s and between 17000 to 24000 for 261 g/s. It was further predicted that those times can be reduced by ~3600 s if a special procedure for water pool preheating is performed.

Furthermore, opened top and bottom IPs in the experiment will introduce counter-current two-phase flows that will be difficult to measure and model, suggesting that both IP should be closed.

System pressurization is sensitive to the depth of the hot layer. Initial water position at 0.5 m above the sparger head would be desirable. However, more intensive erosion of the cold layer may occur if the hot layer is too thin to dissipate momentum. In addition, reduced sparger submergence may increase the likelihood for steam bypass (incomplete condensation in the pool). A pre-test could be useful to clarify these phenomena.

Comparison of shallow and deep water pool configuration suggests that deep water pool provides faster pressurization and in addition is a “safer” choice for maintaining the

thermocline during the whole transient. There is no data on the behavior of the stratified pool when steam is injected into near saturated water in in-stable condensation regime. Loss of stratification will make any other stage of the test (except for spray activation) meaningless.

As a result of the analysis four options have been developed for the test configuration. Those are currently under consideration by the PANDA experimental team. From phenomenological perspective the best configuration is a deep pool setup with closed interconnecting pipes, opened top and bottom interconnecting lines. Steam injection at 262 g/s and sparger submergence 1 m. Sprays should be located above the pool surface to separate effect of steam condensation on the surface of the pool over steam condensation in the gas space above.

At present time several concerns have been raised by the experimentalist and scoping simulations. First is the possibility of rapid pressure rise during sparger actuation due to the water evaporation from the hot walls of the vessel 3. Such situation may lead to the rupture of pressure safety diaphragm or operator opening of venting valve. Both will disrupt the experiment. Another concern is possibility of volumetric boiling in the pool upon spray activation. Due to the rapid cooling and condensation in the gas space the system pressure may fall below the saturation point and promote rapid pool expansion. This may lead to the damage of instrumentation in the pool and disrupt the spray injection phase of the H2P4 test. Both issues are currently being investigated.

7. Analysis of SEF-POOL tests

7.1. Motivation and background

SEF-POOL is a separate effect experimental facility build and operated at LUT (Finland) for measurement of the effective momentum generated by direct condensation of steam in a water pool and investigation of the relevant physical mechanisms. Specifically, the facility is used to experimentally determine a relation between a theoretical momentum rate M_{th} of steam and effective momentum rate M_{eff} developed in water induced by the injected steam:

$$M_{eff} = CM_{th} = C\rho_s A_0 U_s^2,$$

where ρ_s is steam density; A_0 nozzle cross-section; and U_s steam velocity at the nozzle outlet; C is a proportionality coefficient that can be a function of different parameters including steam mass flux or Mach number, water pool subcooling, steam superheat, nozzle geometry, etc.

The ultimate goal of the experiments at the SEF facility is to provide data for the development of EMS model for prediction of the time-averaged momentum generated by steam injection through sparger in pressure suppression pool of a nuclear reactor in sonic and subsonic regimes. The EMS model introduces (time averaged) momentum source that creates a single phase liquid jet with specific characteristics such as (i) effective momentum, (ii) centerline velocity, and (iii) two-dimensional expansion ratio. The centerline velocity U_c can be related to the jet expansion using momentum conservation equation for an expanding circular jet:

$$U_c(x) = U_0 \frac{d_0}{x - x_0} B$$

where U_0 is jet inlet velocity at initial centreline position x_0 ; d_0 is initial jet injection diameter; x is centreline coordinate; and B is proportionality coefficient or jet decay rate.

The jet initial velocity can be deduced from the measurement of the momentum rate in the SEF-POOL facility. Coefficient B is not known for a jet induced by steam injection but is related to the jet entrainment rate E :

$$B = \frac{\pi d_0 \rho_l U_0}{2E}$$

The jet entrainment rate E is defined as the rate at which the volumetric flux (within the jet cross-section) grows with distance x due to the entrainment of the surrounding liquid.

Entrainment rate can be deduced from the velocity field around the jet. Measurement of the flow velocity was suggested by KTH for the new tests in SEF-POOL facility. The following sections describe the status of the experimental and analytical work carried out to measure effective momentum and entrainment generated by condensing jet and estimate velocity field in the vicinity of the jet.

7.2. Experimental setup

The schematic of the experimental setup is show in Figure 68. It consists of a test section with 0.4x0.5x1.2 m water pool and an injection nozzle for steam supply. The nozzle is positioned in

the middle of the pool on a rotating pipe. During steam injection, the force exerted on the pipe / nozzle is measured using a force sensor located on an external rigid frame and connected to the rotating pipe using a steel rod. The experimental facility is instrumented with thermocouples to measure water and steam temperature, vortex flow meter to measure the steam mass flux and pressure transducers inside the steam line and water pool.

A fast video camera is used to record the process of steam injection and condensation inside the pool through one of the two Plexiglas windows at the sides of the test section. During the test, the condensation process is periodically recorded at different water pool temperatures. Each recording is performed at ~6000 fps for a period of 0.25-0.50 s.

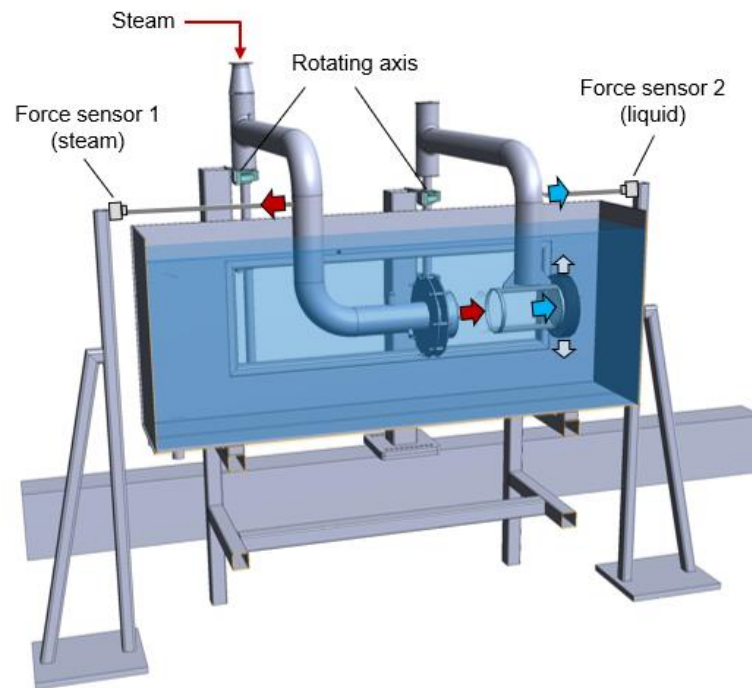


Figure 68. SEF-POOL test facility

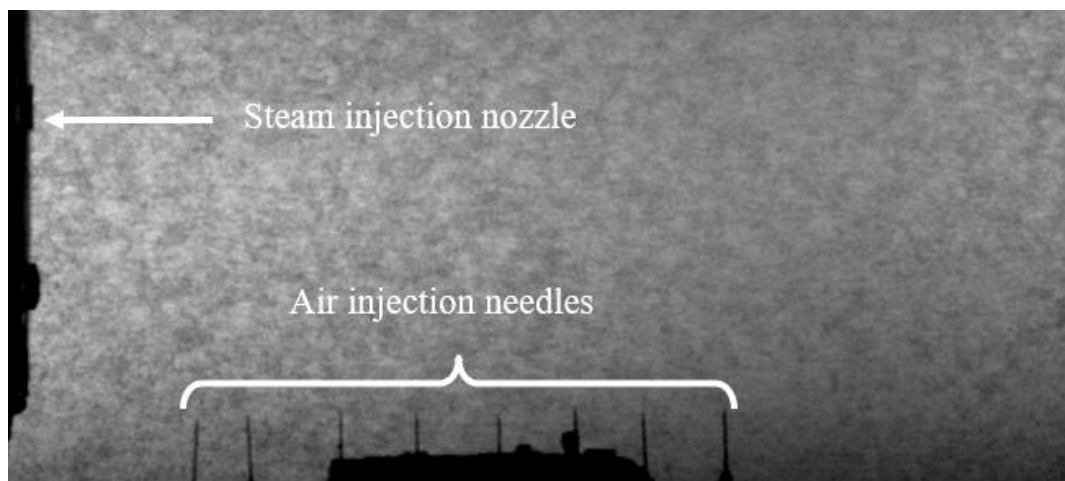


Figure 69. Gas injection needles

To measure the flow velocity around the condensing jet, it was suggested to track movement of gas bubbles inside the pool. Two modifications to the experimental setup were introduced:

1. Eight needles (ID 0.2mm) connected to a collector have been placed at the bottom of the test section pool underneath the steam condensation region. The nozzles were positioned in the plane of the jet. The pitch between the needles is 15-18 mm. Compressed air supplied into the collector will flow through the needles and generate $\sim \varnothing 2$ mm bubbles inside the pool (see Figure 69).
2. Two fast video cameras were placed in front of the test section side window for stereoscopic video recording of the pool. The cameras would film the same region of view from two different angles (see Figure 70); the two video recordings are used for triangulation and 3D tracking of individual bubbles in the flow. The stereo imaging is needed to track bubbles position relative to the jet.



a



b

Figure 70. Snapshots of the stagnant pool from left (a) and right (b) cameras

The method would require first to measure characteristic bubble velocity in a stagnant pool and then use it as a reference for the estimation of the flow velocity in a pool with condensing jet.

7.3. Entrainment rate analysis

7.3.1. Image calibration and error analysis

Testing stereoscopic setup has been carried out at KTH in conditions similar to the potential setup at LUT. Mapping of distances between the cameras, error in image analysis and respective error in the estimation of depth was obtained (see Figure 71). Results suggested that optimal distance between the cameras is in the range between 350 to 550 mm, further increase in the distance is not likely to improve image accuracy and will make it difficult to correlate objects between the two video footages. Specific recommendation for alignment, distance between the cameras and image calibration procedure were then provided to LUT.

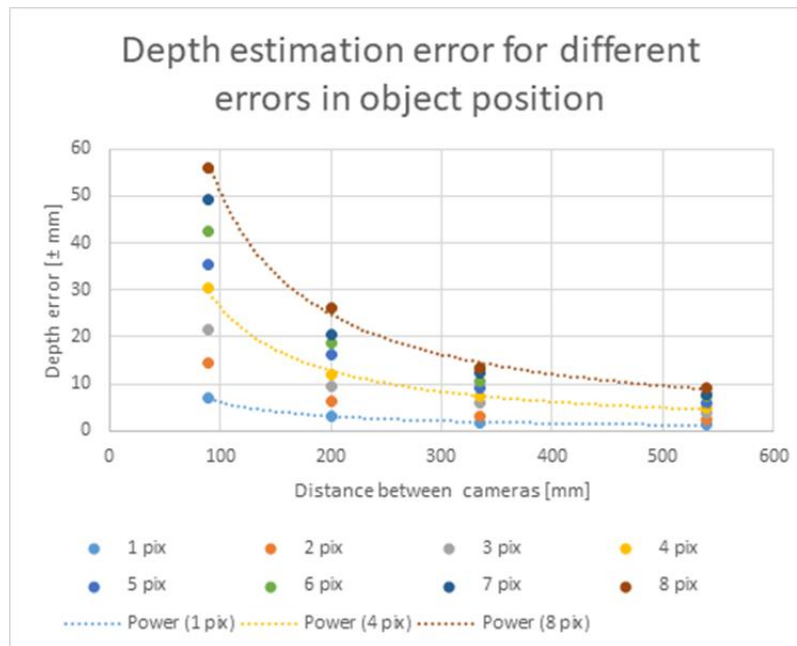


Figure 71. Error in depth estimation as a function of distance between the cameras

The stereoscopic imaging calibration was carried out using >160 pair of snapshots of a checkerboard plate inside the water pool. The results of the calibration and estimation of the reprojection error are shown in Figure 72. The mean reprojection error appeared to be <0.5 pix, which is sufficient for our application.

Uncertainty in 3D position of the bubble is expected to be dominated by the error in the estimation of the bubble position in the video images. The components of the maximal error vector (i.e. vector between the actual bubble position and the estimated one) resulting from random sampling of point location within given ranges of image error are listed in Table 11. For an average bubble diameter of 2-3 mm an image error in bubble position is not likely to exceed ± 0.7 mm. This corresponds to a maximal error vector with magnitude of 3.11 mm and for the vertical component of the position ± 0.68 mm.

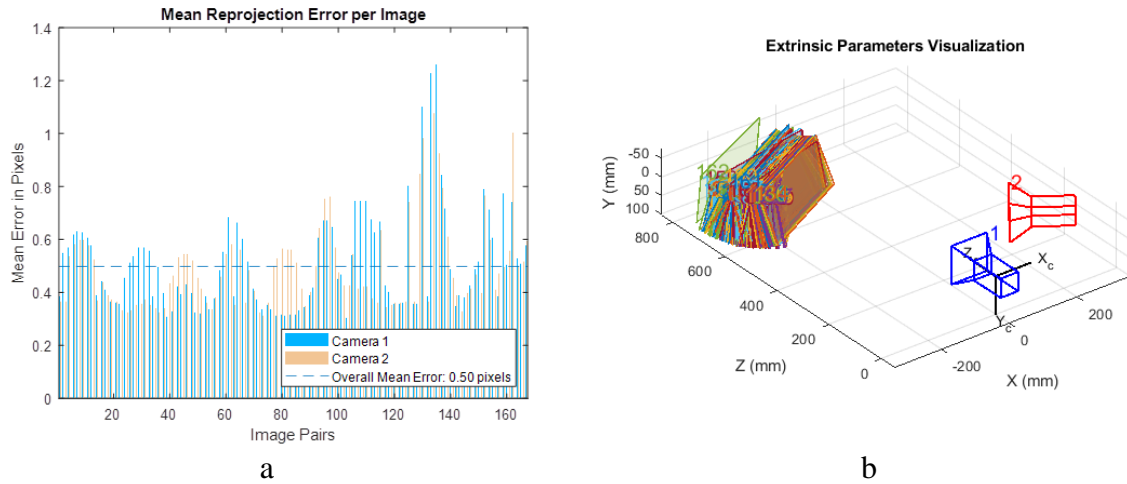


Figure 72. MATLAB generated figures for mean reprojection error (a) and visualization of extrinsic parameters (b)

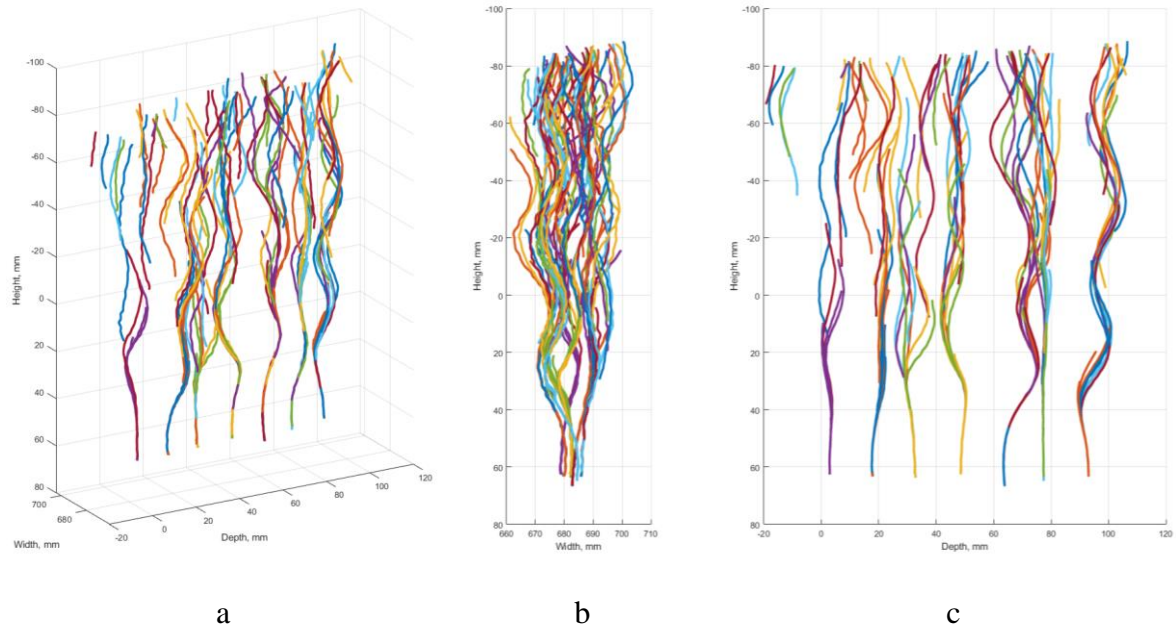
Table 11. Error assessment for bubble triangulation

Error in image coordinates		Error in world coordinates [*]			
Col, Row [pix]	Col, Row [mm]	Z, mm	Y, mm	X, mm	Magnitude
± 1	± 0.34	± 1.28	± 0.39	± 0.79	1.55
± 2	± 0.69	± 2.60	± 0.68	± 1.57	3.11
± 3	± 1.03	± 3.70	± 1.23	± 2.33	4.54
± 4	± 1.38	± 4.98	± 1.50	± 2.90	5.95
± 5	± 1.72	± 6.05	± 1.90	± 3.88	7.43
± 6	± 2.07	± 6.92	± 2.53	± 4.20	8.48

^{*}Refer to coordinate system in Figure 3b

7.3.2. SEF stagnant pool

A video of bubbles rising in a stagnant pool has been recorded in SEF-POOL facility. The recording was done at 6300 fps for a period of 261 ms. The snapshots of the first frame from left and right cameras with superposition of coordinates of the tracked bubbles are shown in Figure 74. Table 11 Results from the 3D triangulation of 146 bubbles are shown in Figure 73.



a b c
Figure 73. Trajectories of 146 bubbles in stagnant pool
(a – isometric projection; b – ZY projection; c – XY projection)

Upon detachment from the needle each bubble for ~40 mm follows a trajectory characteristic to the needle by which the bubble is generated. The difference in the initial trajectories seems to be due to the different orientation of the needles (which are cut at some angle at the top). Once the memory of the “origin” effect is gradually lost in random fluctuations, all bubbles follow more stochastic helicoidal paths. During the rise all bubbles remain within the vicinity of vertical central plane of the jet.

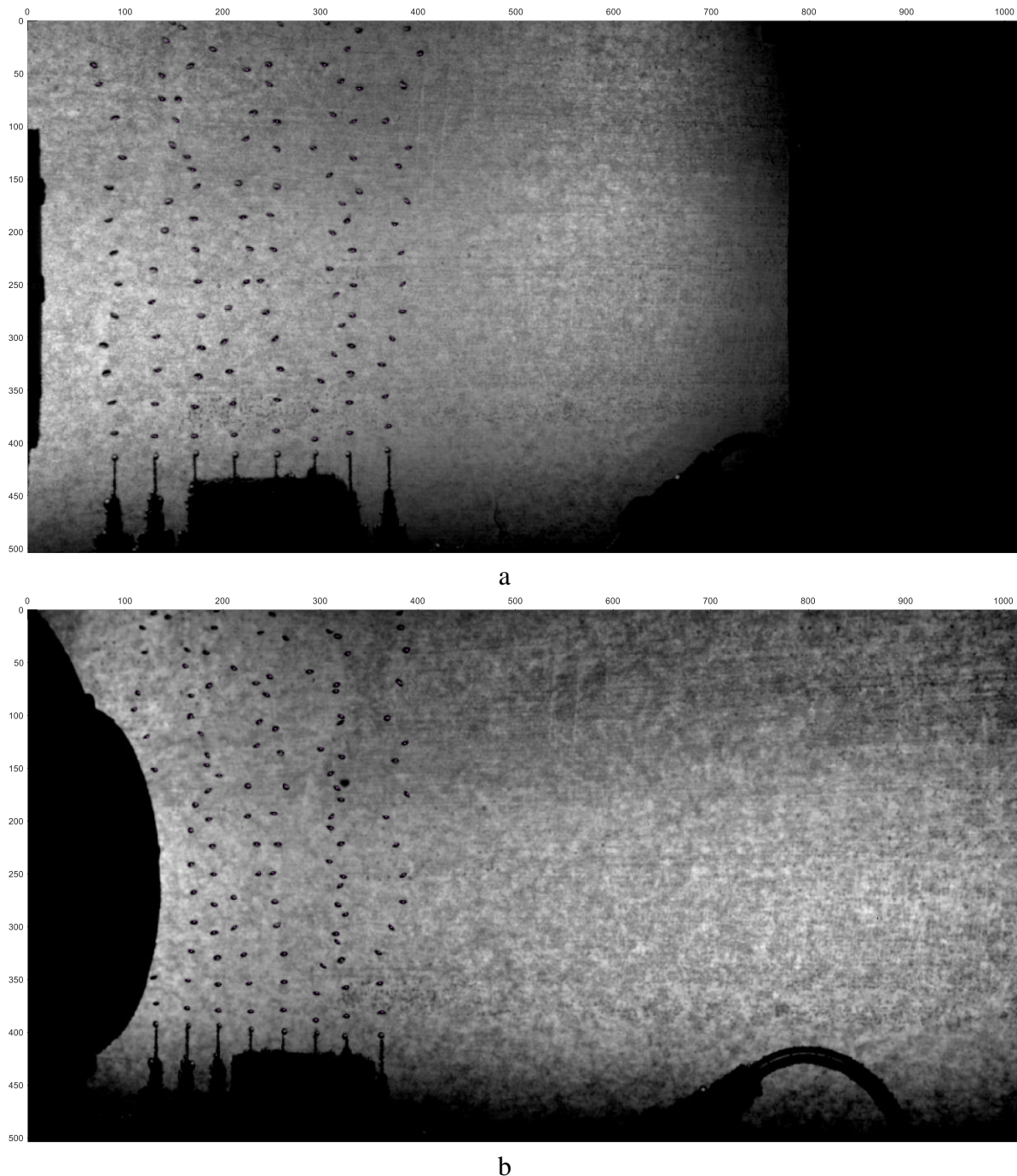


Figure 74. Snapshots of bubbles in a stagnant pool
(a – left camera; b – right camera)

The results of the estimation of the vertical velocity component for bubbles originating from several needles and covering the distance from release till the steam ejection nozzle are shown in Figure 75. The magnitude of the velocity vector shows periodic oscillations, which are attributed to the periodic oscillation of bubbles shape. In the range between 60 to 15 mm bubbles velocities reproduce each other well. Difference is mainly between the nozzles. The average (expected) value of the vertical velocity component from the full history of 146 bubbles is 0.322 m/s.

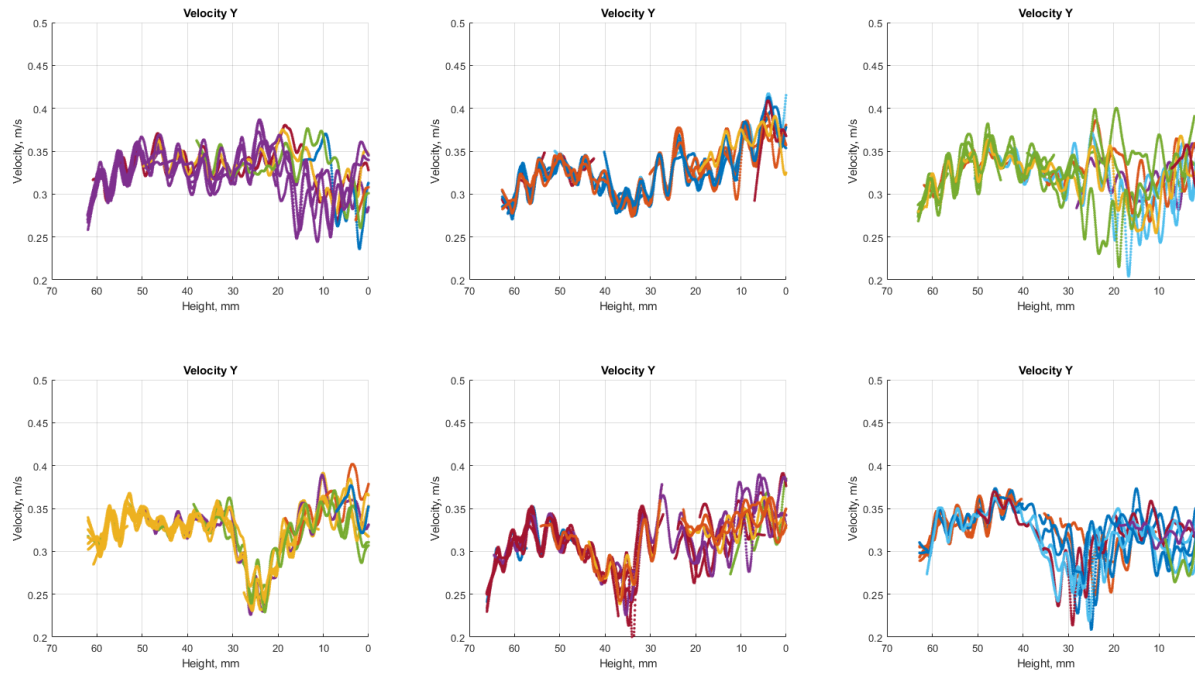


Figure 75. Vertical velocity component from different nozzles.
(zero in the abscissa corresponds to the elevation of the nozzle)

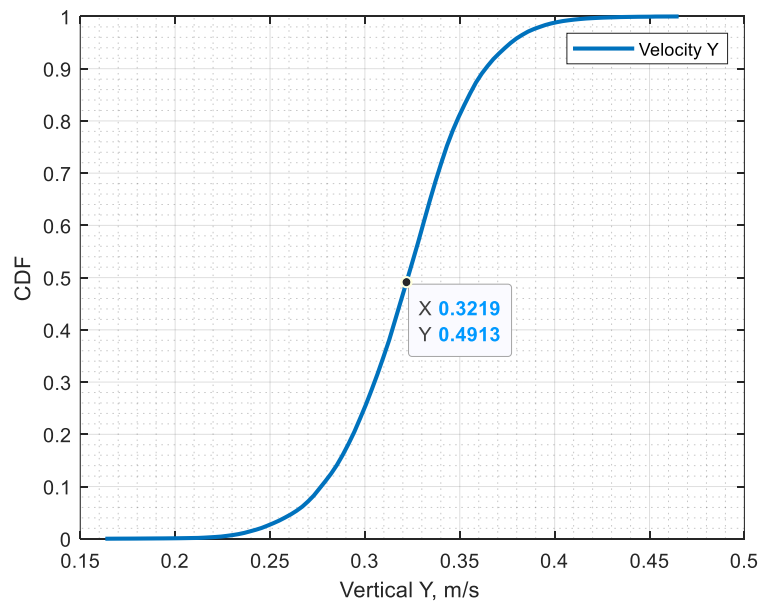


Figure 76. Cumulative distribution of the vertical velocity component

7.3.3. Discussion of the results

Image analysis of bubble trajectories inside a stagnant pool show some promising results. The bubbles can be tracked and their 3D trajectory and velocity vectors can be estimated with sufficient accuracy. However, the data suggests that few issues should be addressed for measurement of the fluid flow velocity and estimation of the entrainment rate:

- There is a periodic variation of the bubble velocity. This phenomenon is likely to be due to the oscillation of the bubble shape. Such oscillations can be suppressed if smaller bubbles could be generated. Several solutions are currently investigated:
 - Change the shape and/or diameter of the bubble injection needle.
 - Increase wettability at the needle tip by applying a hydrophilic coating. The aim is to achieve earlier pinch-off and detachment of the bubble. Possible caveats are stability of the introduced coating during steam injection and variation in the bubble sizes and respective terminal velocity.
 - Reduce surface tension of the liquid in which bubbles are released. A possible solution is to install a sleeve around each needle filled with oil. One may expect 2-10 times reduction in the surface tension and respective reduction in the bubble size. Possible caveats are (i) bubble penetration through oil / water interface, (ii) oil back flow into the needle and adverse effects of the oil higher viscosity.
- Bubbles have two characteristic parts in their trajectories: one that is well reproduced and dominated by the bubble injection needle, and another one that has a more stochastic nature. By placing needles closer or farther away from the jet it will be possible to impose desired reference velocity profile.
- Phenomena of steam condensation has periodic nature which effectively results in the periodic variation of the flow velocity around jet. To obtain / measure entrainment velocity one would need somewhat longer data acquisition sequences to provide more data for proper statistical treatment of the bubble's movement in the water pool.

7.4. Summary of development of image analysis for SEF-POOL experiment

The first data from the analysis of the bubbles rise in a stagnant pool was obtained and results are being analyzed. The current work is focused on the further analysis of bubbles flow during steam injection and the data from SEF S-29 test has been already processed.

Further work will aim to optimize (i) experimental setup to resolve several issues related to bubble formation and size, and (ii) image analysis and develop reliable approach to the estimation of flow velocity and entrainment rate.

8. SUMMARY

Containment is an essential part of the reactor safety design and is the last physical barrier that prevents the release of radioactive fission products into the environment. Pressure Suppression Pool (PSP) in Boiling Water Reactor (BWR) is used to condense steam released from the primary system in normal operation and in accident conditions. The PSP also serves as a source of water for the Emergency Core Cooling System (ECCS), spray, and as a scrubber in case of a core damage accident with release of radioactive aerosols. The PSP and overall containment performance can be affected by physical phenomena such as mixing and stratification. A stratified pool will have higher temperature at the surface compared to a completely mixed pool with the same averaged temperature. The pool surface temperature determines the steam partial pressure in the containment gas space. Higher pool temperature results in higher partial pressure of steam in the containment atmosphere and respectively higher total containment pressure, while the bottom layer of the pool remains cold. For instance, in Fukushima Daiichi Unit 3 containment pressure was rapidly increasing, which was attributed to the development of thermal stratification in the PSP.

The prediction of thermal stratification and mixing in a PSP remains a challenging task, due to the lack of models for steam direct contact condensation phenomena that could be effectively used for modeling of large-scale pools with numerous steam injection devices operated during long-term transients.

Effective Heat Source (EHS) and Effective Momentum Source (EMS) models have been proposed to enable the prediction of thermal stratification and mixing phenomena in a BWR containment PSP. The aim of this project is to provide pre- and post-test analytical support to the HYMERES-2 and NKS-THEOS experimental activities that were proposed to support development and validation of the EHS/EMS models. In this report we describe the progress achieved in addressing main tasks, i.e: (i) development and validation of the EHS/EMS models for spargers using OECD/HYMERES-1 PANDA HP5 test series; (ii) pre-test analysis in support of the experimental for SEF-POOL facility at LUT and PANDA facility at PSI; (iii) post-test analysis using the new test data.

In Section 3 we provide an overview of previous works on direct contact condensation and pool phenomena and modeling approaches. The need and the progress in further development of the EHS/EMS models for spargers is described in Sections 4. Two approaches to EMS model implementation are discussed (i) based on the source terms in the momentum equation and (ii) using boundary conditions for liquid velocity. Advantages and disadvantages of both approaches are discussed in detail. Results of the model calibration and validation against the data available from the PANDA HP5 tests are presented.

In Section 5 application of the developed EHS/EMS models to pre-test analysis in support of the PANDA H2P3 tests with sparger injection are presented. Scoping calculations were carried out to specify geometrical setup (pool depth, elevation of the sparger and number of open LRR holes), initial pool temperature, injection procedures, arrangement of thermocouples, PIV setup, for sparger tests (H2P3-1,2,3) and LRR tests (H2P3-4,5,6).

In Section 6 we present results of the pre-test analysis for the integral H2P4 test series in PANDA facility. The aim of the tests is to study the effect of pool stratification and mixing phenomena on containment pressurization. Results of the analysis are used for selection of the test configuration, i.e. the vessels to be used and connections between them, water pool level,

duration and mass flow rates for different injection phases. Results of the analysis suggest that it is feasible to achieve prototypic levels of pressurization during a reasonable time for the tests.

In Section 7 the progress in development of the image analysis for post-processing of the data from the SEF-POOL tests are presented. Gas bubbles are used in the tests in order to visualize water velocity in the vicinity of the jet induced by steam injection. The first data from the analysis of the bubbles rise in a stagnant pool was obtained and results are being analyzed. The current work is focused on the further analysis of bubbles flow during steam injection and the data from SEF S-29 test has been processed. Further work will aim to optimize (i) experimental setup to resolve several issues related to bubble formation and size, and (ii) image analysis and develop reliable approach to the estimation of flow velocity and entrainment rate.

ACKNOWLEDGEMENTS

Financial support from the SSM and Nordic Nuclear Safety Program (NKS) is greatly acknowledged. The authors are grateful to all the countries participating in the OECD/NEA HYMERES and HYMERES-2 projects. The authors would like to thank the secretariat and all the members of the Management Board and the Programme Review Group of the HYMERES and HYMERES-2 project for their help in defining the test programme and evaluating the test results.

GOTHIC is developed and maintained by the Numerical Applications Division of Zachry Nuclear Engineering under EPRI sponsorship. We would like to acknowledge NAI for providing access to the program for educational and research purposes.

NKS conveys its gratitude to all organizations and persons who by means of financial support or contributions in kind have made the work presented in this report possible.

DISCLAIMER

The views expressed in this document remain the responsibility of the author(s) and do not necessarily reflect those of NKS. In particular, neither NKS nor any other organization or body supporting NKS activities can be held responsible for the material presented in this report.

REFERENCES

1. Pershagen, B., 1994. Light Water Reactor Safety. Pergamon Press.
2. Lahey, R.T., Moody, F.J., 1993. The Thermal Hydraulics of a Boiling Water Nuclear Reactor, 2nd edition, American Nuclear Society, La Grange Park, Ill, USA.
3. Li, H., Kudinov, P., 2010. Effective Approaches to Simulation of Thermal Stratification and Mixing in a Pressure Suppression Pool. OECD/NEA & IAEA Workshop CFD4NRS-3, Bethesda, MD, USA, September 14-16, 2010.
4. Li, H., Villanueva, W., Kudinov, P., 2014. Approach and Development of Effective Models for Simulation of Thermal Stratification and Mixing Induced by Steam Injection into a Large Pool of Water. Science and Technology of Nuclear Installations, 2014, Article ID 108782, 11 pages.
5. Laine, J., Puustinen, M., Räsänen, A., 2013. PPOOLEX experiments on the dynamics of free water surface in the blowdown pipe. Nordic Nuclear Safety Research, NKS-281.
6. J. Laine, M. Puustinen, A. Räsänen, PPOOLEX Experiments with a Sparger, Nordic Nuclear Safety Research, 2015, NKS-334.
7. Mizokami, S., Yamada, D., Honda, T., Yamauchi, D., Yamanaka, Y., 2016. Unsolved issues related to thermal-hydraulics in the suppression chamber during Fukushima Daiichi accident progressions. Journal of Nuclear Science and Technology, 53, 630-638.
8. Mizokami, S., Yamanaka, Y., Watanabe, M., Honda, T., Fuji, T., Kojima, Y., PAIK, C.Y., Rahn, F., 2013. State of the art MAAP analysis and future improvements on TEPCO Fukushima-Daiichi NPP accident. NURETH-15: The 15th International Topical Meeting on Nuclear Reactor Thermal Hydraulics, Pisa, Italy, May 12-17, paper number 536.
9. Tanskanen, V., Jordan, A., Puustinen, M., Kyrki-Rajamäki, R., 2014. CFD simulation and pattern recognition analysis of the chugging condensation regime. Annals of Nuclear Energy, 66, 133-143.
10. Patel, G., Tanskanen, V., Hujala, E., Hyvärinen, J., 2017. Direct contact condensation modeling in pressure suppression pool system. Nuclear Engineering and Design, 321, 328-342.
11. Pellegrini, M., Naitoh, M., 2016. Application of two-phase flow DFC to the phenomena expected in Fukushima Daiichi S/C. OECD/NEA & IAEA Workshop CFD4NRS-6.
12. Li, H., Villanueva, W., Puustinen, M., Laine, J., Kudinov, P., 2014. Validation of Effective Models for Simulation of Thermal Stratification and Mixing Induced by Steam Injection into a Large Pool of Water. Science and Technology of Nuclear Installations, 2014, Article ID 752597, 18 pages.
13. Li, H., Villanueva, W., Puustinen, M., Laine, J., Kudinov, P., 2017. Thermal stratification and mixing in a suppression pool induced by direct steam injection. Annals of Nuclear Energy, 111, 487-498.
14. Villanueva, W., Li, H., Puustinen, M., Kudinov, P., 2015. Generalization of experimental data on amplitude and frequency of oscillations induced by steam injection into a subcooled pool. Nuclear Engineering and Design, 295, 155-161.
15. Li, H. and Kudinov, P., 2009. An Approach to Simulation of Mixing in a Stratified Pool with the GOTHIC code. ANS Transactions, paper 210976.
16. Li, H., Villanueva, W., Kudinov, P., 2011. Development and implementation of effective models in GOTHIC for the prediction of mixing and thermal stratification in a BWR pressure suppression pool. Proceedings of ICAPP 2011, Nice, France, May 2-5, 2011, Paper 11256.
17. Li, H. and Kudinov, P., 2008. An approach toward simulation and analysis of thermal stratification and mixing in a pressure suppression pool. NUTHOS-7, Seoul, Korea, October 5-9, Paper 243.

18. Gallego-Marcos, I., Villanueva, W., Kudinov, P., 2018. Modelling of Pool Stratification and Mixing Induced by Steam Injection through Blowdown Pipes. *Annals of Nuclear Energy*, 112, 624-639.
19. Li, H. and Kudinov, P., 2009. Condensation, Stratification and Mixing in a Boiling Water Reactor Suppression Pool. NORTHNET Roadmap 3 Report, Division of Nuclear Power Safety, Royal Institute of Technology (KTH), Stockholm, Sweden, 70p.
20. Li, H., Villanueva, W., Kudinov, P., 2010. Investigation of containment behavior with activation of rupture disks in system 361/362 with GOTHIC simulation. Swedish Radiation Safety Authority (SSM) Project Report, Royal Institute of Technology (KTH), Stockholm, Sweden, 25p.
21. Li, H., Kudinov, P., Villanueva, W., 2010. Modeling of Condensation, Stratification and Mixing Phenomena in a Pool of Water. NKS Report, NKS-225, Division of Nuclear Power Safety, KTH, Stockholm, Sweden, 91p.
22. Li, H., Kudinov, P., Villanueva, W., 2010. Condensation, Stratification and Mixing in a Boiling Water Reactor Suppression Pool. NORTHNET Roadmap 3 Report, Division of Nuclear Power Safety, Royal Institute of Technology (KTH), Stockholm, Sweden, 88p.
23. Li, H., Villanueva, W., Kudinov, P., 2012. Development, Implementation and Validation of EHS/EMS Models for Spargers. Westinghouse project report. Division of Nuclear Power Safety, Royal Institute of Technology (KTH), Stockholm, Sweden, 98p.
24. Li, H., Villanueva, W., Kudinov, P., 2012. Effective Momentum and Heat Flux Models for Simulation of Stratification and Mixing in a Large Pool of Water. NKS-ENPOOL Research report, NKS-266, 58p.
25. Li, H., Villanueva, W., Kudinov, P., 2012. Effective Models for Prediction of Stratification and Mixing Phenomena in a BWR Suppression Pool. NORTHNET Roadmap 3 Report, Division of Nuclear Power Safety, Royal Institute of Technology (KTH), Stockholm, Sweden, 87p.
26. Li, H., Villanueva, W., Kudinov, P., 2014. Effective Models for Simulation of Thermal Stratification and Mixing Induced by Steam Injection into a Large Pool of Water. Nordic Nuclear Safety Research, NKS-316.
27. Gallego-Marcos, I., Villanueva, W., Kapulla, R., Paranjape, S., Paladino, D., Kudinov, K., 2016. Modeling of thermal stratification and mixing induced by steam injection through spargers into a large water pool. OECD/NEA & IAEA Workshop CFD4NRS-6, Cambridge, MA, USA, September 13-15.
28. Gallego-Marcos, I., Villanueva, W., Kapulla, R., Paranjape, S., Paladino, D., Kudinov, K., 2016. Scaling and CFD Modelling of the Pool Experiments with Spargers Performed in the PANDA Facility. NUTHOS-11: The 11th International Topical Meeting on Nuclear Reactor Thermal Hydraulics, Operation and Safety Gyeongju, Korea, October 9-13, N11P0670.
29. Gallego-Marcos, I., Villanueva, W., Kudinov, P., 2016. Scaling of the Erosion of a Thermally Stratified Layer in a Large Water Pool during a Steam Injection Through Spargers. NUTHOS-11: The 11th International Topical Meeting on Nuclear Reactor Thermal Hydraulics, Operation and Safety, Gyeongju, Korea, October 9-13, N11P0525.
30. Gallego-Marcos, I., Villanueva, W., Kudinov, P., 2016. Modeling of Thermal Stratification and Mixing in a Pressure Suppression Pool Using GOTHIC. NUTHOS-11: The 11th International Topical Meeting on Nuclear Reactor Thermal Hydraulics, Operation and Safety, Gyeongju, Korea, October 9-13, N11P0524.
31. Gallego-Marcos, I., Villanueva, W., Kudinov, P., et al., 2019. Pool Stratification and Mixing Induced by Steam Injection through Spargers: CFD modeling of the PPOOLEX and PANDA experiments. *Nuclear Engineering and Design*, 347, 67-85.

32. Gallego-Marcos, I., Filich, L., Villanueva, W., Kudinov, P., 2015. Modelling of the Effects of Steam Injection through Spargers on Pool Thermal Stratification and Mixing. NKS Report 347.
33. Gallego-Marcos, I. Villanueva, W., Kudinov, P., 2016. Thermal Stratification and Mixing in a Large Pool Induced by Operation of Spargers, Nozzles, and Blowdown Pipes". NKS Report 369.
34. Gallego-Marcos, I., Villanueva, W., Kudinov, P., 2017. Modelling of a Large Water Pool during Operation of Blowdown Pipes, Spargers, and Nozzles. NKS-393.
35. Puustinen, M., Laine, J., Räsänen, A., 2009. PPOOLEX experiments on thermal stratification and mixing. Research report CONDEX 1/2008, NKS-198.
36. Gallego-Marcos, I., Villanueva, W., Kudinov, P., et al., 2018. Pool Stratification and Mixing Induced by Steam Injection through Spargers: analysis of the PPOOLEX and PANDA experiments. Nuclear Engineering and Design, 337, 300-316.
37. Song, C.H., Cho, C., Him, H.Y., et al., 1998. Characterization of direct contact condensation of steam jets discharging into a subcooled water, Proceedings of IAEA Technical Committee Meeting, PSI, Villigen.
38. Kerney, J., Feath, G.M., Olson, D.R., 1972. Penetration characteristics of a sub-merged steam jet. AIChE Journal 18(3) 584-553.
39. Gulawani, S.S., Dahikar, S.K., Mathpati, C.S., et al., 2009. Analysis of flow pattern and heat transfer in direct contact condensation. Chemical Engineering Science, 64 1719-1738.
40. Wu, X.Z., Yan, J.J., et al., 2009. Experimental study on sonic steam jet condensation in quiescent subcooled water. Chemical Engineering Science, 64 (23), 5002-5012.
41. Y.J. Choo, C.H. Song, PIV measurements of turbulent jet and pool mixing produced by a steam jet discharge in a subcooled pool, Nuclear Engineering and Design 240 (9) (2010) 2215-2224.
42. Ju, S.H., et al., 2000. Measurement of heat transfer coefficients for direct contact condensation in core makeup tanks using holographic interferometer. Nuclear Engineering and Design, 199, 75-83.
43. Chan, C.K., Lee, C.K.B., 1982. A regime map for direct contact condensation. International Journal of Multiphase Flow, 8, 11-20.
44. Simpson, M.E., Chan, C.K., 1982. Hydrodynamics of a subsonic vapor jet in subcooled liquid. Journal of Heat Transfer, 104 (2), 271-278.
45. Fukuda, S., 1982. Pressure Variations due to Vapor Condensation in Liquid, (II). Journal of the Atomic Energy Society of Japan, 24 (6), 466-474.
46. Hong, J., Park, G.C., Cho, S., Song, C.H., 2012. Condensation dynamics of submerged steam jet in subcooled water. International Journal of Multiphase Flow 39, 66-77.
47. Cho, S., Chun, S.Y., Baek, W.P., Kim, K., 2004. Effect of multiple holes on the performance of sparger during direct contact condensation. Experimental Thermal and Fluid Science, 28 (6), 629-638.
48. Tang, J., Yan, C., Sun, L., 2015. A study visualizing the collapse of vapor bubbles in a subcooled pool. International Journal of Heat and Mass Transfer, 88, 597-608.
49. Aya, I., Nariai, H., Kobayashi, M., 1980. Pressure and Fluid Oscillations in Vent System due to Steam Condensation, (II) High-Frequency Component of Pressure Oscillations in Vent Tubes under at Chugging and Condensation Oscillation. Journal of Nuclear Science and Technology, 20(3), 213-227.
50. Youn, D.H., Ko, K.B., Lee, Y.Y., Kim, M.H., Bae, Y.Y., Park, J.K., 2003. The Direct Contact Condensation of Steam in a Pool at Low Mass Flux. Nuclear Science and Technology 40(10), 881-885.

51. E. Aust, D. Seeliger. Pool dynamics and dynamic loads in pressure suppression containment systems. Transactions of the American Nuclear Society 41 (1982) 696-699.
52. Aya, I., Nariai, H 1987. Boundaries between regimes of pressure oscillations induced by steam condensation in pressure suppression containment. Nuclear Engineering and Design, 99, 31-40.
53. Liang, K.S., Griffith, P., 1994. Experimental and analytical study of direct contact condensation of steam in water, Nuclear Engineering and Design, 147 (3), 425-435.
54. Cho, S., Song, C.H., Park, C.K., Yang, S.K., Chung, M.K., 1998. Experimental study on dynamic pressure pulse in direct contact condensation of steam jets discharging into subcooled water. Proceedings of NTHAS98. Korea-Japan symposium on nuclear thermal hydraulics and safety; Pusan Korea, 291-298.
55. A. Petrovic de With, R.K. Calay, G. de With, 2007. Three dimensional condensation regime diagram for direct contact condensation of steam injected into water. International Journal of Heat and Mass Transfer, 50 (9-10), 1762-1770.
56. G. Gregu, M. Takahashi, M. Pellegrini, R. Mereu, 2017. Experimental study on steam chugging phenomenon in a vertical sparger, International Journal of Multiphase Flow 88, 87-98.
57. X.Z. Wu, J.J. Yan, W.J. Li, D.D. Pan, G.Y. Liu, W.J. Li, 2009. Condensation regime diagram for supersonic/sonic steam jet in subcooled water, Nuclear Engineering and Design 239 (12), 3142-3150.
58. Song, 2010. PIV measurements of turbulent jet and pool mixing produced by a steam jet discharge in a subcooled pool. Nuclear Engineering and Design 240 (9) 2215-2224.
59. R.J.E. Van Wissen, K.R.A.M. Schreel, C.W.M Van Der Geld, 2005. Particle image velocimetry measurements of a steam-driven confined turbulent water jet. Journal of Fluid Mechanics 530, 353-368.
60. F. D'Auria, G.M. Galassi, Scaling of nuclear reactor system thermal-hydraulics, Nuclear Engineering and Design 240 (10) (2010) 3267-3293.
61. MARVIKEN-FSCB-I, 1973. Marviken Full Scale Containment Blowdown Experiments Series I.
62. W. Kennedy, D. McGovern, R. Maraschin, K. Wolfe. Rigid and flexible vent header testing in the quarter scale test facility. Mark I containment program, task 5.3.3. Technical report, General Electric Co., San Jose, CA (USA), 1978. Alternate Energy Division.
63. T.R. McIntyre, M.A. Ross, L.L. Myers. Mark II pressure suppression test program: Phase I tests. Technical report, General Electric Co., San Jose, CA (USA), 1976. Boiling Water Reactor Systems Dept.
64. W.A. Grafton, T.R. McIntyre, M.A. Ross. Mark II pressure suppression test program: Phase II and III tests. Technical report, General Electric Co., San Jose, CA (USA), 1977. Boiling Water Reactor Projects Dept.
65. T.R. McIntyre, L.L. Myers, J.E. Torbeck, R.J. Booker. Mark III confirmatory test program: one third scale, three vent air tests. Technical report, General Electric Co., San Jose, Calif. (USA), 1975. Boiling Water Reactor Systems Dept.
66. A.M. Varzaly, W.A. Grafton, H. Chang, M.K. Mitchell. Mark III confirmatory test program: 1/root 3 scale condensation and stratification phenomena, test series 5807. Technical report, General Electric Co., San Jose, Calif. (USA), 1977. Boiling Water Reactor Systems Dept.
67. T.H. Chuang. Mark III one-third area scale submerged structure tests. Technical report, General Electric Co., San Jose, CA (USA), 1977. Boiling Water Reactor Systems Dept.

68. K. Namatame, Y. Kukita, I. Takeshita, 1983. Evaluation of primary blowdown flow rate and vent pipe steam mass flux (Tests 00002, 0003, 0004, 1101, 2101, 3101, 3102) - Full-Scale Mark II CRT program Test Evaluation Report No 1, JAERI-M 83-185.
69. Y. Kukita, I. Takeshita, K. Namatame, M. Kato, K. Moriya, M. Shiba, 1981. Statistical evaluation of steam condensation loads in pressure suppression pool (1) – Full-Scale Mark II CRT program. Test Evaluation Report No. 2, JAERI-M 9665.
70. J. Hart, W.J.M. Slegers, S.L. de Boer, M. Huggenberger, J. Lopez Jimenez, J.L. Munoz-Cobo Gonzalez, F. Reventos Puigjaner., 2001. TEPSS-Technology enhancement for passive safety systems. Nuclear Engineering and Design 209, 243-252.
71. C.D. Walsche, F.D. Cachard., 1996. Experimental investigation of condensation and mixing during venting of a steam/non-condensable gas mixture into a pressure suppression pool. Technical report, IAEA Report 53-61.
72. Y.T. Moon, H.D. Lee, G.C. Park., 2009. CFD simulation of steam jet-induced thermal mixing into a subcooled water pool, Nuclear Engineering and Design 239, 2849-2863.
73. Y. Zhang, D. Lu, Z. Wang, X. Fu, Q. Cao, Y. Yang, G. Wu., 2016. Experimental research on the thermal stratification criteria and heat transfer model for the multi-holes steam ejection in IRWST of AP1000 plant, Applied Thermal Engineering 107, 1046-1056.
74. J. Laine, M. Puustinen., 2005. Condensation Pool Experiments with Steam Using DN200 Blowdown Pipe, Nordic Nuclear Safety Research NKS-111.
75. J. Laine, M. Puustinen., 2006. Thermal stratification experiments with the condensation pool test rig, Nordic Nuclear Safety Research NKS-117.
76. J. Laine, M. Puustinen., 2009. A. Räsänen, PPOOLEX Experiments on Thermal Stratification and Mixing, Nordic Nuclear Safety Research NKS-198.
77. M. Puustinen, J. Laine., 2011. A. Räsänen, Multiple blowdown pipe experiments with the PPOOLEX facility, Nordic Nuclear Safety Research NKS-241.
78. J. Laine, M. Puustinen., 2013. A. Räsänen, PPOOLEX experiments on the dynamics of free water surface in the blowdown pipe, Nordic Nuclear Safety Research NKS-281.
79. J. Laine, M. Puustinen, A. Räsänen., 2014. PPOOLEX Mixing Experiments, Nordic Nuclear Safety Research, NKS-309.
80. Kapulla, R., Mignot, G., Paranjape, P., Paladino, D., Fehlmann, M., Suter, S., 2015. OECD/NEA HYMERES project: HP5 Test Results. In: 6th Meeting of the Programme Review Group and Management Board of the HYMERES Project, PSI Villigen, Switzerland, 17–19 November.
81. M. Solom, K.V. Kirkland, Experimental investigation of BWR Suppression Pool stratification during RCIC system operation, Nuclear Engineering and Design 310 (2016) 564-569.
82. H.J.S. Fernando., 1991. Turbulent mixing in stratified fluids, Annual Review of Fluid Mechanics 23, 455-93.
83. D. Song, N. Erkan, B. Jo, K. Okamoto, 2014. Dimensional analysis of thermal stratification in a suppression pool, International Journal of Multiphase Flow 66, 92-100.
84. H.J.S. Fernando, Turbulent mixing in stratified fluids, Annual Review of Fluid Mechanics 23 (1991) 455-93.
85. H.J.S. Fernando, J.C.R. Hunt, 1997. Turbulence, waves and mixing at shear-free density interfaces. Part 1. A theoretical model, Journal of Fluid Mechanics 347, 197-234.
86. J.L. McGrath, H.J.S. Fernando, J.C.R. Hunt, 1997. Turbulence, waves and mixing at shear-free density interfaces. Part 2. Laboratory experiments, Journal of Fluid Mechanics 347, 235-261.
87. C.H. Chen, V.K. Dhir. Hydrodynamics of a bubble formed at vent pipe exit. International Journal of Multiphase Flow 8(2) (1982) 147-163.

88. F. Yuan, D. Chong, Q. Zhao, W. Chen, J. Yan, Pressure oscillation of submerged steam condensation in condensation oscillation regime, *International Journal of Heat and Mass Transfer* 98 (2016) 193-203.
89. J.H. Pitts, Steam chugging in a boiling water reactor pressure-suppression system, *International Journal of Multiphase Flow* 6 (1980) 329-344.
90. M. Ali, V. Verma, A.K. Ghosh, Analytical thermal hydraulic model for steam chugging phenomenon, *Nuclear Engineering and Design* 237(19) (2007) 2025-2039.
91. C. Brennen, A Linear Dynamic Analysis of Vent Condensation Stability, Annual Meeting of the American Society of Mechanical Engineers, Chicago, Illinois, November 16-21, 1980.
92. T.J.H. Pättikangas, J. Niemi, J. Laine, M. Puustinen, H. Purhonen. 2010. CFD modelling of condensation of vapor in the pressurized PPOOLEX facility. *CFD4NRS-3*, 14-16 September, Washington D.C., USA.
93. R.E. Gamble., T.T. Nguyen., B.S. Shiralkar., P.F. Peterson., R. Greifc., H. Tabatad., 2001. Pressure suppression pool mixing in passive advanced BWR plants, *Nuclear Engineering and Design* 204, 321-336.
94. H.S. Kang., C.H. Song., 2008. CFD analysis for thermal mixing in a subcooled water tank under a high steam mass flux discharge condition. *Nuclear Engineering and Design*, 238. 492-501.
95. H.S. Kang., C.H. Song., 2010. CFD analysis of a turbulent jet behavior induced by a steam jet discharge through a single hole in a subcooled water tank. *Nuclear Engineering and Design*, 240, 2160-2168.
96. C.H. Song., S. Cho., H.S. Kang., 2012. Steam Jet Condensation in a Pool: From Fundamental Understanding to Engineering Scale Analysis. *Journal of Heat Transfer*, 134, 031004-1.
97. Gallego-Marcos, I., Grishchenko, D., Kudinov, P., 2019. Thermal stratification and mixing in a Nordic BWR pressure suppression pool. *Annals of Nuclear Energy*, 132, 442-450.
98. Gallego-Marcos, I., Kudinov, P., et al., 2019. Effective momentum induced by steam condensation in the oscillatory bubble regime. *Nuclear Engineering and Design*, 350, 259-274.
99. GOTHIC Thermal Hydraulic Analysis Package, Version 8.1(QA). EPRI, Palo Alto, CA: 2014.
100. RELAP5/MOD3.3 Code Manual Volume IV. US Nuclear Regulatory Commission, Washington DC, 2006.
101. I. Aya, H. Nariai. Chugging Phenomenon Induced by Steam condensation into pool water (amplitude and frequency of fluid oscillation). Translated from: *Transactions of the Japan Society of Mechanical-Engineers* 50 (1984) 2427-2435.
102. C.E. Brennen. *Fundamentals of Multiphase Flow*. Cambridge University Press (2005), section 15.6.3.
103. C.K.B Lee, C.K. Chan, Steam chugging in pressure suppression containment: final report July 1976 - July 1979, US Nuclear Regulatory Commission (1980).
104. I. Gallego-Marcos, W. Villanueva, P. Kudinov. Possibility of Air Ingress into a BWR Containment during a LOCA in case of Activation of Containment Venting System. NUTHOS-10: The 10th International Topical Meeting on Nuclear Reactor Thermal Hydraulics, Operation and Safety, Okinawa, Japan, December 14-18, (2014) paper number 1292.

105.

106. Gallego-Marcos, I., 2018. Steam condensation in a water pool and its effect on thermal stratification and mixing. PhD thesis, KTH Royal Institute of Technology, Stockholm, Sweden.
107. A.A. Sonin. Scaling laws for small-scale modeling of steam relief into water pools, *Nuclear Engineering and Design* 65 (1) (1981) 17-21.
108. Paladino, D., Dreier, J., 2012. PANDA: a multipurpose integral test facility for LWR safety investigations. *Science and Technology of Nuclear Installations*, Article ID 239319.
109. Kapulla, R., Mignot, G., et al., 2018. PIV Measurements in the Vicinity of a Steam Sparger in the PANDA Facility. *Nuclear Engineering and Design*, 336, 112-121.
110. X. Li, M. Zhang, Z. Du, X. Fu. Scaling analysis of coolant spraying process in automatic depressurized system, *Annals of Nuclear Energy* 72 (2014) 350-357.
111. N.W.M. Ko, K.K. Lau, Flow structures in initial region of two interacting parallel plane jets, *Experimental Thermal and Fluid Science* 2 (4) (1989) 431-449.
112. D. Heinze, T. Schulenberg, L. Behnke. A Physically Based, One-Dimensional Two-Fluid Model for Direct Contact Condensation of Steam Jets Submerged in Subcooled Water. *Journal of Nuclear Engineering and Radiation Science*, 1(2) (2015) 8 pages.
113. E.S Gadis, A. Vogelpohl. Bubble formation in quiescent liquids under constant flow conditions. *Chemical Engineering Science* 41 (1986) 97-105.
114. S. Ramakrishnan, R. Kumar, N.R. Kuloor. Studies in bubble formation - Bubble formation under constant flow conditions. *Chemical Engineering Science* 24 (1969) 731-747.
115. L. Zhang, M. Shoji. Aperiodic bubble formation from a submerged orifice. *Chemical Engineering Science* 56 (2001) 5371-5381.
116. I. Aya, H. Nariai. Evaluation of heat-transfer coefficient at direct-contact condensation of cold water and steam. *Nuclear Engineering and Design* 131 (1991) 17-24.
117. O. Zeitoun, M. Shoukri, V. Chatoorgoon. Interfacial Heat Transfer Between Steam Bubbles and Subcooled Water in Vertical Upward Flow. *Journal of Heat Transfer* 117 (2) (1995) 402-407.
118. G.R. Warrier, N. Basu, V.K. Dhir. Interfacial heat transfer during subcooled flow boiling. *International Journal of Heat and Mass Transfer* 45 (2002) 3947-3959.
119. A. Prosperetti, M.S. Plesset. Vapour-bubble growth in a superheated liquid. *Journal of Fluid Mechanics* 85 (2) (1978) 349-368.
120. Pope. S.B., 2020. *Turbulent Flow*. Section 5.1, Cambridge University Press, Cambridge UK.
121. Hussein. H., et al., 1994. Velocity measurements in a high-Reynolds-number, momentum-conserving axisymmetric, turbulent jet. *Journal of Fluid Mechanics*, 258, 31-75.
122. T.B. Benjamin, A.T. Ellis. The collapse of cavitation bubbles and the pressures thereby produced against solid boundaries. *Philosophical Transactions of the Royal Society* 260 (1966) 221-240.
123. J.R. Blake. The Kelvin Impulse: Application to Cavitation Bubble Dynamics. *Journal of the Australian Mathematical Society* 30 (1988) 127-146.
124. D. Obreschkow, M. Tinguely, N. Dorsaz, P. Kobel, A. Bosset, M. Farhat. A Universal Scaling Law for Jets of Collapsing Bubbles. *Physical Review Letters* 107 (2011) 204501.
125. O. Supponen, D. Obreschkow, M. Tinguely, P. Kobel, N. Dorsaz, M. Farhat. Scaling laws for jets of single cavitation bubbles. *Journal of Fluid Mechanics* 802 (2106) 263-293.
126. ANSYS® Academic Research, Release 17.0, ANSYS Fluent Theory Guide, ANSYS, Inc.

127. A.M. Bahari, K. Hejazi. Investigation of Buoyant Parameters of k- ϵ Turbulence Model in Gravity Stratified Flows. World Academy of Science, Engineering and Technology 55 (2009).
128. J.W. Miles. On the stability of heterogeneous shear flows. Journal Fluid Mechanics 10 (1961) 496-508.
129. H.D. Abarbanel, D.D. Holm, J.E. Marsden, T. Ratiu. Richardson Number Criterion for the Nonlinear Stability of Three-Dimensional Stratified Flow. Physical Review Letters 52 (1984) 2352-2355.
130. I.P.D. De Silva, A. Brandt, L.J. Montenegro, H.J.S. Fernando. Gradient Richardson number measurements in a stratified shear layer. Dynamics of Atmospheres and Oceans 30 (1999) 47-63.
131. P. Van Gastel, J.L. Pelegrí. Estimates of gradient Richardson numbers from vertically smoothed data in the Gulf Stream region. Scientia Marina 68 (4) (2004) 459-482.
132. Paranjape. S, Fehlmann. M, Kapulla, R. et al., 2016. OECD/NEA HYMERES project: PANDA Test HP5_3 Quick-Look Report. Paul Scherrer Institute, (report restricted to project participants).
133. Cha. J.H, et al., 2017. The effect of the Reynolds number on the velocity and temperature distributions of a turbulent condensing jet. International Journal of Heat and Mass Transfer, 67, 125-132.
134. Benoit. C.R, 2008. Environmental Fluid Mechanics, Chapter 9: Turbulent Jets, Wiley-Blackwell.
135. Wang, X.C., Grishcehnko, D., Kudinov, P., 2020. Development of Effective Momentum Model for Steam Injection through Multi-hole Spargers. ICAPP2020. Abu Dhabi, UAE, March 15-19.
136. Mignot G. R. Kapulla, S. Paranjape, R. Zboray, M. Fehlmann, W. Bissels, S. Sutter, D. Paladino, OECD/NEA HYMERES project: PANDA test facility description and geometrical specifications, HYMERES-P-13-03, 2013.

Appendix B

SEF-POOL tests on small-scale phenomena of steam discharge into subcooled water

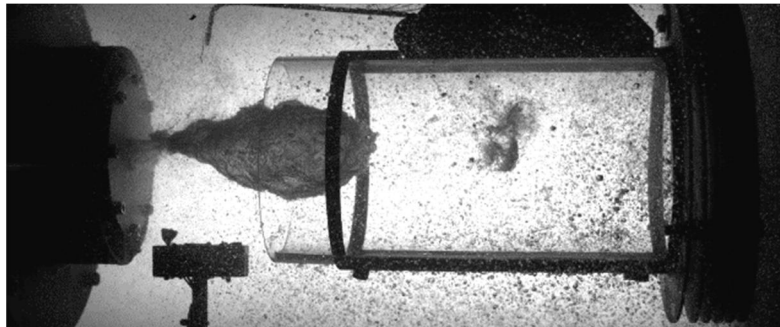
Technical Report
LUT University
Nuclear Engineering

SPASET 1/2019 (D1.2.1)

**SEF-POOL tests on small-scale
phenomena of steam discharge into sub-
cooled water**

Markku Puustinen, Antti Räsänen,

Eetu Kotro, Kimmo Tielinen



Lappeenranta-Lahti University of Technology LUT
School of Energy Systems
Nuclear Engineering
P.O. Box 20, FIN-53851 LAPPEENRANTA, FINLAND
Phone +358 294 462 111

Lappeenranta, 27.1.2020

Research organization and address LUT University School of Energy Systems Nuclear Engineering P.O. Box 20 FIN-53851 LAPPEENRANTA, FINLAND Project manager Markku Puustinen Diary code 360/322/2018	Customer VYR / SAFIR2022 SSM NKS Contact person Jari Hämäläinen (SAFIR2022) Francesco Canidu (SSM) Ari-Pekka Leppänen (NKS) Order reference Drno SAFIR 18/2019				
Project title and reference code SAFIR2022-SPASET	<table> <tr> <th>Report identification & Pages</th><th>Date</th></tr> <tr> <td>SPASET 1/2019 (D1.2.1) 26 p. + app. 3+1 p.</td><td>27.1.2020</td></tr> </table>	Report identification & Pages	Date	SPASET 1/2019 (D1.2.1) 26 p. + app. 3+1 p.	27.1.2020
Report identification & Pages	Date				
SPASET 1/2019 (D1.2.1) 26 p. + app. 3+1 p.	27.1.2020				

Report title and author(s)

SEF-POOL TESTS ON SMALL-SCALE PHENOMENA OF STEAM DISCHARGE INTO SUB-COOLED WATER
Markku Puustinen, Antti Räsänen, Eetu Kotro, Kimmo Tielinen

Summary

The main goal of the SEF-POOL tests in 2019 was to provide data of the characteristics of small-scale phenomena, which affect the effective momentum sources in case of steam injection through a sparger into a sub-cooled pool of water. This information will then be used in the validation of the simplified EHS/EMS models for spargers by KTH. Furthermore, the SEF-POOL tests support the validation effort of the DCC and interfacial area models of CFD codes for steam injection through spargers at VTT and LUT.

With high-frequency measurements and high-speed cameras, the small-scale phenomena and steam bubble properties such as bubble velocity, radius and collapse frequencies can be captured.

Effect of high Ja number on the effective momentum, effective momentum in the transition regime, i.e. effect of transition from sub-sonic to sonic flow conditions, effective momentum at mass fluxes higher than $300 \text{ kg/m}^2\text{s}$ and effect of nozzle chamfer were studied in 2019.

Both the Jakob and Mach number have a significant effect on the effective momentum coefficient C (i.e. the ratio of liquid momentum rate to the theoretical value of the momentum rate of steam). At very large Ja numbers (~ 0.16 - 0.2) the condensation rate is very large which leads to rapid reduction of the effective momentum coefficient. There is no apparent dependency of the effective momentum coefficient on chamfer in the injection holes.

The results fit well with the previous data and are very helpful for the understanding of the key effects and factors that can be neglected when the EMS/EHS models are developed further.

Distribution

Members of the SAFIR2022 Reference Group 4

F. Cadinu (SSM), A-P. Leppänen (NKS), P. Kudinov (KTH), W. Villanueva (KTH), J. Hämäläinen (VTT), V. Suolanen (VTT), T. Pättikangas (VTT), I. Karppinen (VTT), S. Hillberg (VTT)

Principal author or Project manager

Markku Puustinen
Senior Research Scientist

Approved by

Heikki Purhonen
Research Director

Reviewed by

Joonas Telkkä
Project Researcher

Availability statement

SAFIR2022 limitations

PREFACE

Tests done in the Separate Effect Facility (SEF-POOL) have been planned together by Kungliga Tekniska Högskolan (KTH) and the Nuclear Engineering research group at Lappeenranta-Lahti University of Technology LUT (LUT University). The work has been performed under the Finnish Research Programme on Nuclear Power Plant Safety 2019–2022 (SAFIR2022) in the SPASET project. Financial support for the work has been provided by the National Nuclear Waste Management Fund (VYR), Strålsäkerhetsmyndigheten (SSM), Nordic Nuclear Safety Research (NKS) and LUT.

CONTENTS

NOMENCLATURE.....	5
1 INTRODUCTION	7
2 EMS/EHS MODELS AND EFFECTIVE MOMENTUM.....	8
3 SEF-POOL FACILITY	9
3.1 GENERAL	10
3.2 CONDENSATION POOL	10
3.3 SPARGER SYSTEM.....	11
3.4 FORCE MEASUREMENT.....	11
3.5 OTHER MEASUREMENTS.....	11
3.6 DATA ACQUISITION.....	12
3.7 CAMERA SYSTEM.....	12
4 SEF-POOL TESTS	12
4.1 TESTS ON REGIME TRANSITION AND EFFECT OF SUB-COOLING.....	16
4.2 TEST ON HIGH FLOW RATE.....	18
4.3 TESTS OF EFFECT OF CHAMFER.....	19
4.4 QUALITATIVE ANALYSIS OF VIDEO IMAGES.....	20
5 CONCLUSIONS	23
REFERENCES	25
APPENDIX A: TEST RIG DRAWINGS	
APPENDIX B: BASIC INSTRUMENTATION	

NOMENCLATURE

Symbols

A	area
C	ratio of liquid momentum to the theoretical value of momentum of steam
c_{pL}	specific liquid heat at constant pressure
d	injection hole diameter
ΔT	sub-cooling
h_{fg}	latent heat of condensation
Ja	Jacob number
M	Mach number
\dot{m}	mass flow rate
M_{eff}	effective momentum
M_s	steam momentum
Re	Reynolds number
T_p	pool temperature
ρ	density
We	Weber number

Abbreviations

BWR	Boiling Water Reactor
CFD	Computational Fluid Dynamics
DCC	Direct Contact Condensation
DP	Differential pressure measurement
EHS	Effective Heat Source
EMS	Effective Momentum Source
INSTAB	Couplings and INSTABilities in Reactor Systems Project
KTH	Kungliga Tekniska Högskolan
LUT	Lappeenranta-Lahti University of Technology LUT, LUT University
NKS	Nordic Nuclear Safety Research
P	Pressure measurement
PACTEL	PARallel Channel TEST Loop
PC	Polycarbonate
PPOOLEX	Pressurized Condensation POOL EXperiments Test Facility
SAFIR	Safety of Nuclear Power Plants - Finnish National Research Programme

SEF-POOL	Separate Effect Test Facility
SPASET	Sparger Separate Effect Tests Project
SRV	Safety Relief Valve
SSM	Strålsäkerhetsmyndigheten
T	Temperature measurement
TC	ThermoCouple
VTT	Technical Research Centre of Finland Ltd
VYR	National Nuclear Waste Management Fund

1 INTRODUCTION

Steam injection through spargers induces heat, momentum and mass sources that depend on the steam injection conditions and can result in thermal stratification or mixing of the suppression pool. The development of thermal stratification in the suppression pool is of safety concern since it reduces the steam condensation capacity of the pool, increases the pool surface temperature, and thus leads to higher containment pressures, compared with completely mixed pool conditions.

Prediction of thermal stratification and mixing induced by steam injection into a sub-cooled pool with computational fluid dynamics (CFD) codes is time consuming and requires lots of computational capacity because the associated direct-contact condensation (DCC) phenomenon needs to be solved. The simplified effective heat source (EHS) and effective momentum source (EMS) models for simulation of steam injection into a pool filled with sub-cooled water, proposed by KTH, would reduce the needed computational capacity [1, 2]. The models have been implemented in the GOTHIC code and validated against PPOOLEX experiments with blowdown pipes done at LUT University (LUT) under the SAFIR2018/INSTAB project [3, 4]. However, the EHS/EMS models can be used in any thermal-hydraulic code, which currently cannot reliably model direct contact condensation phenomena.

The concepts of the EHS/EMS models are being extended to the condensation regimes, particularly the oscillatory bubble and oscillatory cone jet regime, appearing in safety relief valve (SRV) spargers. The oscillatory bubble and oscillatory cone jet regimes are relevant for BWR plant conditions when spargers inject steam at mass fluxes between 75-300 kg/(m²s) [5]. A validation effort has been carried out against the PANDA and PPOOLEX experiments done with a model of a SRV sparger [6]. This validation effort has shown that the injection angle, total momentum, and momentum profile have a large effect on the pool behaviour [7]. Due to the uncertainty on these parameters, a separate effect test facility named SEF-POOL, has been designed at LUT in collaboration with KTH to measure/define the effective momentum and reduce the uncertainty of the simulations. Effective momentum induced by steam injection through the sparger can be measured directly for different condensation regimes with the help of force sensors. High-speed camera will allow recordings of the condensation regimes and collapsing bubbles. With high frequency pressure measurements, the detachment and collapse frequency of the bubbles will be obtained.

VTT also has been developing, improving and validating numerical simulation models of direct contact condensation for steam discharge through blowdown pipes on the basis of PPOOLEX experiments. In 2018, VTT tested the suitability of these CFD models for direct contact condensation phenomenon associated with a sparger operation. A simulation model based on the LUT's separate effect test facility for sparger studies was developed and a selected test case was calculated [8].

The SEF-POOL facility was constructed at LUT and a series of preliminary and characterizing tests were conducted with the facility in autumn 2017. The first tests with the facility revealed that some modifications for the design are needed in order to be able to define the effective momentum. After these modifications were implemented more

preliminary tests were run at the end of the year [9]. The test campaign continued in 2018, first with the same facility design as at the end of 2017 and later in spring with a design that had been changed considerably by adding a second support arm for an independent propulsion volume to allow a direct measurement of the effective momentum [10].

In 2019, the SEF-POOL tests concentrated on the effect of chamfer at the injection holes, regime transition and high steam mass fluxes. The basic design of the SEF-POOL facility remained unchanged in the 2019 tests. However, part of the tests was done with the propulsion volume in use and part without it. Different options for the high-speed camera arrangement were tested during the test campaign in 2019. Particularly, stereo imaging was tried in couple of last tests.

Experiments in the SEF-POOL facility at LUT will provide necessary data to understand which characteristics of small-scale phenomena affect the effective heat and momentum sources and will thus help in the validation of the simplified EHS/EMS models. Furthermore, the SEF-POOL tests support the validation effort of the DCC and interfacial area models of CFD codes for steam injection through spargers as well as implementation of the EHS/EMS models to the Apros system code. As a result of this validation effort of simulation tools, capabilities for realistic evaluation of the steam condensation capacity of the suppression pool in different thermal stratification scenarios will improve.

This report summarizes the SEF-POOL tests done in 2019. The concept behind the EMS/EHS models is first shortly discussed in chapter 2. Next, the geometry and the installed instrumentation of the SEF-POOL facility are introduced in chapter 3. The main observations from the tests done with the SEF-POOL facility in 2019 and some related preliminary analysis results obtained from KTH are then presented in chapter 4. Conclusions are drawn in chapter 5.

2 EMS/EHS MODELS AND EFFECTIVE MOMENTUM

The general idea behind the EMS/EHS models is that, to predict the global pool behaviour, the small scale phenomena occurring at the level of direct contact condensation does not need to be resolved [1, 2]. Instead, it is the time averaged heat and momentum transferred from the steam to the large scale pool circulation that needs to be provided. The premise behind this idea is that averaged effects of the small-scale direct contact condensation phenomena determine the integral heat and momentum sources, which in turn determine the large-scale pool circulation and temperature distribution. With this approach computational efficiency can be improved considerably, when large domains such as pressure suppression pools of BWRs and long term transients, are modelled. Particularly the modelling of steam jets at the injection holes of a sparger requires very fine meshes and small time steps. Furthermore, instability issues will arise if we attempt to resolve the direct contact condensation of such jets.

In the EMS/EHS model approach, simplified conservation equations of mass, momentum, and energy in a control volume, where the steam jets are expected to condense completely, are solved and a mean (time-averaged) condensate flow at the

control volume boundary is defined. Steam momentum M_s is defined as momentum of the steam right at the injection hole (before condensing) and can be expressed by $\dot{m}^2/(\rho A)$, where \dot{m} is steam mass flow rate, ρ steam density and A cross sectional flow area. Effective momentum M_{eff} is the amount of momentum transferred from the steam to the liquid. These two momentums are not equal in two phase flow (for example: chugging). It is the M_{eff} term that needs to be known in the EMS model approach. Separate-effect tests in the SEF-POOL facility allow to measure and visualize directly the difference between M_s and M_{eff} . The tests help to map the effective momentum of different condensation regimes and will thus provide closures for the EMS model development for spargers by KTH.

Focus in the test series with the SEF-POOL facility in 2018 was to determine the effect of the injection hole diameter, number of holes, pool temperature, steam mass flux, etc., on the effective momentum [10]. Furthermore, the bubble radius and velocity as well as the detachment and collapse frequencies of the bubbles could be obtained with the help of high frequency measurements and high-speed video recordings.

However, important variables affecting the effective momentum magnitude in full-scale plant need to be further analysed in order to provide closures for the EMS model development for spargers. Tests in SEF-POOL in 2019 thus concentrated on the effect of chamfer at the injection holes, regime transition and high steam mass fluxes.

3 SEF-POOL FACILITY

The reference system for the SEF-POOL facility is a SRV sparger pipe of a BWR plant. Hence, the SEF-POOL facility is designed in such a way that discharge of steam through injection holes at the sparger lower end into sub-cooled pool water can be simulated representatively.

The goal in the tests with the facility is to define the effective momentum for a given steam condensation regime, particularly for the oscillatory bubble regime. For this purpose, the design of the test facility is such that the effective momentum can be directly measured with a force sensor or it can be calculated on the basis of measured steam momentum. Because the focus is on measuring separate effects of steam injection through the sparger holes and not on the stratification/mixing phenomenon, the water pool itself, where the sparger is submerged, is relatively small in volume.

For helping to recognize different flow regimes and for obtaining the bubble diameter as a function of time, the test facility allows high-speed video recordings of the DCC of steam. In addition, a high frequency pressure measurement helps to obtain the detachment and collapse frequencies of the bubbles. Steam needed in the tests is generated with the nearby PACTEL test facility [11]. The design principles, geometry and installed instrumentation of the SEF-POOL facility are presented in more detail in reference [12]. Appendix A presents some drawings on the facility geometry and Appendix B the locations of the measurements. The flexibility of the facility provides appropriate possibilities to extend the facility set-up according to the future research needs.

3.1 GENERAL

The main parts of the SEF-POOL facility are the sparger piping and the condensation pool. The sparger piping is connected with a pipeline to the PACTEL test facility which supplies steam needed in the tests. The sparger pipe is pivoted on a vertical axis with low friction bearings in order to allow the direct force measurement. The lower end of the sparger pipe mounts a flow plate with injection holes. Steam is discharged through the injection holes and it condenses in the pool.

In front of the flow plate there is a polycarbonate (PC) pipe, which is independent from the sparger piping and it has its own support arm which is allowed to rotate around its axis. The purpose of the PC pipe is to act as a propulsion volume and to create a parallel flow pattern so that the amount of momentum transferred from the steam to the liquid at the outlet of the PC pipe can be estimated. The condensed flow is guided through the PC pipe to impinge on the disk stack. The disk stack is designed to maximize the amount of flow driven radially outwards from the PC pipe. Backflow in the axial direction would induce an artificial increase of the force measured at the PC pipe. Axial distance between the disks is 5 mm. The steam force at the injection hole and the liquid force carried by the condensate liquid (effective momentum) can thus be measured independently by using force sensors connected to fixed supports in the floor. The current configuration of the SEF-POOL facility is shown in Figure 1.

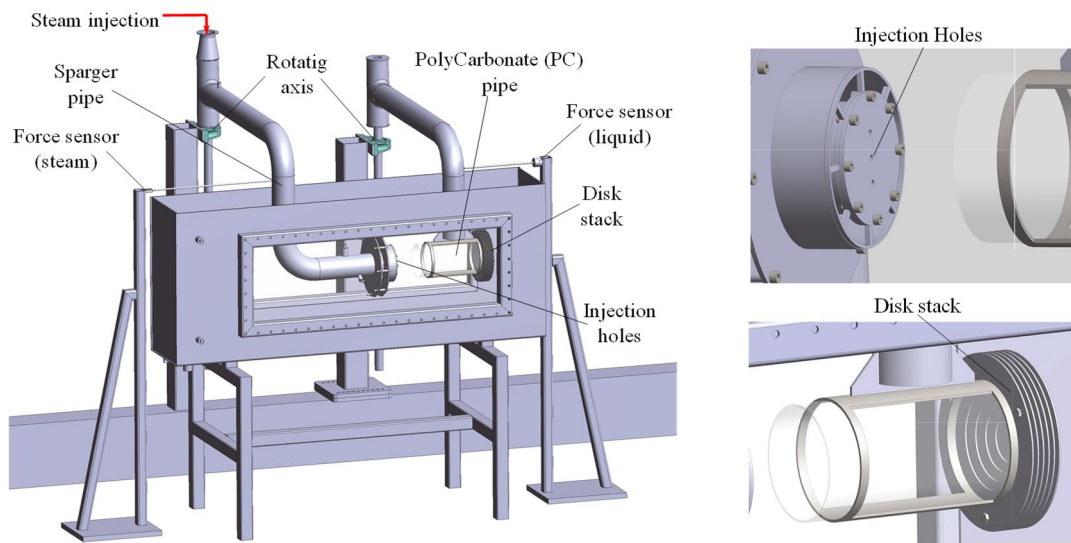


Figure 1. General view of the current SEF-POOL facility configuration where the propulsion volume (PC pipe) is independent and attached to its own support arm.

3.2 CONDENSATION POOL

The condensation pool is made of stainless steel. It is 1500 mm long, 300 mm wide and 600 mm tall. The pool is open on top and it is uninsulated. Windows on both sides are 1000 mm wide and 300 mm tall. The pool is mounted on a support made of 50x50 box section. A cover (lid) can be installed to the top to prevent any spill over or splashing of water to the laboratory site during the tests. As the pool is open on top, atmospheric

pressure will prevail in the pool in all the tests. Figure 1 in Appendix A presents the condensation pool in more detail.

3.3 SPARGER SYSTEM

The sparger piping is made of sections of DN80 stainless steel pipes and it is insulated with 13 mm thick AP Armaflex® XG flexible elastomeric thermal insulation. Dimensions of the piping are shown in Figure 2 in Appendix A. A perforated flow plate for steam injection is mounted to the end of the sparger pipe. Configuration of the flow plate can be easily changed. A set of plates with different diameter injection holes and pitch have been manufactured.

The independent PC pipe is 250 mm long and its inner diameter is ~127 mm. The distance between the injection plate and the PC pipe is 100 mm. A disk stack at the outlet of the PC pipe directs the flow radially outwards from the PC pipe. An assembly drawing of the current PC pipe configuration is shown in Figure 4 in Appendix A.

3.4 FORCE MEASUREMENT

The direct force measurements are arranged with load cells. They are located outside the condensation pool and are attached to support poles made of 50x50 mm box section bolted to the floor of the laboratory. The first load cell is at that end of the condensation pool, where the sparger piping is submerged. Another cell is at the end of the pool, where the support arm of the PC pipe is installed. Force is transmitted from the sparger piping and support arm to the sensors via thin horizontal rods. When steam is injected through the sparger piping and perforated flow plate, momentum is created and as a result the sparger piping tends to rotate around the pivot bearing. Momentum transferred to the pool liquid tends to rotate the support arm of the PC pipe. These rotating movements cause compression to the load cells and the generated forces can be thus measured. Because the force measurement compression distances are almost non-existent, the angle of the sparger piping or the angle of the support arm compared to the condensation pool does not change during the tests.

3.5 OTHER MEASUREMENTS

Two pressure transducers for steam pressure measurement are mounted in the sparger piping. One is near the steam inlet point and the other one is 140 mm upstream from the perforated flow plate. The measurement range of both transducer is 0.1-1.0 MPa.

A kHz range pressure sensor is used for capturing the detachment and collapse frequencies of the steam bubbles. It is fixed to a vertical support structure laying at the pool bottom and it can be positioned in front of the flow plate with a desired distance from the plate. The range of the sensor can be up to 0.2 MPa, 1 MPa or 2 MPa depending on the test in question. An additional pressure sensor with the range of 0-0.2 MPa was attached near the pool bottom for the 2019 tests.

Temperatures are measured with calibrated k-type thermocouples (TC). Temperature of incoming steam is measured with one TC near the inlet point at the same location as the

pressure. Steam temperature is also measured in the sparger piping at about 190 mm before the perforated flow plate. In the pool side one TC is positioned inside the PC pipe, one at the inlet of the PC pipe and one at the outlet of the PC pipe close to the disk stack. In addition, pool water temperature is also measured with three TCs attached to the pool wall on different elevations.

Water level in the condensation pool is measured with a Yokogawa® differential pressure transducer. The transducer is mounted to the base of the pool. Water level is calculated from the differential pressure reading with the help of liquid density. Temperature measurements in the pool are used to define the liquid density. Steam flow rate is measured with a vortex flow meter in the steam line.

Figure 1 in Appendix B shows the locations of the measurements of the sparger system and PC pipe. The type/frequency/range of different sensors/instrumentation can be found in Table 1 at the end of Appendix B.

3.6 DATA ACQUISITION

The National Instruments PXIe PC-driven measurement system is used for data acquisition. The system enables high-speed multi-channel measurements. The maximum recording capacity depends on the number of measurements and is in the region of mega samples per second. The measurement software is LabView 2015.

3.7 CAMERA SYSTEM

Windows on the both side walls of the condensation pool allow the capture of the DCC phenomenon of steam with a high-speed video system. Different flow regimes can be recognized and bubble diameters obtained with the help of the system.

The high-speed camera system consists of two monochromatic Phantom Miro 310 cameras. The maximum resolution is 1280x800 px, but in practise the picture area is cropped in order to increase the maximum amount of the images the 12 GB internal memory can hold, thus increasing the total time of the recordings.

For the 2019 tests, the horizontal angle of the camera was re-adjusted so that the view was closer to parallel to the front surface of the sparger plate. It was hoped that this would help to reduce some difficulties in the identification of the bubble shape at the early stage of the bubble growth.

Compared to the earlier SEF-POOL tests, an increased frame rate (but reduced length of video clips) was used in the 2019 tests. Most of the tests were done with one high-speed camera, but in a few tests stereo imaging was tried with two cameras.

4 SEF-POOL TESTS

The main goal of the SEF-POOL tests in 2019 was to provide data of the characteristics of small-scale phenomena, which affect the effective heat and momentum sources. This information will then be used in the validation of the simplified EHS/EMS models by KTH. Furthermore, the SEF-POOL tests support the validation effort of the DCC and

interfacial area models of CFD codes for steam injection through spargers at VTT and LUT.

KTH is developing a unit cell model to predict the effective momentum distribution on a coarser mesh when pool and injection characteristics are given. The previous results from the SEF-POOL tests suggest that with respect to the effective momentum there is no noticeable difference between single and multiple holes, nor between holes with different diameters. This may suggest that the effect of the chamfer of the injection hole (or other geometrical modifications) might be also relatively small. On the other hand, it was found that there is a significant difference between the sonic and subsonic injection regimes. The data indicates that different regimes might exist for Jakob number values larger than 0.12. Jakob number represents the ratio of sensible heat to latent heat absorbed (or released) during the phase change process. It is defined as

$$Ja = \frac{c_{pL}(\Delta T)}{h_{fg}}$$

where c_{pL} is specific liquid heat at constant pressure, ΔT sub-cooling and h_{fg} latent heat of condensation.

On the basis of the findings listed above it was decided with KTH that the following issues will be addressed in the 2019 tests:

- i. Effect of high Ja numbers on the effective momentum, i.e. steam injection into initially highly subcooled pool, (at least $T_p \leq 10^\circ\text{C}$), in sonic and subsonic regimes
- ii. Effective momentum in the transition regime, i.e. the effect of transition from subsonic to sonic flow conditions (steam injection at Mach numbers $\sim 0.9 < M < 1.1$)
- iii. Effective momentum at mass fluxes higher than $300 \text{ kg/m}^2\text{s}$
- iv. Effect of nozzle chamfer

A total of 12 steam injection tests were performed in the SEF-POOL facility in 2019. The first one was a shake-up test to check the systems. Two tests had to be repeated due to some problems during the test procedure. Thus, nine actual tests were carried out.

The test parameters and procedures were obtained from KTH. The effective momentum and other parameters were measured during the tests. In addition, high-speed video clips of the DCC phenomenon of steam were recorded. Based on this high-resolution measurement data KTH will refine the semi-empirical correlations for

- the effective momentum, and
- the bubble collapsing frequency, radius, velocity, pressure gradient and heat transfer coefficients.

The semi-empirical correlations for the effective momentum are currently used at KTH to model the behaviour of the full-scale pressure suppression pool during a steam injection through spargers in a Nordic BWR. Table 1 lists the main parameters of the tests done in 2019.

Table 1. SEF-POOL tests in 2019

Test	PC tube	Force sensor	Steam flow rate [g/s]	Initial pool water level/temp [m/°C]	Flow plate	High speed video
SEF-S0 (shake-up)	yes	two	~28-64	0.50/9	1x16 mm	2800 fps
SEF-S20 (failed)	yes	two	~27	0.42/11	1x16 mm	2800 fps
SEF-S20R (repeat of S20)	yes	two	~31	0.44/6	1x16 mm	2800 fps
SEF-S21	yes	two	~65	0.45/3	1x16 mm	2800 fps
SEF-S22	yes	two	~50	0.46/5	1x16 mm	6600 fps
SEF-S23	yes	two	~115	0.45/2	1x16 mm	6600 fps
SEF-S24	yes	two	~42	0.45/2	1x16 mm	6600 fps
SEF-S25	no	one	~50	0.44/2	1x16 mm	6600 fps
SEF-S26	no	one	~46	0.44/5	1x16 mm	6600 fps Two cameras
SEF-S27 (failed)	no	one	~29	0.45/3	1x16 mm Chamfer 125°	6600 fps Two cameras
SEF-S27R (repeat of S27)	no	one	~32	0.45/4	1x16 mm Chamfer 125°	6600 fps Two cameras
SEF-S28	no	one	~69	0.45/4	1x16 mm Chamfer 125°	6600 fps Two cameras

The following chapters present selected results from the steam injection tests in 2019 and discuss the key observations based on those results. The shake-up test (SEF-S0) as well as the two unsuccessful tests (SEF-S20, SEF-S27) are not presented here.

Figure 2 presents a regime map for direct contact condensation developed by Chan and Lee [5]. The boundaries of various condensation modes on the flow regime map are established by two criteria: (a) the location of the steam region relative to the pipe exit and (b) the location at which steam bubbles detach from the source. The horizontal boundary (solid line from the left edge to the right edge) in Figure 2 shows whether the steam region is completely below the pipe exit or has expanded to encapsulate part of the pipe. The vertical boundaries indicate how steam is being released from the pipe exit.

The flow modes covered in the previous SEF-POOL steam injection tests are the oscillatory bubble regime, the oscillatory cone jet regime and partly the ellipsoidal jet regime. The oscillatory bubble and cone jet regimes are relevant for BWR plant conditions when spargers inject at mass fluxes between 75-300 kg/m²s [5]. In the SEF-POOL tests in 2019, the steam mass flux varied between 135- 345 kg/m²s placing the

tests mainly in the oscillatory cone jet regime on the map. In one test (SEF-S23) the steam mass flux was about $572 \text{ kg/m}^2\text{s}$. With this mass flux value, the flow mode can be described as a stable jet. In all tests, the injection flow plate had a single 16 mm orifice.

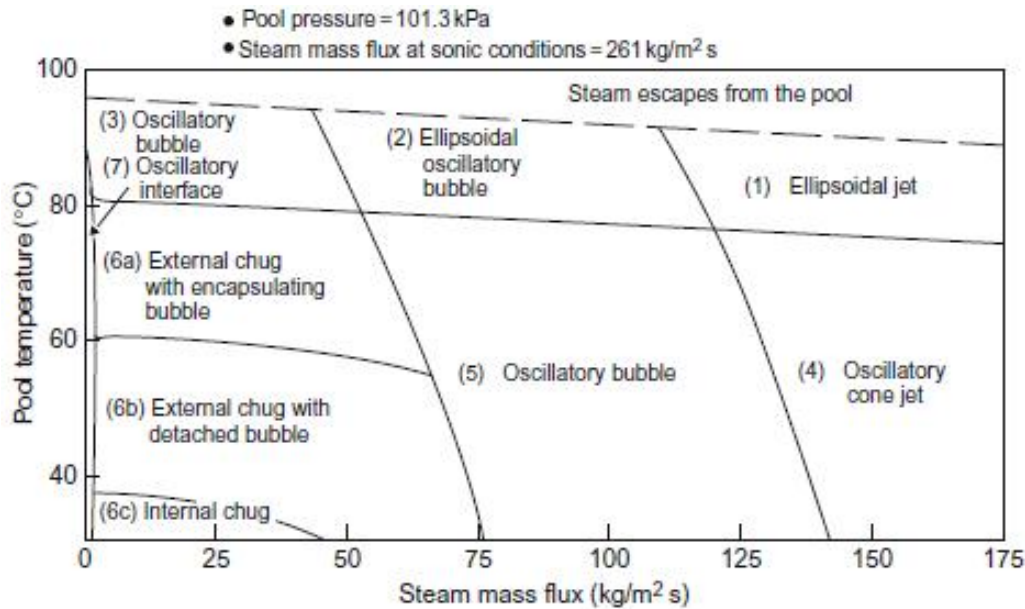


Figure 2. Condensation regime map for a single-hole sparger [5].

One goal of the tests in 2019 was to verify the validity of the EMS/EHS models in highly sub-cooled conditions. Therefore, during the preparations for most of the tests a few kilograms of ice was put in the pool before filling it with water. The initial pool water temperature in those tests was between 2°C and 6°C . The parameter range covered in the 2019 tests was thus extended from the previous tests by using both high steam flow rates and initially highly sub-cooled pool water.

In each test, the steam mass flow rate was first adjusted to the desired value and then it was kept constant for the rest of the test. Adjustment of the flow rate was challenging, especially with the small flow rates, and could take 200-300 seconds. The tests were usually continued until the pool water temperature was approaching $98-99^\circ\text{C}$. A couple of tests were terminated earlier when the temperature was around $85-90^\circ\text{C}$ and one test at about 65°C . Fast data (pressure, forces and video) was recorded from 8-10 short sequences as the pool temperature increased. In two tests, the high-speed video clips were recorded with the frame-rate of 2800 fps (clip length 1.03 s). In the rest of the tests, the frame-rate was increased to 6600 fps (clip length 0.262 s). In the three last tests, two cameras were used in order to get stereo images of collapsing steam bubbles and thus to improve possibilities to evaluate bubble properties on the basis of the video recordings.

For the four last tests, the PC tube and its support arm was removed from the pool to get a better view of the DCC phenomenon. It was also noticed earlier that when the pool water temperature exceeded $85-90^\circ\text{C}$ at the final stages of the tests, the steam bubbles survived without condensing so long that they collided to the disk stack at the end of the PC tube. Naturally, there was only one force measurement available in those tests where the PC tube support arm was in its place.

4.1 TESTS ON REGIME TRANSITION AND EFFECT OF SUB-COOLING

The effect of high Ja numbers on the effective momentum, i.e. steam injection into initially highly subcooled pool in sonic and sub-sonic regimes as well as effective momentum in the transition regime i.e. steam injection at Mach numbers $\sim 0.9 < M < 1.1$ were studied in tests SEF-S20R, SEF-S21, SEF-S22, SEF-S24, SEF-S25 and SEF-S26.

For example, in the SEF-S20R test, sub-sonic flow conditions prevailed (steam mass flux was about $154 \text{ kg/m}^2\text{s}$) while in SEF-S21 the flow conditions were sonic (steam mass flux was about $323 \text{ kg/m}^2\text{s}$). Both tests were started with highly sub-cooled pool water. Figures 3 and 4 present the time averaged steam mass flow rate, force values and pool temperature from those two tests. It can be seen that in the sub-sonic case (Figure 3) the measured force values first jump to about 3.0-3.5 N when the steam injection is started and after that have an increasing trend until the pool temperature reaches 80°C . In the sonic case (Figure 4) the force values quite fast increase to about 28-30 N with the initiation of steam injection but after that they have only a very gradual increasing trend.

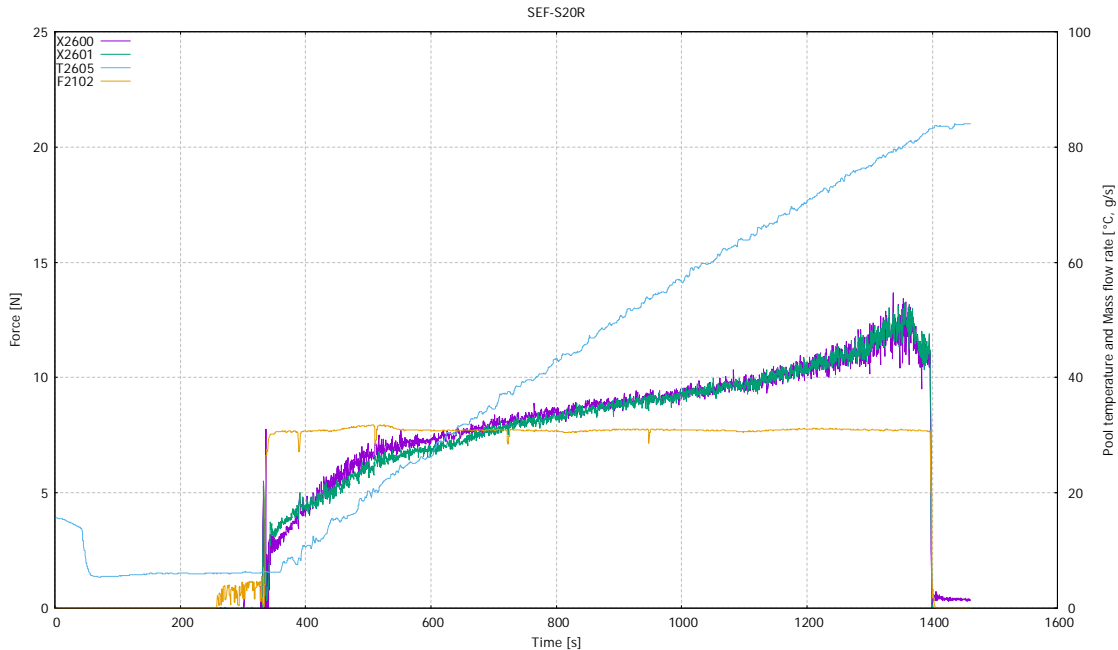


Figure 3. Measured forces (X2600, X2601), flow rate (F2102) and pool temperature (T2605) from the SEF-S20R test (relevant time period begins at about 350 s when the flow rate has been adjusted to the desired value).

KTH has made a preliminary analysis of the effect of sub-cooling on the effective momentum coefficient C , i.e. the ratio of liquid momentum rate to the theoretical value of momentum rate of steam. Figure 5 shows C coefficient as a function of Ja number from the SEF-S20R and SEF-S21 tests among the earlier SEF-POOL tests. As it was anticipated, there is a different tendency for the effective momentum (C coefficient) at water temperatures below 15 degrees. The SEF-S20R and SEF-S21 tests confirm that

high subcooling doesn't affect sonic jets, while it has a significant influence on the subsonic injection.

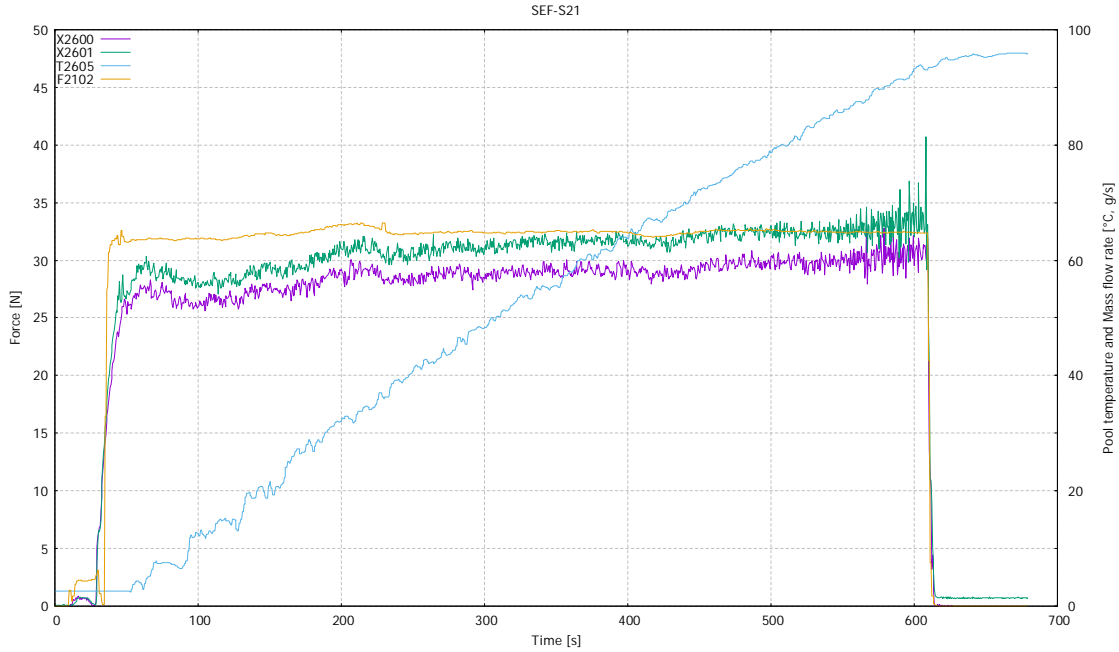


Figure 4. Measured forces (X2600, X2601), flow rate (F2102) and pool temperature (T2605) from the SEF-S21 test (relevant time period begins at about 60 s when the flow rate has been adjusted to the desired value).

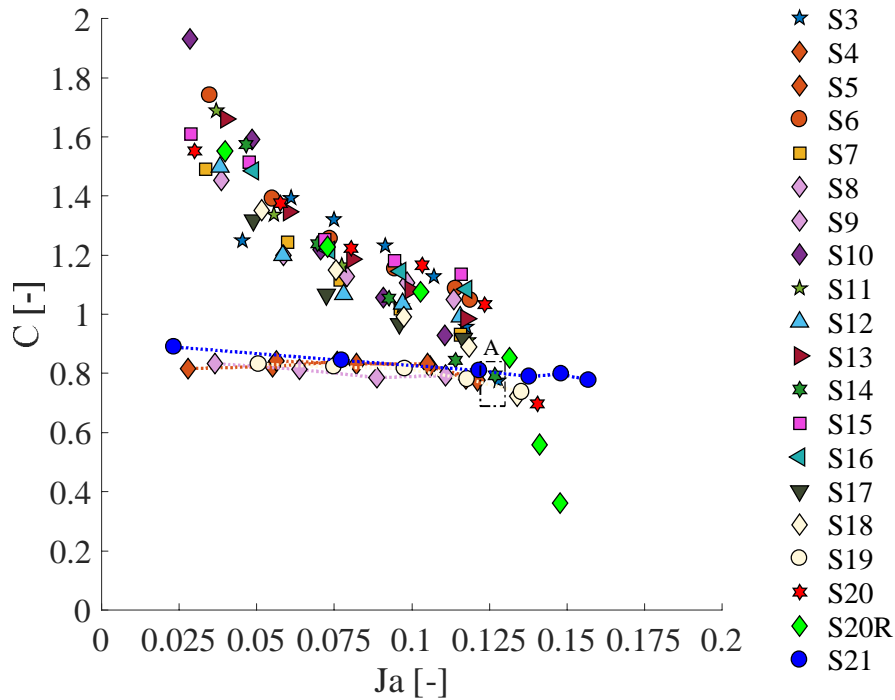


Figure 5. Effect of sub-cooling on the effective momentum coefficient in various SEF-POOL steam injection tests (Figure composed by KTH).

Figure 6 shows an example of a test (SEF-S25), where the steam mass flux (about $248 \text{ kg/m}^2\text{s}$) is in the transition region, i.e. not clearly in the sub-sonic or sonic region. It also shows what happens when a test is continued almost to saturated pool conditions. In this test the PC pipe was not in the pool and only one force sensor was thus in use. The rather strong dependency of M_{eff} on the combination of the Mach and Jakob numbers in the transition region can be seen from the measured force curve. The decreasing trend of the force curve at pool water temperatures above 80°C is illustrated, too.

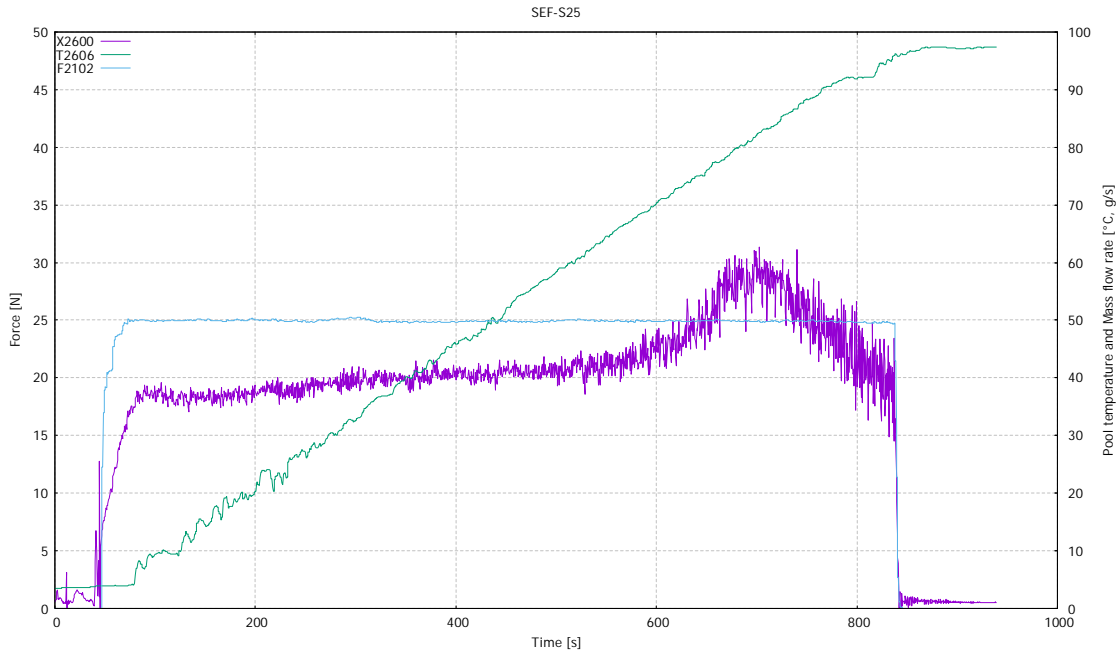


Figure 6. Measured force (X2600), flow rate (F2102) and pool temperature (T2606) from the SEF-S25 test (relevant time period begins at about 80 s when the flow rate has been adjusted to the desired value).

4.2 TEST ON HIGH FLOW RATE

In the SEF-S23 test, the main point was to check if there is any different tendency or anything unexpected in the range of very high steam flow fluxes ($\sim 500\text{--}600 \text{ kg/m}^2\text{s}$) compared to the highest cases ($\sim 320\text{--}330 \text{ kg/m}^2\text{s}$) studied before. The used steam mass flux in the SEF-S23 test was about $572 \text{ kg/m}^2\text{s}$. Figure 7 shows the time averaged steam mass flow rate, force values and pool temperature from the test.

The shapes of the force measurement curves (except after the failure of the X2601 sensor at the end) are similar as in the SEF-S21 test, which was done also with sonic flow conditions but with about half smaller steam mass flux. The absolute values of the measured forces are of course higher with the larger mass flux, but the almost linear and very slightly increasing trends with the rising pool temperature are common to both cases. The results of the test thus suggest that the higher mass flow rates have no effect on the effective momentum coefficient. Therefore, no additional tests were done at such conditions with high mass flow rates in this test series.

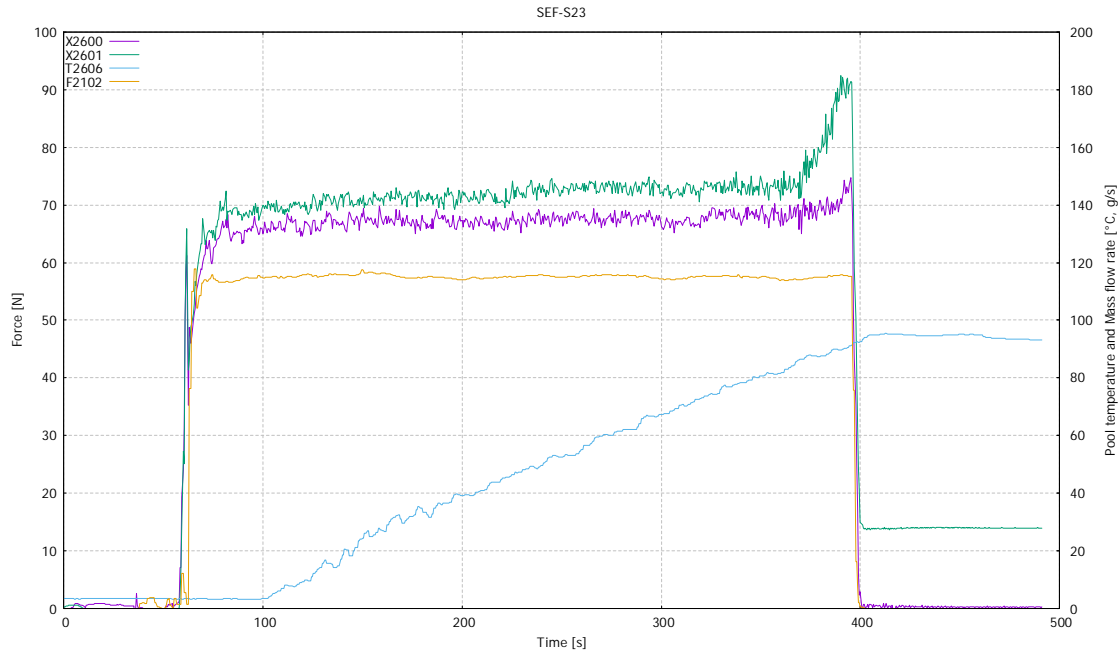


Figure 7. Measured forces (X2600, X2601), flow rate (F2102) and pool temperature (T2605) from the SEF-S23 test (relevant time period begins at about 95 s when the flow rate has been adjusted to the desired value). Note that the zero point of the force sensor X2601 shifted at about 370 s and its readings after that are invalid!

4.3 TESTS OF EFFECT OF CHAMFER

The last two tests (SEF-S27R, SEF-S28) of the test campaign in 2019 concentrated on the effect of the chamfered injection hole. This means that the injection plate used in those tests was manufactured so that a 125° chamfer on the outlet edge of the 16 mm orifice was formed. Practically all the injection holes in plant spargers are drilled with chamfers. The earlier experiments in the SEF-POOL facility (or in the PPOOLEX facility) have not addressed the chamfer effect, i.e. all the tests have been run with straight holes.

The SEF-S27R test was done with sub-sonic flow conditions (steam mass flux about 159 kg/m²s) while the SEF-S28 test with sonic flow conditions (steam mass flux about 343 kg/m²s). The SEF-S20R and SEF-S21 tests, done with a straight injection hole, can be used as reference cases, because the sub-sonic and sonic flow conditions in those tests were almost the same as in the chamfer cases.

Figure 8 shows the time-averaged steam mass flow rate, force value and pool temperature from the sonic chamfer case, i.e. from the SEF-S28 test. If we compare it to the straight hole reference case (SEF-S21) shown earlier in Figure 4 we can see that the measured force values in these two tests are close to each other. Soon after the steam injection flow reaches its desired value, the force measurements stabilize to about 27-29 N and then increase steadily as the pool water temperature rises. At 90 °C pool temperature, the force values are about 33-35 N.

The straight-hole reference case was done with the PC pipe in the pool while the chamfer case was done without the PC pipe and only with one force sensor in use. The small

difference in the measured force values between the straight and chamfered hole cases are believed to originate rather from the effect caused by the PC pipe than the effect caused by the chamfer. This conclusion bases on the fact that the existence of the PC pipe in the pool has earlier been found to have a small effect on the measured force value.

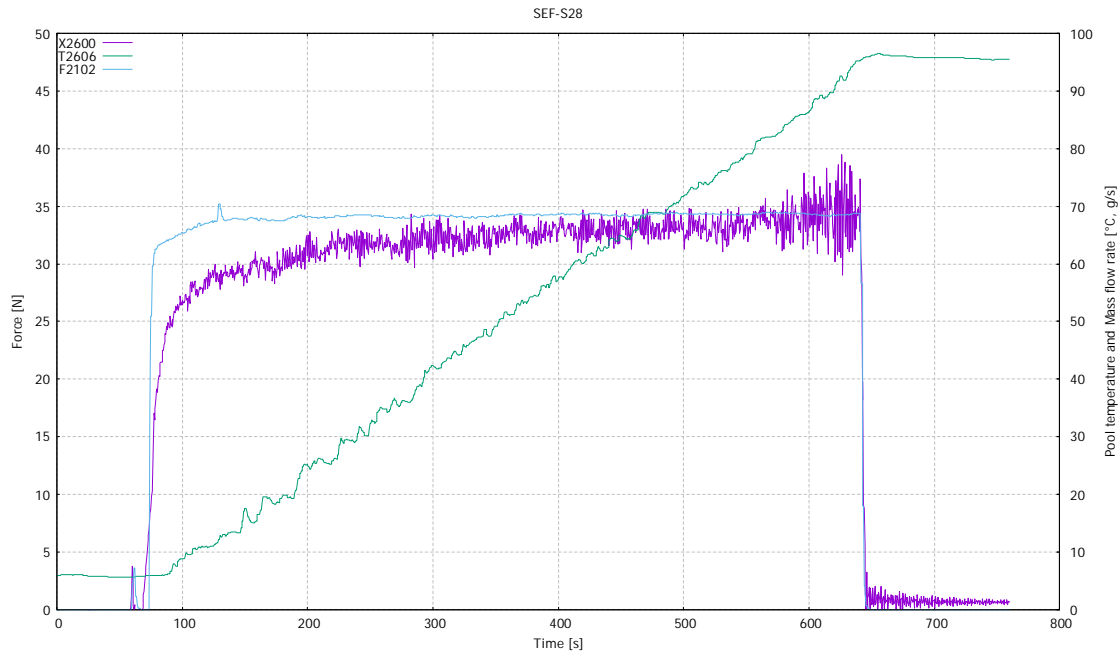


Figure 8. Measured force (X2600), flow rate (F2102) and pool temperature (T2606) from the SEF-S28 test (relevant time period begins at about 140 s when the flow rate has been adjusted to the desired value).

It can be concluded that the chamfer effect on the effective momentum magnitude was found almost insignificant. No additional tests on this topic are needed.

4.4 QUALITATIVE ANALYSIS OF VIDEO IMAGES

The oscillatory motion of the steam bubbles can be divided into three parts. That is, the bubble begins to grow attached to the injection holes, detaches when the force balance becomes positive in the direction of the steam injection, and collapses as the neck connecting the bubble to the injection hole reduces the steam flow into the bubble.

At low sub-cooling, detached bubbles can move a large enough distance from the injection holes and allow the formation of a new bubble before their collapse. It can also be observed that the collapse phase at large sub-cooling leads to a steam-water cloud with no clear boundary between vapour and liquid.

In 2019 tests, one objective was to develop the image analysis approach to evaluate flow velocity around the steam jet. The goal was to be able to estimate water entrainment along the jet. Currently, KTH relies on the movement of bubbles in the image to compute flow velocity. One disadvantage with this approach is that it is not known if the bubbles are located in the same plane as the jet or not. Two possible methods were thought of. Bubbles/tracers could be highlighted with light/laser to indicate which ones belong to the

central plane, or extra bubbles/traces could be generated in the central plane. The latter method was chosen for experimenting in the last four tests in 2019. For that purpose, a horizontal pipe with small holes drilled on the upper side was installed to the central line of the pool below the elevation of the steam jet. During the tests, a small amount of air was injected into the pipe so that a stream of small bubbles escaping from the holes on the upper side was formed. The air bubbles were then drawn into the by-passing liquid flow before finally being entrained into the steam jet.

Due to space limitations, the PC tube cannot be used at the same time with the air bubble injection system and therefore the SEF-S25...SEF-S28 tests were done without the PC tube. Furthermore, stereo imaging with two high-speed cameras was tried in the last three tests. Figure 9 presents a series of image frames captured from a high-speed video (6600 fps) where the air bubble system was tested during the preparations to the SEF-S28 test before steam injection into the pool was initiated.

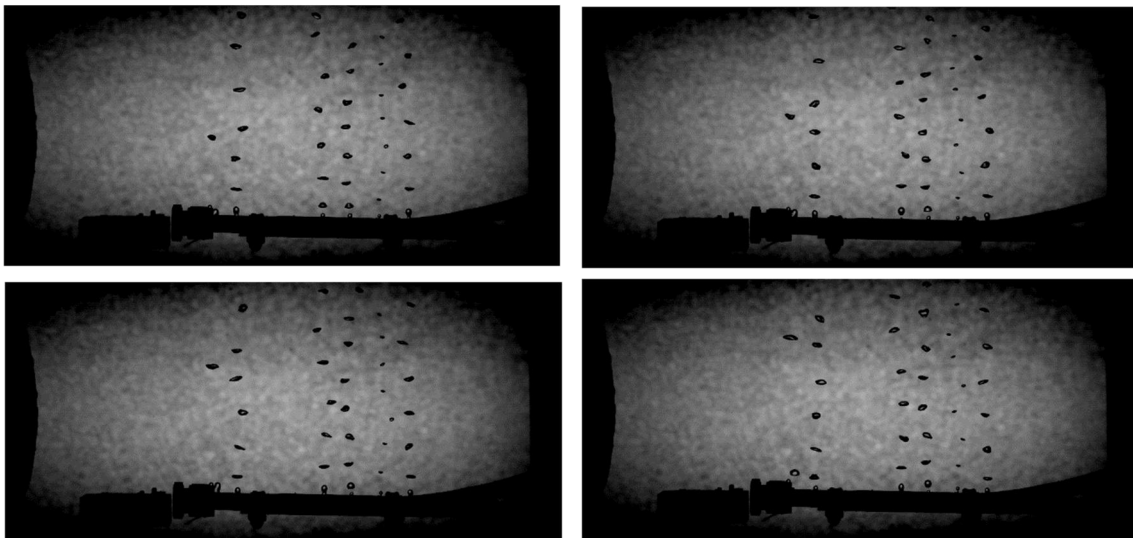


Figure 9. Video frames from air bubble test ($\Delta t = 0.06$ s).

An example of stereo imaging with two high-speed cameras is presented with captured image frames in Figure 10. The frames are from the SEF-S28 test and they are from a recording sequence of the high-speed cameras (6600 fps) when the water pool temperature had increased to about 42 °C. The steam mass flux in the test was about 343 kg/m²s. The interval between the captured images is 20 frames, which means that they are taken about 0.003 seconds from each other. Six images are presented both from the left-side and right-side camera. With frozen images, only an incomplete conception of the speed and route of drifting air bubbles can be accomplished. By looking at the live video recordings, a much more precise understanding of how the air bubbles accelerate along the fluid flow can be gained.

The image analysis approach developed by KTH and applied to the recorded high-speed clips from the SEF-POOL tests has given some encouraging preliminary results in determining the flow velocity around the jet. Also bubble radius, velocity and collapsing frequencies will be obtained through the analysis of the video images, as the work with the clips continues at KTH.

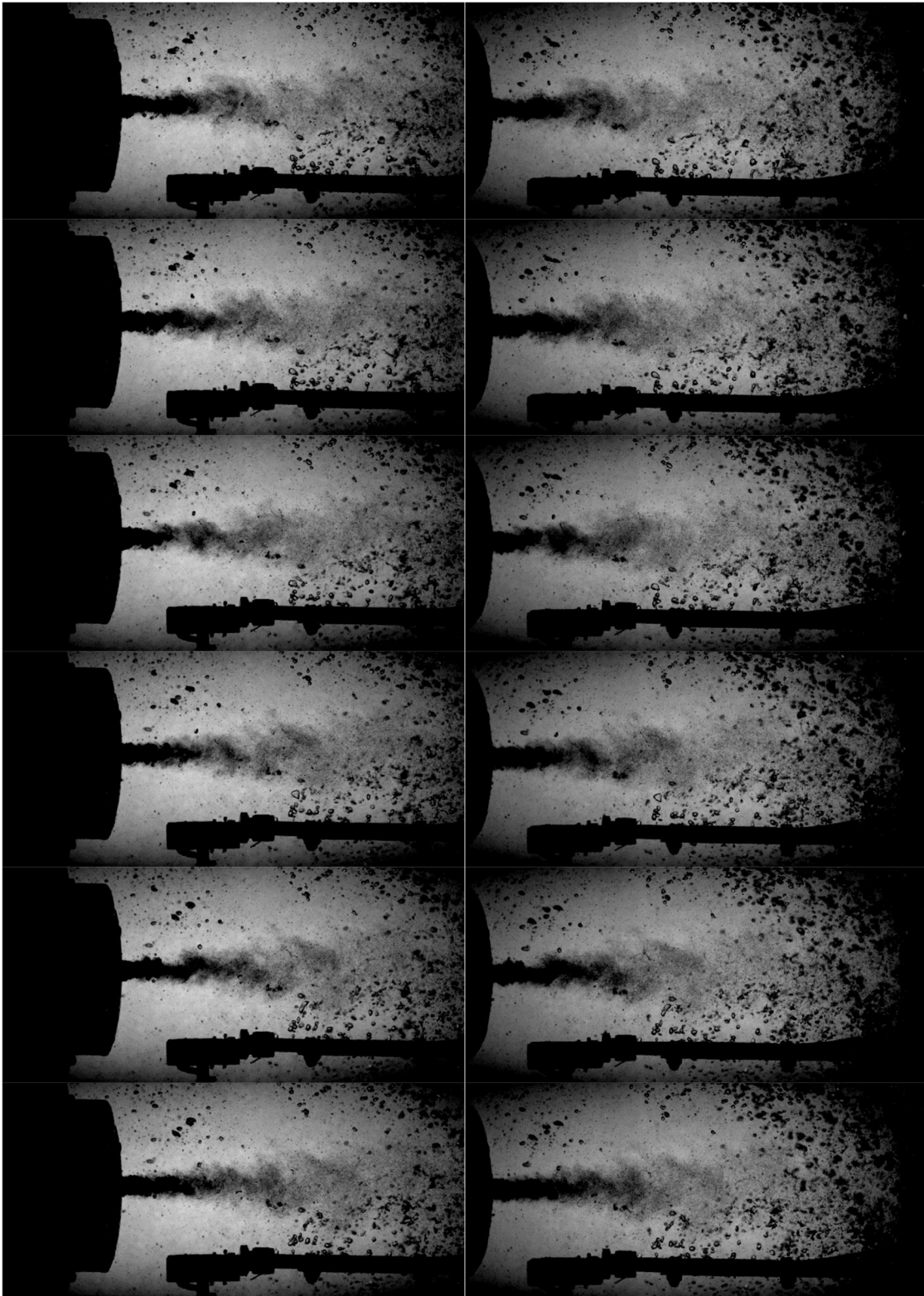


Figure 10. Stereo video images from the SEF-S28 test with steam (from left) and air bubbles (from bottom) injection. Images on the left are from the left-side camera and images on the right are from the right-side camera.

5 CONCLUSIONS

Prediction of the effective momentum induced by the oscillatory bubble and oscillatory cone jet regimes is necessary for the modelling of the pool behaviour. This is especially relevant for BWRs, where the development of thermal stratification or mixing during a steam injection through spargers can affect the performance of the suppression pool. In order to directly measure the effective momentum, the SEF-POOL facility was built at LUT University and an extensive test series is being carried out. The reference system for the SEF-POOL facility is an SRV sparger pipe of a BWR plant. Hence the facility is designed in such a way that discharge of steam through the injection holes at the sparger lower end into the sub-cooled pool water can be simulated representatively.

Analysis of the previous tests by KTH has shown that oscillatory bubble motions are a very efficient mechanism of transferring the force from the steam to the mean flow liquid. The main goal of the SEF-POOL tests in 2019 was to provide data of the characteristics of the small-scale phenomena, which affect the effective momentum sources in case of steam injection through a sparger into a sub-cooled pool of water. This information will then be used in the validation of the simplified EHS/EMS models for spargers by KTH. Furthermore, the SEF-POOL tests support the validation effort of the DCC and interfacial area models of CFD codes for steam injection through spargers at VTT and LUT.

Nine actual steam injection tests were performed in the SEF-POOL facility in 2019. The following issues were addressed:

- i. Effect of high Ja number on the effective momentum, i.e. steam injection into initially highly subcooled pool in sonic and sub-sonic regimes
- ii. Effective momentum in the transition regime, i.e. effect of transition from sub-sonic to sonic flow conditions
- iii. Effective momentum at mass fluxes higher than $300 \text{ kg/m}^2\text{s}$
- iv. Effect of nozzle chamfer

Preliminary analysis of the tests by LUT and KTH reveal that the results fit well with the previous data and are very helpful for the understanding of the key effects and factors that can be neglected when the EMS/EHS models are developed further [13]. Based on the results, the following new findings from the SEF-POOL tests in 2019 can be summarized.

- 1) Both the Jacob and Mach number have a significant effect on the effective momentum coefficient C (i.e. the ratio of the liquid momentum rate to the theoretical value of the momentum rate of steam). New data provides a possibility to quantify the effect of the Mach number, which was only qualitatively noticeable in the previous data set.
- 2) In choked flow conditions, except for the cases with a very large Ja number, the steam mass flow rate (or theoretical Mach number) has no effect on the effective momentum coefficient, which is close to ~ 0.8 in this regime.
- 3) The Ja number has a minor and nearly linear effect on the effective momentum coefficient, which is increasing as the Ja number is decreasing.

- 4) At very large Ja numbers ($\sim 0.16-0.2$), the condensation rate is very large, which leads to rapid reduction of the effective momentum coefficient. This effect can be observed even at choked flow conditions (as mentioned above) when the theoretical Mach number for steam is relatively small, $\sim 1-1.3$.
- 5) As the Ja number approaches to zero, the effective (time-averaged) momentum coefficient behaves non-monotonically, i.e. it reaches a maximum value at $Ja \sim 0.02-0.04$ and then decreases.
- 6) There is no apparent dependency of the effective momentum coefficient on chamfer in the injection holes.
- 7) Comparison with the previous data suggests that the hole diameter also doesn't have an effect on the effective momentum coefficient, except with the value of the Ja number at which C reaches its maximum value.
- 8) Comparison of the earlier test results (the S3 and S17 tests with the $\varnothing 8$ mm orifice) indicate that the maximum value of C can be reached with larger values of Ja number when the hole size is smaller. This can be an indication that the Weber and/or Reynolds number might play a role in the transition.

Figure 11 below shows the effective momentum coefficient C as a function of the Mach and Jakob numbers in a combined illustration from the steam injection tests in the SEF-POOL facility in 2018-2019.

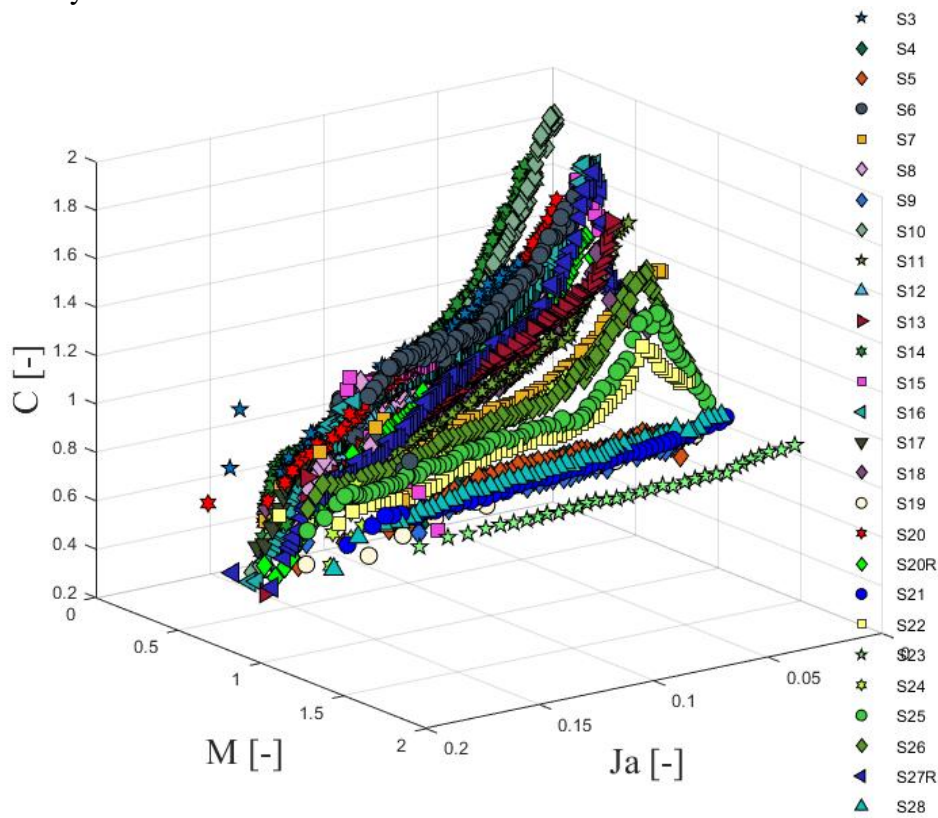


Figure 11. Effective momentum coefficient C as a function of the Mach and Jakob numbers in the steam injection tests in the SEF-POOL facility in 2018-2019 (Figure composed by KTH).

Bubble parameters, which have been estimated through the image processing of the high-speed videos of the SEF-POOL tests by KTH, include the collapse and bubble life frequencies, maximum bubble radius, bubble velocities, pressure gradient, and heat transfer coefficients. A good agreement is observed in the data and proposed correlations. Regarding the heat transfer coefficient, further tests are required to reduce the uncertainties associated with its strong time-dependency and the steam flow entering the bubble.

REFERENCES

- [1] Li, H., Kudinov, P., Effective Approaches to Simulation of Thermal Stratification and Mixing in a Pressure Suppression Pool. OECD/NEA & IAEA Workshop CFD4NRS-3, September 14-16, 2010, Bethesda, MD, USA.
- [2] Li, H., Villanueva, W., Kudinov, P., Approach and development of effective models for simulation of thermal stratification and mixing induced by steam injection into a large pool of water. Sci. Technol. Nucl. Ins. 2014, <http://dx.doi.org/10.1155/2014/108782>, (Article ID 108782).
- [3] Li, H., Villanueva, W., Puustinen, M., Laine, J., Kudinov, P., Validation of effective models for simulation of thermal stratification and mixing induced by steam injection into a large pool of water. Sci. Technol. Nucl. Ins. 2014, <http://dx.doi.org/10.1155/2014/752597>, (Article ID 752597).
- [4] Li, H., Villanueva, W., Puustinen, M., Laine, J., Kudinov, P., Thermal stratification and mixing in a suppression pool induced by direct steam injection. Annals of Nuclear Energy. 2018, 111, <https://doi.org/10.1016/j.anucene.2017.09.014>.
- [5] Chan, C.K., Lee, C.K.B., A regime map for direct contact condensation. International Journal of Multiphase Flow, 8 (1982), pp. 11-20.
- [6] Gallego-Marcos, I., Kudinov, P., Villanueva, W., Kapulla, R., Paranjape, S., Paladino, D., Laine, J., Puustinen, M., Räsänen, A., Pyy, L., Kotro, E., Pool Stratification and Mixing Induced by Steam Injection through Spargers: Analysis of the PPOOLEX and PANDA experiments. Nuclear Engineering and Design, 337 (2018), pp. 300-316. <https://doi.org/10.1016/j.nucengdes.2018.07.004>
- [7] Gallego-Marcos, I., Kudinov, P., Villanueva, W., Kapulla, R., Paranjape, S., Paladino, D., Laine, J., Puustinen, M., Räsänen, A., Pyy, L., Kotro, E., Pool Stratification and Mixing during a Steam Injection through Spargers: CFD modelling of the PPOOLEX and PANDA experiments. Nuclear Engineering and Design, 347 (2019), pp. 67-85. <https://doi.org/10.1016/j.nucengdes.2019.03.011>
- [8] Pättikangas, T., Hovi, V., CFD Simulation of Condensation of Vapor Jets. Research Report VTT-R-00993-18. Espoo 2018.
- [9] Puustinen, M., Laine, J., Räsänen, A., Kotro, E., Tielinen, K., Characterizing Tests in SEF-POOL Facility. Lappeenranta University of Technology, School of Energy Systems, Nuclear Engineering, Research Report INSTAB 3/2017. Lappeenranta 2018.
- [10] Puustinen, M., Laine, J., Räsänen, A., Kotro, E., Tielinen, K., SEF-POOL Tests. Lappeenranta-Lahti University of Technology, School of Energy Systems, Nuclear Engineering, Research Report INSTAB 1/2018. Lappeenranta 2019.

- [11] Tuunanen, J., Kouhia, J., Purhonen, H., Riikonen, V., Puustinen, M., Semken, R. S., Partanen, H., Saure, I., Pylkkö, H., General Description of the PACTEL Test Facility. Espoo: VTT. 1998. VTT Research Notes 1929. ISBN 951-38-5338-1.
- [12] Tielinen, K., Räsänen, A., Kotro, E., Saure, I., General description of SEF-POOL test rig. Lappeenranta University of Technology, School of Energy Systems, Nuclear Engineering, Research Report INSTAB 2/2017. Lappeenranta 2018.
- [13] Gallego-Marcos, I., Kudinov, P., Villanueva, W., Puustinen, M., Räsänen, A., Tielinen, K., Kotro, E., Effective Momentum Induced by Steam Injection in the Oscillatory Bubble Regime. Nuclear Engineering and Design, 350 (2019), pp. 259-274. <https://doi.org/10.1016/j.nucengdes.2019.05.011>

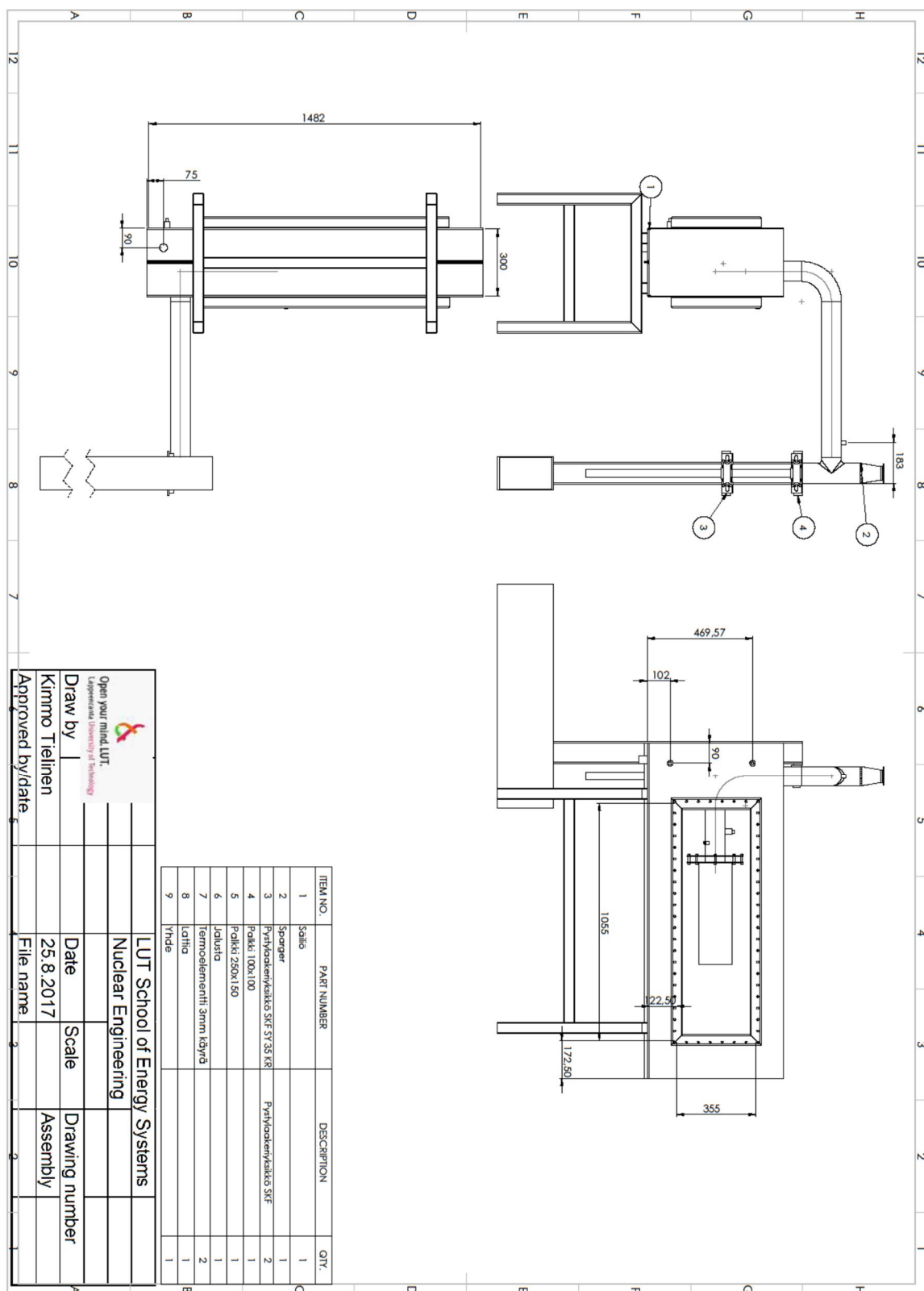


Figure 1. Condensation pool.

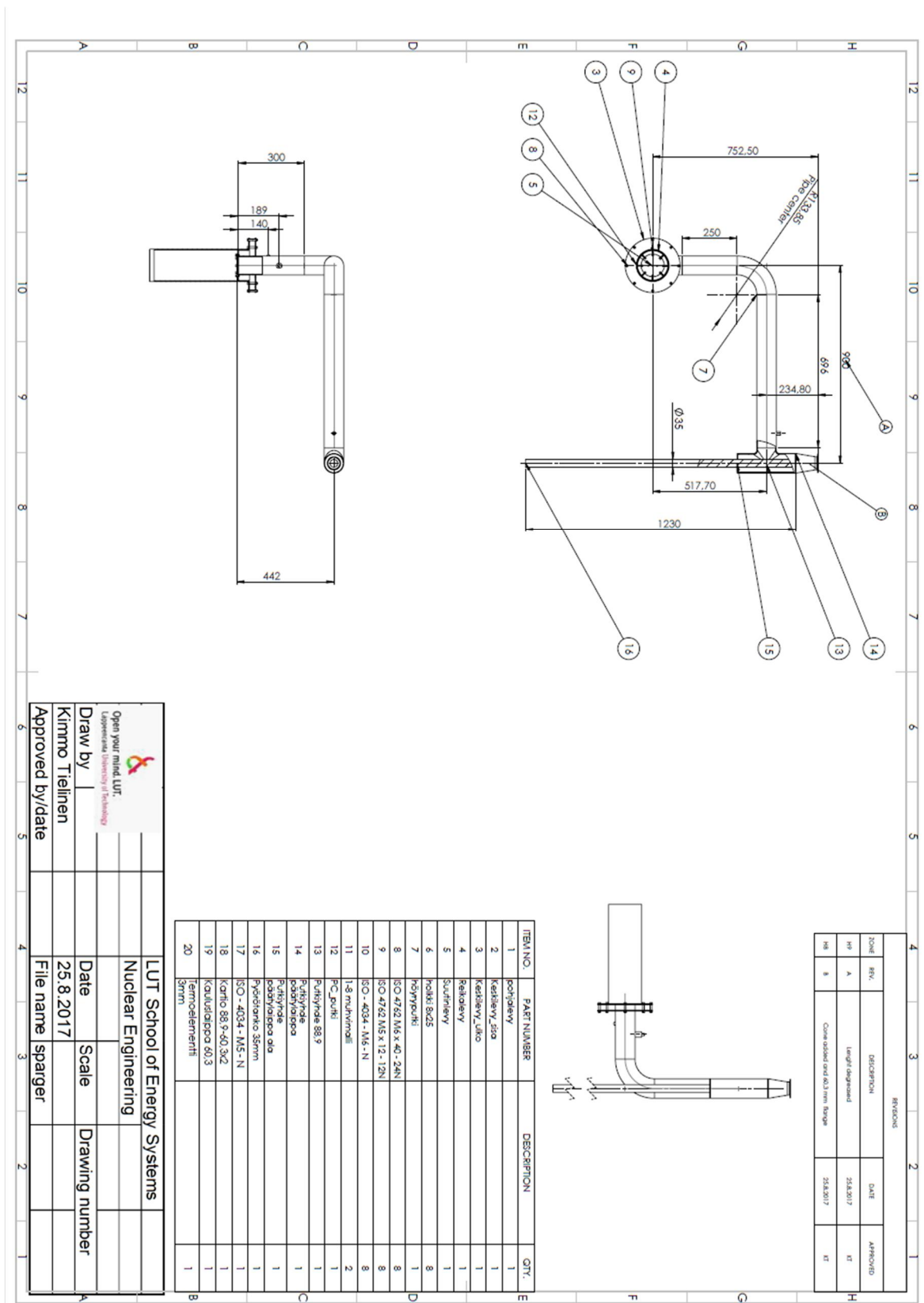


Figure 2. Sparger piping.

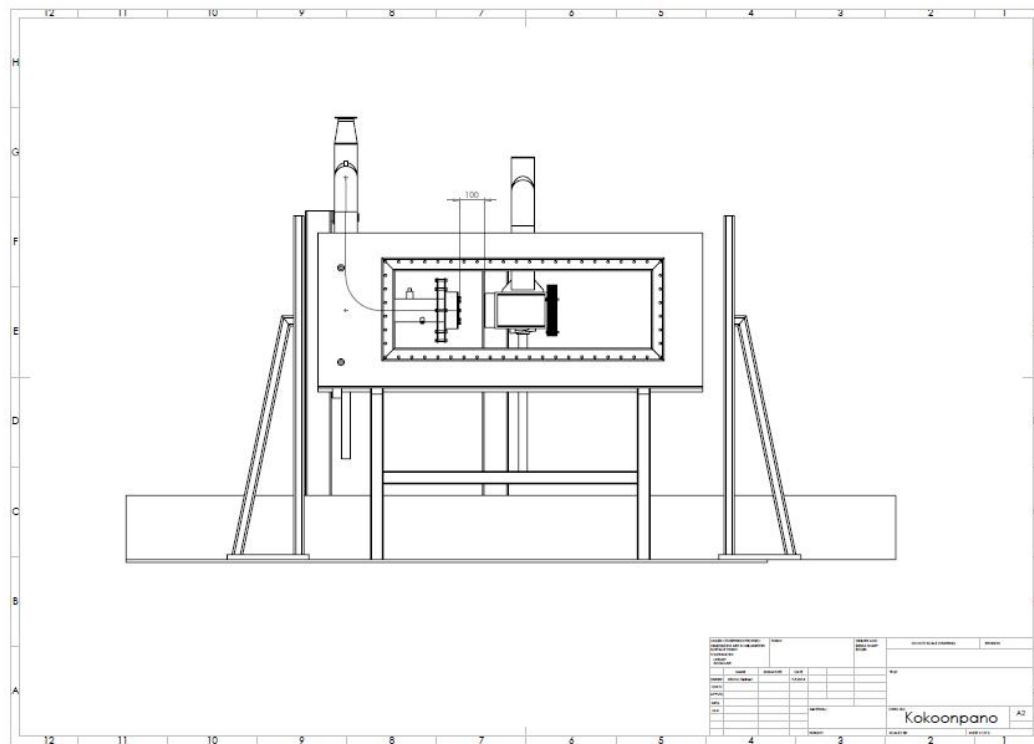


Figure 3. Sparger system and independent PC pipe of the current facility configuration.

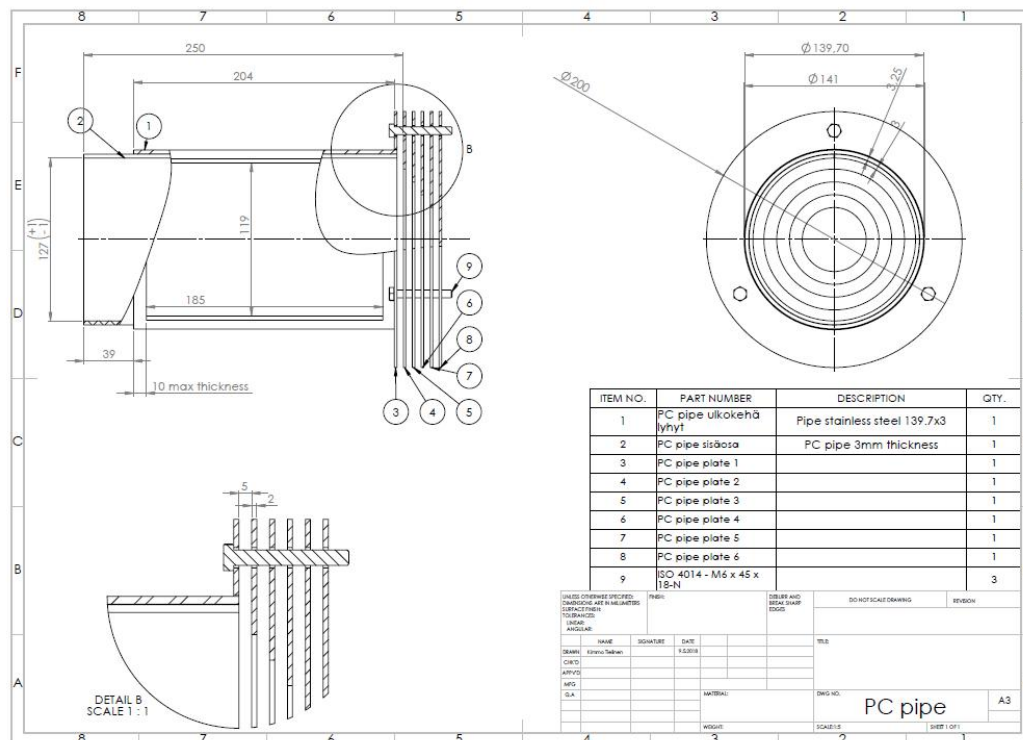


Figure 4. PC pipe and attached disk stack in the current facility configuration.

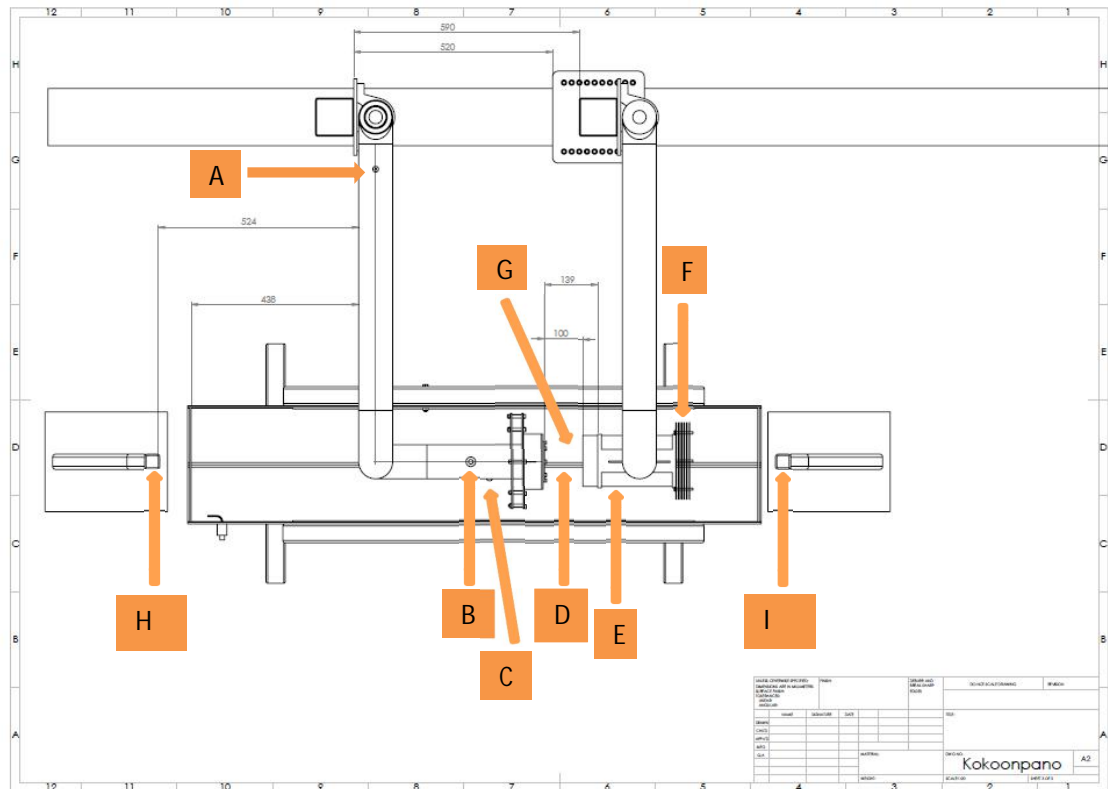


Figure 1. Measurements of the sparger system and PC pipe in the current facility configuration.

Table 1. Instrumentation of the SEF-POOL facility

Figure code	Data code	Sensor type	Manufacturer/ type	Measurement frequency	Measurement range
A	P2600	Pres. transducer	Wikatronic	2 Hz	0-1 MPa
A	T2600	TC, K- type	Ø3 mm ¹	70 Hz	0-200 °C
B	T2601	TC, K- type	Ø1 mm ¹	70 Hz	0-200 °C
C	P2601	Pressure sensor ²	Kyowa PHS-B	7 kHz	0-1 MPa
D	P2602	Pressure sensor ²	Kyowa PS-2KC ³	7 kHz	0-0.2 MPa
E	T2602	TC, K- type	Ø 0.5 mm ¹	70 Hz	0-200 °C
F	T2603	TC, K- type	Ø 0.5 mm ¹	70 Hz	0-200 °C
G	T2604	TC, K- type	Ø 0.5 mm ¹	70 Hz	0-200 °C
H	X2600	Force sensor ²	Kyowa LUX-B-50N	7 kHz	±50 N
I	X2601	Force sensor ²	FUTEK LRM200	7 kHz	±222 N

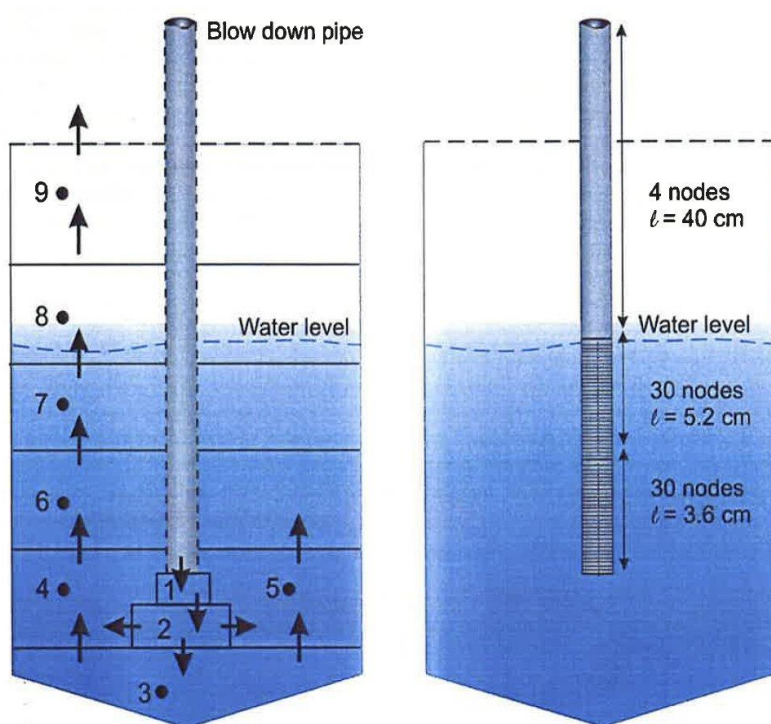
¹ Diameter of the sensing element

² These are used in conjunction with a Strain/Bridge Input Module

³ Type used depends on the range, the number denotes the measurement range in bars

Appendix C


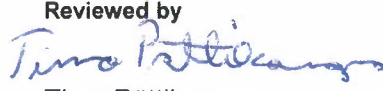

Assessment of implementation of the effective heat and momentum source models in Apros



Assessment of implementation of the effective heat and momentum source models in Apros

Authors: Ari Silde

Confidentiality: Public

Report's title	
Assessment of implementation of the effective heat and momentum source models in Apros	
Customer, contact person, address	Order reference
1. Yli-insinööri Jorma Aurela, Valtion ydinjäterahasto, PI 32, 00023 Valtioneuvosto 2. Cristian Linde, Programme Manager NKS-R, Strålsäkerhetsmyndigheten, Se-171 16 Stockholm, Sweden	Dnro SAFIR 11/2019 AFT/NKS-R(19)130/8
Project name	Project number/Short name
SAFIR2022_CFD4RSA_2019	122262-1.5
Author(s)	Pages
Ari Silde	22
Keywords	Report identification code
Apros, thermal stratification, pool mixing, suppression pool	VTT-R-01029-19
Summary <p>Royal institute of Technology (KTH) has developed a simulation approach based on the Effective Heat Source (EHS) and Effective Momentum Source (EMS) models. The goal of the EHS/EMS models is to introduce the complex DCC effects as appropriate boundary conditions (momentum and heat sources) which can be implemented in the CFD or system codes for modelling of transient thermal stratification and mixing in pool.</p> <p>The main aim of this work was to assess the possible implementation of the EHS/EMS models in Apros. Both the lumped parameter containment model and six-equation thermalhydraulic model of Apros are considered.</p> <p>Due to totally different approach used in the Apros lumped parameter code, the EHS/AMS models cannot be directly used for LP simulation. However, the work revealed some other interesting approaches which might be exploited in the future for Apros LP modelling of pool stratification.</p> <p>The EHS/EMS models could be in principle implemented in the Apros 6-equation model using the suitable correlations for the steam momentum calculated by Apros. The recommendations for future work are that the EHS/EMS models associated with steam injection through spargers will be first implemented in the Apros 6-equation model. Possibility to use 2D nodalisation in the pool to allow circulation flows should be studied. Selected POOLEX experiments (e.g. SPA-T2) could be calculated to verify/validate the new modelling approach. The suitable tests will be selected in consensus with the corresponding work with the Fluent CFD code at VTT.</p> <p>This work shows that adoption of the EHS/EMS model for Apros can be worthwhile. Pool thermal stratification is typically a long-term phenomenon, as seen in the Fukushima accident, and an accurate modelling of stratification phenomena and associated steam condensation regimes is challenging and time-consuming when using the current code models. The EHS/EMS models increase capability of Apros for computational efficient simulation of pool stratification/mixing phenomena in real plant geometry. In the future, implementation of the EHS/EMS models in Apros for blowdown pipe case should also be considered. Final goal is to enable modelling of whole BWR containment parallel with the Apros LP and 6-equation calculations so that the pool stratification is calculated with the 6-equation model, whereas other parts of containment use the LP approach.</p>	
Confidentiality	Public
9.3.2020 Written by  Ari Silde Senior scientist	
Reviewed by  Timo Pättikangas Principal scientist	
Accepted by  Inka Orko Research team leader	
VTT's contact address	
VTT Technical Research Centre of Finland, PL 1000, 02044 VTT	
Distribution (customer and VTT)	
SAFIR2022 Reference Group 4	
The use of the name of VTT Technical Research Centre of Finland Ltd in advertising or publishing of a part of this report is only permissible with written authorisation from VTT Technical Research Centre of Finland Ltd.	

Contents

Contents.....	2
1. Introduction.....	3
2. Effective Heat Source (EHS) and Effective Momentum Source (EMS) Models	4
2.1 Blowdown pipes.....	5
2.2 Spargers.....	5
3. Modelling of Water Stratification in Apros.....	8
3.1 Lumped Parameter Containment Model	8
3.2 Six-Equation Thermalhydraulic Model.....	9
3.2.1 First order upwind discretisation.....	10
3.2.2 Higher order upwind model.....	10
4. Adoption of EHS/EMS Models to Apros	12
4.1 Lumped Parameter Containment Model	12
4.2 6-Equation Model.....	13
5. Discussion	17
6. Conclusions	19
References.....	20

1. Introduction

The Boiling Water Reactor (BWR) Nuclear Power Plants are equipped with a suppression pool system to manage the containment overpressurisation. During the accidents, opened Safety Relief Valves (SRVs) discharge steam from the primary coolant system through the SRV lines to below the surface of a wetwell pressure suppression pool where the steam is condensed. Interconnecting blowdown vent pipes are also provided between the drywell and suppression pool to discharge the steam and water mixture in a LOCA from the upper drywell into the suppression pool. The possible formation of thermal stratification in the pool is of safety concern since it has an influence on the steam condensation and pressure suppression capacity of the pool compared to completely mixed pool. In addition, some safety related systems such as emergency core cooling and containment spray systems use suppression pool as a water source. The development of stratification leads to higher pool surface temperature, and thus higher containment pressurization compared with complete mixed pool. The real example of this is the Fukushima accident (Jo et al 2016; Mizokami et al 2016.)

The numerical modelling of pool mixing/stratification have been widely studied e.g. at KTH Sweden (Gallego-Marcos et al. 2016a; Gallego-Marcos 2018; Li et al. 2014a). The extensive experimental work has been done, e.g. at Lappeenranta-Lahti University of Technology LUT (LUT university) (Li et al. 2014b; Laine et al. 2009; Laine et al. 2014). KTH has developed and validated the Effective Heat Source (EHS) and Effective Momentum Source (EMS) models which are a middle ground approach, between the lumped parameter and CFD approach, providing computational efficiency and sufficient accuracy in the modelling of pool stratification effects (Gallego-Marcos 2018).

The goal of this work is to summarise the current pool stratification modelling of Apros, and assess whether the EHS/EMS models could be implemented in Apros to improve the calculation speed and stability of stratification calculation. Both the Apros lumped parameter containment model and the six-equations thermalhydraulic model are considered. The principles of the EHS/EMS models are also shortly described. This report focuses on the cases where steam is injected through the spargers into the suppression pool. Effects of non-condensables are not treated in this report.

2. Effective Heat Source (EHS) and Effective Momentum Source (EMS) Models

Lumped parameter codes cannot be used for simulating complex phenomena related to e.g., direct contact condensation (DCC) and mixing and thermal stratification in the pool. Use of CFD codes for realistic plant analyses is challenging due to calculation resources needed. Royal institute of Technology (KTH) has developed a simulation approach based on the Effective Heat Source (EHS) and Effective Momentum Source (EMS) models which is a compromise between a simple approach and CFD modelling providing computational efficiency and sufficient accuracy in simulating pool mixing/stratification phenomena (Gallego-Marcos et al. 2016a; Gallego-Marcos 2018; Li et al. 2014a). The model has been validated for flow chugging and internal condensation flow regimes of blowdown pipes, spargers, and mixing nozzles. KTH has implement and tested the approach in the GOTHIC 8.1 and ANSYS Fluent 16.2 computer codes.

The goal of the EHS/EMS models is to predict the pool stratification and mixing without direct modelling of complex DCC phenomena. Instead, the EHS/EMS models introduce the DCC effects as appropriate boundary conditions (momentum and heat source) which can be implemented in the CFD or system codes for modelling of transient thermal stratification and mixing in pool (Figure 2-1).

The EHS/EMS models calculate the time-average of instantaneous variations of the heat and momentum sources induced by different steam condensation regimes. The effective heat Q_{eff} and momentum M_{eff} source are calculated as

$$Q_{eff}(t) = \frac{1}{\Delta t} \int_{t-\Delta t}^t Q(t) dt \quad (2-1)$$

$$M_{eff}(t) = \frac{1}{\Delta t} \int_{t-\Delta t}^t M(t) dt \quad (2-2)$$

where Δt is the considered time period.

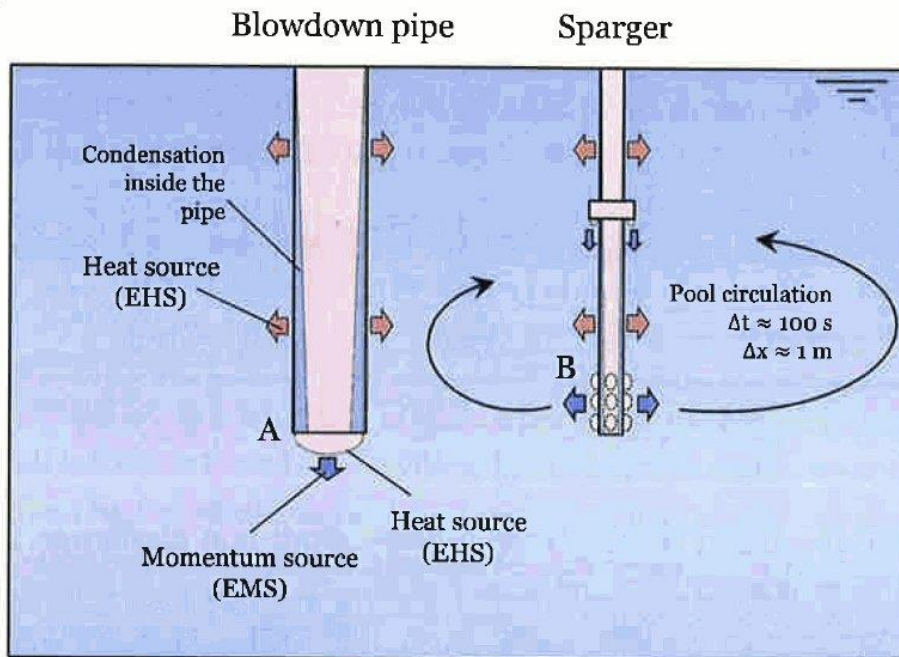


Figure 2-1. Schematic picture of location of the heat and momentum sources induced by a steam injection through blowdown pipe (left) and spargers (right) (Gallego-Marcos 2018).

2.1 Blowdown pipes

In case of blowdown pipe, the injection hole is large and steam injection mass flux is relatively low leading often to chugging or complete condensation regime inside the pipe. As a consequence, flow and pressure oscillations may occur in the pool.

KTH has studied the pool behavior during a steam injection through a blowdown pipe in series of PPOOLEX experiments at Lappeenranta University of Technology LUT (Li et al. 2014a; Li et al. 2014b). They showed that a complete condensation inside the blowdown pipe produces insignificant momentum which allows the development of thermal stratification, whereas chugging regimes were able to mix the pool. They developed the EMS model for chugging regime based on the synthetic jet theory (Smith&Swift 2003), where the effective velocity of the synthetic jet is given by

$$U_{eff} = fA\sqrt{2} \quad (2-1)$$

where, in the chugging regime, f and A are the frequency and amplitude of the steam-water interface (liquid level) inside the pipe, respectively. The effective momentum induced by chugging is

$$M_{eff} = \rho_L \left(\frac{\pi d^2}{4} \right) \cdot U_{eff}^2 \quad (2-2)$$

The frequency and amplitude in Eq. 2-1 are measured experimentally assuming the chugging oscillations behave as a harmonic of the type $z = (A/2)\sin(2\pi f t)$. Some analytical and numerical models are also available to assess these variables as described later, but the models are derived from small scale experiments mostly in limited condensation regimes.

The effect on non-condensables are not addressed in the current EHS/EMS models. Especially, in the initial stage of transient, also non-condensable gas (air) may flow through the blowdown pipes into the pool. Further experiments are needed to provide correlations for the frequency and amplitude in cases where non-condensables exist in the steam flow (Gallego-Marcos 2018). Therefore, this report mostly focuses on cases where pure steam is injected through multi-hole spargers into the suppression pool.

2.2 Spargers

The spargers of Nordic BWR inject steam directly from the primary coolant system through the multi-holes pipe system into the suppression pool. In the upper ring of the pipes, the holes are facing downwards, where in the lower part of the pipes (in sparger head) the steam injection takes place radially (horizontally).

The sparger experiments performed in the PPOOLEX and PANDA facilities are mostly performed in the sub-sonic oscillatory bubble regime (Gallego-Marcos 2018). In this regime, the effective momentum is expected to be dependent on many different condensation parameters such as frequency of bubble collapse, bubble radius etc. Unfortunately, these parameters are not measured in the sparger experiments. Therefore, KTH has developed approach, where the effective momentum of the EMS model for sparger injection is estimated with (Gallego-Marcos 2018)

$$M_{eff} = C \cdot M_{th} \quad (2-3)$$

where C is the coefficient which is dependent on the condensation regime and M_{th} is the theoretical steam momentum at the injection holes defined as

$$M_{th} = \rho_s A_i U_s^2 + A_i (P_i - P_h) \quad (2-4)$$

where ρ_s is the steam density, A_i is the sparger hole area, U_s is the steam velocity at the sparger holes, P_i is the pressure in the sparger hole and P_h is the hydrostatic pressure. For sub-sonic regimes, P_i becomes the hydrostatic pressure P_h . In the KTH study, the calibration of M_{eff} was done by varying the C coefficient (in Eq. 2-3) and comparing the corresponding CFD results to the pool temperature and velocity fields measured in the PPOOLEX and PANDA experiments until a good agreement was obtained. The following correlations for C coefficient were developed. For sub-sonic regimes with certain steam mass flux G the EMS correlations are (Gallego-Marcos 2018)

For $G \leq 120 \text{ kg/m}^2/\text{s}$

$$C_1 = \frac{10.58}{\Delta T^{0.42}} \left(n \frac{\pi d^2}{4} \right)^{0.07}$$

For $150 \leq G \leq 300 \text{ kg/m}^2/\text{s}$

$$C_2 = \frac{2.70}{\Delta T^{0.51}} \left(n \frac{\pi d^2}{4} \right)^{-0.13}$$

For $120 \leq G \leq 150 \text{ kg/m}^2/\text{s}$

$$C_3 = (0.5 - s)C_1 + (0.5 + s)C_2 \quad (2-5)$$

where

$$s = 0.5 \tanh\left(\frac{G - 135}{5}\right)$$

For sonic regimes the EMS correlation is

$$C = \frac{239}{\Delta T^{0.03}} G^{-0.43} \left(n \frac{\pi d^2}{4} \right)^{0.34} \quad (2-6)$$

Since the liquid momentum induced by steam condensation have not been measured in any previous works/experiments, Separate Effect Facility (SEF-POOL) was built at LUT University (Gallego-Marcus 2018, Gallego-Marcus et al. 2019). In these tests, the liquid momentum was measured by specific force sensors. Based on the SEF-POOL data, new correlations were proposed for the EMS model. Also another approach based on the Kelvin Impulse theory was proposed based on the bubble dynamics. The set of experiments showed that the theoretical momentum M_{th} calculated from Eq. 2-4 could capture the order of magnitude of the measured effective momentum M_{eff} , but corrected C coefficient is needed to take into account the effects of condensation regimes. A new fitting based on Jacobs number Ja alone showed good agreement with the SEF-POOL data in the sub-sonic regime. The correlation is

$$C = 0.48 \cdot Ja^{-1/3} \quad (2-7)$$

Another simplified correlation as a function of water subcooling ΔT showed a similar accuracy

$$C = 4.28 \cdot \Delta T^{-0.35} \quad (2-8)$$

In the sonic jet regimes, only a quasi-constant value for the C coefficient could be given, since all SEF-POOL tests performed at the regime where the Mach number is greater than one were run at similar steam mass flux of about $320 \text{ kg}/(\text{m}^2\text{s})$. The value for the C coefficient for sonic jet regimes is

$$C_{G=320kg/(m2s)} = 0.84 \quad (2-9)$$

The study related to SEF-POOL experiments showed that further experiments are needed to study the C coefficient at higher steam fluxes and Ja numbers (Gallego-Marcus 2018).

Another approach based on the Kelvin impulse theory takes into account the momentum transfer of oscillatory bubbles. The C coefficient (C_{KI} here) becomes

$$C_{KI} = 3.48 \frac{G^{0.01}}{d^{0.08} \Delta T^{0.41}} \quad (2-10)$$

where d is the hole diameter and G is the steam mass flux.

If some thermal stratification in the pool is formed, the codes should also be able to calculate possible re-mixing or erosion of stratification in the pool. In mixing, the momentum is sufficient to mix the cold and hot layers. Blowdown pipe with vertical steam injection downwards is more effective for mixing of horizontal layer than radial (horizontal) injection through the sparger holes (Gallego-Marcos et al. 2018). In the erosion, the injected momentum is not sufficient to mix the layers perfectly, and instead, only slow erosion of the layer interface takes place. If the stable thermally stratified pool is formed, the stratified layer can be eroded by shear or shear-free flows (Fernando 1991). Fernando and Hunt (1997) and McGrath et al. (1997) verified that the erosion mechanism of shear-free flow can be expressed by the Richardson number.

$$Ri_s = \frac{\Delta b D}{U^2} \quad (2-11)$$

where

$$\Delta b = \frac{g(\rho_c - \rho_h)}{\rho_c} \quad (2-12)$$

where D is the mixed layer thickness, U is the velocity above the thermocline, and ρ_c and ρ_h are the densities of cold and hot layers, respectively. Fernando (1991) also showed that the vertical erosion velocity U_E at which the cold layer is displaced can be predicted based on the Richardson number as

$$\frac{U_E}{U} = C \cdot Ri_s^{-n} \quad (2-13)$$

where C and n are experimental coefficients.

Gallego-Marcos et al. (2018) analyzed and interpreted the pool stratification experiments performed in the PPOOLEX and PANDA facilities. In the tests, steam was injected through a sparger into the pool. They assumed that the horizontal injection through the sparger holes behaves like a shear source and distributes the momentum along the cross section of the pool. The velocity U in Eq. 2-13 can be then calculated as

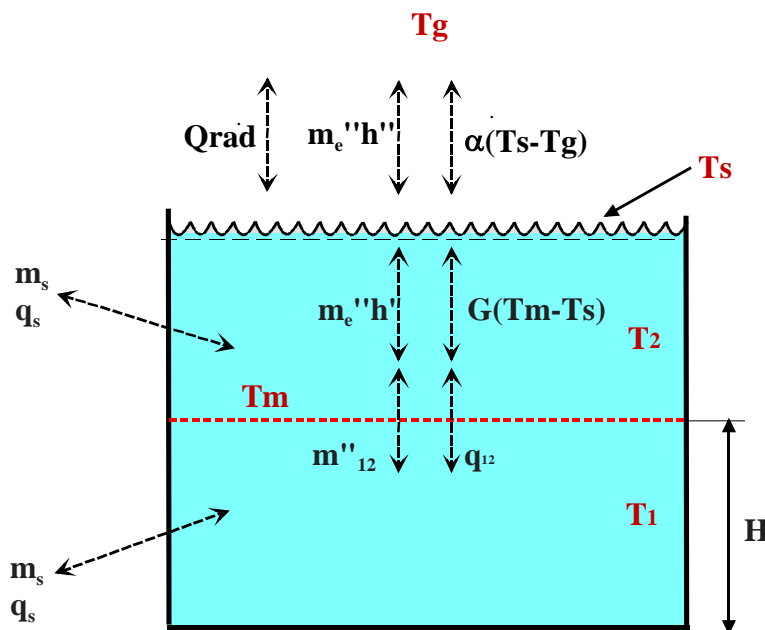
$$U = U_s \sqrt{\frac{\rho_s A_i}{\rho_L A_p}} \quad (2-14)$$

where U_s is the steam injection velocity in the sparger hole, A_i is the injection hole area, A_p is the pool cross section area, and ρ_s and ρ_L are the densities of injected steam and pool water, respectively. Gallego-Marcos et al. (2018) showed that the velocity ratio according to Eq. 2-13 was in good agreement with the erosion velocity of the experiments. Suitable constants for Eq. 2-13 were estimated to be $C = 0.7$ and $n = 1.2$. The thickness of the thermocline layer (D in Eq. 2-11) was about 50 mm during the stratification and slow erosion phases.

3. Modelling of Water Stratification in Apros

3.1 Lumped Parameter Containment Model

The containment model of Apros uses a lumped parameter (LP) approach where water pool is normally assumed to form single-phase, homogeneous liquid (Silde & Ylijoki 2019). However, a separate temperature of infinite small surface layer is solved iteratively due to its strong influence on the combined heat and mass transfer. An alternative parametric approach called a pool stratification model allows to divide the pool to two vertical layers (zones) (Figure 3-1).



- T_g = bulk gas temperature
- T_s = pool surface temperature
- T_m = pool mean temperature
- T_1 = temperature of the lowermost pool layer
- T_2 = temperature of the uppermost pool layer
- H = user-specified elevation of boundary layer from pool (node) bottom
- Q_{rad} = radiation heat flux
- m_e'' = condensation/evaporation mass flux
- h'' = specific enthalpy of saturated steam
- h' = specific enthalpy of saturated water
- α = convective heat transfer coefficient
- G = thermal conductance of water
- m_{12}'' = mass flux between the pool layers
- q_{12} = heat flux between the pool layers
- m_s = mass flow of external sources/sinks
- q_s = heat flow of external sources/sinks

Figure 3-1. Schematic picture of the LP pool stratification model.

Elevation of the stratified layer (H) between the pool layers (location of thermocline) is user specified and fixed value, and does not change during the simulation. If the pool elevation drops below the specified boundary layer, only one homogeneous pool layer remains and the

pool stratification calculation is stopped until the pool elevation exceeds again the determined boundary layer.

Both layers have an own mass and energy balance calculation, and hence, they may be in thermal non-equilibrium and have a different temperature. Heat transfer between the pool layers occurs through heat conductance which can be affected by varying the heat conductance thickness term. Mass flow between the layers takes place only, if the mass or density of the lowermost layer changes. Water flow between separate pools is calculated from the Bernoulli mechanical energy balance equation. Because pool can be divided only into two vertical layers, its clear that 2D/3D flows, and concurrent pool mixing/stratification phenomena inside a pool cannot be modelled.

The LP approach is a parametric model, i.e., pool stratification or mixing calculation should be actuated as input boundary conditions. The current model is not suitable for predictive analysing purposes. If the user activates the stratification calculation with the specific input option, the mass and energy balances are updated separately for both layers during the simulation. If the user inactivates the stratification calculation, the layers will mix instantaneously forming a uniform pool with one temperature. One alternative option allows the automatic actuation of the stratification/mixing calculation according to the velocity of steam-gas mixture inside the blowdown pipes or forced feed injection. When the velocity of gas-steam mixture drops below the certain user-given threshold velocity, the stratification calculation is started. If the velocity exceeds the threshold value, the stratification calculation is stopped, and the pool layers become fully mixed instantaneously.

3.2 Six-Equation Thermalhydraulic Model

The six-equation model of Apros is a one-dimensional two-fluid model which simulates the behaviour of a system containing gas and liquid phases (Hänninen 1992). It is based on the idea shown in reference (Siikonen 1987). The system is governed by six partial differential equation, from which the pressures, void fractions, phase velocities and phase enthalpies are solved.

Technical Research Centre of Finland VTT and Lappeenranta University of Technology LUT studied passive Core Make-up Tank (CMT) behaviour during small-break loss-of-coolant accident. The simulations with conventional one-dimensional thermalhydraulic codes using the upwind discretisation scheme and averaged enthalpy in node showed that accurate simulation of thermal stratification in CMT is not possible (Hänninen 2009; Vihavainen et al. 1999). The sharp enthalpy distribution is unphysically smoothed when the fluid proceeds over several calculation meshes, i.e., numerical diffusion smoothens the temperature distribution inside the tank. The phenomenon can be attenuated by using a dense nodalisation and small time step, but the basic problem cannot be fully removed.

Later on, a new alternative discretization scheme has been applied in Apros, where the liquid first order upwind enthalpy transported from node to node in the area close to the thermally stratified layer was defined using information from three consecutive nodes. The calculation results showed that the numerical diffusion can be largely eliminated and temperature distribution in the CMT becomes much closer to the distribution in the experiment.

The following description of the discretization schemes is taken from reference (Hänninen 2009).

In case of liquid enthalpy, the following equation is obtained from energy conservation equation of the Apros 6-eq model

$$\frac{\partial((1-\alpha)\rho_l h_l)}{\partial t} + \frac{\partial((1-\alpha)\rho_l u_l h_l)}{\partial z} = S \quad (3-1)$$

where subscript refers to liquid, α is the steam volume fraction, u is the velocity, h is the total enthalpy, and S describes the enthalpy sources of energy and pressure derivate.

The staggered mesh scheme and subscript used in the following equations are show in Figure 3-2.

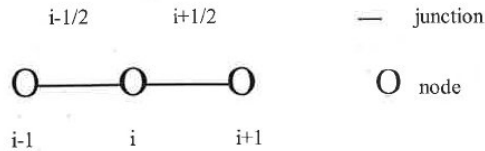


Figure 3-2. Staggered grid discretisation scheme.

3.2.1 First order upwind discretisation

Using the standard upwind discretisation of the equation 3-1 in respect of time and space by using staggered grid gives

$$\begin{aligned} & \frac{V_i \left[(1-\alpha)\rho_{l,i} h_{l,i} - ((1-\alpha)\rho_{l,i} h_{l,i})^{t-\Delta t} \right]}{\Delta t} + A_{i+1/2} ((1-\alpha)\rho_l)_{i+1/2} [u_{l,i+1/2}, 0] h_{l,i}^n \\ & - A_{i-1/2} ((1-\alpha)\rho_l)_{i-1/2} [u_{l,i-1/2}, 0] h_{l,i-1}^n + A_{i-1/2} ((1-\alpha)\rho_l)_{i-1/2} [-u_{l,i-1/2}, 0] h_{l,i}^n \\ & - A_{i+1/2} ((1-\alpha)\rho_l)_{i+1/2} [-u_{l,i+1/2}, 0] h_{l,i+1}^n = S \end{aligned} \quad (3-2)$$

Subscript i for the node and $i - \frac{1}{2}$ and $i + \frac{1}{2}$ are the junctions to and from the node i . Subscript $i-1$ and $i+1$ are for nodes before and after the node i . The notation $[u_{l,i+1/2}, 0]$ means that the maximum of $u_{l,i+1/2}$ or 0 is used. The superscript n means that a quantity is to be solved in the new iteration step, the variables with no superscripts are referring to the current value and the variables with superscript $t-\Delta t$ are referring to the values of the old time step.

3.2.2 Higher order upwind model

In the new higher order upwind model, the liquid enthalpy h_x is defined with three latest iterated enthalpies $h_{l,i}$, $h_{l,i-1}$ and $h_{l,i+1}$ and h_x is calculated as follows

if $u > 0$

$$h_x = h_{l,i+1} + f(h_{l,i-1}, h_{l,i}, h_{l,i+1}) (h_{l,i-1} - h_{l,i+1}) \quad (3-3)$$

or if $u < 0$

$$h_x = h_{l,i-1} + f(h_{l,i-1}, h_{l,i}, h_{l,i+1}) (h_{l,i+1} - h_{l,i-1}) \quad (3-4)$$

The function f defines the behaviour of the change of enthalpy to be transported from node i . If velocity u is positive, $h_{l,i}$ changes from $h_{l,i+1}$ to $h_{l,i-1}$ and if velocity is negative, $h_{l,i}$ changes

from $h_{l,i-1}$ to $h_{l,i+1}$. The desired function f is selected so that it delays the change of the upwind enthalpy.

If the velocity is positive, the following function is used

$$f = \left[\frac{h_{l,i} - h_{l,i+1}}{h_{l,i-1} - h_{l,i+1}} \right]^4 \quad (3-5)$$

The function changes from 0 to 1 when the enthalpy $h_{l,i}$ changes from $h_{l,i+1}$ to $h_{l,i-1}$.

If the velocity is positive, the following function is used

$$f = \left[\frac{h_{l,i} - h_{l,i+1}}{h_{l,i-1} - h_{l,i+1}} \right]^4 \quad (3-6)$$

The function changes from 0 to 1 when the enthalpy $h_{l,i}$ changes from $h_{l,i-1}$ to $h_{l,i+1}$. Because the transported enthalpy is a solved quantity, the equations 3-3 and 3-4 cannot be used directly in the enthalpy solution. The desired enthalpy change is obtained by manipulating the convective term in the equation 3-2. If the flow velocity is positive, the convective term of junction $i + \frac{1}{2}$ is modified as

$$\frac{h_x}{h_{l,i}} A_{i+1/2} ((1-\alpha)\rho)_{i+1/2} u_{i+1/2} h_{l,i}^n \quad (3-7)$$

where h_x is calculated from the equation 3-3 and $h_{l,i}$ is the latest iterated enthalpy.

The higher order upwind model is developed to model thermal stratification in vertical pipes and tanks. It can also be used for simulation of a hot or cold water pulse in a horizontal or vertical pipeline. The user has to define the flow path where the sharp stratification is to be occurred, but one nodes can be connected to several junctions. Sufficient dense nodalisation is needed to capture the real sharp stratification, because the temperature is calculated as function of the solved enthalpy which still represents the average enthalpy of node. The model assumes that $h_{l,i-1} < h_{l,i} < h_{l,i+1}$ or $h_{l,i+1} < h_{l,i} < h_{l,i-1}$. Otherwise the pulse fades away. If the pulse shape enthalpy changes are to be calculated, the pulse length should be at least two nodes or more.

4. Adoption of EHS/EMS Models to Apros

4.1 Lumped Parameter Containment Model

In the Apros LP containment modelling, a pool can be divided into two vertical zones. The pool internal circulation flows induced by momentum and/or buoyancy cannot be not modelled. Exchange of energy between the zones can be modelled using so called heat conductance term which can be affected by the user. The only way in the current model to control the mixing of the two pool zones would be controlling the interconnecting flow between the zones with given boundary conditions. On the other hand, the EHS/EMS models rely on the principal, where the determined momentum and heat sources are added to certain cell(s) in the pool calculation grid, and code then calculates internally the flow field and corresponding stratification and mixing phenomena inside the pool. In conclusion, the EHS/EMS models are not directly applicable for the Apros LP model.

The predictability of the current LP pool model could maybe be increased by exploiting some correlations (or other boundary conditions) to control the intercell flow between two pool zones in order to reach the desired stratification/mixing regime in the pool. Development of such empirical correlations would require a huge amount of experiments and/or simulations where dependency of stratification on several important variables should be studied. Ozdemir and George (2015) have developed such correlations for the GOTHIC code using numerically generated data from the 3D simulations to be used to estimate pool mixing and stratification effects with the lumped parameter pool model. The aim of the GOTHIC simulations was to model a direct contact steam condensation without the need of any alternative methods, such as the EHS/EMS models etc. The pool calculation model was based on the geometric parameters of the MARK I type BFN nuclear power plant. The LP pool was modelled with two vertical zones and a pump component with associated flow connection were ncluded to provide desired mixing between the upper and lower pool zones. The steam was injected into the upper zone of the pool. The pump mass flow between the zones was controlled by correlations developed from the GOTHIC simulations. The pool surface temperature (temperature of the upper zone) was considered the most important target from containment pressurization point of view. The effects of steam injection rate, the injection depth, the temperature difference between the condensed steam and the pool, and the thermal expansion coefficient of the pool water were studied. Results showed that the mixing correlations lead to a good agreement between the detailed 3D and LP simulations, especially when the steam injection rate was small. In spite of the facts that the results rely on the geometric data of one plant type and numerical GOTHIC simulations without any empirical work, the described method could also be suitable for the Apros LP model.

Song et al. (2014) studied criteria of thermal stratification created by DCC using a experimental setup of a suppression pool. The size of the pool was 500 mm x 300 mm x 50 mm. The inner diameter of a vertical blowdown pipe was 4.2 mm. Vertical temperatures were measured and bubbles were visualized in order to examine bubble shape, frequency and amplitude for different DCC regimes. It was found that the criterion for the occurrence of the thermal stratification in the DCC regime could be determined according to the DCC Richardson number which is the ratio of buoyancy to inertial force as

$$Ri_{DCC} = \frac{g\beta(T_{sat}-T_{amb})L}{2f^2\delta^2} \quad (4-1)$$

where g is the gravitational acceleration, β is the thermal expansion coefficient, T_{sat} is the steam saturation temperature, T_{amb} is the temperature of ambient fluid (water), L is the distance between steam injection pipe end and pool bottom, f is the frequency of the oscillations of steam-water interface, and δ is the corresponding amplitude. Their conclusion was that if Ri_{DCC} is higher than 2, thermal stratification takes definitely place. When Ri_{DCC} is between 0.1 and 2.0, DCC should be in encapsulating bubble regime (ECEB) to get thermal

stratification. If Ri_{DCC} is lower than 0.1, it would be difficult to get stratification and the pool is fully mixed. Although the study was only based on the small-scale experiments, the used method and the Richardson number relation could be maybe applied also in the LP modelling. However, it is unclear whether the approach is suitable also for steam injection through spargers.

If some stratification in the pool is formed, the equations from 2-11 to 2-14 could be exploited also for the lumped parameter calculation to estimate the erosion velocity.

4.2 6-Equation Model

An example of implementation method of the EHS/EMS models to the GOTHIC containment model is given by Gallego-Marcos (2018) and Gallego-Marcos et al. (2016b) (Figure 4-1). Despite this example is only for the case where steam injection occurs through the blowdown pipes, the similar principles can be used for sparger injection cases. The similar principles could also be exploited when connecting the EHS/EMS models to the Apros 6-equation model.

To obtain the steam pressure flowing out from the pipe outlet, the pipe is not connected to the wetwell pool, instead, the connection is made to a pressure boundary condition '2P'. The pressure and temperature of '2P' correspond to the hydrostatic pressure and liquid temperature at the injection hole level, respectively. As a consequence, the effective momentum can be predicted from flow into cell '2P' and is transferred into the pool with a pump component '1P'. Liquid and gas injection into '2P' are directed into wetwell pool using the boundary condition modules '3F', '4F' and '5F'. The steam coming out from the pipe outlet (holes) is added in the EMS model always as liquid form into the pool. The latent heat of the artificial steam condensation is added with a heater at the pipe outlet. Steam condensation inside the pipe is also added as a liquid mass source in the EMS model. The heat transfer through the pipe may be modelled internally by the code heat transfer and heat structure models.

In Apros, '2P' could be an external node which has the given pressure, enthalpies for liquid, steam, and non-condensables, and void fraction. Heat transfer through the wall along the pipe will be calculated internally with the code giving the relevant pipe inner temperature as a boundary conditions. The important EHS/EMS variables, such as momentum and heat sources, will be calculated using the Apros 6 SCL script. Finally, the heat sources are added to the desired pool nodes. The velocities for liquid and non-condensables with specified direction should be calculated from the desired momentum of the EMS model, and they are transferred to the external branches (flow paths) between the desired pool nodes of Apros model. The implementation of the EHS/EMS models in Apros 6 could be done purely with the current module types and by means of the Simantics Constraint Language (SCL). Development of an own Apros 6 user component for the EHS/EMS models should also be consider. Significant code modifications are probably not needed.

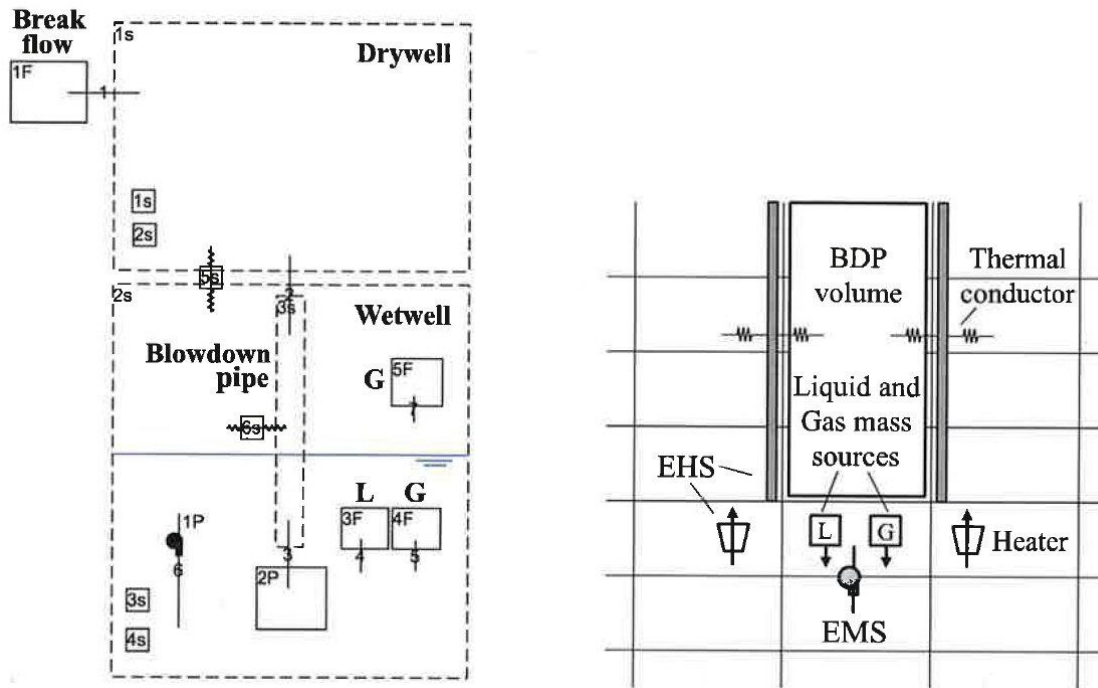


Figure 4-1. EHS/EMS model implemented in GOTHIC. Overview of the control volumes and boundary conditions (left) and location of the source terms at the blowdown pipe (right).

The GOTHIC simulation performed at KTH revealed that numerical oscillations takes place at the blowdown pipe outlet. These oscillations may cause artificial pool mixing. Gallego-Marcos (2018) minimized their effects by time averaging them before the flow is used for the EHS/EMS model. It is still unclear whether similar order of magnitude of oscillations would take place in Apros simulations and in simulations for steam injection through sparger holes. But if needed, a similar averaging could be also applied for Apros using SCL.

There is lack of applications, where the Apros 6-equation model has been directly used for pool stratification calculation. Hänninen (2005) calculated the POOLEX test STB-08-05 using the Apros 6-equation model. The main goal of the work was to increase understanding of different phenomena in the condensation pool during steam injection through a blowdown pipe and verify the ability of Apros to calculate the steam condensation and possible pressure oscillations in the pool. Although Hänninen's work was focused on pressure oscillations during steam condensation and was done only for a blowdown pipe, it provides some important aspects how the Apros 6-equation model could be used for pool stratification/mixing calculation. Therefore, it is shortly described here.

The test was started by the high steam mass flow regime in the blowdown pipe and then water level did not flow back into the blowdown pipe. Thereafter, the mass flow rate was decreased and the oscillation phenomena (chugging regime) started. Because the main goal was to examine the behavior of the steam flow in the blowdown pipe and the steam condensation in the pool, a very dense 1D nodalisation was used in the blowdown pipe (Figure 4-2). The lowest part of the blowdown pipe was submerged in the pool. It was divided into the nodes with length of 3.6 cm, whereas the rest of the pipe in water had nodes with length of 5.2 cm. The pipe nodes above the water elevation have much larger dimensions. A relatively simple 1D nodalisation was used for a pool because the main aim was not to study stratification/mixing phenomena inside the pool. Relatively small node (node 1) was used in the pool near the pipe outlet and the node was connected only to the larger node just below (node 2), which had connections also to side nodes 4 and 5.

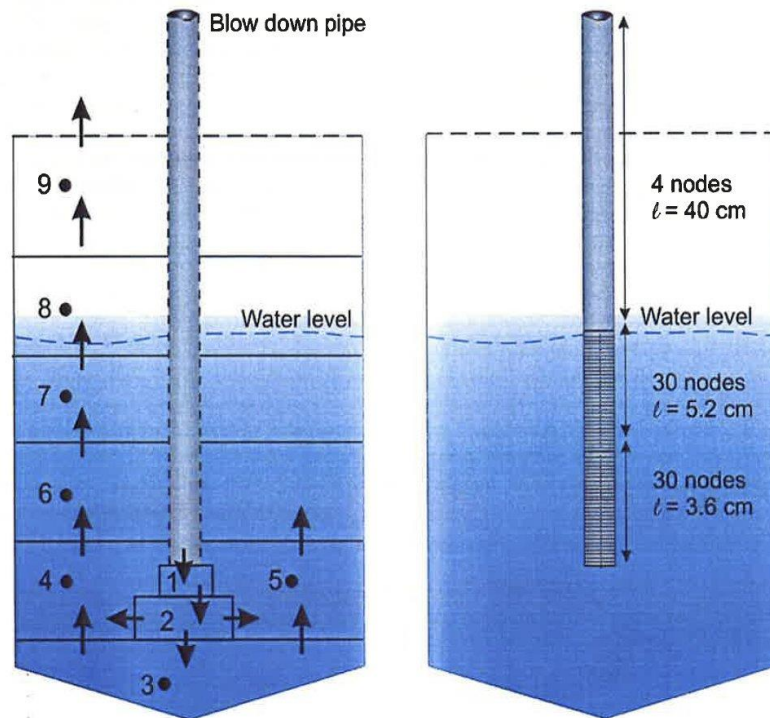


Figure 4-2. Apros nodalisation in the pool and the blowdown pipe for test STB-08-05.

Although the aim the study was not to model pool stratification/mixing phenomena, the study gives an interesting insight into the code capability to model steam condensation inside the pipe, DCC phenomena near the pipe outlet and pool behavior as well. The results showed that the calculated pressure at the pipe outlet corresponded very well to the measured data (Figure 4-3). The pressure oscillations appear both in the simulation and experiment after 500 s, when the steam injection rate becomes low enough. In order to model the oscillation phenomena very short time step had to be used. Also the pipe nodalisation was very dense, which increased also the calculation time. The oscillations cause often instability problems in the calculation. However, the real oscillations depend strongly on the three-dimensional phenomena near the pipe outlet such as bubble formation and collapsing, and therefore these oscillations could not be calculated properly. Some oscillations can be seen also in the calculated steam velocity inside the blowdown pipe beyond 550 s, but the oscillations are not very severe (Figure 4-4). Unfortunately, the simulation time is only 600 s, and behaviour of oscillations after that time instant remains unclear.

The calculated pool temperature near the pipe outlet were slightly higher and the upper temperature much lower than in the experiments, i.e., the mixing of the pool seemed to be smaller than in the experiment. This is understandable since the simple 1D nodalisation of the pool cannot capture the pool mixing due to circulation flows. When using a more dense 2D nodalisation in the pool, the mixing (and stratification) process could be simulated better.

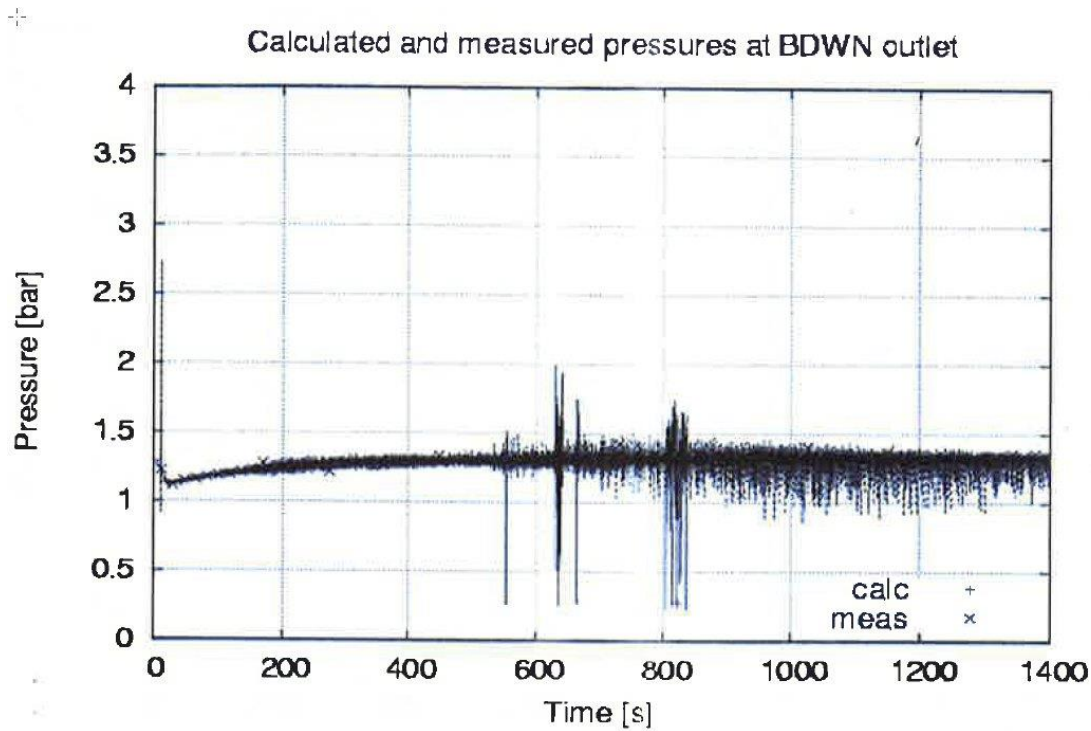


Figure 4-3. Calculated and measured pressure in the blowdown pipe outlet in test STB-08-05 (Hänninen 2005).

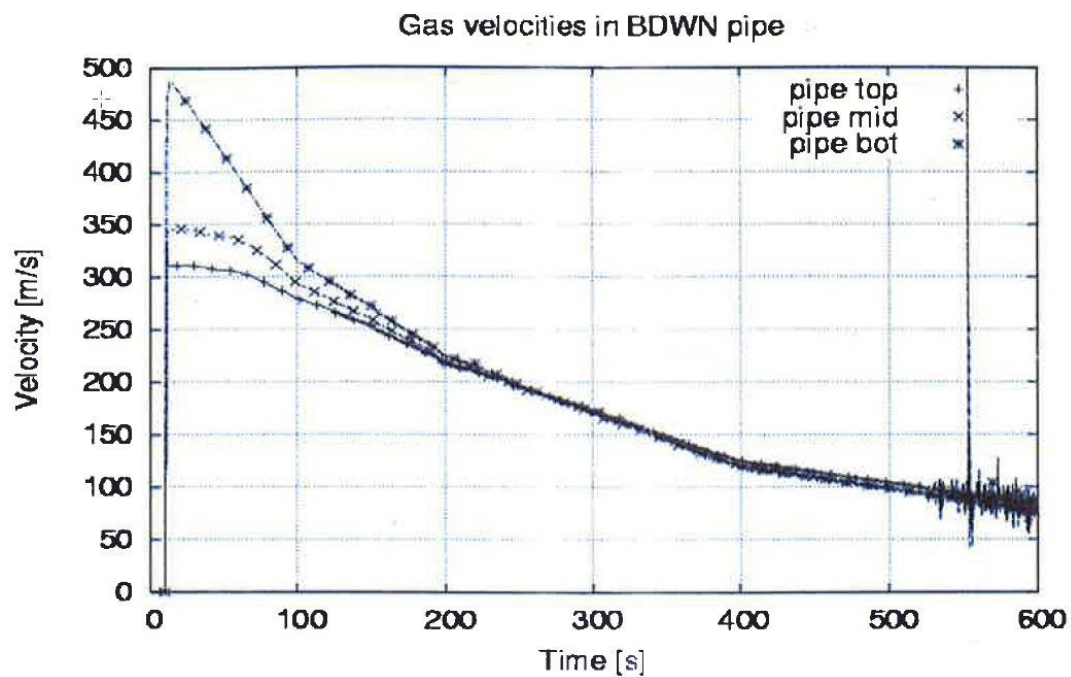


Figure 4-4. Calculated steam velocity in the blowdown pipe in test STB-08-05 (Hänninen 2005).

5. Discussion

Implementation of the EHS/EMS models is studied in the system or CFD codes for the modelling of transient thermal stratification and mixing in pressure suppression pool. The EHS/EMS models can be implemented in the Apros 6-equation model using the suitable correlations, such as Eqs. from 2-5 to 2-8, for the liquid momentum source. The necessary output variables to be transferred from the EHS/EMS models to Apros can be determined using Simantics Constraint Language of the Apros 6 environment.

The pool nodalisation in 6-equation model calculation should be denser than presented in Figure 4-2 to model more accurately the pool stratification and mixing. Also possibility to use 2D nodalisation for pool to model water circulation flows should be studied.

The Apros calculations using the EHS/EMS models could be tested against the selected POOLEX, PPOOLEX or PANDA experiments.

The sparger experiments performed in the PPOOLEX and PANDA facilities so far are mostly performed in the sub-sonic oscillatory bubble regime (Gallego-Marcos 2018) (Figure 5-1). However, from simulation point of view the chugging regime is probably the most challenging and time-consuming due to relatively strong oscillations caused by direct contact condensation near the pipe outlet. Simulation of this regime shows the most likely the benefits of the EHS/EMS models. Figure 5-1 shows that the PPOOLEX test SPA-T2 is mostly performed in the chugging regime, whereas the tests SPA-T3 and SPA-T5 are in the chugging regime only during limited time. All other PPOOLEX tests and the PANDA tests of Figure 5-1 are mostly in the sub-sonic oscillatory bubble or cone jet regime.

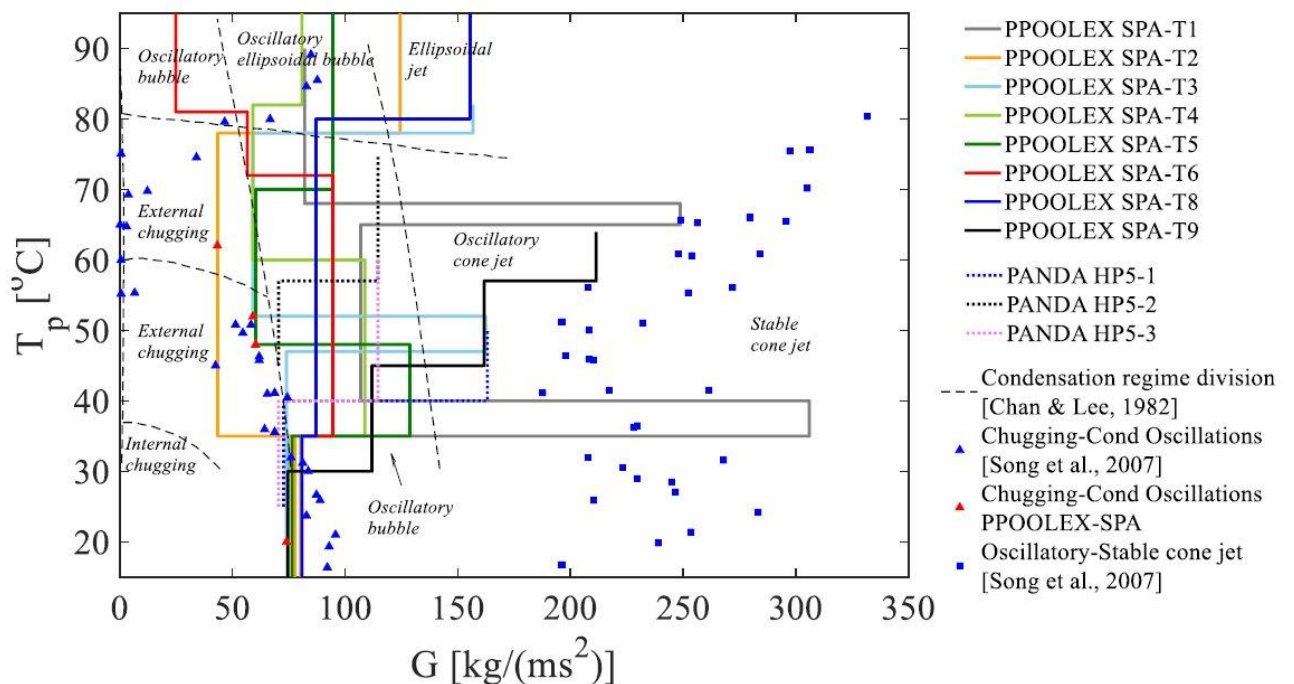


Figure 5-1. Trajectories of the PPOOLEX and PANDA experiments with sparger and expected condensation regimes based on Chand and Lee (1982) and Song et al (2012).

In summary, the recommendations for further work for pool stratification/mixing calculation using Apros 6-equation model are as follows:

- 1) The EHS/EMS models associated with steam injection through spargers will be first implemented in the Apros 6-equation model.
- 2) The implementation could be probably made without code modifications.
- 3) Influence of nodalisation of the injection pipe on the simulation time should be studied.
- 4) Possibility to use 2D nodalisation in the pool to allow circulation flows should be studied.
- 5) The higher order upwind model should be tested for pool stratification calculation to decrease numerical diffusion.
- 6) Selected PPOOLEX experiments should be calculate to verify/validate the new modelling approach. The possible test which is mostly performed in the chugging regime is SPA-T2. The suitable tests will be selected in consensus with the work relating to the Fluent CFD calculations (Pättikangas 2019).

This work shows that adoption of the EHS/EMS model for Apros can be worthwhile. Pool thermal stratification, as seen e.g. in the Fukushima accident, is typically a long-term phenomenon, and an accurate modelling of stratification phenomena and associated steam condensation regimes is challenging and time-consuming when using the current code models. The EHS/EMS models increase capability of Apros for computational efficient simulation of pool stratification/mixing phenomena in real plant geometry. In the future, implementation of EHS/EMS models in Apros for blowdown-pipe case should also be considered. Final goal is to enable the modelling of whole BWR containment parallel with the Apros LP and 6-equation calculations so that pool stratification is calculated with the 6-equation model, whereas other parts of containment use the LP approach. The possibility to connect the Apros LP containment calculation with the pool CFD calculation using Fluent is also of interest.

6. Conclusions

Royal institute of Technology (KTH) has developed a simulation approach based on the Effective Heat Source (EHS) and Effective Momentum Source (EMS) for simulating pool mixing/stratification phenomena. The goal of the EHS/EMS models is to predict the pool stratification and mixing without direct modelling of the complex and time-consuming DCC phenomena. Instead, the EHS/EMS models introduce the DCC effects as appropriate boundary conditions (momentum and heat sources) which can be implemented in the CFD or system codes for modelling of transient thermal stratification and mixing in pool.

The main aim of this work was to assess the implementation of the EHS/EMS models in Apros, i.e., whether the implementation is possible and worthwhile and how it should be done. Both the lumped parameter containment model and six-equation thermalhydraulic model of Apros are considered.

The EHS/EMS models are developed to be implemented in the CFD codes or system codes using a single-phase liquid solver. Due to totally different approach used in the Apros lumped parameter code, the EHS/EMS models cannot be directly used for LP simulation. However, the work revealed some other interesting approaches which might be exploited in the Apros LP modelling for pool stratification/mixing.

The EHS/EMS models could be implemented in the Apros 6-equation model using the suitable *C* coefficient correlations for the steam momentum calculated by Apros. The recommendations for future work are that the EHS/EMS models associated with steam injection through spargers will be first implemented in the Apros 6-equation model. Possibility to use 2D nodalisation in the pool to allow circulation flows should be studied. Selected POOLEX experiments could be calculated to verify/validate the new modelling approach. The suitable experiments are e.g. SPA-T2. The calculated tests should be selected in consensus with the corresponding work with the Fluent CFD code.

This work shows that adoption of the EHS/EMS model for Apros can be worthwhile. Pool thermal stratification, as seen e.g. in the Fukushima accident, is typically a long-term phenomenon, and an accurate modelling of stratification phenomena and associated steam condensation regimes is challenging and time-consuming when using the current code models. The EHS/EMS models increase capability of Apros for computational efficient simulation of pool stratification/mixing phenomena in real plant geometry.

References

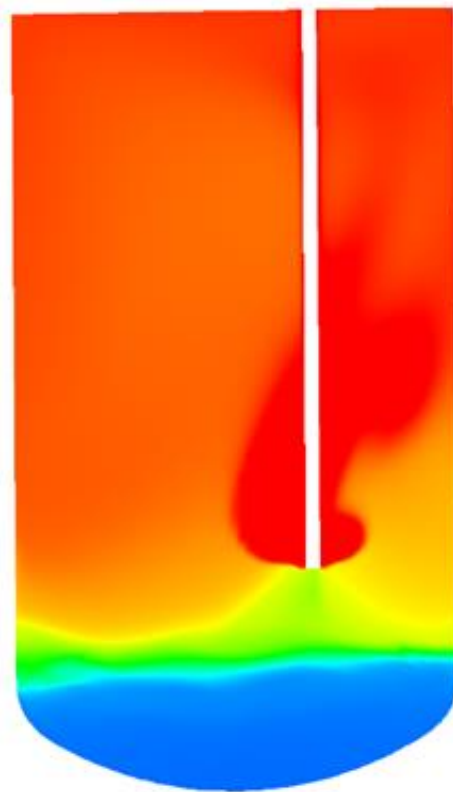
- Jo, B. et al. 2016. Thermal stratification in a scaled-down suppression pool of the Fukushima Daiichi nuclear power plant. *Nuclear Engineering and Design* 305(2016)39-50.
- Chan, C.K. and Lee, K.B. 1982. A regime map for direct contact condensation. *International Journal of Multiphase Flow*, 8, 11-20.
- Fernando, H.J.S. 1991. Turbulent mixing in stratified fluids. *Annual Review of Fluid Mechanics*, 23, 455-493.
- Fernando, H.J.S. and Hunt, J.C.R. 1997. Turbulence, waves and mixing at shear-free density interfaces. Part 1. A theoretical model, *Journal of Fluid Mechanics*, 347, 197-234.
- Gallero-Marcos, I., Villanueva, W., Kudinov, P. 2016a. Thermal stratification and mixing in a large pool induced by operation of spargers, nozzles, and blowdown pipes. *Nordic Nuclear Safety Research, NKS-369*. ISBN 978-87-7893-454-3. July 2016.
- Gallero-Marcos, I., Villanueva, W., Kudinov, P. 2016b. Modeling of thermal stratification and mixing in a pressure suppression pool using GOTHIC. NUTHOS-11, The 11th International Topical Meeting on Nuclear Reactor Thermal Hydraulics, Operation and Safety Gyeongju, Korea, October 9-13, 2016.
- Gallero-Marcos, I. 2018. Steam condensation in a water pool and its effect on thermal stratification and mixing. KTH School of Engineering Sciences. Doctoral thesis.
- Gallero-Marcos, I. et al. 2018. Pool stratification and mixing induced by steam injection through spargers: analysis of the PPOOLEX and PANDA experiments. *Nuclear Engineering and Design* 337(2018) 300-316.
- Gallero-Marcos, I. et al. 2019. Effective momentum induced by steam condensation in the oscillatory bubble regime. *Nuclear Engineering and Design* 350(2019)259 - 274.
- Hänninen, M. 2005. Simulation of POOLEX experiment with Apros six-equation model. VTT Research Report PRO5/7813/04. 23.3.2005.
- Hua, L, Villaneuva, W, Puustinen, M, Laine, J., Kudinov, P. 2014. Validation of effective models for simulation of thermal stratification and mixing induced by steam injection into a large pool of water. *Science and Technology of Nuclear Installations*. Volume 2014, Article ID 752597, 18 pages.
- Hänninen, M. 1992. Apros code for the analyses of nuclear power plant thermal-hydraulics transients. *Proc. of ANS Winter Meeting*, Chicago, Illinois, USA.
- Hänninen, M. 2009. Phenomenological extensions to Apros six-equation model. Doctoral thesis. VTT Publications 720.

- Laine, J., Puustinen, M., Räsänen, A. 2009. PPOOLEX experiments on thermal stratification and mixing. Nordic Nuclear Safety Research, NKS-117.
- Laine, J., Puustinen, M., Räsänen, A. 2014. PPOOLEX mixing experiments. Nordic Nuclear Safety Research, NKS-309.
- Li, H., Villanueva, W., Kudinov, P. 2014a. Approach and development of effective models for simulation of thermal stratification and mixing induced by steam injection into a large pool of water. Science and Technology of Nuclear Installations, 2014, Article ID 108782, 11 pages.
- Li, H., Villanueva, W., Puustinen, M., Laine, J., Kudinov, P. 2014b. Validation of effective models for simulation of thermal stratification and mixing induced by steam injection into a large pool of water. Science and Technology of Nuclear Installations, 2014, Article ID 752597.
- McGrath, J.L, Fernando, H.J.S., Hunt, J.C.R. 1997. Turbulence, waves and mixing at shear-free density interfaces. Part 2. Laboratory experiments, Journal of Fluid Mechanics, 347, 235-261.
- Mizokami, S. et al. 2016. Unsolved issues related to thermal-hydraulics in the suppression chamber during Fukushima Daiichi accident progression. Journal of Nuclear Science and Technology, 53, 630-638.
- Nariaia, H. and Aya, I. 1986. Fluid and pressure oscillations occurring at direct contact condensation of steam flow with cold water. Nuclear Engineering and Design, vol. 95, pp. 35 - 45, 1986.
- Ozdemir, E.O. and George, T.L. 2015. BWR Mark I pressure suppression pool mixing and stratification analysis using GOTHIC lumped parameter modeling methodology. Annals of Nuclear Energy 85(1015) 532 - 543.
- Pättikangas, T. 2019. CFD analysis of pressure suppression pool by using effective heat and momentum source models, VTT Research Report.
- Siikonen, T. 1987. Numerical method for one-dimensional two-phase flow. Numerical Heat Transfer 12(1987), pp-1-18.
- Silde, A. and Ylijoki, J. 2019. Nuclear power plant containment model of Apros 6.09: description of code models. Apros documentation.
- Smith, B.L. and Swift, G.W. 2003. A comparison between synthetic jets and continuous jets. Experiments in Fluids, vol. 34, no. 4, pp. 467 - 472, 2003.
- Song, D., et al. 2014. Dimensional analysis of thermal stratification in a suppression pool. International Journal of Multiphase Flow 66(2014) 92 - 100.
- Dong, C.H, Cho, S., Kang, H.S. 2012. Steam jet condensation in a pool: From fundamental understanding to engineering scale analysis. Journal of Heat Transfer 134(3), 15 pages.
- Vihavainen, J., Hänninen, M., and Tuunanen, J. 1999. Improved thermal stratification modeling in the Apros code simulations of passive safety injection experiments. 9th International Topical Meeting in Nuclear Reactor Thermal Hydraulics (NURETH-9). San Francisco, California, October 3-8, 1999.

Villanueva, W., Hua, L., Puustinen, M., Kudinov, P. 2015. Generalization of experimental data on amplitude and frequency of oscillations induced by steam injection into a subcooled pool. Nuclear Engineering and Design, 295, 155-161.

Appendix D



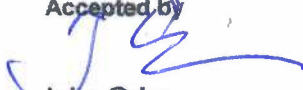


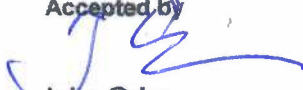


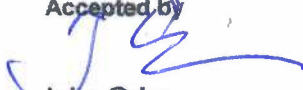
CFD analysis of pressure suppression pool by using effective heat and momentum source models



CFD analysis of pressure suppression pool by using effective heat and momentum source models

Authors: Timo Pättikangas

Confidentiality: Public

Report's title CFD analysis of pressure suppression pool by using effective heat and momentum source models				
Customer, contact person, address 1. Yli-insinööri Jorma Aurela, Valtion ydinjätehuoltorahasto, PL 32, 00023 Valtioneuvosto 2. Ari-Pekka Leppänen, Programme Manager NKS-R, STUK, Lähteentie 2, 96400 Rovaniemi, Finland	Order reference Dnro SAFIR 11/2019 ATF/NKS-R(19)130/8			
Project name CFD methods for reactor safety assessment (CFD4RSA)	Project number/Short name 121103 /SAFIR2022 CFD4RSA 2019			
Author(s) Timo Pättikangas	Pages 16			
Keywords pressure suppression pool, BWR, CFD, EMS/EHS model	Report identification code VTT-R-00228-20			
Summary <p>Test simulation on thermal stratification of pressure suppression pool has been done for an experiment performed with the PPOOLEX test facility. In the experiment, steam was injected into water through a vertical sparger pipe submerged into the pressure suppression pool. The condensation of steam was not calculated directly but it was modelled by using the Effective Momentum Source and the Effective Heat Source (EMS/EHS) models developed by Gallego-Marcos et al. (2018a, 2018b). The calculation was performed with the commercial ANSYS Fluent code, where the EMS/EHS model was implemented with user-defined functions. In the EMS/EHS model, the momentum and enthalpy resulting from the steam condensation are added as source terms directly into liquid water phase.</p> <p>The CFD simulation resulted in qualitatively correct behaviour of the thermal stratification. The calculated pool temperatures were, however, clearly lower than in the experiment. The reason for this was the heat loss on the pool surface. The beginning of the mixing part of the stratified layer was also calculated and the initial phase of the mixing was observed.</p> <p>The present approach must be modified and a new simulation with modified boundary conditions is in progress. It seems, however, that in future some major changes in the simulations method should be made in order get improved results. During the present experiment, the amount of injected steam is so large that the surface level in the pool changes significantly. In order to take this properly into account, Volume Of Fluid Method should be used where the evolution of the surface level can be calculated. This method would also properly treat the problematic heat losses on the pool surface.</p>				
Confidentiality	Public			
Espoo 25.3.2020 <table border="0"> <tr> <td>Written by  Timo Pättikangas, Principal Scientist</td> <td>Reviewed by  Ari Silde Senior Scientist</td> <td>Accepted by  Inka Orko Research Team Leader</td> </tr> </table>		Written by  Timo Pättikangas, Principal Scientist	Reviewed by  Ari Silde Senior Scientist	Accepted by  Inka Orko Research Team Leader
Written by  Timo Pättikangas, Principal Scientist	Reviewed by  Ari Silde Senior Scientist	Accepted by  Inka Orko Research Team Leader		
VTT's contact address VTT Technical Research Centre of Finland Ltd, P.O.B. 1000, FI-02044 VTT, Finland				
Distribution (customer and VTT) SAFIR2022 Reference Group 4, NKS-R Programme Manager				
The use of the name of VTT Technical Research Centre of Finland Ltd in advertising or publishing of a part of this report is only permissible with written authorisation from VTT Technical Research Centre of Finland Ltd.				

Contents

Contents.....	3
1. Introduction.....	4
2. PPOOLEX thermal stratification experiments.....	5
3. Effective momentum and heat source models.....	7
4. CFD model	9
5. CFD simulation of the experiment SPA-T3.....	10
6. Summary and discussion.....	14
References.....	15

1. Introduction

In a Boiling Water Reactor (BWR), the operation of the pressure suppression pool is affected by thermal stratification and mixing phenomena. In particular, thermal stratification can be important in different hypothetical Loss-Of-Coolant-Accident (LOCA) scenarios, where steam line breaks inside the containment or station blackouts. It has been suggested that thermal stratification played a role in the pressure increase in the containment of Fukushima Daichi Unit 3 (Jo et al., 2016). Validated numerical tools for the simulation of such accident scenarios are necessary.

At the Royal Institute of Technology (KTH), the behavior of the pressure suppression pool has been studied during a steam injection through blowdown pipes and spargers. Effective Heat Source (EHS) and Effective Momentum Source (EMS) models have been developed to predict the long-term thermal behavior of the pool (Gallego-Marcos et al., 2016; 2018a; 2018b; 2019a; 2019b; 2019c). At KTH, the EHS/EMS models have been implemented in the GOTHIC code.

At the LUT University, a set of experiments with spargers have been performed in the PPOOLEX facility. The experiments were mainly focused on the oscillatory bubble regime, and exploratory tests were done in chugging and stable jet regimes. The experimental data was used by KTH to address important phenomena governing the pool behavior and validate the computational models. A small-scale Separate Effect Facility (SEF-POOL) was built to measure directly the effective momentum induced by steam injection through a sparger. The experiments enabled the development of the effective momentum source correlations at KTH.

At VTT, Computational Fluid Dynamics (CFD) simulations have been performed for the SEF-POOL experiments of LUT. The simulations have been done by using the commercial ANSYS Fluent code and the open-source OpenFOAM code (Pättikangas et al., 2019). The work has been done in co-operation with KTH, LUT and VTT through the COPSAR (Puustinen et al., 2018) and THEOS projects, which have been funded by NKS.

In the present work, the EHS/EMS models have been used in the CFD simulation of thermal stratification and mixing experiment performed at LUT with the PPOOLEX test facility. The thermal stratification phase is calculated for an experiment, where steam is injected into pressure suppression pool through sparger pipe. Steam is first injected at a low mass flow rate, which leads to thermal stratification of the water pool. In the end, the pool is mixed by injecting steam at a high mass flow rate.

The possibilities to implement the EHS/EMS based modeling approach in the lumped parameter containment model of the Apros system code is studied in a separate report (Silde, 2019).

2. PPOOLEX thermal stratification experiments

Thermal stratification and mixing experiments have been performed at the LUT University with the PPOOLEX test facility (Laine et al., 2015). The PPOOLEX test facility is 7.45 m high and its diameter is 2.4 m. The facility consists of dry well and wet well compartments, which models a BWR containment. The present experiments are performed with the wet well compartment of the facility, where steam is injected into a water pool through a sparger pipe. The PPOOLEX facility is shown in Figure 1.

The sparger pipe is submerged in the water pool, where the water level is at 3 m. The bottom of the 76.1×4.0 pipe is at level 1.2 m, i.e., the submergence depth is initially 1.8 m. The bottom part of the vertical sparger pipe has 32 orifices having a diameter of 8 mm. The orifices are arranged in four rows each containing eight orifices. The bottom part of the sparger pipe is shown in Figure 2.

In the following, the PPOOLEX experiment SPA-T3 is modelled with CFD calculations. Before the experiment the water pool was heated with steam to a uniform temperature of 21 C. In the stratification phase of the experiment, steam was injected into the water pool for 4068 seconds at a low mass flow rate of 120 g/s. The stratification phase was followed by mixing phase, where the mass flow rate of steam was large, 260 g/s. The mixing phase lasted for about 500 s. The parameters of the experiment are summarized in Table 1.

The behaviour of the steam jets injected into the water pool depends on two main parameters: mass flux of steam and pool temperature. Condensation map determined by Gallego-Marcos et al. (2018a, 2018b) and Laine et al. (2015) is shown Figure 3. At low mass flux, chugging oscillations of steam jets occur at the orifices of the sparger pipe. If the pool temperature is low, the oscillation occurs inside the pipe. If the pool temperature is high, oscillating steam jet is located outside the sparger pipe. At high mass fluxes, oscillatory cone jet and stable cone jet are observed.

In the present experiment, the initial pool temperature was 21 C. In the heating phase, the mass flow rate of steam was 120 g/s, which corresponds to mass flux of 74.6 kg/m²s. In the condensation map of Figure 3, this is on the borderline between internal and external chugging regions and the oscillatory bubble region. In the mixing phase, the mass flow rate of steam was increased to 260 g/s, which corresponds to mass flux of 162 kg/m²s. In the condensation map, this is in the stable cone jet region.

Table 1. Parameters of the PPOOLEX experiment SPA-T3.

	Time period [s]	Mass flow rate [g/s]
Stratification phase	235...4303	120
Mixing phase	4303...5005	260

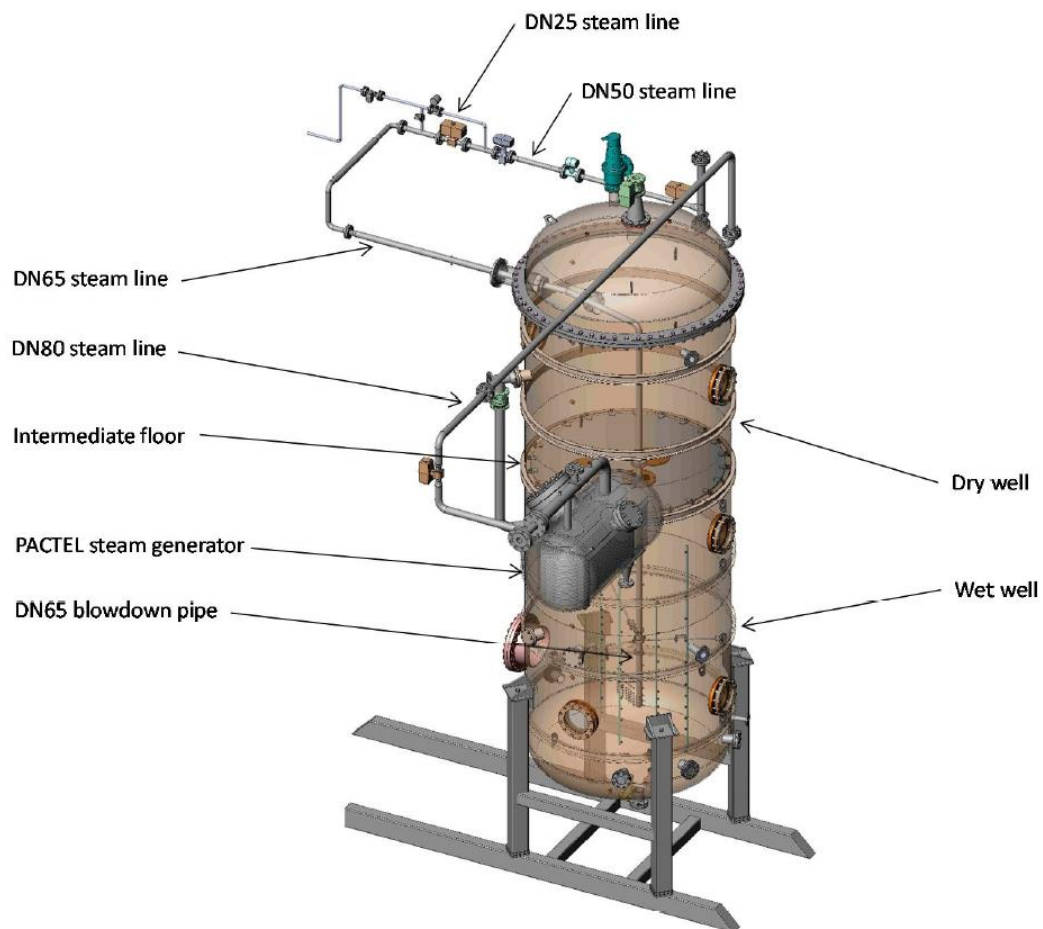


Figure 1. PPOOLEX test vessel at LUT University (Laine et al., 2015).



Figure 2. Sparger pipe in the pressure suppression pool of the PPOOLEX test facility at the LUT University (Laine et al., 2015).

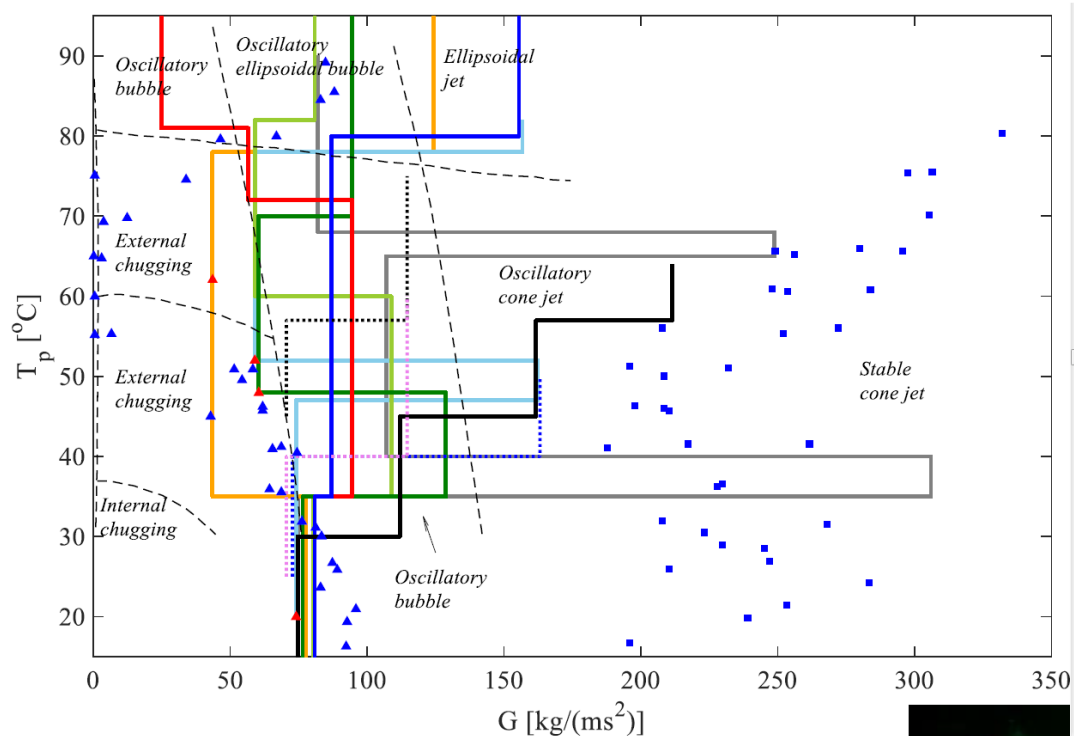


Figure 3. Condensation map obtained from PPOOLEX and PANDA data (Gallego-Marcos, 2018a).

3. Effective momentum and heat source models

In the Effective Momentum Source (EMS) and Effective Heat Source Model (EHS), the condensation of steam in water pool is not directly calculated in GOTHIC or CFD simulations models. Instead, momentum and heat sources are added in the simulation model in the region, where the condensation of the steam jets occurs.

Gallego-Marcos et al. (2019a, 2019b) have formulated EMS/EHS models both for blowdown pipes and sparger pipes submerged in water pools. These two configurations are illustrated in Figure 4. The condensation of the heat jets provides the momentum source and the main part of the heat source into the water pool. Some amount of heat is also transferred into water through the uninsulated wall of the submerged steel pipe. This amount of heat must be taken into account, when the effective heat source is determined.

The idea of the EMS model is illustrated in Figure 5, where a steam jet in a water pool is shown. The picture is taken from the SEF-POOL separate effect test facility of LUT University (Puustinen et al., 2018), where different condensation regimes have been studied experimentally. Part of the momentum of the condensing steam jet is transferred to the water pool as time-averaged momentum of liquid water. Another part of the momentum is converted to turbulence, which is dissipated in the water pool.

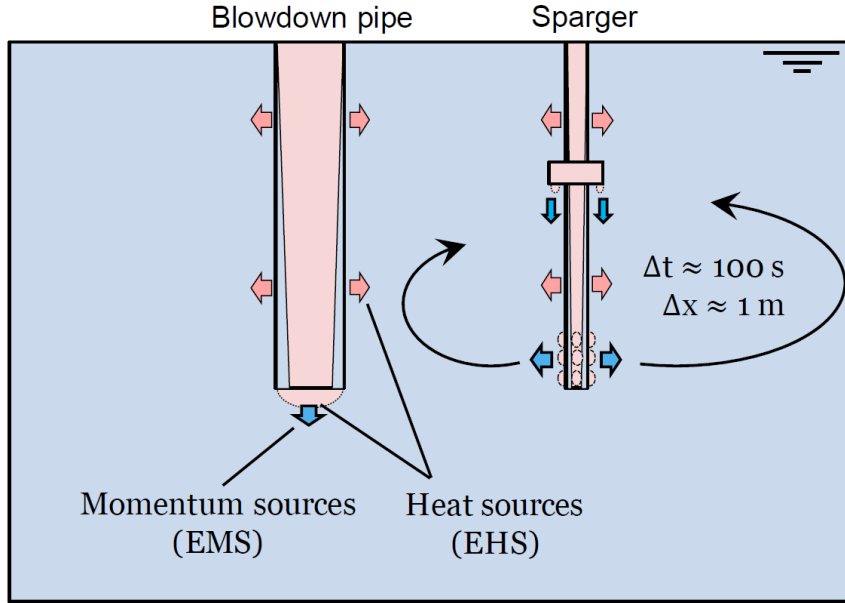


Figure 4. Effective Momentum Source (EMS) and Effective Heat Source models have been developed for the blowdown pipe and sparger pipe at KTH (Wang et al., 2019).

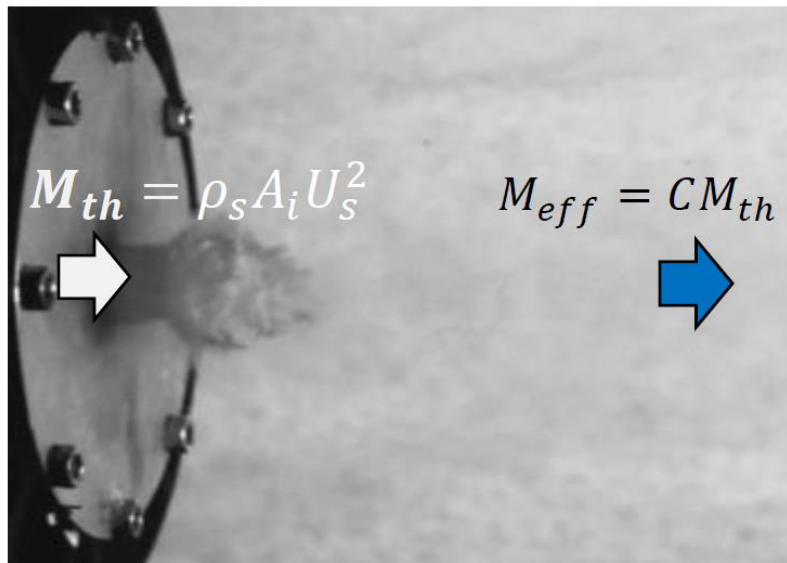


Figure 5. In the EMS/EHS model, correlations for the coefficient C for the momentum transfer from condensing steam to liquid is determined for different mass flow rates and pool temperatures (Wang et al., 2019; Puustinen et al., 2018).

In the EMS model, the effective momentum transferred to liquid water is described as

$$M_{\text{eff}} = C \rho_s A_i U_s^2 \quad (1)$$

where ρ_s is the density of steam, A_i is the area of the orifice and U_s is the mean flow velocity of steam. The coefficient C describes has been determined experimentally for different regions of the condensation map of Figure 3 by using the data obtained from the SEF-POOL facility (Gallego-Marcos, 2018a; Puustinen et al., 2018). The advantage of this approach is that the details of the condensation process do not need to be modelled. In GOTHIC or CFD simulations, this is advantageous in particular in the oscillating regime of the condensation

map. The EMS/EHS approach makes possible to simulate long transients, which are relevant to analysis of hypothetical accidents in BWRs.

In his Doctoral Thesis, Ignacio Gallego-Marcos summarized correlations for the effective momentum transfer coefficients in subsonic regimes of the condensation map (Gallego-Marcos, 2018a):

$$C = \begin{cases} C_1 = \frac{10.58}{\Delta T^{0.42}} \left(n \frac{\pi d^2}{4} \right)^{0.07} & G \leq 120 \\ C_2 = \frac{2.70}{\Delta T^{0.51}} \left(n \frac{\pi d^2}{4} \right)^{-0.13} & 150 \leq G < 300 \\ C_3 = (0.5 - s)C_1 + (0.5 + s)C_2 & 120 < G < 150 \\ s = 0.5 \tanh\left(\frac{G - 135}{5}\right) & 120 < G < 150 \end{cases} \quad (2)$$

Here, the momentum transfer coefficient depends on the mass flux of steam (G), the number of orifices (n) and their diameter (d), and the subcooling of the pool water (ΔT). In the present simulations, the values the coefficient were $C = 1.0$ in the beginning of the stratification phase and $C = 0.77$ in the mixing phase.

Some other forms for the momentum transfer coefficient have recently been determined from the SEF-POOL experiments in terms of Jacob number (Gallego-Marcos et al., 2019a; Wang et al., 2019).

4. CFD model

Thermal stratification phase of the experiment SPA-T3 was modelled with CFD calculations by using ANSYS Fluent version 19 R3. Single phase calculation with EMS/EHS model was performed by using standard $k-\varepsilon$ turbulence model with “enhanced wall treatment”. In the enhanced wall treatment of Fluent, the turbulence dissipation is calculated from an algebraic equation in the regions where wall-distance based Reynolds number is small. This improves the behaviour of the $k-\varepsilon$ in the regions where turbulence level is small.

The SIMPLE scheme was used for the pressure-velocity coupling, where second order discretization was used for the pressure. Second order upwind method was used for momentum, turbulence and energy. Bounded second order implicit time discretization was used, where the time step was 0.05 s in the stratification phase and 0.02 s in the mixing phase. Therefore, 80 000 time steps were needed for 4000 s stratification phase.

The CFD mesh consisted of 537 000 hexahedral control volumes. The regions for the EMS/EHS sources were implemented with user-defined functions of Fluent in the regions, where the orifices of the sparger pipes were located. The CFD mesh is illustrated in Figure 6.

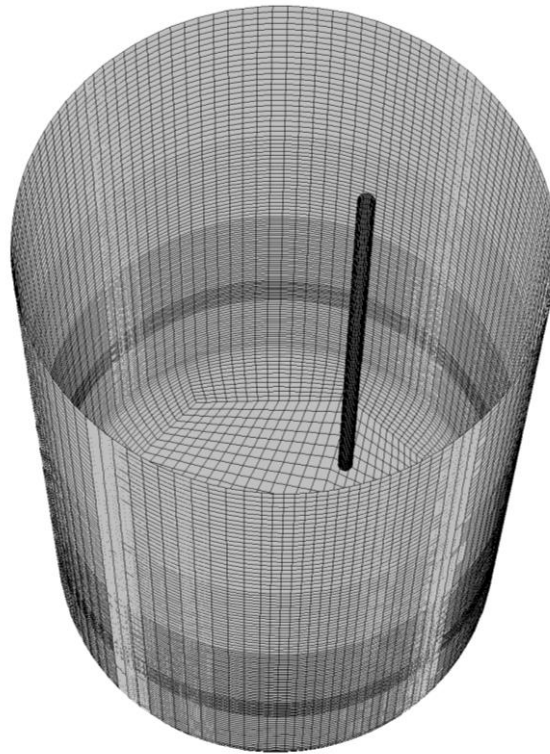


Figure 6. Surface mesh of the CFD model of the bottom part of the PPOOLEX wet well.

5. CFD simulation of the experiment SPA-T3

The thermal stratification phase of the experiment SPA-T3 is illustrated in Figure 7, where the temperature of the water pool is shown. In the beginning of the experiment, the pool is fully mixed with homogeneous temperature of 21 C. The injection of steam heats the liquid water near the bottom part of the pipe. In addition, the liquid water in the vicinity of the hot pipe heats up. Gradually the temperature rises in the region above the pipe bottom. Later, the temperature gradient moves downwards towards the bottom of the pool. The temperature in the bottom part of the pool remains close the initial temperature of 21 C.

The mixing phase is started at time $t = 4200$ s by increasing the mass flow rate of the injected steam. This increases the flow velocity and the return flow is formed, which returns from the top part of the pool towards the thermocline in the bottom part of the pool. Mixing of the cold water layer in the pool bottom starts. In the end of the simulation, the cold layer is not yet fully mixed.

The magnitude of flow velocity is shown in Figure 8. In the stratification phase, the cold water layer in the bottom part of the pool is still. The maximum flow velocities in the top part of the pool are above 0.2 m/s, in some regions about 0.9 m/s. The circulation of the flow from the top part of the pool makes the thermocline region to oscillate, which increases the mixing of the bottom part of the pool.

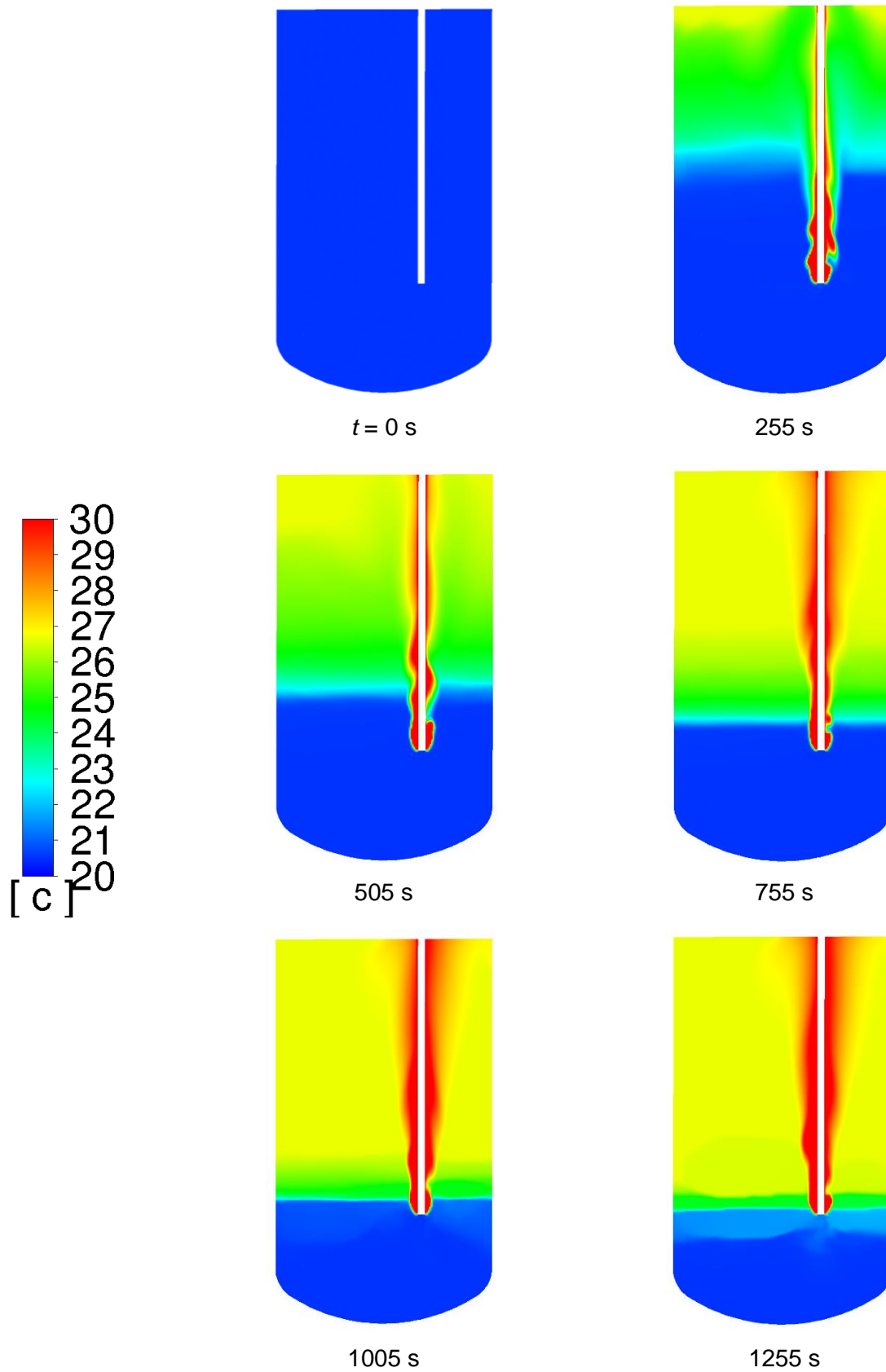


Figure 7. Calculated temperature in the pressure suppression pool of PPOOLEX test facility during the stratification experiment SPA-T3. In the temperature scale, all temperatures above 30 °C as shown as red.

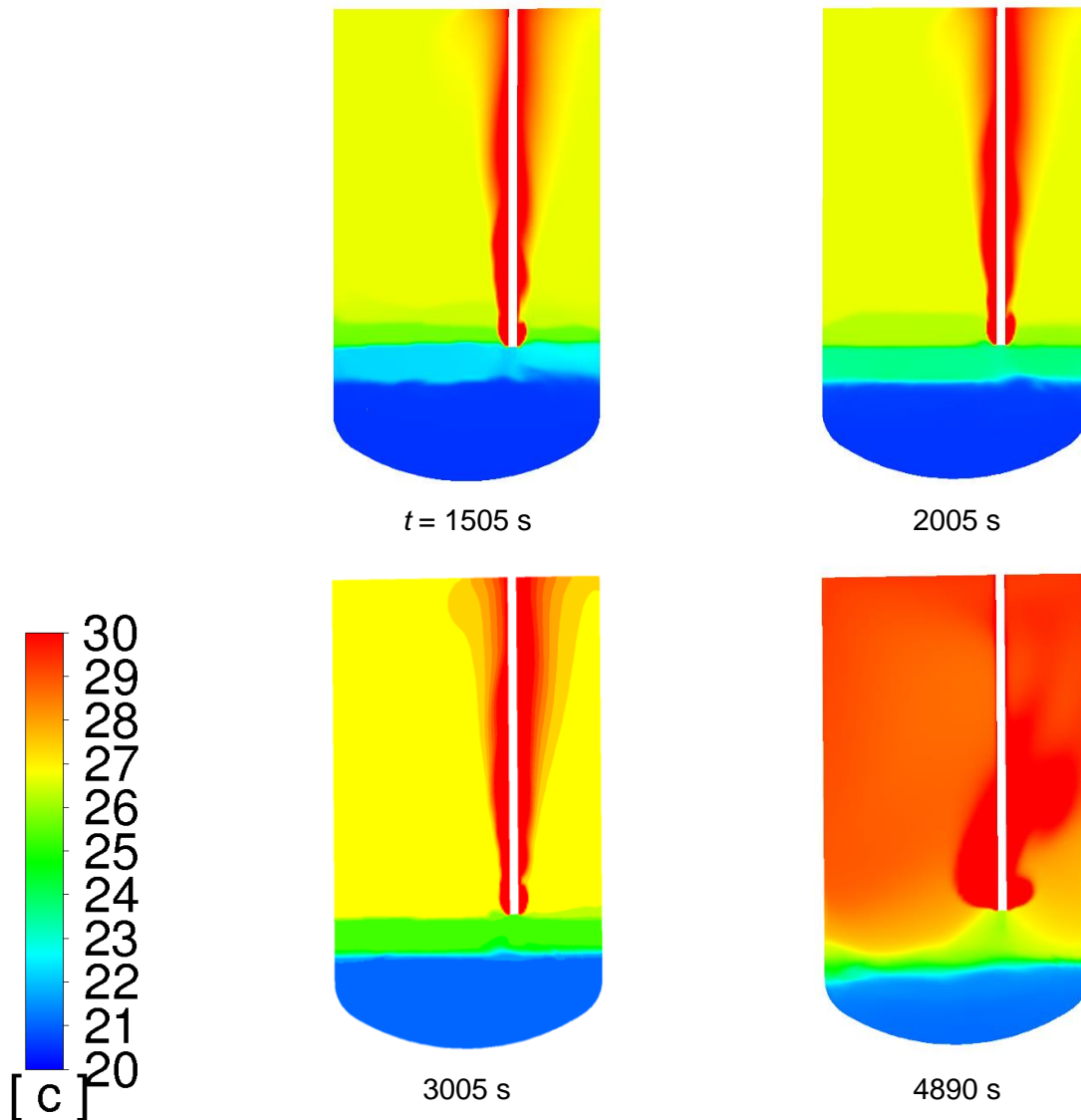


Figure 7. Temperature of the pressure suppression pool. Continues from the previous page.

At the end of the simulation, the calculation of the mixing phase is started by increasing the mass flow rate of injected steam. The deterioration of the stratification is accelerated at this phase as can be seen in the temperature field at time $t = 4890$ s. The condensing steam jet drives flow that returns to the thermocline area as is seen in the flow velocity at time $t = 4890$ s.

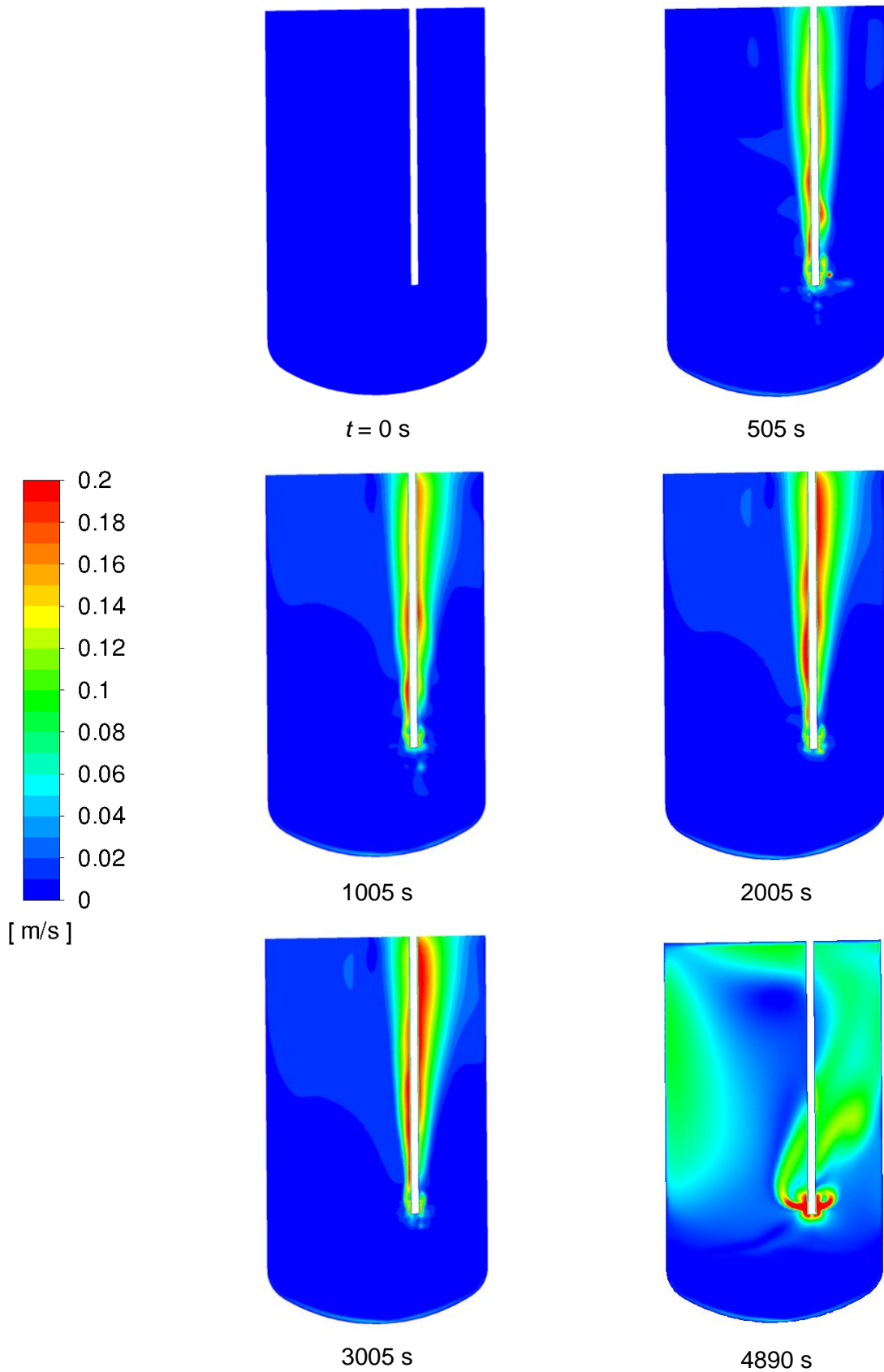


Figure 8. Calculated magnitude of flow velocity in the pressure suppression pool of PPOOLEX test facility during the stratification experiment SPA-T3. All velocities larger than 0.2 m/s are shown as red.

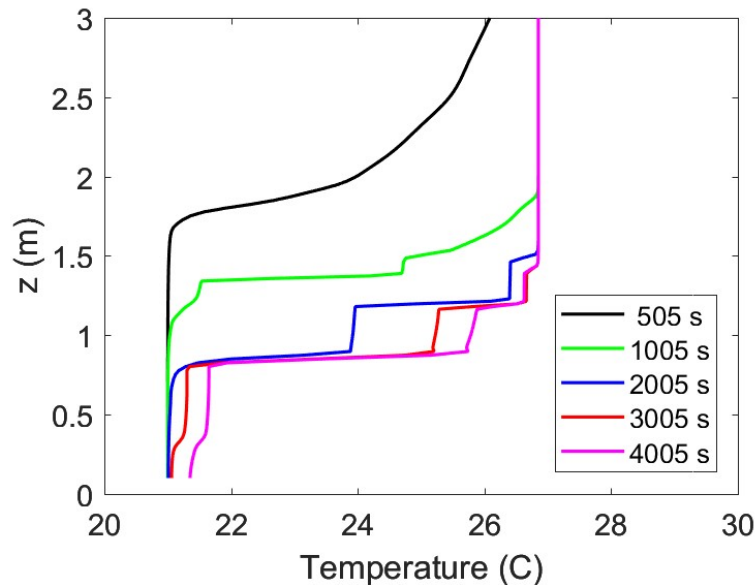


Figure 9. Calculated temperature along the vertical L1 measurement line at different instants of time.

The calculated temperature during the stratification phase is shown in Figure 9 at different instants of time. The results are shown along the vertical line L1 that is located at a distance of 40 cm from the pool center and 82 cm from the sparger pipe. The temperature profile behaves qualitatively in the expected manner. Thermal stratification occurs during the simulation and the thermocline moves downwards during the experiment. The calculated temperatures are, however, clearly lower than in the experiment. The heat loss at the pool surface is clearly larger than in the experiment.

6. Summary and discussion

Test simulation on thermal stratification of pressure suppression pool has been done for an experiment performed with the PPOOLEX test facility. In the experiment, steam was injected into water through a vertical sparger pipe submerged into the pressure suppression pool. The condensation of steam was not calculated directly but it was modelled by using the Effective Momentum Source and the Effective Heat Source (EMS/EHS) models developed by Gallego-Marcos et al. (2018a, 2018b). The calculation was performed with the commercial ANSYS Fluent code, where the EMS/EHS model was implemented with user-defined functions. In the EMS/EHS model, the momentum and enthalpy resulting from the steam condensation are added as source terms directly into liquid water phase.

The CFD simulation resulted in qualitatively correct behaviour of the thermal stratification. The calculated pool temperatures were, however, clearly lower than in the experiment. The reason for this was the heat loss on the pool surface. The beginning of the mixing part of the stratified layer was also calculated and the initial phase of the mixing was observed.

The present approach must be modified and a new simulation with modified boundary conditions is in progress. It seems, however, that in future some major changes in the simulations method should be made in order to get improved results. During the present experiment, the amount of injected steam is so large that the surface level in the pool changes significantly. In order to take this properly into account, Volume Of Fluid Method should be used where the evolution of the surface level can be calculated. This method would also properly treat the problematic heat losses on the pool surface.

References

- Cai, J., Jo, B., Erkan, N., Okamoto, K., 2016. Effect of non-condensable gas on thermal stratification and flow patterns in suppression pool, *Nuclear Engineering and Design* 300, 117–126.
- Gallego-Marcos, I., Villanueva, W., and Kudinov, P., 2016. Thermal stratification and mixing in a large pool induced by operation of spargers, nozzles and blowdown pipes, *Nordic nuclear safety research, NKS-369*, 50 p.
- Gallego-Marcos, I., 2018a. Steam condensation in a water pool and its effect on thermal stratification and mixing, *Doctoral Thesis, KTH Royal Institute of Technology, Stockholm, Sweden*.
- Gallego-Marcos, I., Kudinov, P., Villanueva, W., Kapulla, R., Paranjape, S., Paladino, D., Laine, J., Puustinen, M., Räsänen, A., Pyy, L., Kotro, E., 2018b. Pool stratification and mixing during a steam injection through spargers: analysis of the PPOOLEX and PANDA experiments. *Nuclear Engineering and Design* 337, 300–316.
- Gallego-Marcos, I., Kudinov, P., Villanueva, W., Puustinen, M., Räsänen, A., Tielinen, K., Kotro, E., 2019a. Effective momentum induced by steam condensation in the oscillatory bubble regime. *Nuclear Engineering and Design* 350, 259–274.
- Gallego-Marcos, I., Kudinov, P., Villanueva, W., Kapulla, R., Paranjape, S., Paladino, D., Laine, J., Puustinen, M., Räsänen, A., Pyy, L., Kotro, E., 2019b. Pool stratification and mixing induced by steam injection through spargers: CFD modelling of the PPOOLEX and PANDA experiments, *Nuclear Engineering and Design* 347, 67–85.
- Gallego-Marcos, I., Grishchenko, D., Kudinov, P., 2019c. Thermal stratification and mixing in a Nordic BWR pressure suppression pool, *Annals of Nuclear Energy* 132, 442–450.
- Jo, B., Erkan, N., Takahashi, S., Song, D., Sagawa, W., Okamoto, K., 2016. Thermal stratification in a scaled-down suppression pool of the Fukushima Daiichi nuclear power plants, *Nuclear Engineering and Design* 3015, 39–50.
- Li, H., Villanueva, W., Puustinen, M., Laine, J., Kudinov, P., 2018. Thermal stratification and mixing in a suppression pool induced by direct steam injection, *Annals of Nuclear Energy* 111, 487–498.
- Laine, J., Puustinen, M., Räsänen, A., 2015. PPOOLEX experiments with a sparger, *Nordic nuclear safety research, NKS-334*, 19 p. + app. 17 p.
- Pättikangas, T., Peltola, J., Hovi, V., Puustinen, M., Räsänen, A., Kotro, E., 2019. CFD simulations of direct-contact condensation of horizontal vapor jets, *Proceedings of the 18th International Topical Meeting on Nuclear Reactor Thermal Hydraulics (NURETH-18)*, August 18–22, 2019, Portland, USA, pp. 1583–1596.
- Puustinen, M., Pättikangas, T., Kudinov, P., 2018. COPSAR-NKS Project, Summary report 2017, *Nordic nuclear safety research, NKS-409*, 201 p.
- Silde, A., 2019. Assessment of implementation of the effective heat and momentum source models in Apros, *VTT Technical Research Centre of Finland Ltd, VTT Research Report VTT-R-01029-19*, 22 p.
- Wang, X., Gallego-Marcos, I., Grishchenko, D., Kudinov, Pavel, 2019. *Proceedings of the 18th International Topical Meeting on Nuclear Reactor Thermal Hydraulics (NURETH-18)*, August 18–22, 2019, Portland, USA, pp. 6176–6189.

Title	Thermal Hydraulic Phenomena of the Suppression Pool
Author(s)	Pavel Kudinov ¹ , Xicheng Wang ¹ , Dmitry Grishchenko ¹ Markku Puustinen ² , Antti Räsänen ² , Eetu Kotro ² , Kimmo Tielinen ² Timo Pättikangas ³ , Ari Silde ³
Affiliation(s)	¹ Division of Nuclear Engineering, Kungliga Tekniska Högskolan (KTH), ² Lappeenranta-Lahti University of Technology (LUT), ³ VTT Technical Research Centre of Finland Ltd
ISBN	978-87-7893-531-1
Date	June 2020
Project	NKS-R / THEOS
No. of pages	184
No. of tables	13
No. of illustrations	108
No. of references	226
Abstract max. 2000 characters	<p>KTH reports further development and validation of the Effective Momentum Source and the Effective Heat Source (EMS/EHS) models for spargers using source terms and boundary conditions approaches. Fluent and GOTHIC codes have been applied in the analysis to design sparger (H2P3) and integral (H2P4) test series in PANDA facility. Results of the analysis suggest that proposed design allows to achieve test objectives and obtain PIV data needed for model development and validation from H2P3, and to reach prototypic levels of pressurization within a reasonable time in H2P4. The progress on development of the image analysis for post processing the data from the SEF-POOL tests is presented.</p> <p>Nine steam injection tests in SEF-POOL facility at LUT University. Analysis of the tests helps to understand the key effects and factors that can be neglected in model development. Main findings are: both the Jacob and Mach number have a significant effect; at large Ja effective momentum is significantly reduced; effective momentum has a maximum at Ja ~0.02-0.04; injection hole diameter and chamfer have no significant influence on the effective momentum except for the maximum value of C, which is reached at larger values of Ja number for smaller holes.</p> <p>Result of VTT work suggest that the EHS/EMS models could be implemented in the Apros 6-equation model. The EHS/EMS models</p>

can increase capability of Apros for computationally efficient simulation of pool stratification/mixing phenomena in plant geometry. Simulation on thermal stratification has been done with Fluent for an experiment performed in the PPOOLEX test facility with steam injection through a vertical sparger. The effect of steam injection was modelled by using the EMS/EHS. Qualitatively correct behavior of the thermal stratification was obtained, however, pool temperature was lower than in the experiment due to the heat loss on the pool surface. Further analysis is ongoing in order improve the results.

Key words

Steam Condensation, Pool Stratification, Mixing, Pressure Suppression Pool, Thermal Hydraulic, BWR, Containment, CFD, GOTHIC